Computational Investigation of Tunable Steel Plate Shear Walls for Improved Seismic Resistance

Manasa Koppal

Thesis submitted to the faculty of

Virginia Polytechnic Institute and State University

in partial fulfillment of the requirements for the degree of

MASTER OF SCIENCE

IN

CIVIL ENGINEERING

Matthew R. Eatherton, Chairman

Cristopher D. Moen

Kamal B. Rojiani

August 3rd, 2012

Blacksburg, VA

Keywords: Steel Plate Shear Walls, Finite element modeling, Perforated plate, Seismic Behavior

Computational Investigation of Tunable Steel Plate Shear Walls for Improved Seismic Resistance

Manasa Koppal

ABSTRACT

Steel plate shear walls (SPSWs) are popular lateral force resisting systems whose practical applications range from high seismic regions to medium and low seismic areas and wind load applications. The factors which make SPSW attractive include its energy dissipation capacity, excellent ductility, constructability, speed of construction compared to concrete shear walls, reduced architectural footprint compared to concrete shear walls, and increased inelastic deformation capacity as compared to braced frames. The principle behind current SPSW design is that the post-buckling tension field capacity of the thin web plate is proportioned to resist the full lateral load. The resulting web plate is typically quite thin, buckles at low loads, possesses low stiffness, and does not provide resistance when the lateral loads are reversed until the tension field engages in the opposite direction. To compensate for these shortcomings, moment connections are required at the beam to column connections to improve energy dissipation, increase stiffness, and provide lateral resistance during load reversal. The resulting SPSW designs with very thin web plates, moment connections, and beams and columns significantly larger than comparable braced frames, can result in inefficient structural systems.

The objective of this work is to develop steel plate shear wall systems that are more economic and efficient. In order to achieve this, approaches like shear connections between beams and columns, allowing some yielding in columns and increasing plate thicknesses were attempted. But these approaches were not effective in that there was no reduction in the amount of steel required since stiffness controlled the designs. This necessitated the creation of tunable steel plate shear wall systems in which strength and stiffness could be decoupled. Preliminary analyses of seven steel plate shear wall systems which allow tunability were conducted and two configurations namely circular holes and butterfly shaped links around the perimeter, that showed promising results were chosen. The solid plate in the middle of the panel contributes significant pre-yield stiffness to the system while the geometry of the perimeter perforations

controls strength and ductility. An example panel was designed using the two approaches and compared to panels designed using current SPSW design methods. The proposed configurations resulted in improved overall performance of the system in terms of energy dissipation, stable hysteresis, required less steel and no moment connections between beams and columns. This was also observed from the parametric study that was performed by varying the thickness of the web plate and the geometry of the configurations. Thus it was concluded that the two proposed configurations of cutouts were promising concepts that allow separate tuning of the system strength, stiffness and ductility and could be adopted in any seismic zone for improved seismic resistance.

Acknowledgements

I would like to express my sincere gratitude to my advisor Dr. Matthew R. Eatherton for being my mentor and guiding me through the entire course of my research at Virginia Tech. I thank him for being a constant support and inspiration to me. I have learnt from every discussion with him. The high standards he sets for his work and his research team, his meticulous teaching methodologies have made me not only a better civil engineer but also a better person. I feel highly privileged to have been his student and to have been given this opportunity to work in his research team. I would also like to thank my co-advisors, Dr. Cristopher D. Moen and Dr. Kamal B Rojiani for their constructive advice and valuable inputs for my research.

I express my profound gratitude to all my teachers at Virginia Tech and NITK, Surathkal for making me the engineer I am today. An immense amount of gratitude goes to my parents, Dr. K P Vittal and Mainavathi Vittal because of whom all this has been possible today. Their love, affection and relentless support are the backbone for everything in my life. Thanks to my brother, Vivek for being there for me all along. Thanks are due to Dr. Badrinath and Anasuya Kulkarni, Madhu and Uma Bangalore who are my guardians in the States and have been there for me from the moment I landed in the USA.

Thanks also go to all my friends here at Tech for giving me memories that will be cherished forever. Thanks to Jeena Rachel Jayamon, Sudeeksha Murari, Chainika Jhangu, Abhilasha Maurya, Natalya Egorova, Saranya Prabhakaran, Amber Verma, Chirag Kapadia, David Padilla-Llano, Amey Bapat, Rakesh Naik, Pradeep Naga, Krishnan Gopalan, Siddharth Vijayaraghavan, Pavan G Srinivas and to all my fellow graduate students in SEM and many more friends who I have not been able to mention here. Special thanks to Karthik Kumaresan and Gargi Singh for everything.

I truly appreciate the endless support extended by all my family members back in India. Finally I thank God for everything I have and I am today.

Table of Contents

List of Tables ..... **ix**

List of Figures ..... **xi**

Chapter 1. INTRODUCTION **1**

1.1 Steel Plate Shear Walls – An Overview: 1

1.2 Motivation and Approach 3

1.3 Organization of the thesis 4

Chapter 2. LITERATURE REVIEW **5**

2.1. System behavior, mechanics and Strip model representation of SPSWs: 5

2.2. SPSW with solid panels 7

2.2.1. Thorburn, Kulak and Montgomery (1983) 8

2.2.2. Xue and Lu (1994) 9

2.2.3. Berman and Bruneau (2005) 10

2.2.4. Vian and Bruneau (2005) 11

2.3. SPSW with Perforations, Slits and Other Cut-outs 12

2.3.1. Roberts and Sabouri-Ghomi (1992) 12

2.3.2. Vian and Bruneau (2005) 13

2.3.3. Purba and Bruneau (2007) 16

2.3.4. Hitaka and Mastui (2006) 16

2.3.5. Borchers, Peña, Krawinkler, and Deierlein (2010) 18

2.4. High Seismic Design of SPSW 19

2.4.1. Requirements of the AISC Seismic Provisions – ANSI/AISC 341-10 20

2.4.2. Web Panel Design 20

2.4.3. Horizontal Boundary Element (HBE) Design 21

2.4.4. Vertical Boundary Element (VBE) Design 24

2.4.5. Implications of Current High Seismic Design Approach 25

Chapter 3. VALIDATION OF FINITE ELEMENT MODELING IN ABAQUS 6.10 27

3.1 SPSW with a solid panel 27

3.1.1 Experimental Set-up 27

3.1.2 Details of FE Modeling in ABAQUS 6.10 28

3.1.3 Comparison of Experimental and FE Model Results 32

3.2 SPSW with a Perforated Panel 35

3.2.1 Experimental Set-up 35

3.2.2 Comparison of experimental and FE model results 36

3.3 Conclusions Regarding FEM Modeling of SPSWs 38

Chapter 4. ADAPTATION OF HIGH SEISMIC DESIGN FOR MODERATE SEISMIC ZONES 39

4.1 High Seismic Design Procedure for SPSW 39

4.2 Modified Design Approach 1 – Capacity Design of VBE with no HBE Moment Connections. 44

4.3 Modified Design Approach 2 – Over-Strength Factor Design of VBE with no HBE Moment Connections 53

4.4 Modified Design Approach 3 – Plastic Design of Columns with no HBE Moment Connections56

4.5 Conclusions 63

Chapter 5. ALTERNATE SPSW DETAILING TO CREATE MORE EFFICIENT SOLUTIONS FOR SPSW 64

5.1 Background and Concept 64

5.2 New Ideas - SPSW with Solid Panels 64

5.2.1 Approach 1 – Web Panel Connected to the HBE Only 65

5.2.2 Approach 2 – Thick Fish Plate around a Thin Web Panel 66

5.2.3 Approach 3 – Small Thin Plates around a Thicker Web Panel 67

5.3 New Ideas – SPSW with Perforated Panels 69

5.3.1 Circular Perforations along the Plate Diagonal 70

5.3.2 Circular Holes of Decreasing Diameter along the Plate Diagonal 71

5.3.3 Circular Holes along the Perimeter of the Web Panel 72

5.3.4 Butterfly Shaped Cutouts along the Perimeter of the Web Panel 75

5.4 Comparison of Two of the New Approaches with Conventional SPSW Design 78

Chapter 6. PARAMETRIC STUDY 82

6.1 Application of Initial Imperfections and Mesh Size Selection 82

6.1 Parametric Study Plan 87

6.1.1 Perimeter Circular Hole Configuration 87

6.1.2 Butterfly Shaped Cutouts along the Perimeter of the Web Panel 90

6.1.3 Input Parameters 92

6.1.4 Output Parameters 93

6.2 Load Deformation Results for some Typical Models 96

6.3 Output Parameter Plots 100

6.3.1 Results for Perimeter Circular Hole Configuration – Varying Size and Spacing 101

6.3.2 Results for Perimeter Circular Hole Configuration – Varying Thickness 108

6.3.3 Butterfly Shaped Cutouts along the Perimeter of the Panel 112

6.4 Behavioral Trends Observed from Hysteresis Curves and Force – Displacement Plots of the Parametric Study 116

6.4.1 Perimeter Circular Holes with Varying Size and Spacing 116

6.4.2 Perimeter Circular Holes with Varying Thickness 116

6.4.3 Perimeter Butterfly Links 117

Chapter 7. CONCLUSIONS 118

7.1 Finite Element Modeling of SPSW 118

7.2 Adaptation of High Seismic Design for Moderate Seismic Zones 118

7.3 Alternate SPSW Detailing to Create More Efficient Solutions for SPSW 118

7.4 Parametric Study for the Two Proposed Configurations of Cutouts 119

7.5 Recommendations for Future Work 120

References: 122

APPENDIX A 126

List of Tables

Table 4-1 Story shears, Web panel thicknesses, VBE and HBE sections for the six-story SPSW 41
Table 4-2 Force acting on the VBE [From (ICC/SEAOC, 2012)] 42
Table 4-3 Comparison of the values for column shear, moment and compression force from hand calculations and SAP 2000 model 44
Table 4-4 Comparison of plate thicknesses for a 6 story shear wall with and without moment connections 47
Table 4-5 Column shear, moment and compression force obtained from the SAP2000 model for the proposed design 48
Table 4-6 Comparison of Column Shear for a six story shear wall with and without moment connections 48
Table 4-7 Comparison of Column moment at the story level (not at mid-span) for a six story shear wall with and without moment connections 49
Table 4-8 Comparison of Column compression force for a six story shear wall with and without moment connections 49
Table 4-9 Comparison of Deflections for a six story shear wall with and without moment connections... 50
Table 4-10 Comparison of Inter-story drift (inches) for a six story shear wall with and without moment connections 50
Table 4-11 Comparison of VBE section for the high seismic design and proposed design approach..... 51
Table 4-12 Comparison of HBE sections obtained from the high seismic design and proposed design approaches..... 51
Table 4-13 Comparison of steel weight for high seismic design and proposed design approach..... 51
Table 4-14 Comparison of the total weight of steel in the high seismic design approach and proposed design method without moment connections including an over strength factor 55
Table 4-15 Applied moments for the six stories of the example SPSW building..... 60
Table 4-16 Interaction equation check for the columns at each story level of the six story building..... 61
Table 4-17 Deflections and drifts at each story level for the six story building 61
Table 4-18 Comparison of VBE sizes for the high seismic design and proposed plastic design approach 62
Table 4-19 Comparison of the HBE sizes for high seismic design and proposed plastic design approach 62
Table 4-20 Comparison of plate sizes for high seismic design and proposed plastic design approach..... 62

Table 4-21 Amount of steel used in the shear wall for the high seismic design and proposed plastic design approach 63
Table 5-1 Comparison of New Approaches and Conventional SPSW Design 81
Table 6-1 Values of Pressure load applied to the plate to simulate the Out of plane deformations 83
Table 6-2 Values of yield strength of the plate for varying values of pressure load applied 84
Table 6-3 Values of input parameters for comparison of a course and a finer mesh size in Abaqus models 86
Table 6-4 Values of the output parameters for comparison of a course and finer mesh in Abaqus models 86
Table 6-5 Geometry and input parameters for the first set of 20 models for perimeter circular holes with varying size and diameter 89
Table 6-6 Geometry and input parameters for the set of 10 models for perimeter circular holes with varying thickness 90
Table 6-7 Geometry and input parameters of set of 10 models with butterfly shaped links for varying plate thickness 91
Table 6-8 Strength, stiffness and energy dissipation ratio of the set of 20 models for the perimeter circular holes with varying size and spacing 104
Table 6-9 Length of cutting and openness of the panel for the set of 20 models for the perimeter circular holes with varying size and spacing 107
Table 6-10 Strength, stiffness and energy dissipation ratio for the set of 10 models with perimeter circular holes configuration with varying thickness 110
Table 6-11 Length of cutting and openness of the panel for the set of 10 models for the perimeter circular holes with varying thickness 111
Table 6-12 Strength, stiffness and energy dissipation ratio for the set of 10 models with strong and weak perimeter butterfly shaped cutout configurations 114
Table 6-13 Length of cutting, openness of panel and maximum out of plane deformation for the set of 10 models with perimeter strong and weak butterfly shaped cutouts 115

List of Figures

Figure 2-1 Idealized tension-field action in a typical SPW – Strip Model Representation [From (Sabelli and Bruneau, 2007)]..... 7
Figure 2-2 Schematic representation of the Strip model of a SPSW (Thorburn et al. 1983)..... 9
Figure 2-3 (a) Experimental Test set-up (Berman and Bruneau, 2005), (b) Hysteresis behavior of the SPSW (Berman and Bruneau, 2005)..... 10
Figure 2-4 (a) Experimental Set-up for Specimen S – at MCEER Laboratory, University of Buffalo, Tests conducted by Vian and Bruneau, 2005, (b) Hysteresis curve for Specimen S 11
Figure 2-5 (a) SPSW Panel with a central circular hole, (b) Hinge assembly – Schematic of the test specimen (Roberts and Sabouri-Ghomi, 1992)..... 13
Figure 2-6 (a) Experimental Set - up for the specimen P – at MCEER Laboratory for the test conducted by Vian and Bruneau, 2005, (b) Hysteresis curve for quasi-static cyclic loading for Specimen P..... 14
Figure 2-7 (a) Schematic representation of SPSW with slits, (b) Experimental test set up, Hitaka and Mastui, (2006)..... 18
Figure 2-8 Typical butterfly shaped fuse with the terms in the plate strength equation explained diagrammatically..... 19
Figure 2-9 SPSW divided into parts to show the forces [From (ICC/SEAOC, 2012)]..... 23
Figure 2-10 Components of expected web strength applied to HBE and VBE [From (ICC/SEAOC, 2012)] 24
Figure 3-1 Test set-up at MCEER test facility for specimen S [From (Vian and Bruneau, 2005)]..... 28
Figure 3-2 Stress Strain curve for LYS steel for the web plate, [From (Vian and Bruneau, 2005)]..... 29
Figure 3-3 Reduced Beam Section detailing incorporated in the experiment and the FE model, [From (Vian and Bruneau, 2005)] 30
Figure 3-4 (a) Plot showing a comparison between the hysteresis curves obtained from experiment and FE analysis in ABAQUS 6.10. (b) Rendering of Von Mises Stress contour on the SPSW in ABAQUS 6.10 33
Figure 3-5 (a) Applied force Versus horizontal reactions from FE model in ABAQUS 6.10, (b) Applied Force Versus vertical reactions from FE model in ABAQUS 6.10 34
Figure 3-6 (a) Panel damage – buckling and yielding of the specimen S at 3% drift [From (Vian and Bruneau , 2005)], (b) Panel damage of the finite element model of Specimen S at the end of analysis at 3% drift 35

Figure 3-7 Experimental set up for specimen P at the MCEER Laboratory, [From (Vian and Bruneau, 2005)] 36
Figure 3-8 (a) Plot showing a comparison between the hysteresis curves obtained from experiment and FE analysis in ABAQUS 6.10. (b) Rendering of Von Mises Stress contour on the SPSW in ABAQUS 6.10 for specimen P 37
Figure 3-9 (a) Damage to panel at the end of testing for specimen P at 3% drift [From (Vian and Bruneau, 2005)], (b) Deformed panel at the end of the analysis at 3% drift from the finite element model 38
Figure 4-1 Building Elevation [From (ICC/SEAOC, 2012)] 40
Figure 4-2 Typical floor and roof framing plan [From (ICC/SEAOC, 2012)] 40
Figure 4-3 (a) Figure showing the columns at each story level and the applied lateral forces, (b) Column axial forces at each story level 42
Figure 4-4 (a) Column Shear and column moment at each story level, (b) Column compression at each story level [From (ICC/SEAOC, 2012)] 43
Figure 4-5 (a) Story shears applied at the floor levels, (b) Figure showing the applied axial forces on the VBE at each story in SAP2000, (b) Applied lateral forces at each story level. 46
Figure 4-6 Comparison of plate, HBE and VBE sizes in (a) high seismic design using the code specifications, (b) proposed design approach without moment connections 52
Figure 4-7 Incremental shears amplified by the over strength factor applied at the floor levels for the finite element model in SAP 2000 54
Figure 4-8 Flow chart explaining the design procedure for the proposed design methodology with over strength factor and without moment connections 54
Figure 4-9 Figure showing the comparison of plate, HBE and VBE sizes for (a) high seismic design using the code specifications, (b) proposed design approach without moment connections including an over-strength factor 55
Figure 4-10 Figure showing one story of the column with plastic hinge locations 56
Figure 4-11 Figure showing plastic hinging mechanism for the first story of the column 58
Figure 4-12 (a) Figure showing the plastic hinging mechanism in a column in the bottom three stories of a six story building, (b) plastic hinging mechanism in the top three stories of a six story building 59
Figure 5-1 Deformed shape, HBE and VBE sections and plate thickness for a SAP2000 model of a SPSW with web plate connected to HBE only 65
Figure 5-2 Deformed shape, HBE and VBE sections and plate thicknesses for a SAP2000 model of a SPSW with a thick fish plate surrounding a thin web plate 67

Figure 5-3 Deformed shape and HBE and VBE sections and plate thickness of a SPSW model in SAP2000 with thin fish plates around a thicker web plate 69
Figure 5-4 (a) Deformed Shape with Von Mises stress distribution of SPSW with circular holes along the diagonals of the web panel as rendered in ABAQUS 6.10, (b) Hysteresis behavior 71
Figure 5-5 (a) Deformed Shape with Von Mises stress distribution of SPSW with circular holes of decreasing diameter along the diagonals of the web panel as rendered in ABAQUS 6.10, (b) Hysteresis behavior 72
Figure 5-6 Figure showing the typical layout of circular perforations along the perimeter 73
Figure 5-7 (a) Deformed Shape with Von Mises Stress Distribution – Circular holes Along the perimeter, (b) Hysteresis behaviour - cyclic loading 74
Figure 5-8 Figure showing the forces applied by the plate on the boundary elements on a SPSW with circular perforations along the perimeter of the web panel 74
Figure 5-9 Typical layout of Butterfly shaped cutouts along the perimeter of the web panel 76
Figure 5-10 (a) Deformed Shape with Von Mises Stress Distribution – Butterfly shaped cut outs along the perimeter of the web panel, (b) Figure showing the fine mesh in the links and coarse mesh in the plate and the BE 76
Figure 5-11 Figure showing the forces exerted by each link on the boundary elements in a SPSW with butterfly shaped cutouts 77
Figure 5-12 (a) Force Vs Displacement plot for monotonic loading for a SPSW with butterfly shaped cutouts, (b) Hysteresis behavior 77
Figure 5-13 (a) FE model of SPSW with a solid panel with moment connections in Abaqus 6.10, (b) Force-Displacement curve for monotonic loading 80
Figure 5-14 (a) FE model of SPSW with a solid panel with moment connections in Abaqus 6.10, (b) Force-Displacement curve for monotonic loading 80
Figure 6-1 Force Vs Displacement plot for different values of out of plane pressure loads on the plate ... 84
Figure 6-2 (a) FE model of SPSW with coarser mesh (2.5-8), (b) FE model of SPSW with finer mesh (1.75-6) 85
Figure 6-3 Force Vs Displacement plot for a coarser and a finer mesh 86
Figure 6-4 Typical layout of the weak and strong configurations of the butterfly shaped cutout 91
Figure 6-5 (a) Layout of circular perforations with the coarse mesh, (b) Hysteresis curve for the cyclic displacement history applied 96
Figure 6-6 (a) Layout of circular perforations with the coarse mesh, (b) Hysteresis curve for the cyclic displacement history applied 97

Figure 6-7 (a) Layout of butterfly shaped cutouts B3 with the coarse mesh for strong configuration, (b) Hysteresis curve for the cyclic displacement history applied 97
Figure 6-8 (a) Layout of butterfly shaped cutouts B3 with the coarse mesh for weak configuration, (b) Hysteresis curve for the cyclic displacement history applied 98
Figure 6-9 (a) Layout of circular perforations for a plate thickness of 0.1875 inches, (b) Hysteresis curve for the cyclic displacement history applied 98
Figure 6-10 (a) Layout of circular perforations for a plate thickness of 0.75 inches, (b) Hysteresis curve for the cyclic displacement history applied 99
Figure 6-11 (a) Undeformed shape of a 0.375 inch thick plate with D/S = 0.6 and 9 inch diameter holes, (b) Stress contour – S12 from Abaqus 6.10 99
Figure 6-12 (a) Stress Contour – S11 from Abaqus 6.10, (b) Stress Contour – S22 from Abaqus 6.10 .. 100
Figure 6-13 Plot showing the variation of shear strength of the panel with D/S ratio for varying hole diameter 101
Figure 6-14 Plot showing the variation of stiffness of the panel with D/S ratio for varying hole diameters 102
Figure 6-15 Plot showing the variation of energy dissipation ratio of the web panel with D/S ratio for varying hole diameters 103
Figure 6-16 Plot showing the variation of length of cutting in the wall with D/S ratio for varying hole diameters 105
Figure 6-17 Variation of the openness of the web panel with D/S ratio for varying hole diameters 106
Figure 6-18 Variation of shear strength of the web panel with thickness of the plate for varying hole diameters 108
Figure 6-19 Variation of stiffness of the web panel with thickness of the plate for varying hole diameters 109
Figure 6-20 Variation of the energy dissipation capacity of the web panel with thickness of the panel for varying hole diameters 109
Figure 6-21 Variation of maximum out of plane deformation in the plate with the thickness of the plate for varying hole diameter 111
Figure 6-22 Plot showing the variation of shear strength of the web panel with thickness of the panel for strong and weak configurations 112
Figure 6-23 Plot showing the variation of the stiffness of the panel with thickness of the panel for strong and weak configurations 113

Figure 6-24 Plot showing the variation of energy dissipation capacity of the panel with the thickness of the panel for strong and weak configurations 113
Figure 6-25 Variation of the maximum out of plane deformation with the thickness of the plate for strong and weak configurations of cutouts 115

Chapter 1. INTRODUCTION

1.1 Steel Plate Shear Walls – An Overview:

Steel plate shear walls (SPSW) have been used in the construction industry for several decades starting from the 1970's. The use of these systems has increased significantly in the recent years due to research demonstrating SPSW behavior and inclusion in U.S. building codes. They are now being used not only in the high seismic areas, but also for wind and low seismic applications (Sabelli and Bruneau, 2007). SPSW are commonly used for structures with moderate wall lengths. SPSW are suitable not only for high rise buildings but also for mid-rise construction. As per the recent research in this field (Berman and Bruneau, 2003a), it is shown that SPSW may be used for the retrofit of existing structures as well as installation in new buildings.

A steel plate shear wall is a lateral load resisting element which is made up of three components, namely the web plate, the beams which are referred to as horizontal boundary elements (HBE) and the columns which are referred to as vertical boundary elements (VBE). The vertical steel web plates are typically connected to the surrounding beams and columns through small connection plates referred to as fish plates. SPSWs are installed in one or more bays along the full height of the structure to form a cantilever wall. SPSW subjected to cyclic inelastic deformations exhibit high initial stiffness (prior to plate buckling), are ductile and are capable of dissipating energy as the web plate yields. These characteristics make them suitable to resist and dissipate seismic loading.

There are two types of steel plate shear walls used in building construction: stiffened and unstiffened SPSWs. Early design procedures prevented buckling and were designed for shear yielding of the web plate in the post elastic range. But this resulted in relatively thick web plates or heavily stiffened plates. Stiffening increased the shear buckling strength of the web plate and also increased its post-buckled stiffness. Stiffening also substantially increased the amount of steel required and the cost of construction.

Research in the 1980's brought a change in the basic approach of designing SPSWs (Thorburn, Kulak and Montgomery, 1983). The current approach allows shear buckling of the web panels and development of post buckling diagonal tension which is the primary mode of lateral force resistance in a SPSW and thus requires no stiffening of the panels. Unstiffened SPSW became popular in the United States starting in 2000. The unstiffened SPSW is included as a basic seismic force resisting system in ASCE 7-10 and AISC 341-10 (ASCE 2010, AISC 2010). Vertical boundary elements are designed to remain essentially elastic for the fully yielded panel allowing the HBE to undergo plastic hinging. For high seismic design, SPSWs are designed to permit the web plates to reach their expected yield stress across the entire panel. Very high strength can be provided by unstiffened steel web plates of moderate thickness.

Steel plate shear walls offer advantages over other shear wall systems in terms of cost, performance, and ease of design. Compared to concrete shear walls (CSW), the reduced thickness of the web plate offers significant reduction in the self-weight of the system and foundations. The plan area devoted to SPSW is smaller than CSWs. Most importantly, however, steel plate shear walls can be erected in significantly less time than concrete shear walls. SPSW may be considered as an alternative to braced frames. They can provide equivalent strength and require the same or less plan area. The speed of construction of SPSW is comparable to that of braced frames as well. The strength and pre-buckling stiffness of the system encourages good performance under moderate lateral loads. The large ductility of steel web plates in SPSW promotes good performance under severe seismic loading. Because SPSWs can provide significant strength, shorter bays can be used. This results in greater flexibility for use of the space in a particular bay.

Though SPSW find a range of applications, there are limitations. SPSW designed using the current provisions in U.S. Building codes result in very conservative designs especially for the boundary elements and the web plate thicknesses obtained are also very small. The current design procedures also require moment connections between beam and columns. Because the beams and columns are resisting the inward pull of the web plate, have moment connections between them and are capacity designed, they become excessively large. Very thin plates designed to resist the entire story shear possess negligible compressive strengths and hence

buckle at small values of loads. The load-deformation behavior exhibits low stiffness associated with early buckling and pinched hysteresis with limited energy dissipation. The constructability issues and reduced energy dissipation associated with thin plates of small gauge sizes make it difficult for implementation in the construction site. Thus the resulting SPSW system has thin web plates and boundary elements that are significantly larger than comparable braced frames and load-deformation performance that is not ideal. It can be concluded that the current SPSW design methodology results in inefficient and expensive seismic force resisting systems.

1.2 Motivation and Approach

The motivation for this work is to develop more efficient, cost effective, and better performing SPSW systems. First, concepts for increasing the economy and efficiency of SPSW systems for moderate seismic zones were investigated. Approaches included removing moment connections, allowing some yielding in columns, and increasing web plate thickness. It was found that stiffness controlled the designs so the approaches were ineffective at reducing the amount of required steel and thus this was not an appealing solution. Based on these results, it was determined that to make SPSWs more efficient, it would be necessary to create a tunable SPSW system in which stiffness and strength could be decoupled. Seven SPSW systems that allow tunability will be investigated. Different configurations of perforations in the web plate will be modeled and preliminary analyses will be performed in a finite element environment. The modeling techniques were validated against the available literature. Based on the results of the preliminary analyses, the two configurations that show the most promise (plates with circular holes cut around the perimeter of the plate, and plates with butterfly shaped links around the perimeter) will be chosen. The concept behind these configurations is that the solid plate in the middle of the panel contributes significant pre-yield stiffness to the system while the geometry of the perimeter perforations controls strength and ductility. An example panel will be designed using the two proposed configurations and compared to panels designed using current SPSW design methods.

A parametric study will be conducted using the chosen configurations. The effect of thickness of the plate, perforation diameter and spacing on the strength, stiffness and ductility of the system

will be studied. Conclusions are made about the performance of the prototype structures and applicability of the proposed design methodology. Scope for further study will be proposed.

1.3 Organization of the thesis

The thesis is organized into 7 chapters. Chapter 1 gives a brief overview of SPSWs and the objectives of the work. Chapter 2 gives a detailed background about SPSWs in the form of a literature review. Validation of finite element modeling in ABAQUS 6.10 and SAP 2000 is described in Chapters 3 and 4 respectively. Chapter 5 presents the various approaches that were attempted before arriving at configurations of perforations which resulted in a desired hysteretic behavior and satisfied the objectives listed in in previous section. The parametric study is described in Chapter 6. Chapter 7 gives the summary of the thesis with the conclusions and recommendations for future work which is followed by the references and the Appendices.

Chapter 2. LITERATURE REVIEW

2.1. System behavior, mechanics and Strip model representation of SPSWs:

Steel plate shear walls resist lateral loads primarily through diagonal tension in the web plate and overturning forces in the adjoining columns. Typical web plates are unstiffened and very slender, and their compressive strength is negligible. The development of tension field action and the transfer of these forces from the plate to the boundary elements constitute a significant part of the behavior of SPSWs. When lateral load applied to the plate generates compressive stresses that exceed the compressive strength of the plate, the plate buckles creating folds in the plate in a direction that is perpendicular to the tension diagonal. The lateral loads are then transferred to the boundary elements through the principal tension stresses in the plate. Thus the tension field action is the limit state for design of SPSWs similar to that for plate girders.

The behavior of a SPSW can be adequately predicted by inelastic finite element analysis by modeling the web panels using a large number of shell elements (Elgaaly et al., 1993). This has to be done to incorporate the geometric and material non-linearities which are inherently present in the real system (Driver et al., 1998b).

The behavior of a SPSW is similar to that of a plate girder. An analogy between the plate girder and the SPSW system has been suggested. The VBEs act like flanges of the plate girder and the HBEs act like stiffeners and steel web panels in the SPSWs act like the web of the plate girder. Unstiffened SPSWs which are designed to buckle in shear and develop a diagonal tension field are similar to vertical plate girders in a qualitative manner only. The difference in the two systems results from the stiffness of the boundary elements. Where plate girder flanges are typically plates with a small weak axis bending stiffness, the vertical boundary elements of a SPSW are typically wide flange sections which have a substantial in-plane bending stiffness. While the VBE resist the forces associated with the full yielding of the web plate, the flanges of the plate girders buckle and yield before the plate girder web yields. The angle of inclination of the diagonal tension field that develops in SPSW, (defined with respect to the vertical), depends on the stiffness of these boundary elements. On the other hand in plate girders, the stiffness of

the boundary elements is typically neglected in determining this angle because of their low in-plane stiffness (Basler, 1961). As a result, plate girder shear strength equations considerably underestimate the strength of SPSWs (Bruneau et al., 2005).

Therefore for seismic design in particular, it is recommended in the Canadian Steel codes (CAN/CSA S16-01) that the strip model be used to model SPSWs, to calculate the angle of inclination of the tension field and strips, and to calculate the ultimate strength of SPSWs (Sabelli and Bruneau, 2007). The strip model representation of a SPSW has been one of the popular and convenient methods of describing the system behavior. It has been observed that the strip model analysis of a SPSW is capable of capturing the behavior of SPSWs to an adequate degree of accuracy when the SPSW is modeled with at least 10 strips along the diagonal of the web panel (Thorburn, Kulak and Montgomery, 1983). Figure 2-1 shows the strip model representation of a SPSW. Timler and Kulak (Timler and Kulak, 1983) derived the equation for the inclination angle of the tension field as the angle between the direction of the strip and the vertical direction as given below:

$$\alpha = arctan\left(\frac{1+\frac{tL}{2A_c}}{1+th\left(\frac{1}{A_b}+\frac{h^3}{360I_{c\,L}}\right)}\right)^{1/4} \ldots\ldots\ldots\ldots\ldots\ldots\ldots\ldots\ldots\ldots\ldots\ldots\ldots\ldots Eqn(1)$$

where t = thickness of the web plate

h = story height

L = bay width

I_c = moment of inertia of the vertical boundary element

A_c = cross sectional area of the vertical boundary element

A_b = cross sectional area of the horizontal boundary element

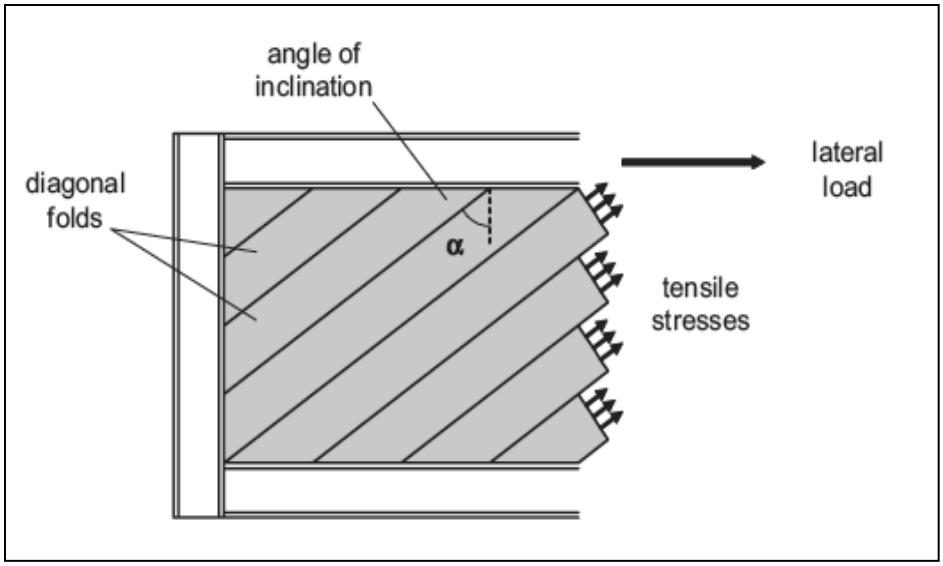

Figure 2-1 Idealized tension-field action in a typical SPW – Strip Model Representation [From (Sabelli and Bruneau, 2007)]

2.2. SPSW with solid panels

Analytical studies and various component and multi-story tests on SPSWs have been conducted by various researchers in the past. These tests have given a better insight into the understanding of the behavior of SPSWs. A selected few are presented here.

Experimental research (Tromposch and Kulak, 1987; Roberts and Sabouri-Ghomi, 1991; Caccese et al., 1993; Elgaaly and Liu, 1997; Driver et al., 1998a; Lubell et al., 2000) suggests that, when subjected to cyclic deformation levels well beyond the elastic limit, SPSW possess adequate hysteretic response characteristics. In the experiments conducted, single- and multistory SPSW models of various scale levels were subjected to quasi-static cyclic loads. In all cases, resulting experimental hysteresis loops were stable up to relatively large ductility ratios, and indicated that a significant amount of energy is dissipated through inelastic deformations. Experimental evidence, however, indicates that pinching effects are less pronounced in SPSW having moment-resisting beam-to-column connections than in those having simple connections. (Sabelli and Bruneau, 2007). The requirement of moment connections between the beams and columns, thin steel plates having highly pinched hysteretic response with little energy dissipation, little resistance to load reversal and small buckling resistance prove to be the

motivation to alleviate these concerns and thus the research was an attempt in this direction. Specific testing programs conducted in the past by various researchers are presented in the following sections.

2.2.1. Thorburn, Kulak and Montgomery (1983)

Thorburn et al. (1983) developed a simple analytical model which simulated the diagonal tension field action in a thin steel wall subjected to shear forces by inclined tension strips. This model was developed based on the work by Wagner (1931) who first presented the theory for thin webs subjected to shear utilizing the post-buckling strength. By assuming that the beams and columns in a SPSW remained rigid in bending and that the web panel would buckle under a diagonal compressive load, the following equation was derived for the inclination angle:

$$tan^4\alpha = \frac{1 + \frac{Lt}{2A_c}}{1 + \frac{Ht}{A_b}} \ldots\ldots\ldots\ldots\ldots\ldots\ldots\ldots\ldots\ldots\ldots\ldots\ldots\ldots\ldots\ldots\ldots\ldots\ldots\ldots\ldots\ldots\ldots\ldots\ldots\ldots Eqn\ (2)$$

where H = story framing height

L = frame bay width

t = panel thickness

A_b and A_c = cross sectional areas of the story beam and the column respectively

The investigation suggested that in order to adequately represent the web panel, at least ten tension strips would be required. Figure 2-2 shows the tension strip model with rigid beams. This is considered to be a valid assumption for an interior panel in a multi-story structure since the vertical component of the tension field from the adjacent stories would oppose each other and the net vertical beam deflection would be negligible.

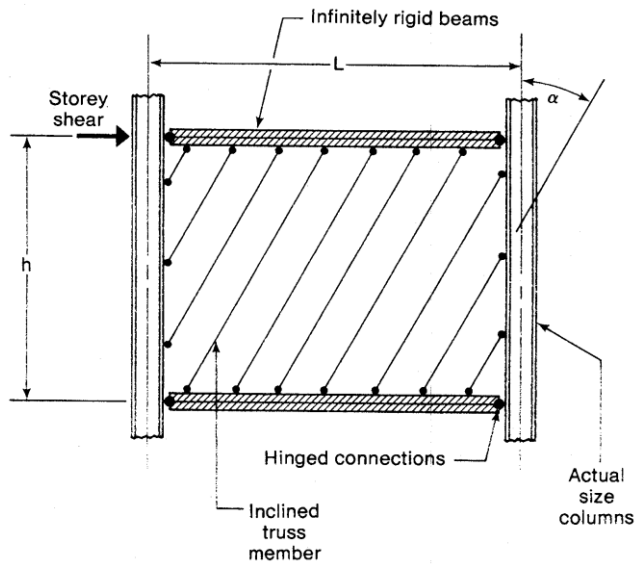

Figure 2-2 Schematic representation of the Strip model of a SPSW (Thorburn et al. 1983)

2.2.2. Xue and Lu (1994)

An analytical study on a three bay, 12-story structure was performed (Xue and Lu, 1994). The beam-column connections were moment resistant. The structure had SPSWs only along the height of the center bay. The effect of beam-to-column and plate connections was the focus of this study. Four cases were considered:

1. Moment-resisting beam-to-column connections and web plates fully connected to the surrounding frame.
2. Moment-resisting beam-to-column connections and the web plates attached to only the beams.
3. Simple beam-to-column connections and fully-connected web plates.
4. Simple beam-to-column connections with web plates connected only to the beams.

Plate thicknesses were the same for each configuration but varied along the height. It was found that the type of beam-to-column connection in a SPSW system had an insignificant effect on the global force-displacement behavior of the system. Connecting the web plates to the columns provided only a slight increase in the ultimate capacity of the system. It was also concluded that SPSW systems with the web plates connected to only the beams and using simple beam-to-

column connections was the optimal configuration because this drastically reduced the shear forces in the vertical boundary elements and helped avoid plastic hinging in the columns before plastic hinging in the beams. However, since a large number of tests were not conducted, this concept has not yet been implemented in the NEHRP Provisions or AISC 341-10.

2.2.3. Berman and Bruneau (2005)

The tests performed by Berman and Bruneau (2005) aimed at using light-gauge steel for the web plate in order to reduce the system weight and also provide adequate ductility. Figure 2-3(a) shows the experimental set-up for the tests conducted and Figure 2-3(b) shows the hysteresis for the light gauge steel web plate. A SPSW test specimen utilizing a light-gauge web plate with 0.0396 in. (1.0 mm) thickness was used. The specimen used W12×96 (W310×143) columns and W12×86 (W460×128) beams. This test was performed using quasi-static cyclic loading. The contribution to hysteretic behavior of the web plate was separated from that of the boundary frame to individually study them. This specimen reached a ductility ratio of 12 and drift of 3.7 percent, and the web plate was found to provide approximately 90 percent of the initial stiffness of the system. The failure limit state of the specimen was due to fractures in the web plate propagating from the corners.

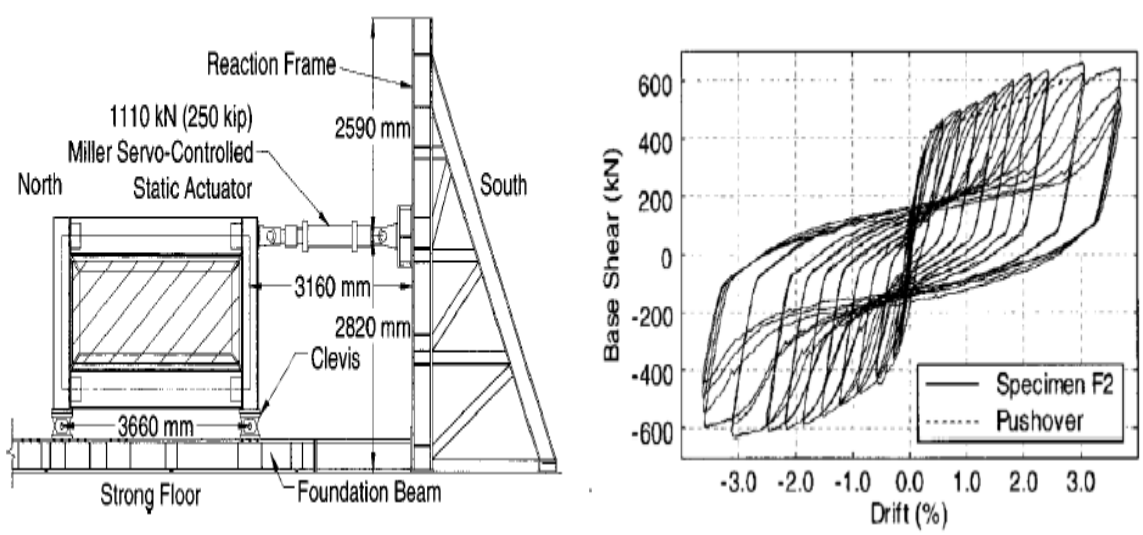

(a) (b)

Figure 2-3 (a) Experimental Test set-up (Berman and Bruneau, 2005), (b) Hysteresis behavior of the SPSW (Berman and Bruneau, 2005)

2.2.4. Vian and Bruneau (2005)

Vian (2005) conducted test on a single-story single-bay SPSW specimen at the MCEER Laboratory. The specimen was called Specimen S signifying a Solid panel. The loading was quasi static cyclic loading applied as a displacement history at the center of the top beam. Figure 2-4 (a) shows the experimental set up for Specimen S and Figure 2-4 (b) shows the experimental hysteresis curve for specimen S. The specimens had rigid beam to column connections, reduced beam sections in the beams and web plates made of LYS steel. The solid panel was the reference panel. The frame dimensions were 4000 mm x 2000 mm overall. W18x65 and W18x71 sections made of A572 Gr. 50 steel were used for the beams and columns respectively. The web plates were 2.6 mm thick. In all three specimens a 6 mm thick fish plate was provided along the perimeter of the web plate to facilitate the connection of the web plate to the surrounding beams and columns. Specimens S was loaded upto an inter-story drift of 3%. Finite element models of the three specimens were modeled in the FE package ABAQUS. Excellent agreement was observed between the experimental and analytical hysteretic results for the specimen S. There was good agreement in the prediction of the overall behavior of the specimens by the analytical models.

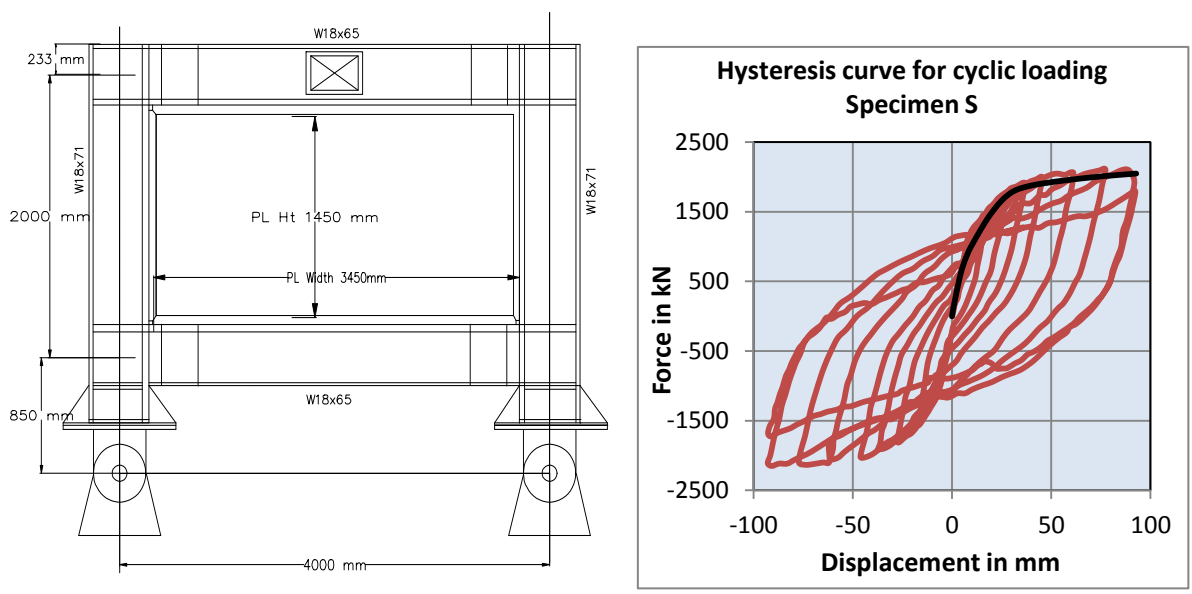

(a) (b)

Figure 2-4 (a) Experimental Set-up for Specimen S – at MCEER Laboratory, University of Buffalo, Tests conducted by Vian and Bruneau, 2005, (b) Hysteresis curve for Specimen S

2.3. SPSW with Perforations, Slits and Other Cut-outs

SPSW with Perforations were implemented by researchers starting in the 1990's. The behavior of SPSW with perforations was investigated in experimental programs including those undertaken at the MCEER Laboratory. Introduction of perforations in the web plate reduces the strength, allowing the use of thicker plates which increase the stiffness and energy dissipation capacity without increasing the sizes of the boundary elements. Also perforations would allow the utilities to pass through them without having to divert the utilities through a different path which would add to the construction costs. The following section describes some of the studies on perforated SPSW.

2.3.1. Roberts and Sabouri-Ghomi (1992)

Roberts and Sabouri-Ghomi (1992) conducted a series of 16 quasi-static cyclic loading tests on unstiffened steel plate shear panels with centrally placed circular openings. The test setup consisted of a plate clamped between pairs of stiff, pin-ended frame members. Figure 2-5(a) shows the web panel with a central circular perforation and Figure 2-5(b) shows the hinge and the panel assembly used in the test set up. Two diagonally opposite pinned corners were connected to the hydraulic grips of a 56.2 kip (250 kN) servo-hydraulic testing machine, which applied the loading. Specimen panel depth, *d*, was 11.8 in. (300 mm) for all specimens; panel width, *b*, was either 11.8 in. or 17.7 in. (300 mm or 450 mm); panel thickness, *h*, was either 0.033 in. or 0.048 in. (0.83 mm or 1.23 mm), with the panels having 0.2 percent offset yield stress values of 32 ksi (219 MPa) and 22 ksi (152MPa), respectively; and four values were selected for the diameter of the central circular opening, *D*= 0 in., 2.4 in., 4.1 in., and 6.0 in. (0 mm, 60 mm, 105 mm, and 150 mm). On the basis of experimental results, the researchers recommended an equation for the strength and stiffness of a perforated panel introducing a reduction factor with respect to that of a solid panel as follows:

$$\frac{V_{yp.perf}}{V_{yp}} = \frac{K_{perf}}{K_{panel}} = 1 - \frac{D}{d} \quad \ldots\ldots\ldots\ldots\ldots\ldots\ldots \; Eqn. (3)$$

where D = diameter of the circular hole

d = depth of the web plate

$V_{yp.perf}$ = yield strength of the perforated web plate

V_{yp} = yield strength of the solid web plate

K_{perf} = stiffness of the perforated web plate

K_{panel} = stiffness of the solid web plate

The researchers observed a reasonable agreement between the hysteresis curve of the theoretical and the experimental models.

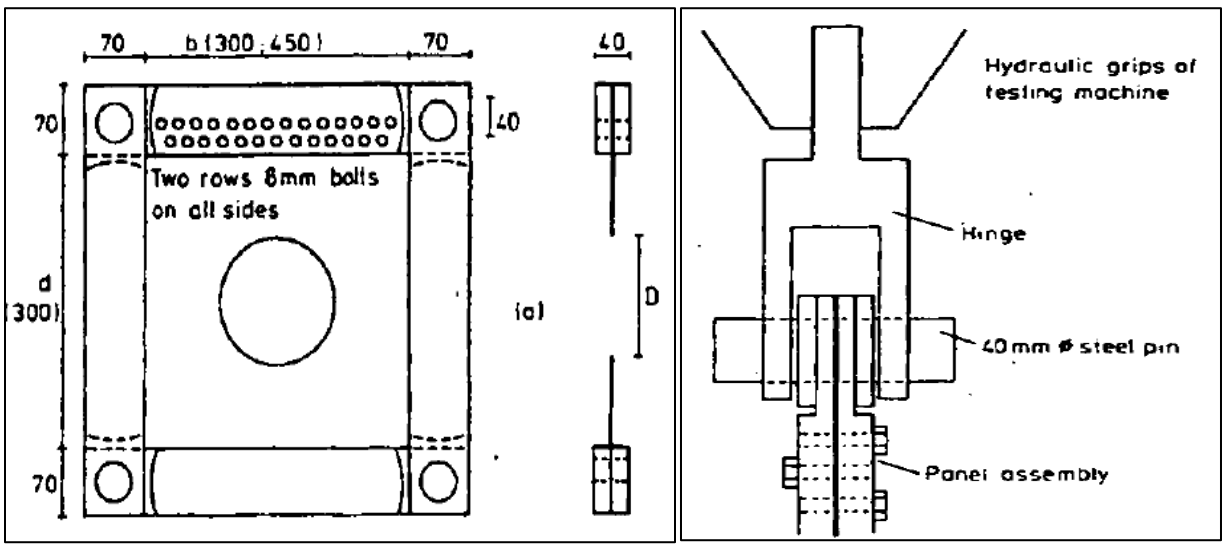

(a) (b)

Figure 2-5 (a) SPSW Panel with a central circular hole, (b) Hinge assembly – Schematic of the test specimen (Roberts and Sabouri-Ghomi, 1992)

2.3.2. Vian and Bruneau (2005)

Vian and Bruneau (2005) investigated the behavior of SPSW with a staggered arrangement of perforations and with a corner cut out with the aid of experiments and FE modeling. They tested two specimens which were designated as specimen P for the perforated panel and specimen CR for the specimen with quarter circle corner cut outs. The description of the loading protocol and the test set up are the same as those mentioned for the solid panel specimen in the previous

section. Figure 2-6 (a) shows the experimental set-up for specimen P and Figure 2-6(b) shows the hysteresis curve for specimen P. The specimen P had multiple regularly placed holes through-out the panel - 200 mm diameter holes were arranged in a staggered manner at a 45 degree angle and 300 mm center to center spacing in four strips wit 4 holes in each strip. The specimen CR had quarter circle cut outs at the four corners of the web plate, each of 500 mm radius. Flat plate reinforcement along the cut outs was provided. The specimen P was tested to a maximum interstory drift limit of 3% and the specimen CR upto 4%. It was found that the analytical models of specimens P and CR underestimated the experimental strength.

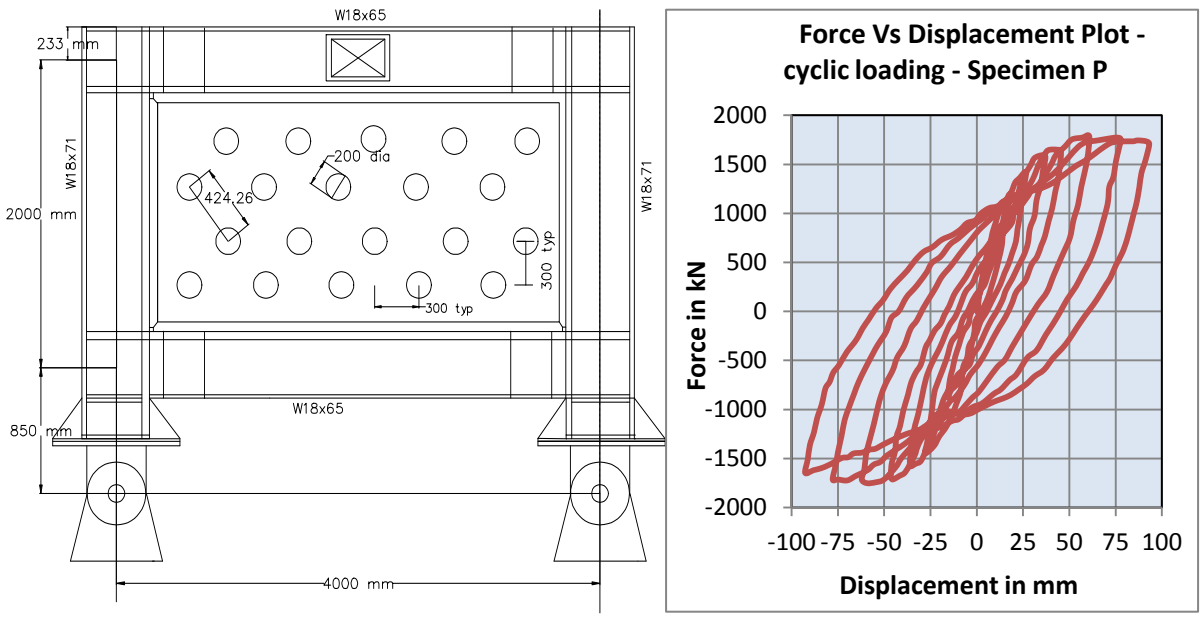

(a) (b)

Figure 2-6 (a) Experimental Set - up for the specimen P – at MCEER Laboratory for the test conducted by Vian and Bruneau, 2005, (b) Hysteresis curve for quasi-static cyclic loading for Specimen P

Vian and Bruneau (2005) developed equations for estimating the reduction in panel stiffness due to the presence of perforations. For a panel with multiple perforations, arranged in diagonal strips, such as the tested specimen, a stiffness reduction factor was derived assuming that the elastic behavior of a typical perforated strip can represent the strips in the entire panel, as a group of parallel axially loaded members. Five variables define the panel perforation layout geometry: the perforation diameter, D; the diagonal strip spacing, S_{diag}; the number of horizontal rows of

perforations, *Nr*; the panel height, H_{panel}; and the diagonal strip angle, θ. K_{perf} is the stiffness of the perforated web plate and K_{panel} is the stiffness of the solid web plate. Using these parameters, the total displacement of the perforated strip can be calculated, and the resulting stiffness is set equal to the stiffness of a tension member of uniform effective width. This effective width, divided by the gross width of the perforated strip, is the stiffness reduction factor proposed by them (Sabelli and Bruneau, 2007). This equation gives good results when the factor $\frac{D}{S_{diag}} \leq 0.50$.

$$\frac{K_{perf}}{K_{panel}} = \frac{1 - \left(\frac{\pi}{4}\frac{D}{S_{diag}}\right)}{1 - \left(\frac{\pi}{4}\frac{D}{S_{diag}}\right)\left(1 - \frac{N_r\, D\ \sin\theta}{H_{panel}}\right)} \ldots\ldots\ldots\ldots\ldots\ldots\ldots\ldots\ldots\ldots\ldots\ldots\ldots\ldots Eqn.(4)$$

Vian and Bruneau (2005) also proposed geometric constraints to ensure ductile performance of the perforated web plates. It was recommended that the ratio of perforation diameter to spacing, D/S_{diag}, be such that

$$\frac{D}{S_{diag}} \leq 1 - Y_t\left(\frac{F_y}{F_u}\right) \ldots\ldots\ldots\ldots\ldots\ldots\ldots\ldots\ldots\ldots\ldots\ldots\ldots\ldots\ldots\ldots\ldots\ldots\ldots\ldots\ldots\ldots\ldots\ldots Eqn.(5)$$

where F_y and F_u are the yield and tensile strength, respectively, of the web plate material, and it is recommended to use values of Y_t equal to 1.0 for $F_y / F_u \leq 0.8$, or 1.1 otherwise, as suggested by Dexter et al. (2002) and specified for design of tension flanges with holes by AISC (2005b). It was also recommended that the steel moment frames with perforated SPSW be designed for maximum inter-story drifts of 1.5 percent. For simplicity, it was suggested that the perforation layout angle, θ, be adopted as a constant 45° angle. Vian and Bruneau (2005) proposed the following equation for the calculation of the perforated panel strength as related to the strength of the solid panel with the terms in the equation explained before.

$$V_{yp.perf} = \left(1 - \frac{D}{S_{diag}}\right) V_{yp} \ldots\ldots\ldots\ldots\ldots\ldots\ldots\ldots\ldots\ldots\ldots\ldots\ldots\ldots\ldots\ldots\ldots\ldots\ldots\ldots\ldots\ldots Eqn.(6)$$

Vian and Bruneau (2005) concluded that loading assembly rotation, subsequent column twisting, distortion of the top beam and lateral support frames, RBS connection fractures account for the discrepancy between experimental and analytical results at large drifts as the FE model was not developed to account for such distortions and material failure.

2.3.3. Purba and Bruneau (2007)

Purba and Bruneau (2007) revisited the work done by Vian and Bruneau (2005). The analytical model of the perforated SPSW was used to develop many more FE models with varying diameter of the perforations in order to study the behavior by Vian and Bruneau (2005). The results from these models were compared to the simpler strip models for the same. It was found that the elongation predicted by the finite element models for a single strip and a full SPSW for a monitored maximum strain closed to the perforation edges was significantly different. This difference could not be explained then. Some jaggedness in the curves of total strip elongation versus perforation ratio calculated using the individual perforated strip model was also observed. For the cutout comer SPSW, the thick fish plate added to the "arching" flat-plate reinforcement along the cutout edges (to allow connection of the web plate to the boundary frame) was expected to modify the behavior of the SPSW from that predicted by the idealized model (Purba and Bruneau, 2007). Finite element models of individual perforated strips were developed. Mesh refinement techniques and various meshing algorithms were used to resolve the issues. With fine mesh sizes smooth curves of strip elongation versus perforation ratio were obtained. It is suggested that the $D/S_{diag} \leq 0.6$ for using strip models to represent a full SPSW model and obtain comparable results. Shear strength of a perforated panel can be calculated by reducing the strength of a solid panel by the factor $[1 - (\alpha\ D/S_{diag})]$ where α is the correction factor equal to 0.70. The full strength of the SPSW is obtained by adding the strength contribution from the bare frame to the panel strength obtained using the above formula.

2.3.4. Hitaka and Mastui (2006)

Hitaka and Mastui (2006) performed static monotonic and cyclic tests on various specimens in Japan. Cyclic loading tests were conducted on three story one bay composite frames braced by

Steel Plate Shear Wall with slits under constant axial load. The panels were connected to beams only as opposed to the conventional SPSW where the panels are connected to both the HBE and the VBE. Figure 2-7 (a) shows the schematic representation of the SPSW with slits and Figure 2-7(b) shows the experimental set-up used by the researchers. Test parameters were shape of the segments between vertical stiffeners and stiffening method to restrain out-of-plane deformation of the shear plates. All specimens underwent roof drift angle of more than 0.05 radians. without losing axial strength. Response of the shear wall was similar to the response observed in the tests on the walls not integrated with the frame.

In this system, the steel plate segments between the slits behave as a series of flexural links, which provide fairly ductile response without the need for heavy stiffening of the wall. The authors conducted static monotonic and cyclic lateral loading tests on forty-two wall plate specimens. The results showed that when properly detailed and fabricated to avoid premature failure due to tearing or out-of-plane buckling, the wall panels respond in a ductile manner, with a concentration of inelastic action at the top and bottom of the flexural links. For transverse stiffening, two methods utilizing steel edge stiffeners and un-bonded mortar panels were proposed (Hitaka, 2003). The test specimens were designed to simulate lower stories of a mid-rise building.

The observed experimental data and the subsequent FE analysis suggested that the contribution of the steel stiffeners to the stiffness in the initial stage is negligible for calculating the initial stiffness. The specimens displayed a stable hysteresis behavior for the cyclic loading applied and strength degradation owing to the transverse buckling was observed later. A few specimens experienced ductile fractures at the ends of the slits. It was observed that welded edge stiffener specimens displayed less strength degradation and more stable hysteresis behavior as compared to the unstiffened panel of similar slit configuration.

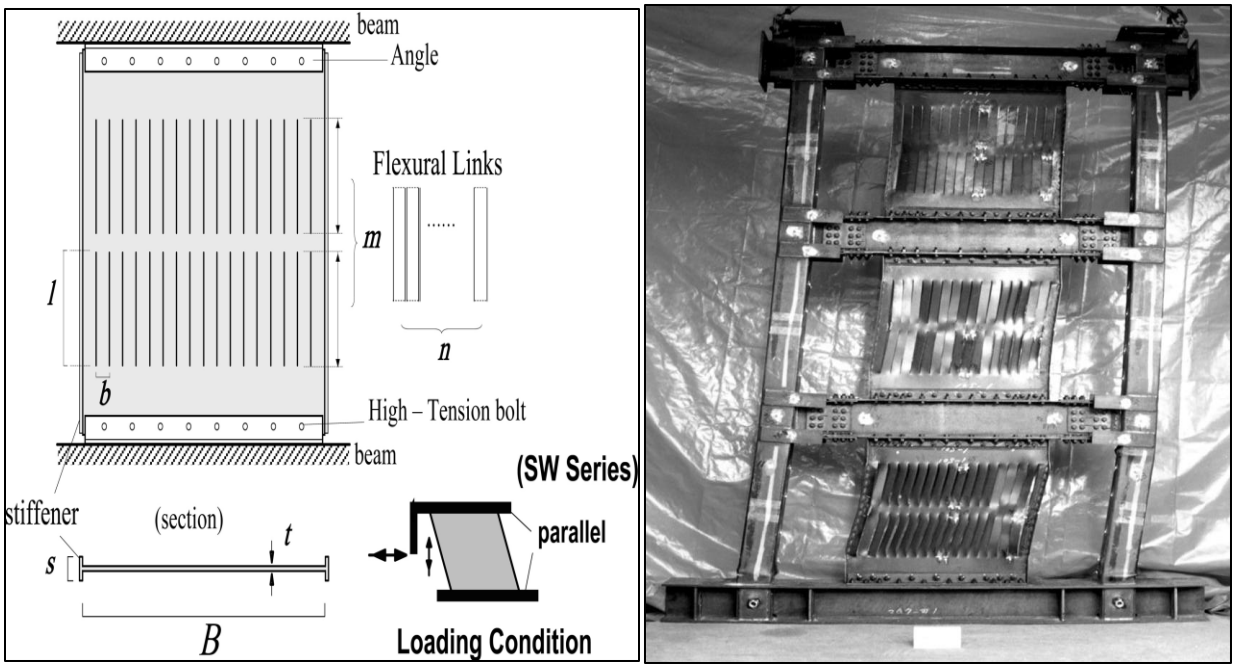

(a) (b)

Figure 2-7 (a) Schematic representation of SPSW with slits, (b) Experimental test set up, Hitaka and Mastui, (2006)

2.3.5. Borchers, Peña, Krawinkler, and Deierlein (2010)

Borchers, Peña, Krawinkler, and Deierlein (2010) at Stanford University conducted tests on specimens with butterfly shaped fuses. Figure 2-8 shows a typical butterfly shaped fuse. The test results showed that yielding was initiated at quarter height of the butterfly cut outs as opposed to initiation of yielding at the ends of the slits in the panels with slits introduced by Hitaka and Mastui (2006). At the end of the tests, buckling of the slits increased rapidly and became so severe that the links turned 90 degrees and became perpendicular to the loading direction. However, it was observed that butterfly fuse could sustain more deformation and was able to withstand higher load at large drifts. Two major reasons were suggested for this behavior. The first reason was that the uniform yielding along the edge of the link in the butterfly fuse reduced strain concentration at a particular point on the link and thus, delayed crack initiation. The second reason stated is that since the plastic hinge formation took place at quarter height sections in the butterfly link, the effective length of the link in tension was shorter as compared to the links in the slit fuse where the hinges are formed at the slit ends. Due to shorter length of the

tension portion, it could contribute more to the lateral strength. Panels with butterfly fuses displayed a very stable hysteresis behavior. It was also found that the butterfly fuses have better ductility as compared to the slits. The following equation was proposed to calculate the strength of the wall with butterfly fuses.

$$V_{fp} = \frac{4b^2t}{9L}\, n\, F_{yp} \ldots\ldots\ldots\ldots\ldots\ldots\ldots\ldots\ldots\ldots\ldots\ldots\ldots\ldots\ldots\ldots\ldots\ldots\ldots\ldots\ldots\ldots\ldots\ldots\ldots\ldots Eqn.(7)$$

where V_{fp} is the strength of the strength of the plate with a butterfly shaped fuse, $F_{yp,}$ the yield strength of the plate material, n is the number of links or fuses and the other terms in the above equation are explained in the Figure 2-8.

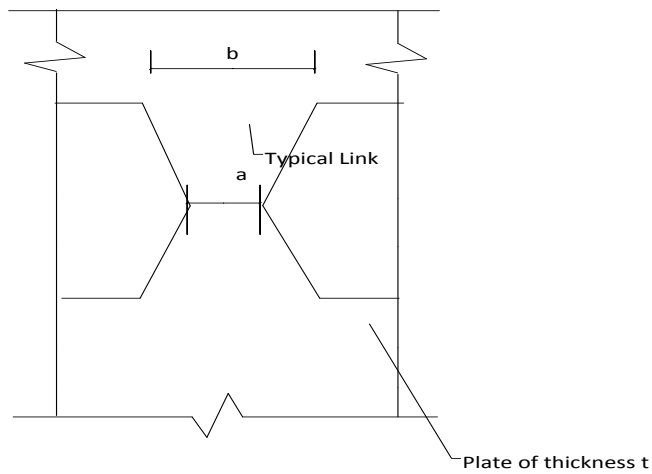

Figure 2-8 Typical butterfly shaped fuse with the terms in the plate strength equation explained diagrammatically

2.4. High Seismic Design of SPSW

The high seismic design of SPSW as specified in the current building codes is summarized in this section. It includes the design of the web plate and the boundary elements.

2.4.1. Requirements of the AISC Seismic Provisions – ANSI/AISC 341-10

Unstiffened steel plate shear walls are typically designed as Special Plate Shear Walls (SPSW). AISC 341 (AISC 2010) includes seismic design provisions for SPSWs for high ductility (Part I, Section 17); no seismic design provisions for the lower ductility systems exist.

Typical SPSW have slender webs that are capable of resisting large tension forces but little or no compression. This behavior is analogous to tension-only bracing, which relies on beams in compression to transmit the horizontal component of a brace force to the brace at the level below, and in which overturning forces are imposed on columns. Overturning forces are resisted by the columns and are delivered by the vertical component of the brace forces. Where braces only resist tension, the beams are typically subject to large compression forces. The tension in the SPSW web plate acts along the length of the boundary elements, rather than only at the intersection of beams and columns, as is the case for tension-only bracing. As such, large inward forces can be exerted on the boundary elements. HBEs and VBEs of SPSW are designed to provide sufficient stiffness to anchor the tension field, and resist the full tension strength of the web plate yielding along the tension field diagonal. (AISC 341-10)

2.4.2. Web Panel Design

The panel design shear strength ΦV_n (LFRD - load and resistance factor design) according to the limit state of shear yielding shall be determined as follows:

$$V_n = 0.42\, F_y t_w L_{cf} \sin 2\alpha \ldots\ldots\ldots\ldots\ldots\ldots\ldots\ldots\ldots\ldots\ldots\ldots\ldots\ldots\ldots\ldots\ldots\ldots\ldots\ldots\ldots\ldots Eqn.(8)$$

where V_n – nominal shear strength of the link

F_y – specified minimum yield stress of steel of the plate

t_w – thickness of the web plate

L_{cf} – clear distance between VBE flanges

α – angle of web yielding measured in radians given by the expression shown below

$$tan^4\alpha = \frac{1 + \left(\frac{t_w L}{2\,A_c}\right)}{1 + (t_w h)\left(\frac{1}{A_b} + \frac{h^3}{360\,I_c\,L}\right)} \ldots\ldots\ldots\ldots\ldots\ldots\ldots\ldots\ldots\ldots\ldots\ldots\ldots\ldots\ldots\ldots Eqn.(9)$$

where h - Distance between the HBE centerlines in mm

A_b – cross sectional area of a HBE in mm^2

A_c – cross sectional area of a VBE in mm^2

I_c – moment of inertia of a VBE taken perpendicular to the direction of the web plate line in mm^4

L – Distance between the VBE centerlines in mm

The code also specifies the values for variables used in design: Seismic response modification coefficient R = 7; Over strength factor $\Omega_o = 2$; Deflection amplification factor $C_d = 6$. For a dual system with special moment frames the modifications required are: R = 8, $\Omega_o = 3$, $C_d = 5.5$.

2.4.3. Horizontal Boundary Element (HBE) Design

For boundary-element design, AISC 341 Section 17.4a (AISC 2010) states that boundary members are to be designed for the forces corresponding to the expected yield strength, in tension, of the web calculated at an angle α. The definition of the expected yield strength at an angle α consists of multiplying F_y by R_y to get the expected yield stress given by equation 10.

$$F = F_y R_y t_w \ldots\ldots\ldots\ldots\ldots\ldots\ldots\ldots\ldots\ldots\ldots\ldots\ldots\ldots\ldots\ldots\ldots\ldots\ldots\ldots\ldots\ldots\ldots\ldots\ldots\ldots Eqn.(10)$$

For the design of the HBE, however, it is necessary to separate the force, F, into components. Figure 2-9 shows SPSW divided into different parts to show the forces on each part. The design example in ICC/SEAOC, 2012 (ICC/SEAOC, 2012)] presents a derivation of the resulting horizontal and vertical forces acting on the HBE and VBE:

$$F_{11} = \frac{Force}{Length} = \frac{R_y F_y t_w \Delta \cos\alpha}{\Delta / \cos\alpha} = R_y F_y t_w \cos^2\alpha \ldots\ldots\ldots\ldots\ldots\ldots\ldots\ldots\ldots\ldots\ldots\ldots Eqn.(11)$$

$$F_{12} = \frac{R_y F_y t_w \Delta \sin\alpha}{\Delta / \cos\alpha} = R_y F_y t_w \sin\alpha \cos\alpha = R_y F_y t_w \left[\frac{1}{2}\sin(2\alpha)\right] \text{.....} Eqn.(12)$$

$$F_{21} = \frac{R_y F_y t_w \Delta \cos\alpha}{\Delta / \sin\alpha} = R_y F_y t_w \sin\alpha \cos\alpha = R_y F_y t_w \left[\frac{1}{2}\sin(2\alpha)\right] \text{.....} Eqn.(13)$$

$$F_{22} = \frac{R_y F_y t_w \Delta \sin\alpha}{\Delta / \sin\alpha} = R_y F_y t_w \sin^2\alpha \text{.....} Eqn.(14)$$

The HBE is designed for the vertical force, F_{11} and the shear force F_{12}. The components of the expected web strength applied to the HBE are shown in Figure 2-10. Additional notes on the design of HBE include:

- The roof HBE resists the force of the tension field on one side only. In some cases this will result in a heavier top HBE than in floors below.
- At intermediate floors, if the plate is the same thickness above and below, the HBE does not resist vertical forces other than gravity loads. When the plates are of different thickness above and below, the HBE is designed for the forces associated with the difference.
- The HBE is not required to be designed for end moments, unless using a dual system where the moment frame is to be designed to resist 25% of the load.
- The HBE must satisfy the lateral bracing requirements and the width-thickness ratios as per section 17.4c of AISC 341-10 in order to ensure that the plastic hinges to occur and so that the full mechanism takes place (AISC 2010).

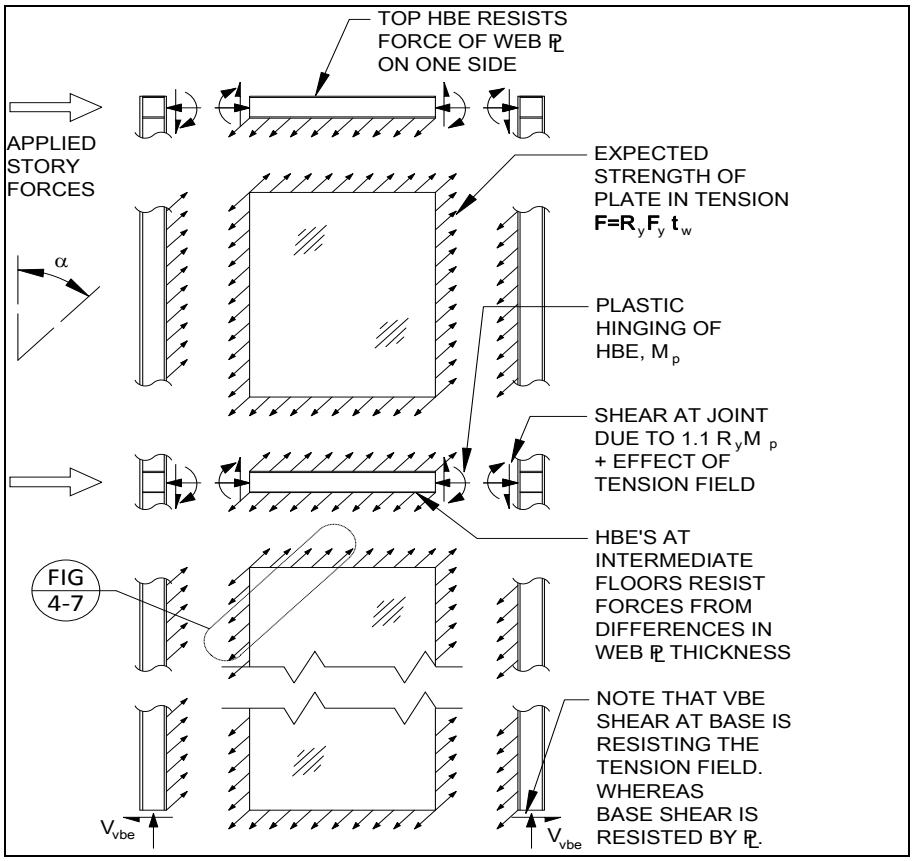

Figure 2-9 SPSW divided into parts to show the forces [From (ICC/SEAOC, 2012)]

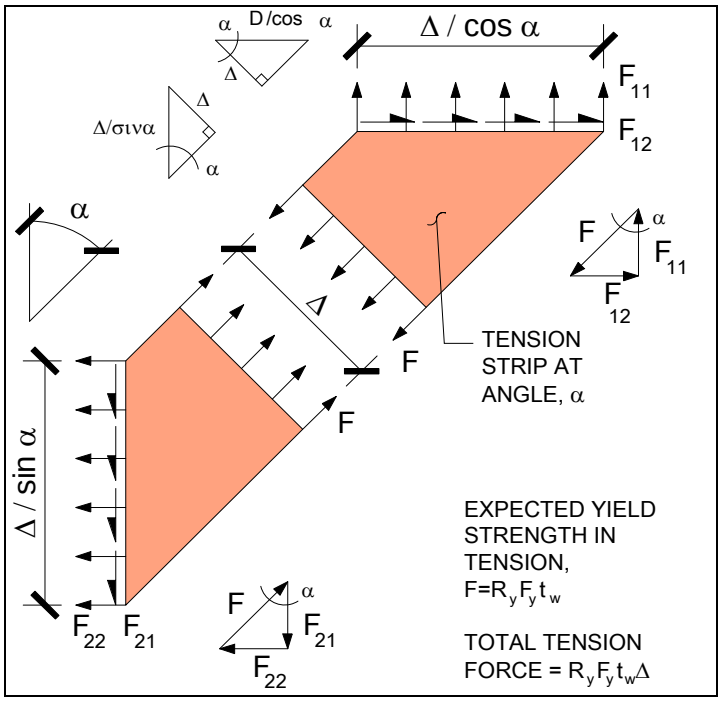

Figure 2-10 Components of expected web strength applied to HBE and VBE [From (ICC/SEAOC, 2012)]

2.4.4. Vertical Boundary Element (VBE) Design

Section 17 of AISC 341 (AISC 2010) has several requirements for the VBE. Similar to HBE's, the VBE should be designed to resist the forces associated with the expected yield strength of the plate ($F_yR_yt_w$) acting at an angle α. Figure 2-10 shows the components of the expected web strength applied to the VBE. For VBE design, the moment and compression forces are separated and examined individually and then interaction is considered in accordance with Chapter H of AISC 360 (AISC 2010). The design checks for the VBE include the following:

1. Combined axial and flexure considering - Moment due to expected yield strength of the web plate acting at the angle α in addition to plastic hinging of the HBE and Compression / tension due to overturning loads
2. Width-Thickness ratio limits
3. Minimum moment of inertia requirement
4. Strong-column / weak beam check

Design is iterative and hence the boundary elements are designed and checked to satisfy deflection limits. The connections are designed after the final sizes of the members are obtained.

2.4.5. Implications of Current High Seismic Design Approach

The purpose of the research by Berman (Berman, 2011) was to investigate the seismic performance of SPSW having various configurations when designed as per the provisions in the AISC 341-10 (AISC 2010). The study was conducted by examining the performance of SPSW extending 3,9,14 and 20 stories subjected to non-linear response history analysis. The following quantities were investigated: seismic drifts in code designed SPSW and comparison with the displacement amplification factor, web plate ductility demand, distribution of load between the web plate and the boundary frame, VBE demands and relative design loads and the influence of SPSW aspect ratio and period on the above factors. The HBE were designed to resist the forces from tension field yielding of the web plates and the VBE were designed for the tension field yielding of the web plates and flexural yielding of the HBE. Capacity design procedure was adopted for the design of HBE and VBE as per the AISC provisions. When compared to the results from non-linear response history analysis, it was found that the capacity design approach for the HBE and VBE result in very conservative designs for taller SPSW because of the assumption of simultaneous yielding of all the web plates and HBE which is very unlikely in reality. Very large VBE sections were required in the bottom most stories and in some cases built up structural sections had to be adopted since the biggest sections available were also insufficient as per the design. For the 3 story prototype buildings the first floor column sizes ranged from W14x370 to W14x605 and the web plate thicknesses ranged from 1.59 mm (0.063 in) for the first floor to 4.76 mm (0.19 in) for the third floor. Similarly in the 9 story prototype building, the first floor columns were W14x730 sections and the web plate thicknesses ranged from 1.59 mm (0.063 in) to 6.35 mm (0.25 in).

This shows that the procedure adopted in the current code provisions for the design of VBE can be highly conservative. The current design methodology results in very thin web plates that buckle at very small loads, displaying a pinched load – deformation behavior, low stiffness and low energy dissipation. The design method results in very large boundary element sizes.

Therefore it could be concluded that the current design methodology produces inefficient seismic lateral force resisting systems which are also uneconomical.

Chapter 3. VALIDATION OF FINITE ELEMENT MODELING IN ABAQUS 6.10

In order to develop modeling techniques for SPSW in a finite element environment models were created and compared to experimental results available in the literature. Shell element models were created using ABAQUS 6.10 (Simulia 2010). The developed FE models were validated against the experiments conducted on a SPSW at the Multi-Disciplinary Center for Earthquake Engineering Research (MCEER) facility at The University of Buffalo, New York as described in the Technical Report MCEER-05-0010, (Vian and Bruneau, 2005). A brief summary of the testing and the results is described here. Further details of the experiment are included in Vian and Bruneau (2005).

3.1 SPSW with a solid panel

This section describes the validation of a SPSW with a solid panel. A brief description of the experimental set-up in included. The step-by-step procedure of the modeling technique used in Abaqus 6.10 in described in the next section.

3.1.1 Experimental Set-up

The experimental set up was a half scale single story single bay SPSW frame. Figure 3-1 shows the experimental set up at the MCEER Laboratory (Vian and Bruneau, 2005). Three specimens were tested. They were designated as specimen S for the specimen with a solid panel, specimen P for the specimen with a perforated panel and specimen CR for the specimen with corner cut outs. The test specimens utilized web plates made of Low Yield Strength steel and reduced beam sections at the beam ends. All specimens were tested using quasi-static displacement controlled loading with increasing cyclic displacement history applied to the top beam of the specimen. The specimens were loaded to reach a maximum inter-story drift of 3 percent.

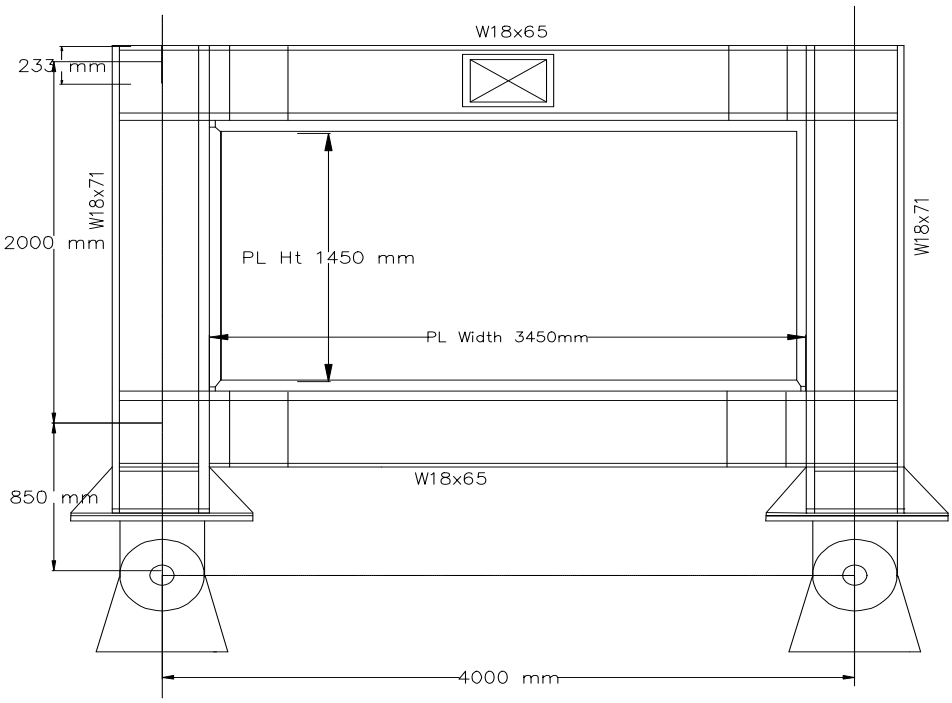

Figure 3-1 Test set-up at MCEER test facility for specimen S [From (Vian and Bruneau, 2005)]

3.1.2 Details of FE Modeling in ABAQUS 6.10

In this section, details of the finite element modeling process in ABAQUS 6.10 are described. Modeling of the boundary conditions and application of load to closely simulate the experimental conditions was attempted.

3.1.2.1 Definition of the Geometry

Local buckling and plastic hinging in the boundary frames observed during the experiment could be understood by modeling each frame member in ABAQUS 6.10 as built up sections of plate elements. Thus instead of using beam or frame elements which are one-dimensional idealizations of a structural member whose range of behavior may be limited by the underlying assumptions, generalized shell elements were used to model the flanges, webs and panel zones of the boundary elements and also the web plate of the SPSW.

The final model may consist of a single part where the entire model is sketched as one unit in the part module or it may consist of an assembly of multiple parts which are connected using

connector elements or constraints. Here the entire SPSW was modeled as a single part without any connector elements to connect the boundary elements to the web plate (shell extrude and shell planar features were used to achieve this geometry). This was done to provide a uniform mesh and to ensure that there are common nodes at the interface of the boundary elements and the web plate. This also guarantees the compatibility of deformations between different parts which constitute the structure.

Fish plates which were used in the actual experiment to connect the web plate to the boundary elements were not included in the ABAQUS model of the SPSW for simplicity. Instead a direct connection was assumed to take place between the elements. This approximation has been found by others to have negligible effects on the results (Driver et al, 1997).

3.1.2.2 Definition of Material Properties

The web plate was made of low yield strength steel. The panel thickness was 2.6mm (0.1024 inches) with yield and ultimate stresses of 165 MPa and 305 MPa respectively.

Calculations were made to determine the yield strength and the corresponding strain and also the stress in the strain hardening region of the curve and the corresponding plastic strain associated with the stress value from the graph shown below in the Figure 3-2.

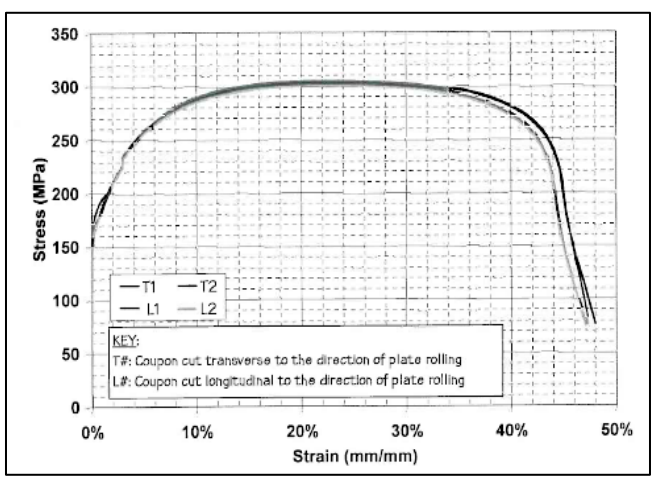

Figure 3-2 Stress Strain curve for LYS steel for the web plate, [From (Vian and Bruneau, 2005)]

The following equations were used:

$$\varepsilon_{true} = \ln(1 + \varepsilon_{eng}) \ldots\ldots\ldots\ldots\ldots\ldots\ldots\ldots\ldots\ldots\ldots\ldots\ldots\ldots\ldots\ldots\ldots\ldots\ldots\ldots\ldots\ldots\ldots\ldots Eqn.(15)$$

$$\sigma_{true} = \sigma_{eng}(e^{\varepsilon_{true}}) \ldots\ldots\ldots\ldots\ldots\ldots\ldots\ldots\ldots\ldots\ldots\ldots\ldots\ldots\ldots\ldots\ldots\ldots\ldots\ldots\ldots\ldots\ldots\ldots Eqn.(16)$$

$$\varepsilon_{plastic\ true} = \ln(1 + \varepsilon_{eng}) - \frac{\sigma_{ytrue}}{E} \ldots\ldots\ldots\ldots\ldots\ldots\ldots\ldots\ldots\ldots\ldots\ldots\ldots\ldots\ldots Eqn.(17)$$

where σ_{true} is the true stress, ε_{eng} is the engineering strain, $\varepsilon_{plastic\ true}$ is the true plastic strain at the chosen second point on the stress strain curve to define the material properties, σ_{ytrue} is the true yield stress; σ_2 and ε_2 are the stress and strain at a second point on the σ-ε curve respectively. The values of stresses and strains used for low yield strength steel for the web plate in the Abaqus 6.10 material model are as follows: σ_{ytrue} = 24 ksi, ε_{eng} = 0.0008 in/in, σ_2 = 44 ksi and ε_2 = 0.1 in/in. E is the modulus of elasticity of steel (E = 29000 ksi) and Poisson's ratio ν = 0.3. Isotropic hardening rule was used for the constitutive model for steel for the web panel and the boundary elements. Yield strength of 50 ksi (345 MPa) was used for boundary elements and 24 ksi (165 MPa) for the web plate.

Reduced Beam Sections (RBS) were implemented in the HBE so that plastic hinging occurs away from the beam to column connection. The detailing of the RBS is shown in Figure 3-3. The same geometry was incorporated in the FE model.

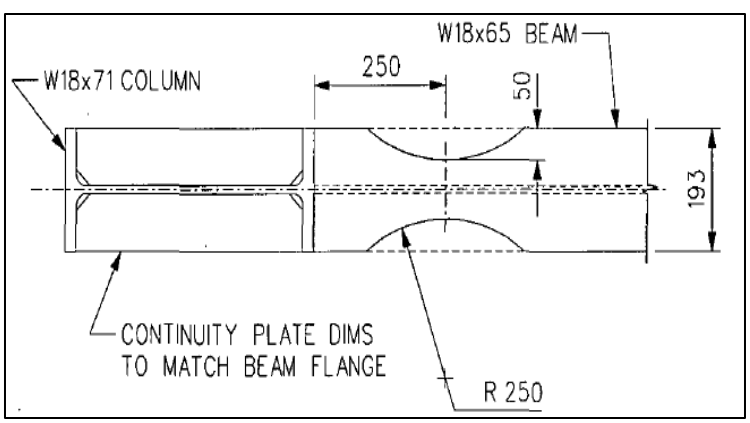

Figure 3-3 Reduced Beam Section detailing incorporated in the experiment and the FE model, [From (Vian and Bruneau, 2005)]

3.1.2.3 Analysis Parameters

Nonlinear geometric effects associated with large deformations were considered in the analysis. Automatic stabilization is used in the model where an appropriate damping factor is used during analysis. The solution technique was Full Newton. Direct method was used for the equation solver.

The experiment was displacement controlled and hence the load was applied as a displacement history. This was implemented in ABAQUS as a boundary condition. The displacement in the global X direction was set to unity and was amplified to the actual displacements by defining a table of values of increasing displacements versus the step times. The displacement history was applied to the top flange region of the top beam. Also a small magnitude of out of plane load was applied at the center of the web plate to account for the initial imperfections in manufacturing of the plate.

The boundary condition at the base of each column in the SPSW is a hinge which was not modeled explicitly in ABAQUS. Instead a connector element–CONN3D2 was defined to connect a reference node at the location of the hinge center with the nodes at the tip of each flange and the intersection of the flange and the web. This connector element allowed all six degrees of freedom to be constrained as per the requirements of the problem. BEAM connector property definition was used to model CONN3D2. This provided a rigid beam connection between the two nodes involved. The node at the hinge center and each of the other nodes were connected using rigid beam connectors and CONN3D2 was assigned to them. All the degrees of freedom were fixed at the reference node except rotation about the out-of-plane axis to replicate the hinge rotation observed during testing. The out-of-plane resistance provided by the lateral supports at the top of the column during the experiment was modeled by fixing the displacement in that direction. This was done by restraining the out-of-plane displacement of the exterior nodes of the flange elements around the perimeter of the panel zones.

3.1.2.4 Finite Element Mesh

The mesh was generated by seeding the edges depending upon the fineness of the mesh required. Since the entire SPSW was a single unit, the mesh of the part was the mesh of the assembly. Mesh controls were assigned to the boundary elements and the web plate separately. The web plate was meshed using free meshing technique and the webs and flanges of the boundary elements were meshed using structured meshing technique. Quadrilateral elements were used for the mesh. All elements are located at the mid thickness of the physical element they represent. Specifically the medial axis theorem was used for the structured meshing. This theorem initially subdivides the region to be meshed into a number of small regions and then it does structured meshing in those small regions and fills the regions with more elements (Simulia 2010).

S4R elements were used for the web plate and boundary elements. An S4R element is a 4 noded quadrilateral doubly curved shell element. Each node has 6 degrees of freedom – 3 translational and 3 rotational degrees of freedom. Transverse shear deformations are allowed by thick shell theory as the thickness of the plate increases and they become thin shell Kirchhoff elements and allow for the reduction in transverse shear deformations when the thickness reduces (Simulia, 2010). The S4R element allows for finite member strains, large rotations and change in thickness. It uses a reduced integration scheme with just one integration point at the center of the element as opposed to 3 points for higher order elements. This significantly reduces the computation time and gives accurate results for elements that are not distorted. However under certain loading conditions, a phenomenon called hour glassing may occur. Mesh refinement and distributing the concentrated loads over multiple nodes are ways to reduce the hour glassing effect. The artificial stiffness which is added automatically by ABAQUS in the shell stiffness formulation is also instrumental in reducing this effect.

3.1.3 Comparison of Experimental and FE Model Results

This section shows the comparison between the hysteresis curves obtained from the experiment conducted by Vian and Bruneau (2005) at the MCEER laboratory and the finite element model developed for the experiment in ABAQUS 6.10. The comparison between force versus

displacement plots for the solid plate experiment (Specimen S) and the finite element analysis is shown in the Figure 3-4(a). The maximum force in the experiment was 2100 kN and in the finite element model it was 2250 kN. There was good agreement in the values of the loading and the unloading stiffnesses from both models. The stiffness of the experimental SPSW obtained from the force versus displacement curve for monotonic loading for Specimen S is 800 kips/in and that from the finite element model is 703 kips/in. Although there were slight differences in the reloading behavior, the overall ability of the finite element model to capture the load-deformation behavior of the solid SPSW is good. The Von Mises stresses on the SPSW as rendered by ABAQUS are shown in the Figure 3-4(b). It is to be noted here that the colors representing the Von Mises stresses might be misleading as to whether the web plate is yielding. This is because the yield strength of the boundary elements is larger than the web plate. Therefore the web plate may be yielding even though it is shown as green in the figure.

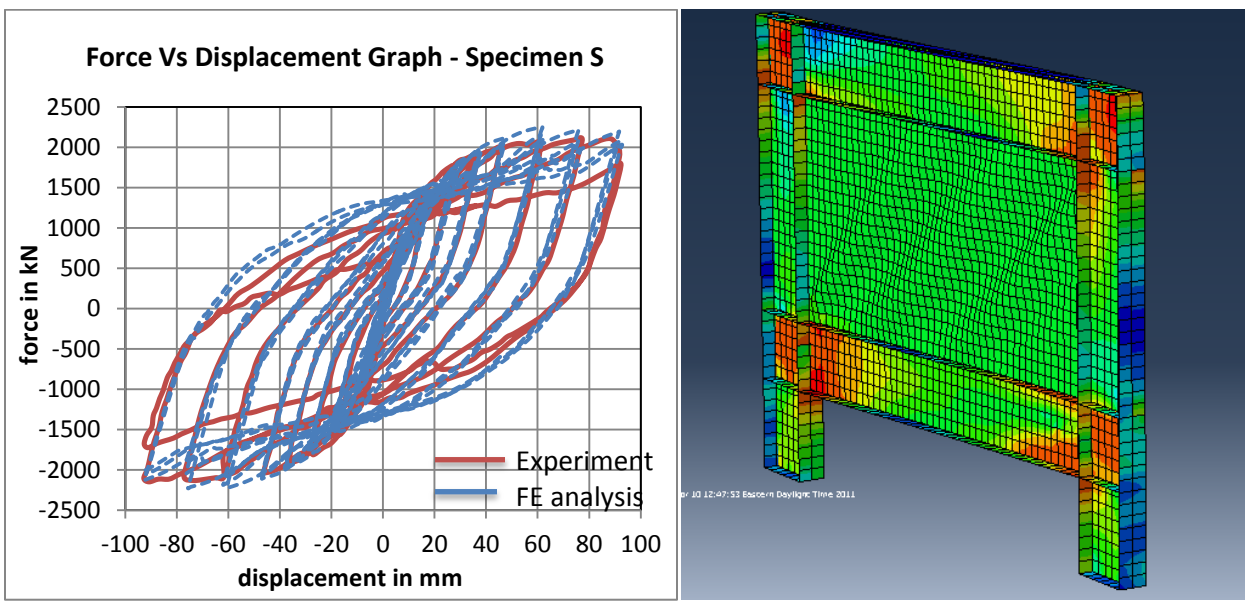

(a) (b)

Figure 3-4 (a) Plot showing a comparison between the hysteresis curves obtained from experiment and FE analysis in ABAQUS 6.10. (b) Rendering of Von Mises Stress contour on the SPSW in ABAQUS 6.10

In order to validate that the model was working as intended, the applied force at the top of the wall was compared with the reaction forces at the bottom of the model. The graphs shown in the

Figure 3-5(a) and Figure 3-5(b) demonstrate that there is very good agreement between the input and the output forces from this model. From the Figure 3-6(a) and Figure 3-6(b) we can see that the deformed shape of the SPSW from the experiment matches well with the deformed shape obtained after the finite element of the model in ABAQUS 6.10. The out of plane buckling of the web panel is found to be similar in both the figures from the experiment and the finite element model with an equal number of fold lines visible on the panel.

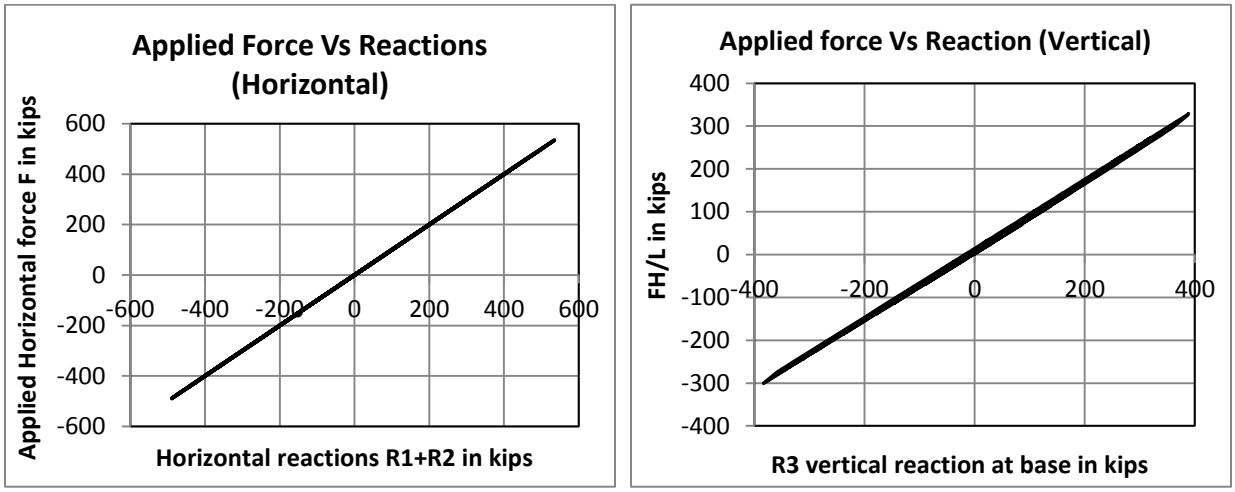

(a) (b)

Figure 3-5 (a) Applied force Versus horizontal reactions from FE model in ABAQUS 6.10, (b) Applied Force Versus vertical reactions from FE model in ABAQUS 6.10

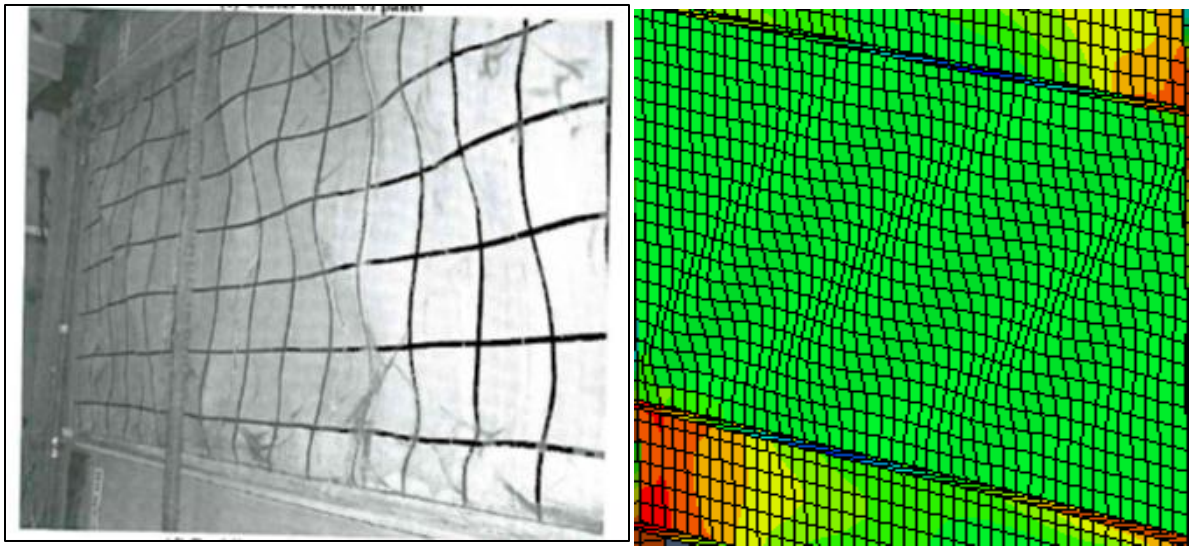

(a) (b)

Figure 3-6 (a) Panel damage – buckling and yielding of the specimen S at 3% drift [From (Vian and Bruneau , 2005)], (b) Panel damage of the finite element model of Specimen S at the end of analysis at 3% drift

3.2 SPSW with a Perforated Panel

This section shows the comparison between the hysteresis obtained from the MCEER experiment on Specimen P with staggered holes in the web panel and the finite element model. The experimental set-up for Specimen P is shown in the Figure 3-7. A shell element model was created using the same approach and details described in the previous section. This comparison is done to validate the behavior of the finite element modeling of perforated SPSW.

3.2.1 Experimental Set-up

Multiple perforations of 200 mm diameter were introduced in the panel at a regular spacing of 300 mm center to center in a staggered manner. Figure 3-7 shows the experimental set-up for the specimen P (Vian and Bruneau, 2005). The finite element modeling aspects for specimen P are exactly the same as those for the specimen S and hence not repeated here. Perforations in the panel are introduced by using the cut extrude feature in the part module. The applied loading also remains the same.

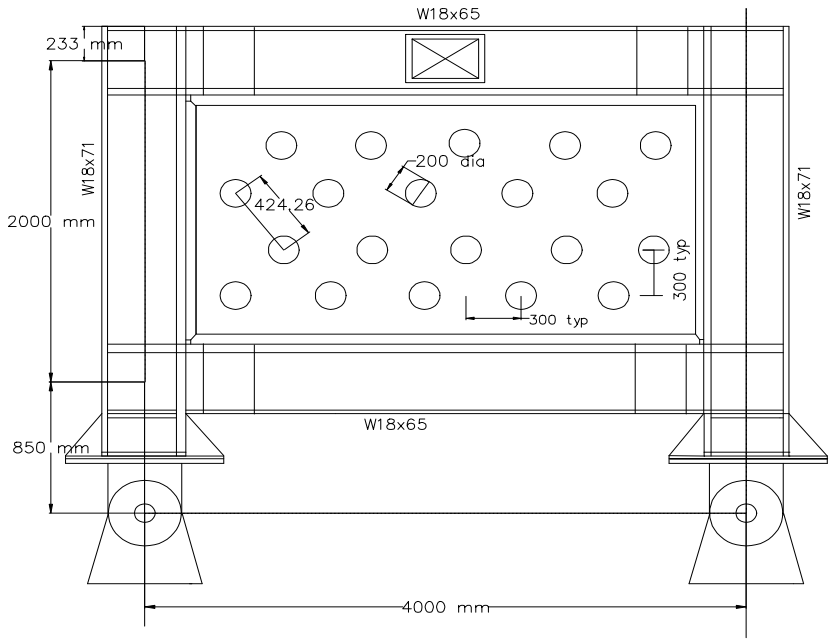

Figure 3-7 Experimental set up for specimen P at the MCEER Laboratory, [From (Vian and Bruneau, 2005)]

3.2.2 Comparison of experimental and FE model results

Figure 3-8(a) shows the comparison of the hysteresis behavior of Specimen P obtained from the experiment conducted by Vian and Bruneau (2005) and the finite element model of the same developed in ABAQUS 6.10. Figure 3-8(b) shows the Von Mises stresses in the SPSW as rendered by ABAQUS 6.10. The peak force from the experimental model is 1800 kN and from the finite element model is 1950 kN. The initial stiffness from the experiment is 615 kips/in and from the finite element model is 710 kips/in. The unloading and the reloading stiffness is observed to be similar. It is seen that there is good agreement between the experimental hysteresis curve and the hysteresis from the finite element model. This validates the adequacy of the proposed modeling techniques to be used in modeling SPSW with perforations.

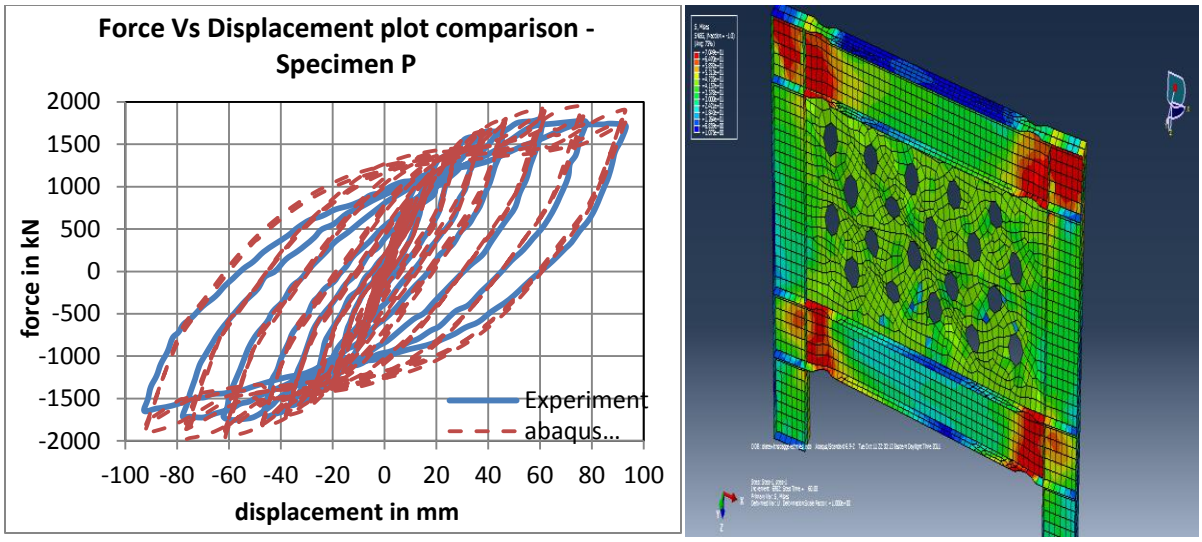

(a) (b)

Figure 3-8 (a) Plot showing a comparison between the hysteresis curves obtained from experiment and FE analysis in ABAQUS 6.10. (b) Rendering of Von Mises Stress contour on the SPSW in ABAQUS 6.10 for specimen P

Figure 3-9(a) shows the buckled shape of specimen P after the test by Vian and Bruneau (2005) at the end of the test at 3 percent drift. The buckled shape compares well with that obtained from the finite element model obtained after the analysis at 3 percent drift in Figure 3-9(b). The deformed shapes have similar pattern of fold lines and distortions along the perforation circumference.

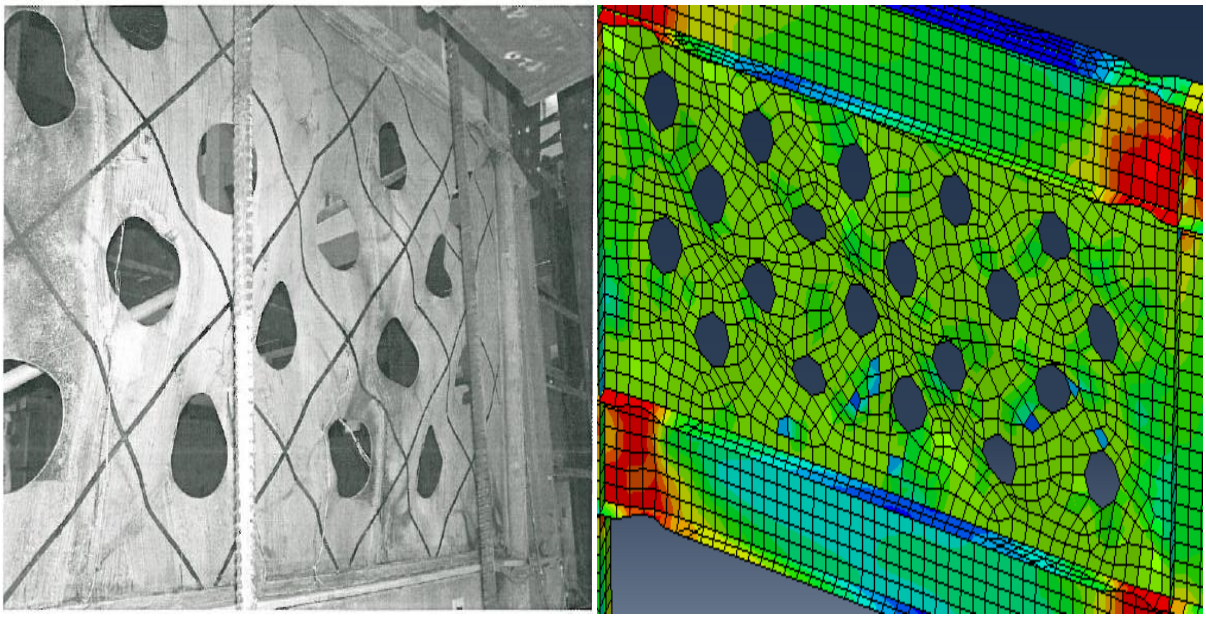

(a) (b)

Figure 3-9 (a) Damage to panel at the end of testing for specimen P at 3% drift [From (Vian and Bruneau, 2005)], (b) Deformed panel at the end of the analysis at 3% drift from the finite element model

3.3 Conclusions Regarding FEM Modeling of SPSWs

Finite element models of SPSWs with shell elements were made and were used to simulate tests found in the literature. It was found that the agreement between the finite element models and the experiments was quite good for solid and perforated panels. Several types of computational tools will be used in the thesis. The modeling techniques validated in this chapter will be used to simulate the behavior of new forms of SPSW henceforth.

Chapter 4. ADAPTATION OF HIGH SEISMIC DESIGN FOR MODERATE SEISMIC ZONES

It was shown in Chapters 1 and 2 that the current SPSW design methodology results in systems with a highly ductile behavior but is inefficient and requires excessively large boundary element sections. In moderate seismic zones, it is desirable to use more economical lateral resisting systems that may have less ductility. The approach that was followed was to start with a high seismic design for a prototype building found in the literature and demonstrate the design procedure and then examine approaches to reduce the cost and sizes of the boundary elements (mostly the VBE), amount of steel required and construction complexity. This will be done by modifying the high seismic design and comparing the above mentioned parameters for the proposed approaches to the results from the conventional design procedure. Conclusions are drawn about the effectiveness of the proposed solutions. This chapter is organized into four sections. The first section validates the high seismic design procedure using a six story building from the literature. The next three sections constitute the three new approaches that were attempted to achieve economic designs. All the four sections include modeling in the FE software SAP 2000 and comparisons of the values of column shears, moments and column axial forces from high seismic design and the proposed approaches.

4.1 High Seismic Design Procedure for SPSW

A design example for a six story building designed with SPSW in a high seismic zone was used in this chapter (ICC/SEAOC 2012). The roof and floor framing plan for the six story prototype building is shown in the Figure 4-2. The building elevation is shown in the Figure 4-1. The web panel is designed such that the panel design shear strength ΦV_n (LFRD - load and resistance factor design) according to the limit state of shear yielding is greater than the story shear at that level. The boundary members are designed for the forces corresponding to the expected yield strength, in tension, of the web calculated acting at an angle α. Design is iterative and hence the boundary elements are designed and checked to satisfy deflection limits. The connections are designed after the final sizes of the members are obtained.

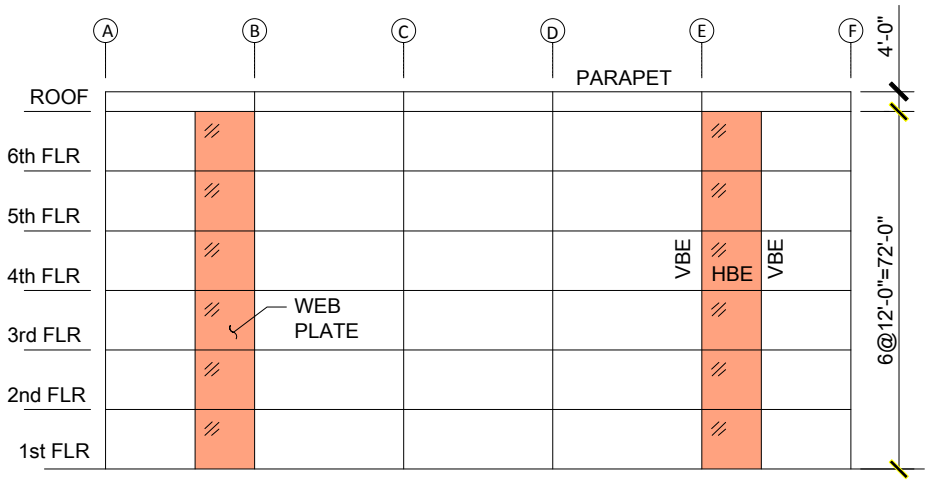

Figure 4-1 Building Elevation [From (ICC/SEAOC, 2012)]

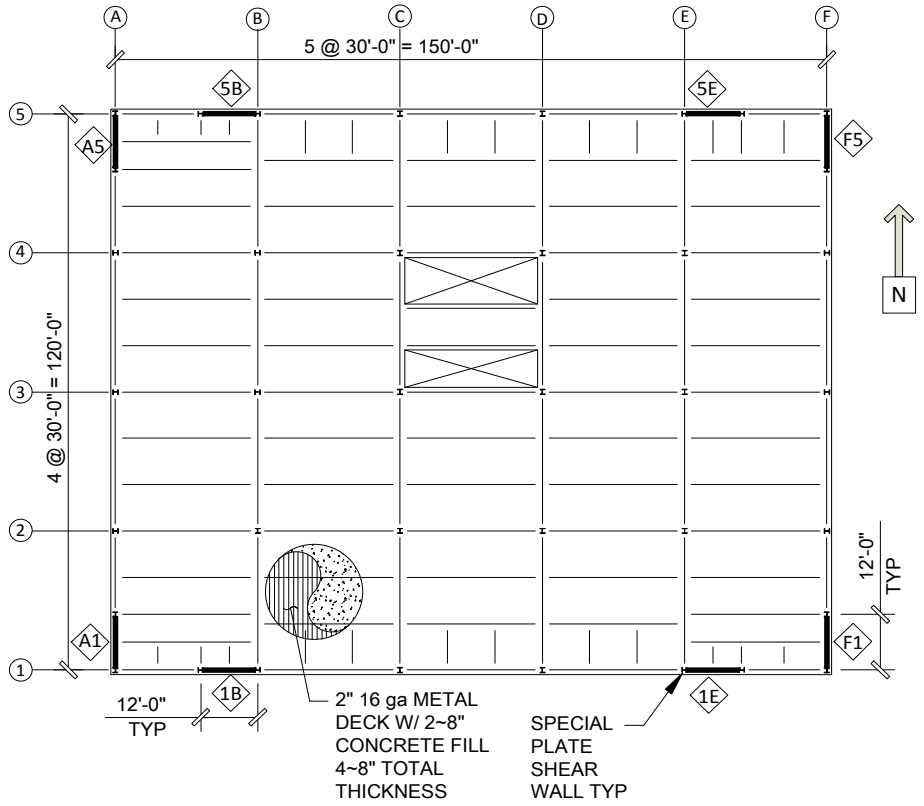

Figure 4-2 Typical floor and roof framing plan [From (ICC/SEAOC, 2012)]

Table 4-1 Story shears, Web panel thicknesses, VBE and HBE sections for the six-story SPSW

Level	Plate Mat'l	Plate Thick.	Design Thick., t_w (inches)	Shear, V_u (kips)	Shear Capacity, ϕV_n, kips	HBE final sizes	VBE final sizes
6th	A1011[1]	14 ga	0.075	40	117	W18x55	W14x145
5th	A1011[1]	12 ga	0.105	116	164	W18x50	W14x145
4th	A1011[1]	10 ga	0.134	175	209	W18x50	W14x145
3rd	A1011[1]	7 ga	0.179	219	279	W18x65	W14x342
2nd	A36	3/16	0.1875	246	319	W18x86	W14x342
1st	A36	3/16	0.1875	259	319	W18x60	W14x342

The high seismic design of a six story building has been summarized in the Table 4-1. The lateral forces were computed using the equivalent lateral force method and the resulting shear forces in the SPSW at each story level are reported in Table 4-1. The web plates were sized using Equation (8) from Chapter 2. The resulting web plate thicknesses are given in Table 4-1. The HBE's were sized for combined compression and flexure including the forces associated with the web plate fully yielding. The final HBE sections obtained are included in Table 4-1.

The primary focus in this section is on the design of the VBE as it is related to the approaches that will be attempted in the next three sections of this chapter to make SPSW more efficient. Similar to HBE's, the VBE should be designed to resist the forces associated with the expected yield strength of the plate ($F_yR_yt_w$) acting at an angle α. For VBE design, the moment and compression forces are separated and examined individually and then interaction is considered in accordance with Chapter H of AISC 360 (AISC 2010). The loads applied to the columns are the forces due to the Tension Field, F_{21} (k/in) and F_{22} (k/in), Beam Shear due to the plate, V_{11} (k) and Beam Shear due to the hinge, V_p (k) and they are shown in the Figure 4-3. The values of these forces on the VBE for the validation example are summarized in the Table 4-2.

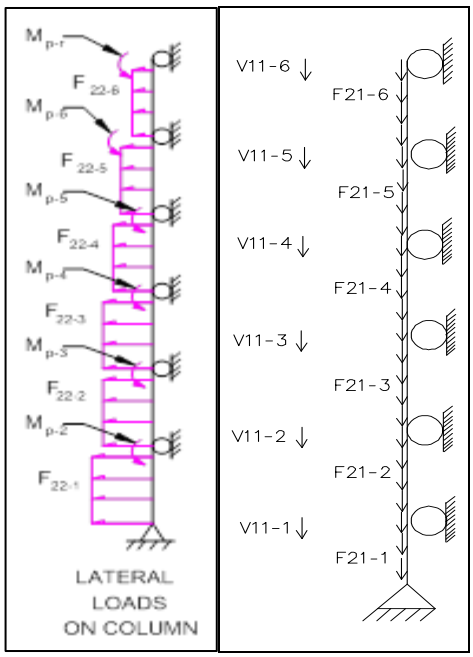

(a) (b)

Figure 4-3 (a) Figure showing the columns at each story level and the applied lateral forces, (b) Column axial forces at each story level

Table 4-2 Force acting on the VBE [From (ICC/SEAOC, 2012)]

Level	Tension Field, F_{22} (k/in)	HBE Plastic Hinge, moment M_p (k-ft)	Tension Field, F_{21} (k/in)	Beam Shear due to Plate, V_{11} (kips)	Beam Shear due to Hinge, V_p (kips)
Roof	-	513	-	102	97
6th	1.12	463	1.34	41	87
5th	1.57	463	1.88	39	87
4th	2.01	610	2.40	61	115
3rd	2.68	853	3.20	85	161
2nd	3.63	564	4.32	0	107
1st	3.63	-	4.32	-	-

A six story column was modeled in SAP 2000 (SAP 2000 User Manual, CSI, 2010) to represent the six stories of a building and the forces at each level from the tension field in the panel, beam shear due to the plate, beam shear due to the hinge and the beam plastic hinge moment were applied. The base of the column is modeled as a hinge support. Roller supports are modeled at the story levels. The values of Column shear (k), Column moment (k ft) and Compression force in the column (k) obtained from the SAP 2000 model are checked with the values obtained using the high seismic design procedure. The equations used to derive the forces on the columns have been summarized in Section 2.4.3. The values from the high seismic design (HSD) procedure as shown in Figure 4-4 and the comparison with those from the SAP 2000 model are given in Table 4-3.

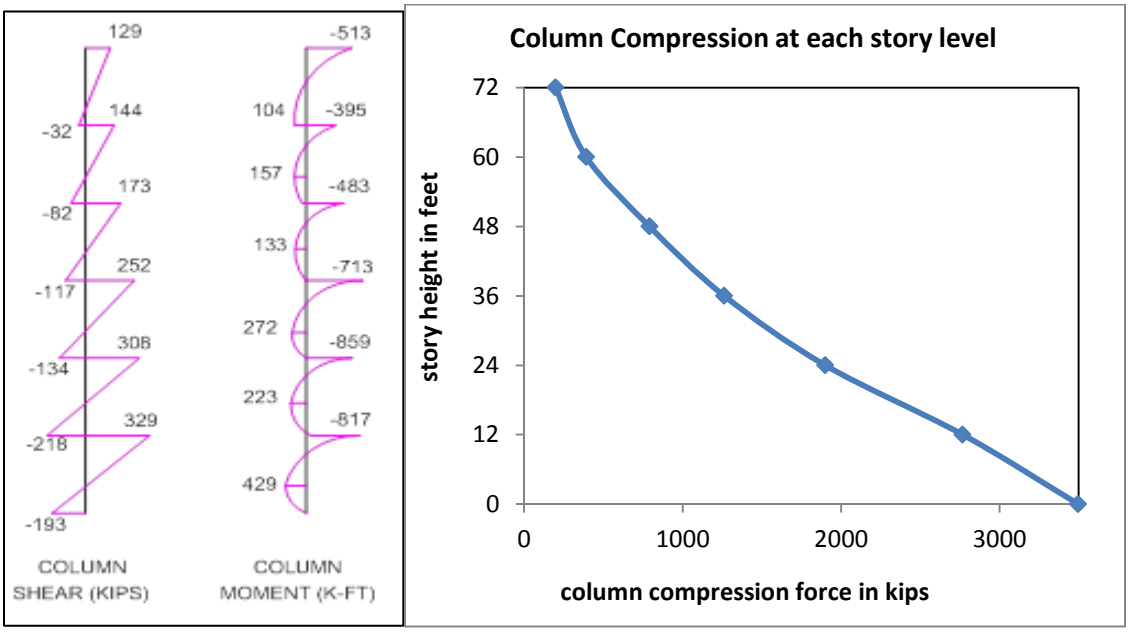

(a) (b)

Figure 4-4 (a) Column Shear and column moment at each story level, (b) Column compression at each story level [From (ICC/SEAOC, 2012)]

Table 4-3 Comparison of the values for column shear, moment and compression force from hand calculations and SAP 2000 model

Story	Column shear V_{22} (kips)		Column moment M_{33} (kip-in)				Column compression (kips)	
			Mid span		ends			
	SAP	HSD	SAP	HSD	SAP	HSD	SAP	HSD
Roof	129	129			513	513	199	199
6th	111	112	106	104			497	392
5th	91	91	154	157	393	395	862	791
4th	137	135	133	133	485	483	1341	1263
3rd	179	174	261	272	744	713	1993	1900
2nd	118	111	225	223	853	859	2646	2768
1st	190	193	413	429	838	817	3193	3497

The values in the Table 4-3 although calculated independently, are in very good agreement with those from the published design example (ICC/SEAOC, 2012). The high seismic design procedure is a capacity design approach. The assumption made in this approach is that every beam undergoes plastic hinging and every plate fully yields at the same time and hence results in large sections for the VBE.

4.2 Modified Design Approach 1 – Capacity Design of VBE with no HBE Moment Connections

The motivation behind this approach is to remove moment connections between the beams and columns and to increase the web plate thickness to satisfy drift limits. Modifications to the high seismic design methodology with minor changes in the forces acting on the VBE would allow the use of a similar design procedure but with a few changes.

The first step in the modeling involves design of the plate elements for strength followed by design to satisfy deflection limits. Since the beam-to-column connections are designed as simple

shear connections in this design approach, the plate thicknesses need to be increased to satisfy deflection limits. A full six story shear wall model in SAP2000 was created. The plate elements were modeled in SAP2000 as membrane area elements. The beams and columns were frame elements. The membrane elements were assigned varying plate thicknesses for each story. The plate material properties were defined for A36 steel. The plate local axes have been rotated to the calculated angle of the tension field for each story. The value of the modulus of elasticity along local 1 axis (the compression diagonal) of the plate was assigned to be 0.1 (very low – axis in compression) and for the tension diagonal – local 2 axis it was given a value of 29000 ksi. The stiffness modifiers for the plate were not modified. The beam-to-column connections for each story were modeled as simple connections – the moments along the minor axis (M22) were released at these nodes. The applied load consisted of the lateral nodal load – unfactored incremental shear at each story as shown in Figure 4-5. Loads were applied at each story level and deflections were checked for the limits. The plate thicknesses were revised to satisfy deflection limits. The columns are designed using a separate SAP2000 model consisting of only the columns at each story and the applied forces consisted of those forces acting on the VBE only. Figure 4-5 (b) shows the axial forces applied to the column and Figure 4-5(c) shows the lateral loads applied to the column in SAP 2000. The beams at each story are designed manually using the provisions of AISC 360-05. This completes the design for high seismic zones without moment connections.

The results for the design are compared in the tables given below and a significant reduction in the forces on the columns is seen. A comparison of the high seismic design with beam to column moment connections and the proposed method without beam to column moment connections is also provided.

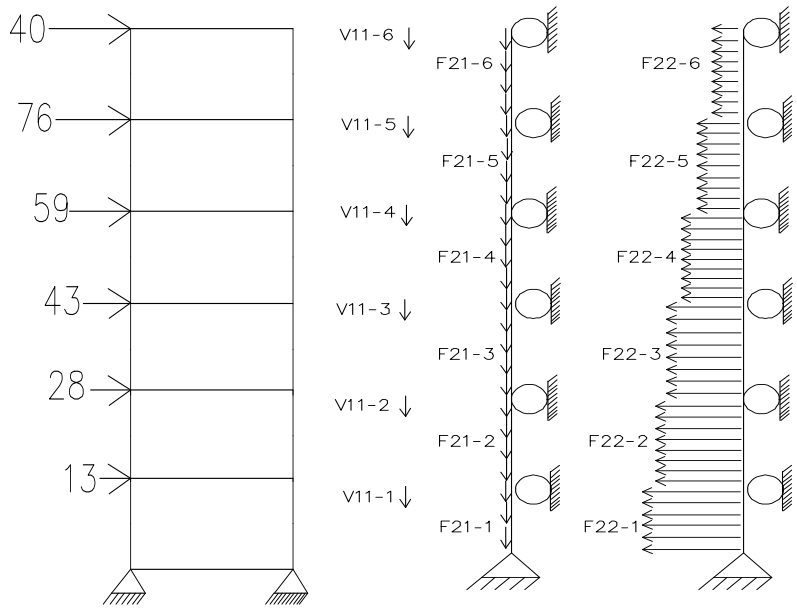

(a) (b) (c)

Figure 4-5 (a) Story shears applied at the floor levels, (b) Figure showing the applied axial forces on the VBE at each story in SAP2000, (b) Applied lateral forces at each story level.

Table 4-4 gives a comparison of the plate thickness for the shear wall with and without moment connections and it can be seen that since drifts controlled the design, there is not a significant reduction in the thicknesses of the web panels for all the six floor levels. Since the proposed design methodology does not require moment connections, slightly thicker plates are required to satisfy drift limits.

Table 4-4 Comparison of plate thicknesses for a 6 story shear wall with and without moment connections

Level	With moment connections	Without moment connections
6th	14 ga plate (0.075 in)	10 ga plate (0.134 in)
5th	12 ga plate (0.105 in)	10 ga plate (0.134 in)
4th	10 ga plate (0.134 in)	7 ga plate (0.179 in)
3rd	7 ga plate (0.179 in)	7 ga plate (0.179 in)
2nd	3/16 in plate (0.1875 in)	3/16 in plate (0.1875 in)
1st	3/16 in plate (0.1875 in)	3/16 in plate (0.1875 in)

Table 4-5 gives the summary of the values obtained from analysis in SAP 2000 for the column shear, moment and the compression force in the column. Table 4-6, Table 4-7, Table 4-8, Table 4-9 and Table 4-10 give the comparisons of the values for different parameters from high seismic design with moment connections and the proposed design methodology without moment connections. They also give the percentage change in the values for the two methods. It can be seen that there is a reduction of more than 50% in the column shear, upto 50% in the column moment and a considerable amount of reduction in the column compression. There is an increase in deflection at the higher story levels but a decrease in the lower levels.

Table 4-5 Column shear, moment and compression force obtained from the SAP2000 model for the proposed design

Story	Column shear kips	Column moment kips-in		Column compression kips
		Mid span	Ends	
Roof	0-62	140		102
6th	98-110	102	220	313
5th	115-139	148	251	591
4th	150-181	195	318	956
3rd	201-243	239	439	1446
2nd	276-313	479	640	1993
1st	206			2540

Table 4-6 Comparison of Column Shear for a six story shear wall with and without moment connections

Level	Column shear - With moment connections	Column shear - Without moment connections	Percent reduction in shear
Roof	129	62	52
6th	111	12	89.2
5th	91	24	73.6
4th	137	31	77.4
3rd	179	42	76.5
2nd	118	40	66.1
1st	190	206	-8.4 (increase)

Table 4-7 Comparison of Column moment at the story level (not at mid-span) for a six story shear wall with and without moment connections

Level	Column moment - With moment connections	Column moment - Without moment connections	Percent reduction in moment
Roof	513		
6th	395	220	44.3
5th	483	251	48
4th	713	318	55.4
3rd	859	439	49
2nd	817	640	22

Table 4-8 Comparison of Column compression force for a six story shear wall with and without moment connections

Level	Column compression -With moment connections	Column compression Without moment connections	Percent reduction in compression force
Roof	199	102	49
6th	497	313	37
5th	862	591	31
4th	1341	956	29
3rd	1993	1446	27
2nd	2646	1993	25
1st	3193	2540	20

Table 4-9 Comparison of Deflections for a six story shear wall with and without moment connections

Level	Deflection - With moment connections	Deflection - Without moment connections	Percent increase in deflection
Roof	2.34	2.3982	2.5
6th	1.97	2.0015	1.6
5th	1.54	1.5414	0.1
4th	1.07	1.0692	-0.1(decrease)
3rd	0.68	0.6528	-4 (decrease)
2nd	0.34	0.2888	-15.1 (decrease)

Table 4-10 Comparison of Inter-story drift (inches) for a six story shear wall with and without moment connections

Level	Drift –with moment connections	Drift – without moment connections	Percent increase in drift	C_d x drift < 2.88 in
Roof	0.37	0.3967	7.22	2.3802
6th	0.43	0.4601	7.00	2.7606
5th	0.47	0.4722	0.47	2.8332
4th	0.39	0.4164	6.77	2.4984
3rd	0.34	0.3640	7.06	2.1840
2nd	0.34	0.2888	-15.06 (decrease)	1.7328

The column sizes are redesigned (as compared to the previous section) for the reduced forces and moments. The HBE are designed according to the provisions for high seismic design from AISC 360 (AISC 2010). Table 4-11 and Table 4-12 show the final designs and comparison of the sections obtained using high seismic design approach and the proposed design methodology. It is

seen that there is an increase in the sizes of the VBE and the plate thicknesses but there is a reduction in the HBE sizes. Although the forces in the boundary elements were reduced, the web plate and boundary element sections had to be increased to satisfy deflection criteria. As a result, there was a net increase in the total amount of steel required as shown in Table 4-13. Figure 4-6 summarizes the comparison and final design using both the methodologies.

Table 4-11 Comparison of VBE section for the high seismic design and proposed design approach

Level	With moment connections	Without moment connections
6, 5, 4	W 14 x 145	W 14 x 193
3, 2, 1	W 14 x 342	W 14 x 370

Table 4-12 Comparison of HBE sections obtained from the high seismic design and proposed design approaches

Level	With moment connections	Without moment connections
6th	W 18x55	W 18x97
5th	W 18x50	W 14x38
4th	W 18x50	W 14x68
3rd	W 18x65	W 14x38
2nd	W 18x86	W 16x77
1st	W 18x60	W 16x50

Table 4-13 Comparison of steel weight for high seismic design and proposed design approach

With moment connections	Without moment connections
Total weight of steel : 126.5 lbs	Total weight of steel : 131.4 lbs

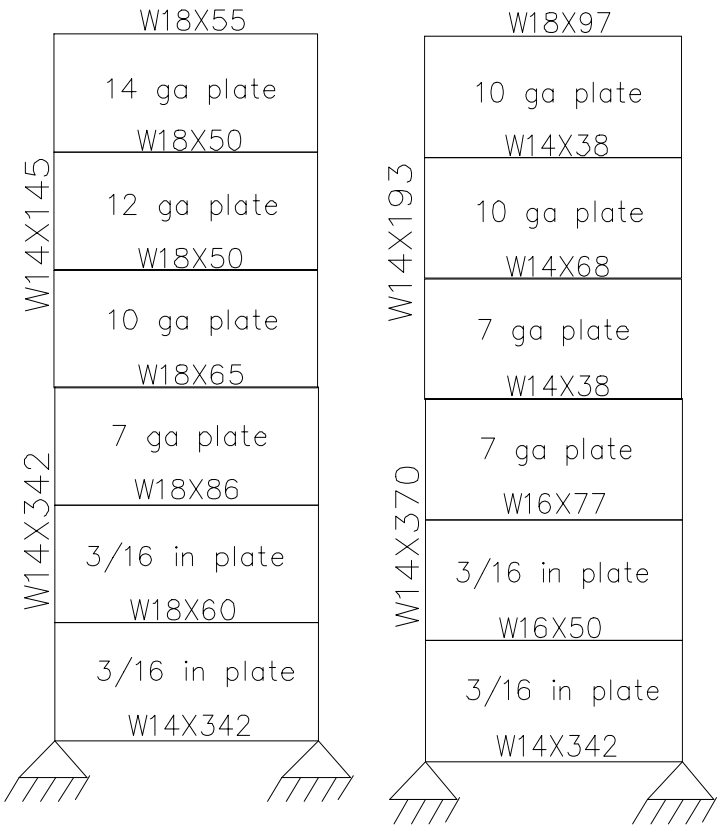

(a) (b)

Figure 4-6 Comparison of plate, HBE and VBE sizes in (a) high seismic design using the code specifications, (b) proposed design approach without moment connections

From this approach it could be concluded that although eliminating moment connections could make construction easier and possibly cheaper, the overall weight of steel increased. It is unclear if this approach would produce a more economical design and it might also worsen the seismic performance without the moment connections. One of the key reasons for the failure of this approach to result in reduction in steel weight is the fact that the design was drift controlled.

4.3 Modified Design Approach 2 – Over-Strength Factor Design of VBE with no HBE Moment Connections

This approach is similar to the previous approach in that there are no moment connections between the HBE and the VBE. The difference between the two methods is the HBE and the VBE were designed using capacity design in Approach 1 and are designed using an over-strength factor in Approach 2.

A full shear wall model in SAP2000 was created without moment connections between the HBE and VBE and a factored incremental shear was applied at each story. The procedure involves designing the plates to satisfy deflections for the unfactored story shears applied at the floor levels (F_i) and boundary elements for a factored incremental shear applied at each story (ΩF_i) where $\Omega = 2.0$. The incremental shears at the floor levels amplified by the over strength factor are shown in the Figure 4-7. This model was analysed in SAP 2000. The built in design tool in SAP 2000 was used to check the design for the VBE. The design code used in SAP 2000 is AISC 360-05. The same finite element model was used in SAP 2000 for the iterative design procedure for plates and the VBE with different load combinations with and without the over strength factor. It is an iterative process. The flow chart in Figure 4-8 explains the procedure followed in this methodology.

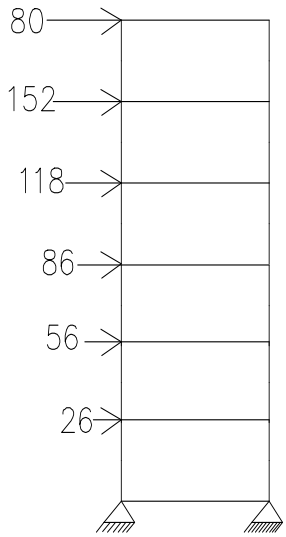

Figure 4-7 Incremental shears amplified by the over strength factor applied at the floor levels for the finite element model in SAP 2000

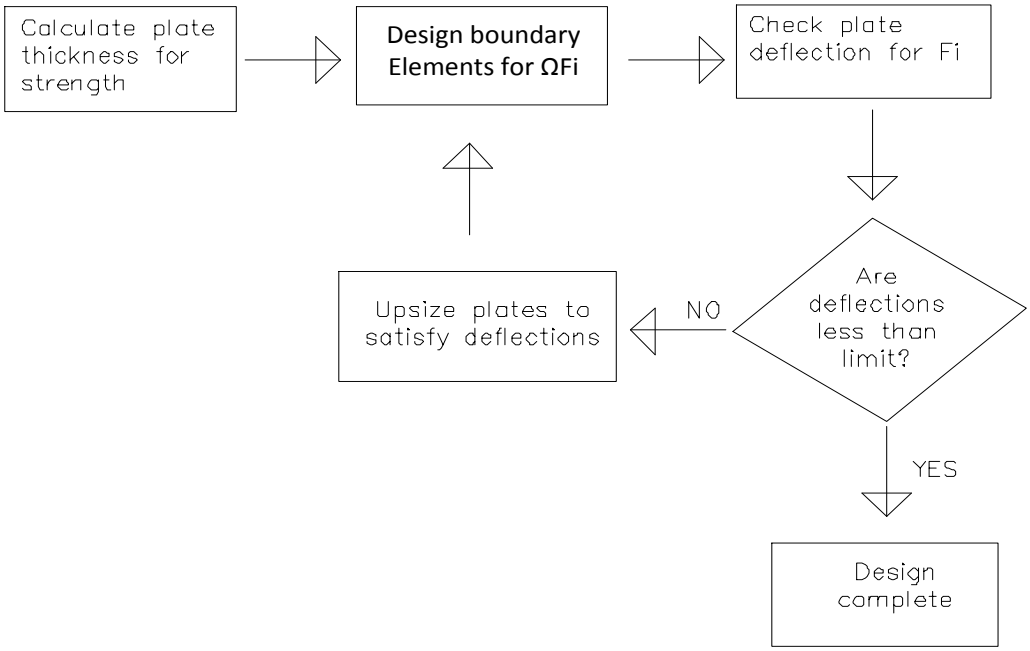

Figure 4-8 Flow chart explaining the design procedure for the proposed design methodology with over strength factor and without moment connections

The Figure 4-9 shows a comparison of the plate, HBE and VBE sizes for the high seismic design using the code specifications and the proposed design methodology using simple beam to column connections including an over strength factor.

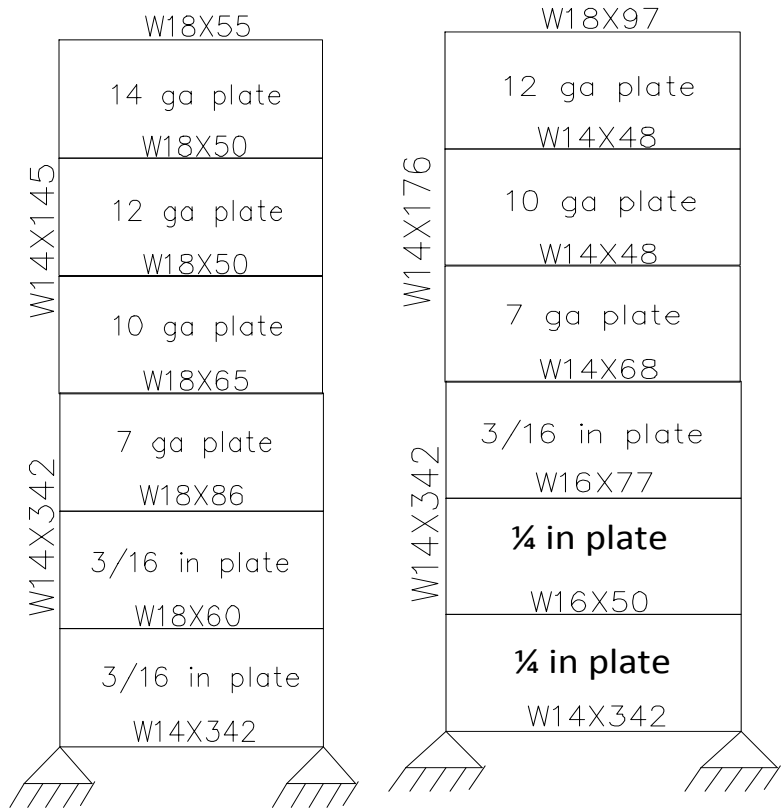

(a) (b)

Figure 4-9 Figure showing the comparison of plate, HBE and VBE sizes for (a) high seismic design using the code specifications, (b) proposed design approach without moment connections including an over-strength factor

Table 4-14 Comparison of the total weight of steel in the high seismic design approach and proposed design method without moment connections including an over strength factor

With moment connections	Without moment connections
Total weight of steel : 126.5 lbs	Total weight of steel : 136.5 lbs

It is seen that the plate thicknesses for all the floors have increased and the HBE sections are comparatively smaller in the proposed design method as compared to the high seismic design approach. But the column section has increased in the top three stories and hence the weight of steel as seen in Table 4-14. The advantage of the method is that there are no moment connections at the beam-column joints. The reason this method failed to reduce the amount of steel required is due to the system being drift controlled. If the web plate and boundary elements were controlled by strength, there would be a significant reduction in their sizes using this method.

4.4 Modified Design Approach 3 – Plastic Design of Columns with no HBE Moment Connections

This design methodology aims at sequencing the formation of plastic hinges in the columns. Consider one story of the column in between beams. Plastic hinges are assumed to form at the 2 ends of the column and at mid-height as shown in the Figure 4-10.

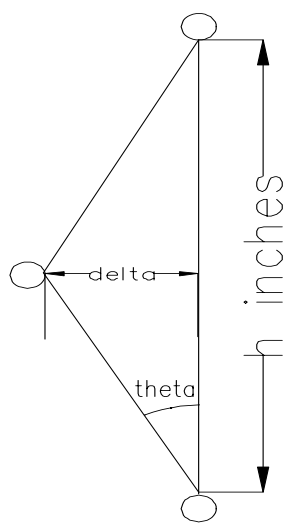

Figure 4-10 Figure showing one story of the column with plastic hinge locations

The terminology used in the following equations is: delta (δ) is the deflection at the mid height of the story, theta (θ) is the angle of the deflected shape of the column with respect to the vertical, w is the distributed load on the column due to the tension field, and the deflection is taken as $\frac{\delta}{2}$. Small angle assumption is made for the angle θ.

$$\delta \text{ (delta)} = \frac{\theta h}{2} \ inches \ldots\ldots\ldots\ldots\ldots\ldots\ldots\ldots\ldots\ldots\ldots\ldots\ldots\ldots\ldots\ldots\ldots\ldots\ldots\ldots\ldots\ldots Eqn. (18)$$

$$\text{External work done } = \frac{\text{w. h. } \delta}{2} \ldots\ldots\ldots\ldots\ldots\ldots\ldots\ldots\ldots\ldots\ldots\ldots\ldots\ldots\ldots\ldots\ldots\ldots\ldots Eqn. (19)$$

$$\text{External work done } = \frac{\text{wh}\theta\text{h}}{4} = \frac{(\text{w}\theta h^2)}{4} \ldots\ldots\ldots\ldots\ldots\ldots\ldots\ldots\ldots\ldots\ldots\ldots . Eqn. (20)$$

$$\text{Internal work done } = \text{ Mp } (\theta + 2\theta + \theta) = \text{ 4Mp } \theta \ldots\ldots\ldots\ldots\ldots\ldots\ldots\ldots\ldots \text{Eqn. (21)}$$

Equating the internal and external work done results in the following equation:

$$M_p = \frac{wh^2}{16} \ldots\ldots\ldots\ldots\ldots\ldots\ldots\ldots\ldots\ldots\ldots\ldots\ldots\ldots\ldots\ldots\ldots\ldots\ldots\ldots\ldots\ldots\ldots\ldots\ldots\ldots\ldots Eqn. (22)$$

Extending the same concept to any floor in the 6 story column gives a similar result. Assuming that the same load is acting on all the spans and the spans are of equal length and two hinges are formed at the ends of each span and one at mid span, we have the following equation after equating the total internal and external work done

$$\frac{6wh^2\theta}{4} = 6Mp(\theta + 2\theta + \theta) \ldots\ldots\ldots\ldots\ldots\ldots\ldots\ldots\ldots\ldots\ldots\ldots\ldots\ldots\ldots\ldots\ldots\ldots\ldots Eqn. (23)$$

$$M_p = \frac{wh^2}{16} \ldots\ldots\ldots\ldots\ldots\ldots\ldots\ldots\ldots\ldots\ldots\ldots\ldots\ldots\ldots\ldots\ldots\ldots\ldots\ldots\ldots\ldots\ldots\ldots\ldots\ldots\ldots Eqn. (24)$$

The plastic moment for all floors of the six story column developing a mechanism is the same as that for the moment derived for a single-story column.

The base of the column has a hinge and so the plastic hinges will form at the story level and at mid-span as seen in the Figure 4-11. A separate equation is derived for the first story of the column when the base of the column is a pin support.

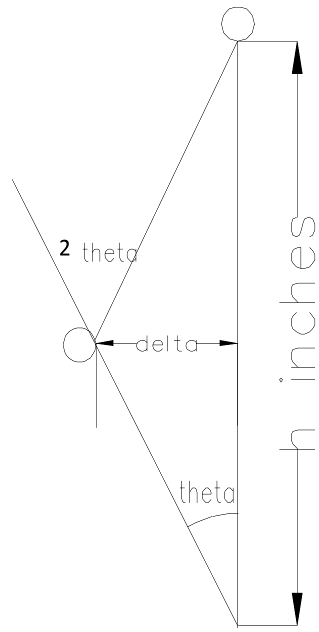

Figure 4-11 Figure showing plastic hinging mechanism for the first story of the column

Equating the internal and the external work done the following equations are obtained.

$$\frac{wL_1\,\delta}{2} = M_p(\theta + 2\theta) = 3\theta M_p \ldots\ldots\ldots\ldots\ldots\ldots\ldots\ldots\ldots\ldots\ldots\ldots\ldots \ldots Eqn. (25)$$

$$\theta = \frac{2\delta}{L_1} \ldots\ldots\ldots\ldots\ldots\ldots\ldots\ldots\ldots\ldots\ldots\ldots\ldots\ldots\ldots\ldots\ldots\ldots\ldots\ldots .. Eqn. (26)$$

$$\delta = \frac{\theta L_1}{2} \ldots\ldots\ldots\ldots\ldots\ldots\ldots\ldots\ldots\ldots\ldots\ldots\ldots\ldots\ldots\ldots\ldots\ldots .. \ldots\ldots\ldots Eqn. (27)$$

$$\frac{w\theta L_1^2}{4} = 3\theta M_p \ldots\ldots\ldots\ldots\ldots\ldots\ldots\ldots\ldots\ldots\ldots\ldots\ldots\ldots\ldots\ldots\ldots\ldots\ldots Eqn. (28)$$

$$M_p = \frac{wL_1^2}{12} \ldots\ldots\ldots\ldots\ldots\ldots\ldots\ldots\ldots\ldots\ldots\ldots\ldots\ldots\ldots\ldots\ldots\ldots\ldots Eqn. (29)$$

The concept of plastic hinge formation is extended to the columns in the six-stories of the building. The equations for the plastic mechanism that have been derived, give the distributed load that causes the plastic mechanism to occur. These equations are used to calculate the applied

moment for design, M_u. When the applied moment reaches the plastic moment capacity M_p, the plastic hinge mechanism will occur. Hence M_u could be compared with M_p in a design equation. This format is useful in implementation with the combined loading equation where the moment and axial forces are combined based on the ratio to their capacities.

The steps involved in the proposed design methodology are summarized as follows. The applied moment M_u is obtained from the plastic mechanism equations above (either Eqn. 22 or Eqn. 29 depending on the boundary conditions). Figure 4-12 shows the displaced shape associated with the plastic mechanism and the locations of the plastic hinges. Here W_1, W_2 and W_3 are the distributed loads for the first three stories of the column. The next three higher level stories will have the same mechanism and the same value of Mu as the third story. W_1= 3.40 k/in, W_2= 3.58 k/in, W_3 = 2.56 k/in, W_4 = 2.33 kips/in, W_5 = 2.20 kips/in, W_6 = 1.63 kips/in (these are F_{22} values) (ICC/SEAOC, 2012).

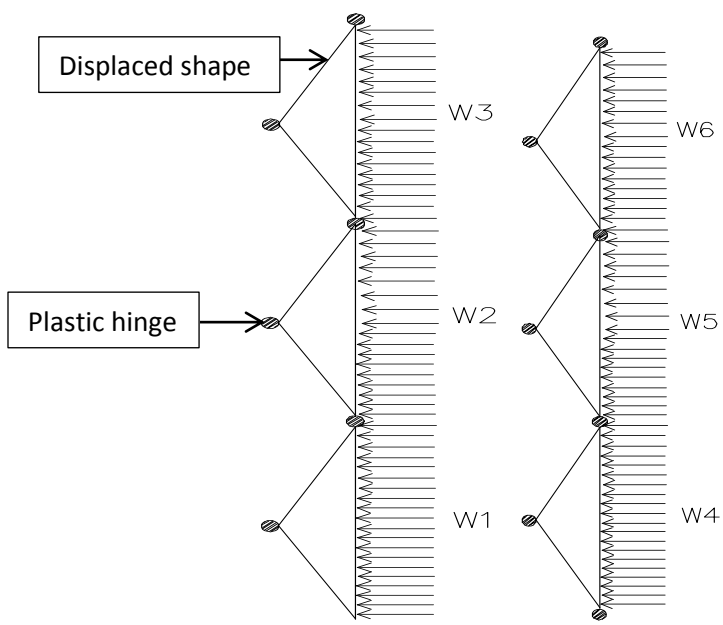

(a) (b)

Figure 4-12 (a) Figure showing the plastic hinging mechanism in a column in the bottom three stories of a six story building, (b) plastic hinging mechanism in the top three stories of a six story building

The base of the first story is a pin support and thus the mechanisms used in the first and the higher story levels are different. Table 4-15 summarizes the values of the applied moment calculated for the six stories of the building.

Table 4-15 Applied moments for the six stories of the example SPSW building

Story	Equation for Design Moment, M_u	Design Moment, M_u (kip ft)
6th	$\frac{W_6 h^2}{16}$	176
5th	$\frac{W_5 h^2}{16}$	237
4th	$\frac{W_4 h^2}{16}$	252
3rd	$\frac{W_3 h^2}{16}$	277
2nd	$\frac{W_2 h^2}{16}$	387
1st	$\frac{W_1 h^2}{12}$	490

The next step in the design process is to obtain the concentrated forces (P_u) on the columns from the idealized model. These values are the values of column compression obtained from the SAP model for the six story column. When the values of the applied moment M_u and the column compression P_u are known the flexural capacities of the sections provided are checked to be adequate using the AISC 360 – 10 provisions and the interaction equation is checked to be satisfied. Table 4-16 summarizes the design for this proposed methodology. The deflections and drifts at each story level are as shown in Table 4-17. Although the design moment for the VBE was reduced, the selected sections had a value from the interaction equation smaller than unity because drift controlled the design instead of strength. As shown in Table 4-17, the interstory drift was just smaller than the limit of 2.88 for the fourth floor.

$$\frac{P_u}{\varphi P_n} + \frac{8}{9}\frac{M_u}{\varphi M_n} \leq 1.0 \ldots\ldots\ldots\ldots\ldots\ldots\ldots\ldots\ldots\ldots\ldots\ldots\ldots\ldots\ldots\ldots\ldots\ldots\ldots\ldots\ldots\ldots\ldots\ldots\ldots\ldots Eqn.(30)$$

Table 4-16 Interaction equation check for the columns at each story level of the six story building

level	M_u	ϕM_n	P_u	ϕP_n	Interaction Equation	VBE section
6th	176	1076	449	1911	0.380	W14x159
5th	237	1076	812	1911	0.621	W14x159
4th	252	1076	1199	1911	0.835	W14x159
3rd	277	2520	1682	4177	0.500	W14x342
2nd	387	2520	2238	4177	0.672	W14x342
1st	490	2520	2780	4177	0.838	W14x342

Table 4-17 Deflections and drifts at each story level for the six story building

Level	Deflection from Elastic Model (in)	Inelastic Drift = C_D x Elastic Drift (in)
6th	2.4332	2.3034
5th	2.0493	2.7048
4th	1.5985	2.8752
3rd	1.1193	2.6418
2nd	0.679	2.2014
1st	0.3121	1.8726

Table 4-18 through Table 4-21 show a comparison of the plate, HBE and VBE sizes using the high seismic design as per the code specifications and the proposed plastic mechanism approach without moment connections between the beams and columns and also the weight of steel used from both approaches.

Table 4-18 Comparison of VBE sizes for the high seismic design and proposed plastic design approach

Level	VBE With moment connections	VBE Without moment connections – plastic mechanism
6, 5, 4	W 14 x 145	W 14 x 159
3, 2, 1	W 14 x 342	W 14 x 342

Table 4-19 Comparison of the HBE sizes for high seismic design and proposed plastic design approach

Level	HBE With moment connections	HBE Without moment connections
6th	W 18x55	W 16x77
5th	W 18x50	W 14x68
4th	W 18x50	W 14x48
3rd	W 18x65	W 14x48
2nd	W 18x86	W 14x82
1st	W 18x60	W 16x50

Table 4-20 Comparison of plate sizes for high seismic design and proposed plastic design approach

Level	With moment connections	Without moment connections
6th	14 ga plate (0.075 in)	12 ga plate (0.105 in)
5th	12 ga plate (0.105 in)	9 ga plate (0.1495in)
4th	10 ga plate (0.134 in)	8 ga plate (0.1644 in)
3rd	7 ga plate (0.179 in)	7 ga plate (0.179 in)
2nd	3/16 in plate (0.1875 in)	3/16 in plate (0.1875 in)
1st	3/16 in plate (0.1875 in)	3/16 in plate (0.1875 in)

Table 4-21 Amount of steel used in the shear wall for the high seismic design and proposed plastic design approach

With moment connections	Without moment connections
Total weight of steel : 126.5 lbs	Total weight of steel : 130.8 lbs

It could be concluded from this approach that moments in the VBE were reduced. However, this did not seem to produce a much lighter VBE section than in Approaches 1 or 2. The main reason for this is that the design is drift controlled. Reducing the strength demands in the VBE did not help in reducing the total amount of steel required.

4.5 Conclusions

SPSW with moment connections increase the cost of construction. For a moderate level of seismicity, the higher cost of providing moment connections between the beams and columns could be used more efficiently to provide slightly bigger sections for the VBE. The HBE sizes and the plate thicknesses are comparatively smaller for the proposed design approaches. Hence investment in a slightly higher amount of steel may be advantageous in that the construction speed would increase and field welding would be reduced. The seismic behavior of the designs created using these approaches was not analyzed, but is expected to be similar to that of tension only braced frames and thus would likely be adequate for moderate seismic zones.

Beyond the elimination of moment connections, the proposed design approaches were intended to reduce the design strength demands on the boundary elements. From the previous sections it is seen that drift controlled the design, the strength was greater than what it needed to be and hence the proposed design approaches did not result in reduced steel weight. To achieve improved efficiency in a SPSW system it is necessary to decouple strength and stiffness. Hence the motivation for the further research would be to develop tunable SPSW for which strength, stiffness and ductility might be separately tuned.

Chapter 5. ALTERNATE SPSW DETAILING TO CREATE MORE EFFICIENT SOLUTIONS FOR SPSW

5.1 Background and Concept

Attempts were made in the previous chapter to make SPSW more economical for moderate seismic zones by eliminating moment connections between beams and column and reducing the strength demands on the boundary elements. Although these approaches may be viable ways to eliminate cost and construction time associated with moment connections, they did not reduce the sizes of the boundary elements. The reason these methods were unsuccessful in reducing the boundary element sizes was because deflection controlled the design instead of strength. To make efficient SPSW systems, it is necessary to reduce the strength of the web plate (to reduce the demands on the boundary elements), but increase the stiffness (to better satisfy the drift criteria).

Various approaches to reduce web plate strength while increasing the web plate stiffness have been attempted in the past by researchers worldwide. The approaches have included introducing perforations in the web plate, detaching the web plate from the VBE, use of low yield point steel for the web plate, cutting vertical slits in the web plate, and other types of web plate cut-outs.

The motivation for this chapter is therefore to investigate several new methods for reducing web plate strength while sustaining or increasing system stiffness. Seven approaches were attempted. The approaches are separated into two parts in this chapter: approaches using solid plates, and approaches with web cut-outs.

5.2 New Ideas - SPSW with Solid Panels

A few ideas with solid panels were attempted. The finite element modeling for these approaches was done in SAP 2000 (SAP 2000 User Manual, CSI 2010) to conduct a preliminary study of the performance of these systems. Analysis in SAP 2000 takes significantly lesser computational time and is a quicker option as compared to ABAQUS 6.10. Thus for the models with solid panels SAP 2000 was used. In this chapter each of the seven approaches includes modeling of a

single story SPSW. This single story is meant to loosely represent the first story of the prototype building used in the previous chapter for validation of high seismic design. The target design shear strength was typically 260 kips.

5.2.1 Approach 1 – Web Panel Connected to the HBE Only

In order to reduce the demand on the columns, a single story SPSW was modeled in SAP2000 with the web plate connected to the HBE only. In this model a membrane area element was used for the web plate. The modulus of elasticity, E along the tension diagonal was specified to be 29000 ksi while along the compression diagonal a low value of 0.1 ksi was specified. The model was used to check the stiffness of the web plate. Boundary elements were designed for strength. The beam to column connection was made simple and to achieve this major and minor axes moment releases were defined. The web plate was sized to satisfy the drift limits. The resulting web plate thickness and boundary element sizes are shown in Figure 5-1.

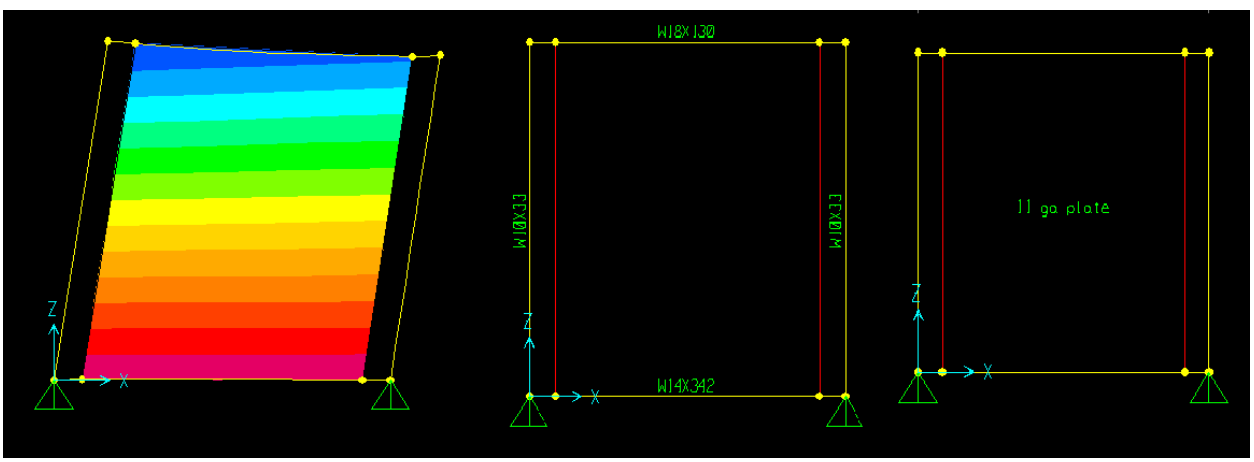

Figure 5-1 Deformed shape, HBE and VBE sections and plate thickness for a SAP2000 model of a SPSW with web plate connected to HBE only

From Figure 5-1 it is seen that when the web panel is connected to the HBE only, the VBE sections can be quite small. The SPSW was designed for a story shear of 260 kips. The shear strength of the web plate calculated using Eqn. 8 for an 11 gauge thick plate was 257 kips. The HBE and VBE sections were designed using the code provisions in AISC 360-10 (AISC 2010). The maximum allowable drift including the displacement amplification factor for the one story

shear wall is 2.88 inches and the drift in the above configuration was 2.76 inches. Although this approach could produce more economical VBE, the buckling and yielding behavior of the plate is not well understood from this elastic 2D analysis. Regardless, it was decided not to further pursue this design approach because it does not provide much ability to separately tune strength and stiffness.

5.2.2 Approach 2 – Thick Fish Plate around a Thin Web Panel

In this approach, a thicker fish plate around the perimeter of the web panel is welded to a thin web plate as shown in the Figure 5-2. The concept behind this approach was to increase stiffness by inclusion of a thicker perimeter plate while controlling strength with the thinner middle plate. This approach was intended to produce a more efficient SPSW system. The modeling techniques used for this model are similar to those described in the previous approach. The VBE and HBE are designed for the tension yielding of the thicker fish plate using the provisions for VBE design in the current building codes – AISC 360-10 (AISC 2010). The maximum allowable drift including the displacement amplification factor for the one story shear wall is 2.88 inches and the drift for this approach was also within the allowable limit.

Figure 5-2 shows that there was not much reduction in the HBE and VBE sizes as compared to the sections for the six story prototype building. But there is a reduction in the amount of steel owing to the reduction in the plate thickness for the web plate. This could be a viable approach for independently adjusting strength and stiffness of the SPSW system, but was not further pursued because of the following challenges:

- The forces on the boundary elements do not reduce if they are designed for yielding of the thicker plate. More analysis would be required to determine if the design forces for the boundary elements could be related to yielding of the thinner plate.
- It is expected that the thick perimeter plates would be welded directly to the column similar to typical fish plates. It is unclear if this will be possible for any width of perimeter plate.

- The corner conditions are important and would require further study. The thicker plates in the corner act to stiffen the beam to column connection and could cause undesirable limit states if not well understood.
- To promote the desired system characteristic, it makes more sense to have the thicker plate in the middle and the thinner plate around the perimeter. The forces on the boundary elements would be reduced, but the stiffness could be controlled by the thicker middle plate. This approach was not pursued, however, because of potential construction issues of using very thin fish plates to weld to the boundary elements. Thin steel sheet can distort with the amount of heat input required for these welds.

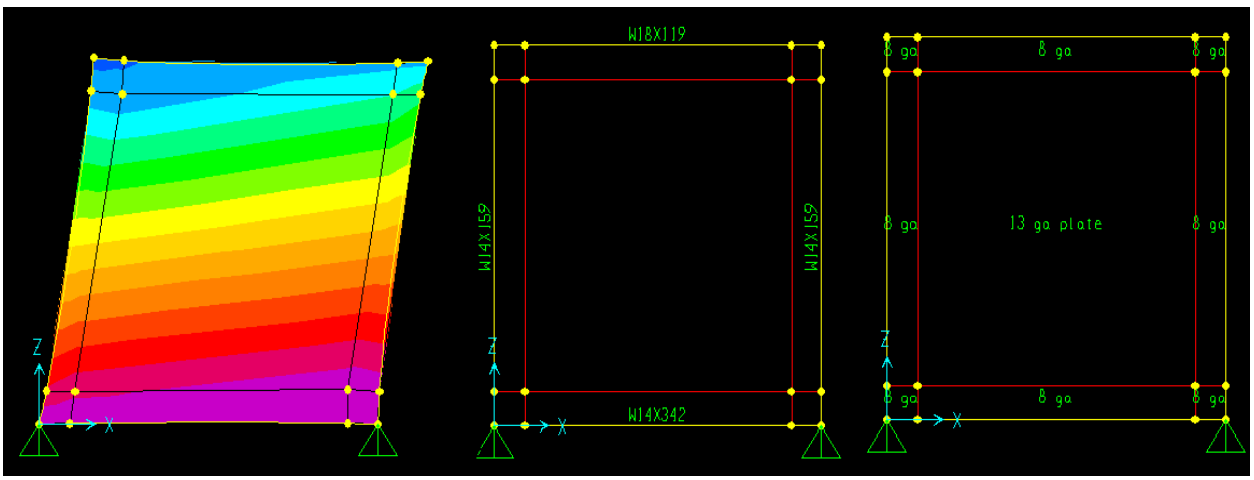

Figure 5-2 Deformed shape, HBE and VBE sections and plate thicknesses for a SAP2000 model of a SPSW with a thick fish plate surrounding a thin web plate

5.2.3 Approach 3 – Small Thin Plates around a Thicker Web Panel

This approach aims at reducing the VBE sizes and also the amount of steel used. Hence a slightly thicker middle web plate is used to increase system stiffness and is connected to the boundary elements using thinner discrete plates as shown in the Figure 5-3. The discrete connection plates control the web plate strength and reduce the demands on the boundary elements. Instead of a thin plate surrounding the entire web panel, smaller length discontinuous plates were selected to

further control the strength of the panel (can be adjusted by plate thickness and length). The model of the central web plate was divided into multiple plates so that there are common nodes between the web plate and the thinner fish plates and there is compatibility in deflections at the common node. The beam to column connection is a simple shear connection. The modeling techniques used in this approach are similar to those in the previous two approaches.

The dimension of the thinner plate and the geometry of the perforation pattern were determined using the equations in Chapter G of the AISC manual (AISC 360-10, AISC 2010). The thinner plates are required to develop tension field action and the shear strength of the web plate will be determined according to the limit state of tension field yielding. The following equation was used to determine the minimum thickness required for the thin perimeter plates.

$$\frac{h}{t_w} = 1.10\sqrt{\frac{k_v E}{F_y}} \ldots\ldots\ldots\ldots\ldots\ldots\ldots\ldots\ldots\ldots\ldots\ldots\ldots\ldots\ldots\ldots\ldots\ldots\ldots\ldots\ldots\ldots\ldots\ldots\ldots\ldots Eqn.(31)$$

where h is the width of the thin plate, t_w is the thickness of the thin plate, E = 29000 ksi, F_y is the yield strength of the plate and k_v is the coefficient that takes different values based on the type of stiffeners provided in the web plate

Considering Cv = 1.0 and since we do not have any transverse stiffeners we can take k_v = 5.0, substituting the following into the above equation, we get the value of the parameter h.

For t_w = 0.1875 inches (the thin plates should have a thickness not less than 3/16 inches to ensure the thin plates do not tear during the development of the tension field) , E = 29000 ksi and F_y = 36 ksi, the value of h obtained was h ≤ 13.1 inches. The width of each thin plate surrounding the central web plate was taken to be 13 inches.

The shear capacity of one such thin plate was calculated using the following equation:

$$V_n = 0.6\, F_y A_w \ldots\ldots\ldots\ldots\ldots\ldots\ldots\ldots\ldots\ldots\ldots\ldots\ldots\ldots\ldots\ldots\ldots\ldots\ldots\ldots\ldots\ldots\ldots\ldots\ldots\ldots\ldots\ldots Eqn.(32)$$

where V_n is the shear capacity and A_w is the cross sectional area of the web plate. Substituting the values the shear capacity of one thin plate was found to be 52.65 kips. To resist a cumulative shear of 260 kips at the first story level, five thin plates would be required.

The resulting designing includes VBE's that are W14x145 sections and the HBE is W18x119 using the provisions in AISC 360-10 (AISC 2010). The thin plates are 3/16 inches in thickness as seen in the Figure 5-3. The central web plate was sized to satisfy drift limits and required a thickness of 0.1875 inches (3/16 in). The maximum allowable drift including the displacement amplification factor for the one story shear wall is 2.88 inches and the drift for this approach was also within the allowable limit.

Although this design approach appeared to provide the desired tunability, this approach was not pursued further because of concerns related to buckling and tearing of the thin perimeter plates.

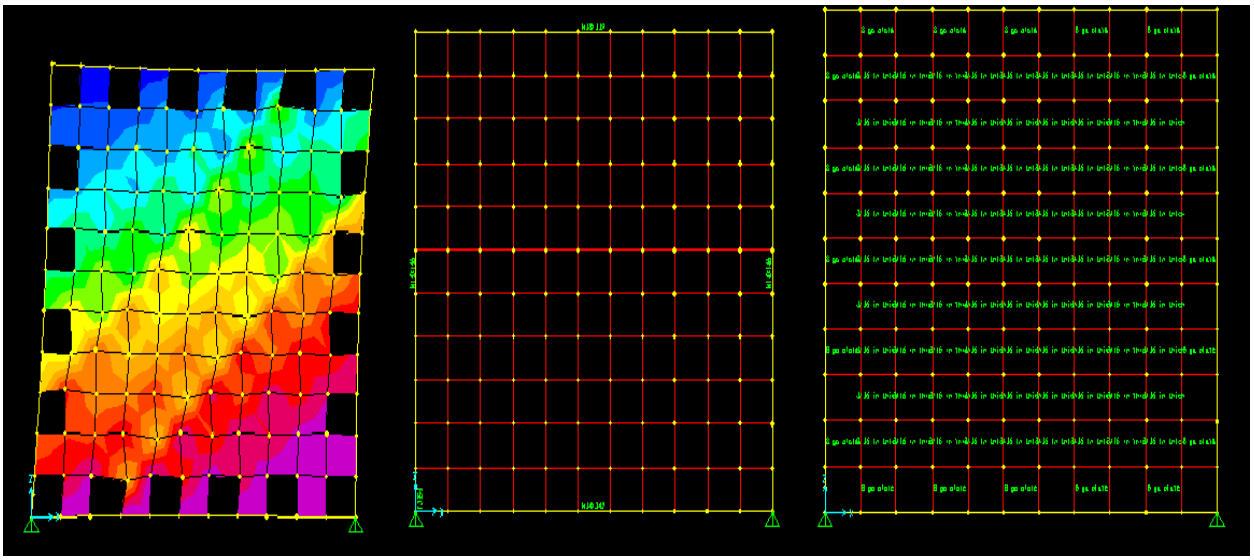

Figure 5-3 Deformed shape and HBE and VBE sections and plate thickness of a SPSW model in SAP2000 with thin fish plates around a thicker web plate

5.3 New Ideas – SPSW with Perforated Panels

Launching from the lessons learned in the previous section, additional approaches were attempted using perforated SPSW. The introduction of perforations into the web plate reduces the strength of the plate while the stiffness remains largely the same. In a drift controlled SPSW, perforations can be used to reduce the forces on the boundary elements while retaining the required stiffness. This section gives a description of these approaches. The work by researchers like Roberts and Sabouri-Ghomi (Roberts and Sabouri-Ghomi, 1992), Vian and Bruneau (Vian and Bruneau, 2005) has provided a good understanding of the behavior of perforated SPSW.

However, in those studies, the perforations were circular holes distributed in a uniform pattern over the entire web plate. New configurations of perforations were investigated and are described below.

The approaches investigated in the following sections were studies using the Finite element software ABAQUS 6.10 (Simulia 2010). The shell element modeling techniques which were validated in Chapter 3 have been used to model the SPSWs. This was done to capture the buckling and yielding behavior of the SPSW better which would not be possible with the two dimensional elastic models used for the previous approaches.

5.3.1 Circular Perforations along the Plate Diagonal

This approach consists of circular perforations oriented along the diagonals of the web panel. The concept was to create short axial yielding links between the perforations to control the strength of the panel. The stiffness of the panel is not significantly reduced by the introduction of these perforations.

The investigated configuration included circular perforations, 9 inches in diameter along the diagonals of the web panel. The perforations were of the same diameter. The VBE were W14x145 sections and the HBE were W18x65 sections. The web plate was 3/16 inches. The spacing of the holes was 4.5 inches. The boundary elements were specified to be made of Gr. 50 steel and the web plate was specified to be made of A36 steel. The flanges of the HBE have been coped out to simulate simple beam-to-column connections. The FE model of the SPSW with this configuration of holes was developed in ABAQUS 6.10 and subjected to a cyclic displacement history and the hysteresis behavior was studied.

Figure 5-4(b) shows the resulting load-deformation behavior obtained from ABAQUS. It was observed that the hysteresis behavior of the SPSW was stable with some pinching. The yielding was concentrated around the perforations as seen from the Figure 5-4 (a) and was found to be more severe at the holes nearer the middle of the plate. The approach appears to provide an efficient method for separately tuning strength and stiffness. However, it was concluded that the ductility demands on the links near the middle of the plate were high and there was not a good way to tune the ductility demands.

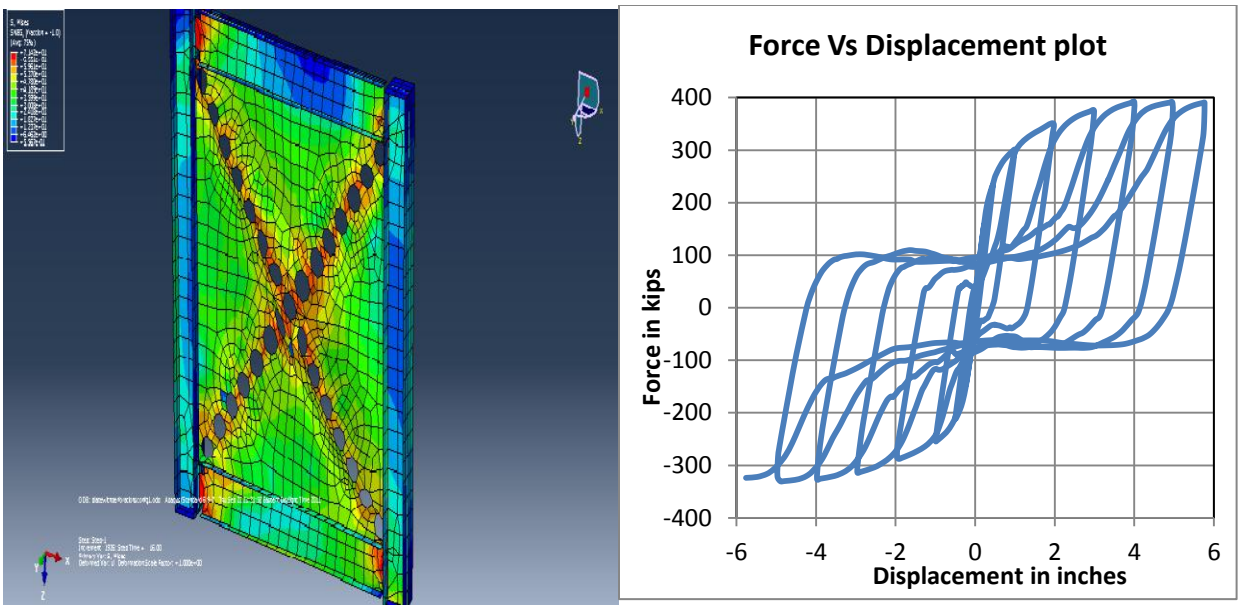

(a) (b)

Figure 5-4 (a) Deformed Shape with Von Mises stress distribution of SPSW with circular holes along the diagonals of the web panel as rendered in ABAQUS 6.10, (b) Hysteresis behavior

5.3.2 Circular Holes of Decreasing Diameter along the Plate Diagonal

Here the diameter of the circular holes was decreased from 18 inches as we moved from the center of the plate to 1.5 inches at the plate boundaries along the diagonal. The properties and the modeling techniques for this SPSW were similar to the previous approach. The concept was to add another variable (variation in hole diameter) to allow the ductility demands to be controlled. Since the major concentration of yielding was at the center of the plate, larger diameter perforations result in longer links and reduced local ductility demands on the steel material. Similar loading and boundary conditions were used as the previous section to maintain consistency and allow comparison. Figure 5-5 shows the layout of the perforations on the web panel of the SPSW. It is seen that the hysteresis behavior is quite similar to that of the panel with constant hole diameter. However, the peak strains in the links near the center of the plate are reduced.

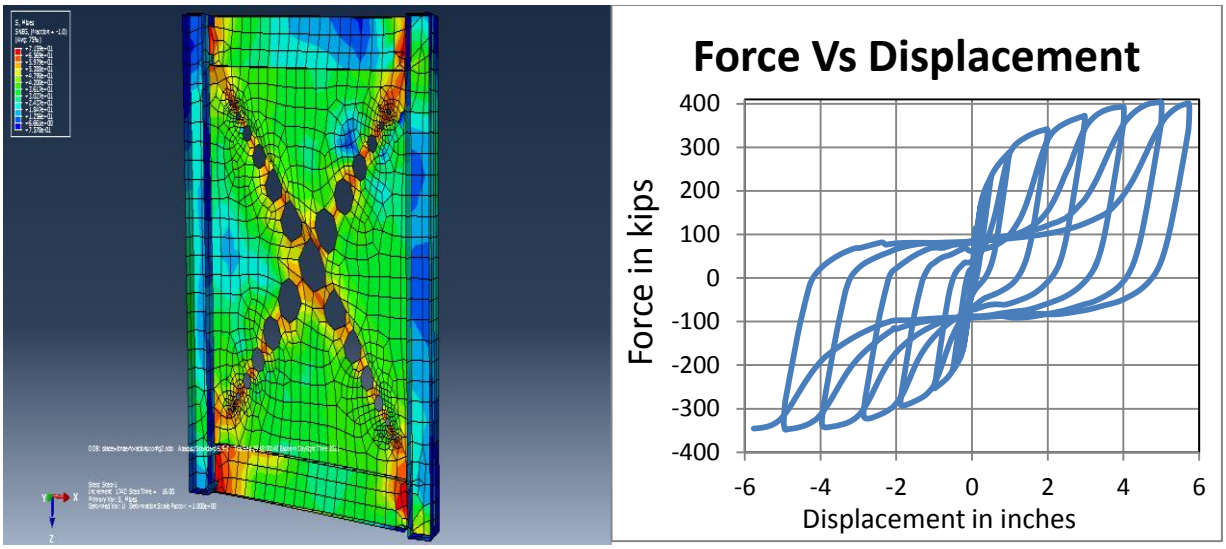

(a) (b)

Figure 5-5 (a) Deformed Shape with Von Mises stress distribution of SPSW with circular holes of decreasing diameter along the diagonals of the web panel as rendered in ABAQUS 6.10, (b) Hysteresis behavior

5.3.3 Circular Holes along the Perimeter of the Web Panel

Although the approaches using diagonal holes produced stable hysteretic behavior and the ability to tune strength, stiffness, and ductility demands, they exhibited a load-deformation behavior that was highly pinched. It was desired to investigate hole patterns that produced more full hysteretic shape. This approach examined in this section includes circular perforations along the perimeter of the web plate as shown in Figure 5-6 .The concept was to create a yielding mechanism based on shear rather than tension.

The finite element model for the web panel was modeled in ABAQUS 6.10 and is shown in the Figure 5-7. The panel was subjected to monotonic and cyclic displacement history. The SPSW was modeled with frame elements for HBE and VBE instead of full beams and columns as in the other models. The frame elements are modeled as 2D beam elements and given the properties of the wide flange sections. The frame elements are connected to the web panel by using tie constraints. The HBE to VBE connection is a simple connection and not moment resistant. This was achieved by releasing the moments at two nodes at the ends of the beams and columns using coupling constraints. Slits are included at the four corners of the SPSW between the corner hole

and the edge of the plate to avoid stress concentrations associated with rotations of the beam relative to the column.

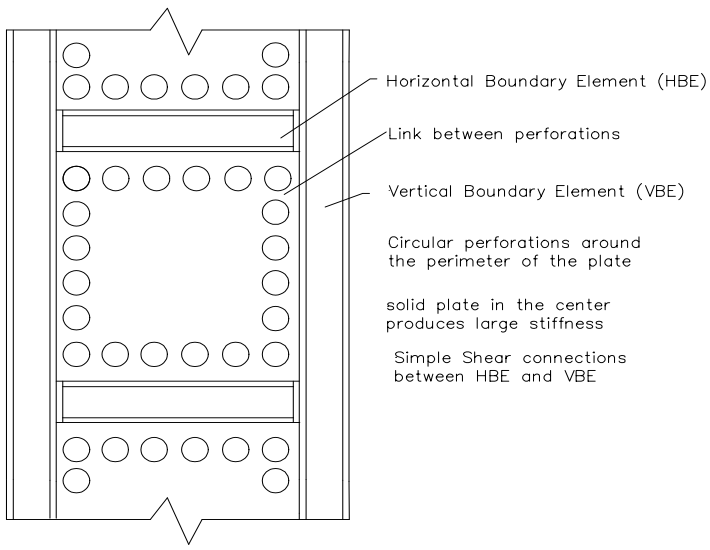

Figure 5-6 Figure showing the typical layout of circular perforations along the perimeter

The deformed shape of the model at 2.8% drift is shown in Figure 5-7(a) with Von Mises stresses. The tension diagonal is clearly visible in the Figure 5-7(a) and the concentration of yielding is along the tension diagonal and around the circular holes. There is very little strength degradation. The boundary elements were designed using the forces on the members obtained from the analysis in ABAQUS 6.10. Figure 5-8 shows the forces on the HBE and VBE due to each of the links. They were obtained by making free body cuts in the middle of the link and the component and resultant forces were obtained at the centroid of the cut. The average of all these forces were taken and divided by the link length to obtain the uniformly distributed load acting on the BE's due to the shear in the plate. The force used to design the HBE and VBE are F_{11} = 1.96 kips/in, F_{22} = 2.37 kips/in, F_{12} = 2.20 kips/in and F_{21} = 2.50 kips/in. These values are lesser when compared to those for a solid web plate [F_{11} = 3.74 kips/in, F_{22} = 2.77 kips/in, F_{12} = 3.22 kips/in and F_{21} = 3.22 kips/in] and hence the demand on the boundary elements for a web plate with circular perforations along the perimeter is lesser than that for a typical solid panel SPSW. The boundary elements are capacity designed using the same procedure described in the AISC 341-10 specifications.

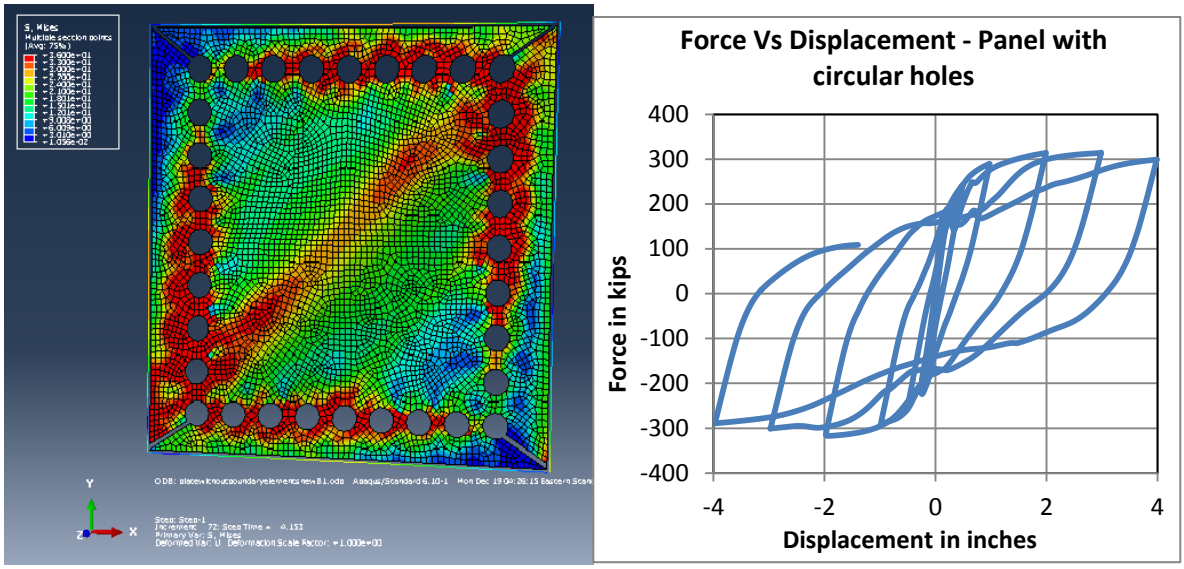

(a) (b)

Figure 5-7 (a) Deformed Shape with Von Mises Stress Distribution – Circular holes Along the perimeter, (b) Hysteresis behaviour - cyclic loading

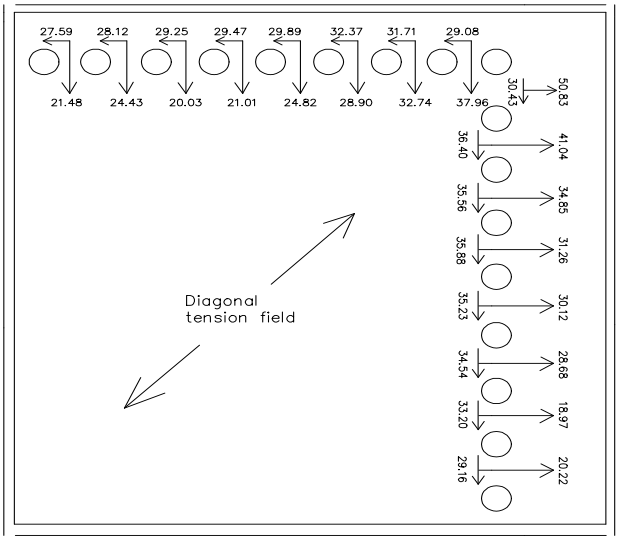

Figure 5-8 Figure showing the forces applied by the plate on the boundary elements on a SPSW with circular perforations along the perimeter of the web panel

The hysteresis beviour is relatively full compared to the diagonal perforations and exhibits little pinching in the absense of moment connections. The system stiffness is expected to be related to

plate thickness, while the strength and ductility might be tuned using the size and spacing of the perforations. These factors make the system a favorable option for further study.

5.3.4 Butterfly Shaped Cutouts along the Perimeter of the Web Panel

The final approach involves Butterfly shaped links along the perimeter of the plate as shown in the Figure 5-9. This panel draws from the work by Borchers et al (2010) in which plates were designed to have a plastic hinging mechanism at the quarter points of the butterfly link. Great ductility and energy dissipation was realized with these configurations.

The boundary elements are beam elements assigned with the properties of wide flange sections as in the previous approach. The connection between the HBE and VBE is a simple connection. The FE model for this configuration was developed in ABAQUS 6.10 and was subjected to cyclic and monotonic loading. The mesh size in the links was specified to be finer and in the plate region a coarse mesh was used as shown in Figure 5-10.

The FE model of the SPSW shows that the links are yielding completely. There is a high stress concentration in the links as seen from Figure 5-10. The forces on the boundary elements from the plate in each of the links are shown in Figure 5-11. Free body cuts are made at the mid height of the links and the force components are obtained at the centroid of the cut. These forces are used to design the BE in an iterative process. The uniformly distributed load on the columns and the beams are obtained by taking the average of all the forces and dividing by the length of the link. The force used to design the HBE and VBE are F_{11} = 1.96 kips/in, F_{22} = 1.86 kips/in, F_{12} = 2.48 kips/in and F_{21} = 2.35 kips/in. These values are lesser when compared to those for a solid web plate of equal strength [F_{11} = 3.74 kips/in, F_{22} = 2.77 kips/in, F_{12} = 3.22 kips/in and F_{21} = 3.22 kips/in] and hence the demand on the boundary elements for a web plate with circular perforations along the perimeter is lower than that for a typical solid panel SPSW.

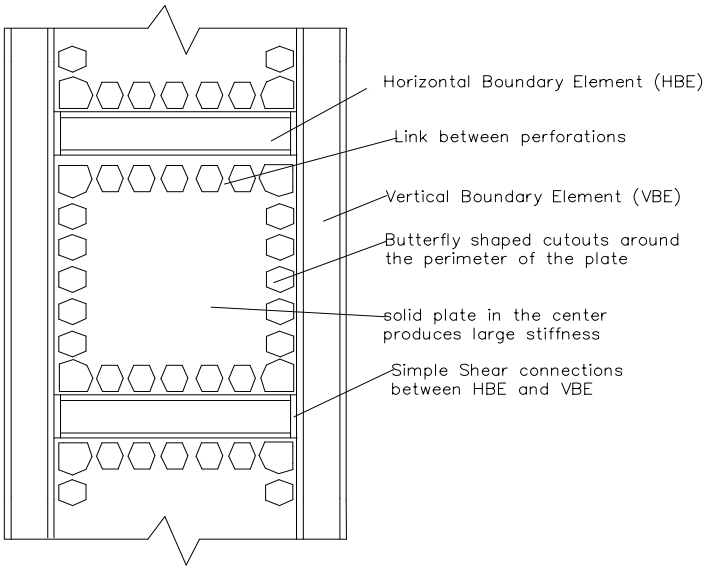

Figure 5-9 Typical layout of Butterfly shaped cutouts along the perimeter of the web panel

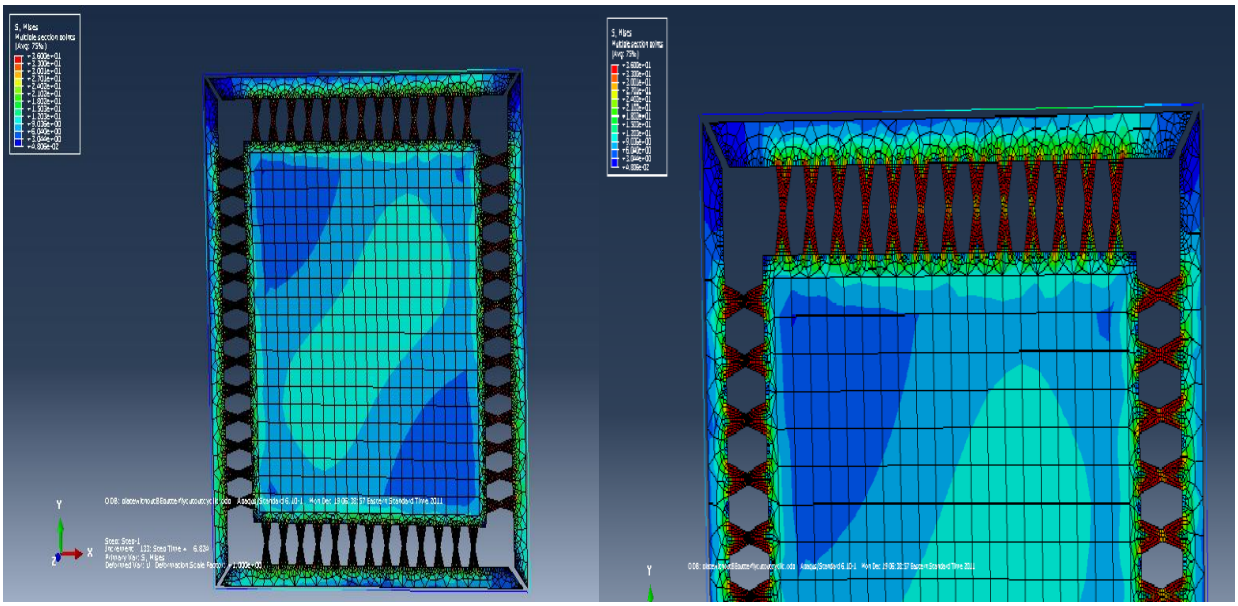

(a) (b)

Figure 5-10 (a) Deformed Shape with Von Mises Stress Distribution – Butterfly shaped cut outs along the perimeter of the web panel, (b) Figure showing the fine mesh in the links and coarse mesh in the plate and the BE

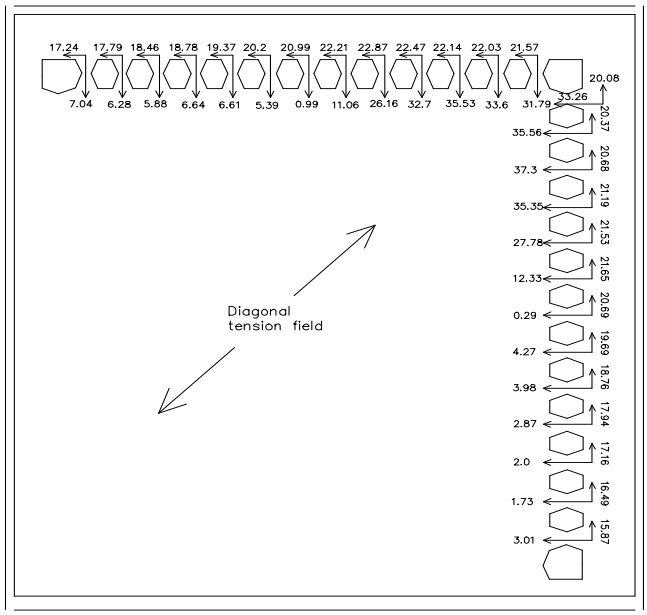

Figure 5-11 Figure showing the forces exerted by each link on the boundary elements in a SPSW with butterfly shaped cutouts

The Force versus Displacement plots for monotonic and cyclic loading are shown below.

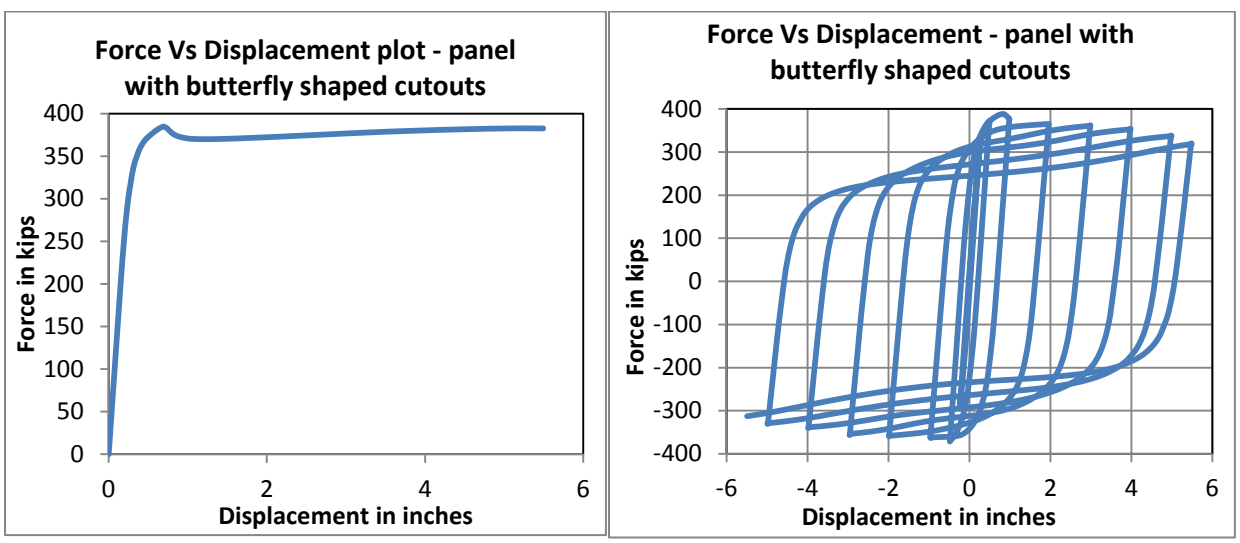

(a) (b)

Figure 5-12 (a) Force Vs Displacement plot for monotonic loading for a SPSW with butterfly shaped cutouts, (b) Hysteresis behavior

The strength of the plate is calculated using the equation: (Borchers et al, 2010)

$$V_{fp} = \frac{4b^2 t}{9L}\, n\, F_{yp} \ldots\ldots\ldots\ldots\ldots\ldots\ldots\ldots\ldots\ldots\ldots\ldots \; Eqn.\,(33)$$

The equation is derived based on an assumed mechanism of plastic hinging at the quarter points of the link assuming reversed shear loading. Actual loading of the links may be different here due to net axial forces in some links. From Figure 5-12 (b) it is seen that there is absolutely no pinching of the hysteresis loop and there is an excellent energy dissipation capacity. There is a slight degradation in strength. The stiffness of the wall is expected to be controlled by the thickness of the plate while the strength and ductility of the system could be related to the geometry and number of links. This is another favorable approach that deserves further study.

5.4 Comparison of Two of the New Approaches with Conventional SPSW Design

Examining the seven approaches described in this chapter helped identify two approaches that allow the strength, stiffness, and ductility to be separately tuned, and also provided favorable hysteretic behavior. In this section, a brief comparison is made between the two selected approaches and the two types of configurations included in the current U.S. building code.

The four walls are designed to have approximately the same shear strength. Each of the four walls is designed for a capacity of 260 kips and is meant to represent the first story of the prototype six story building described at the beginning of the previous chapter. The four designs are as follows:

1) Solid panel with moment connections between the HBE and the VBE
2) Perforated panel with moment connections between the HBE and VBE
3) Panel with circular holes along the perimeter of the plate with simple shear connections between the HBE and VBE
4) Panel with butterfly shaped cutouts along the perimeter of the plate with simple shear connections between the HBE and VBE

The details of the FE models in ABAQUS 6.10 for the four designs are described here. The web plate was a 12ft x 12ft panel. Columns were restrained in all the degrees of freedom except for the out of plane rotation at the bottom. The HBE and VBE were frame elements with properties

of wide flange sections assigned to them. Coupling constraints were defined between the nodes connecting the HBE to VBE allowing definition of the connection between the HBE and VBE to be either moment resistant or simple connection. Tie constraints were defined between the edges of the plate to the boundary elements to ensure they behave as a single unit. Cyclic and monotonic quasi static loading was applied as a displacement history along the top flange of the beam.

The design for the solid panel and perforated panel with moment connections were obtained using the requirements of the AISC Seismic provisions (AISC 2010). The design of the HBE and VBE for the proposed configurations with circular and butterfly links around the perimeter is summarized in the Sections 5.3.3 and 5.3.4. The forces on the BE are also given. The web plate is designed for the shear force at the story level. For the solid panel Eqn. 8 from the literature review section was used. For the plate with staggered holes, Eqn. 6 was used with the D/S ratio multiplied by a factor of 0.7 (Purba and Bruneau, 2007). For the plate with circular holes along the perimeter of the panel, Eqn. 8 from the literature review section was used again with the L_{cf} calculated by subtracting the number of holes times the diameter of one hole from the width of the plate (144 - 9x9 = 63inches), for the panel with butterfly cutouts the Eqn. 33 was used. The shear capacity from ABAQUS 6.10 was calculated from the force-displacement plots that were obtained after a monotonic loading of the SPSWs. These are very preliminary methods for selecting the plate and boundary element section. They were used here only to provide a basic check to know whether the proposed design approaches have the potential to be studied further. Further investigation would be required to develop and verify reliable design methods.

The ABAQUS 6.10 models of the solid and the staggered holes panel with their monotonic force deformation plots are shows in Figure 5-13 and Figure 5-14.

The design of the web panel and boundary elements for the four design approaches is compared in Table 5-1. Included are a comparison of shear capacity, web plate thickness, and sizes of the boundary elements.

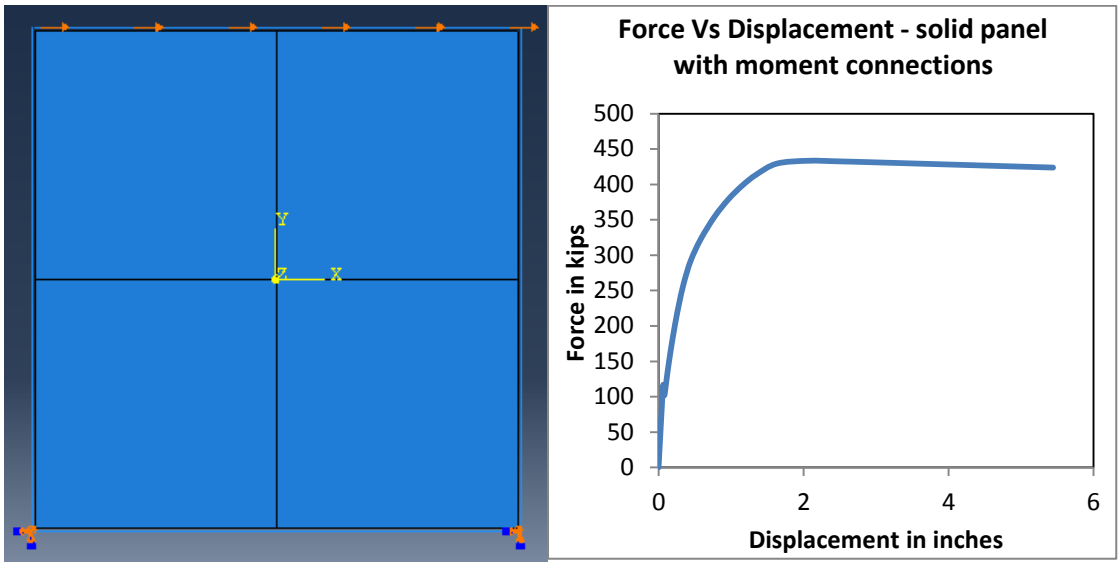

(a) (b)

Figure 5-13 (a) FE model of SPSW with a solid panel with moment connections in Abaqus 6.10, (b) Force-Displacement curve for monotonic loading

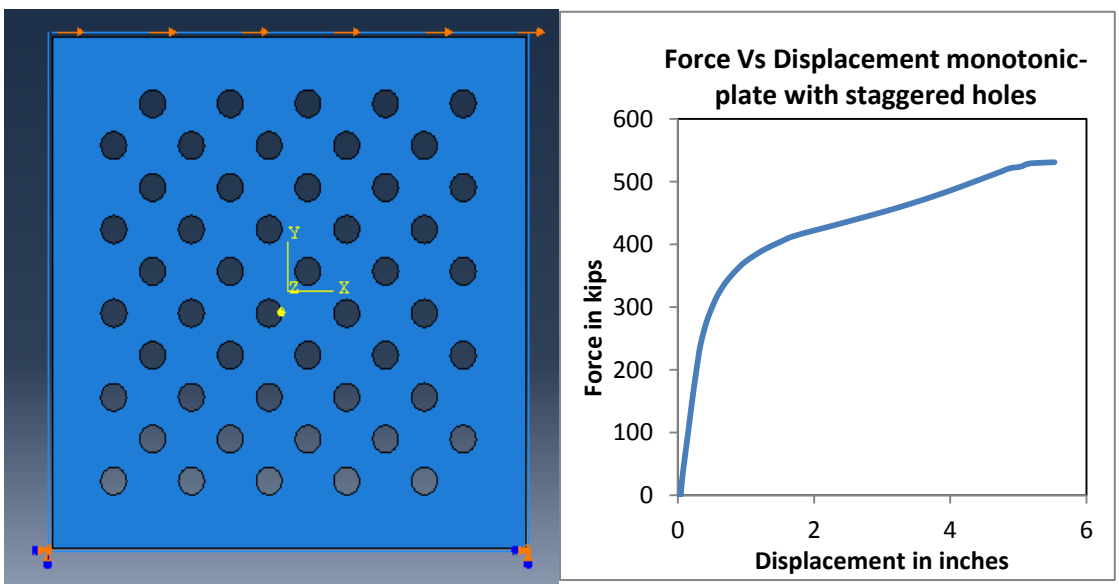

(a) (b)

Figure 5-14 (a) FE model of SPSW with a solid panel with moment connections in Abaqus 6.10, (b) Force-Displacement curve for monotonic loading

Table 5-1 Comparison of New Approaches and Conventional SPSW Design

Configuration	Plate Thickness (in)	HBE section	VBE section	Shear Capacity of plate from ABAQUS (kips)	Capacity of plate from AISC design equations (kips)
Conventional Solid panel with moment connections	7 gauge 0.1793 in	W18x130	W14x233	424	283
Conventional Perforated panel with moment connections	1/4 in 0.25 in	W18x143	W14x257	400	291
New Approach with circular holes and pinned connections	5/16 in 0.3125 in	W18x71	W14x99	323	264
New Approach with butterfly cutouts and pinned connections	3/4 in 0.75 in	W18x86	W14x109	375	263

Since the stiffness of the SPSW is related to the web plate thickness, it was observed that the plate thickness increased for the new approaches in which moment connections were eliminated. Although the design strength of the SPSW was 260 kips, the conventional approaches with moment connections between beam and columns produced significantly higher shear yield capacity. The new approaches allowed the strength and stiffness to be tuned separately and the observed strength was better controlled and closer to the design strength. The boundary elements selected using the preliminary design procedures were dramatically smaller for the new approaches. Furthermore the hysteretic behavior of the two new approaches is significantly better than the typical SPSW as shown in the previous section. Because of the tunability, reduced steel weight, elimination of moment connections and improved energy dissipation, the proposed approaches are considered promising and deserve further study.

Chapter 6. PARAMETRIC STUDY

Two design approaches have shown the most promise for allowing tunability and improved response. Although the initial attempts at producing more efficient SPSW presented in Chapter 4 were intended for moderate seismic zones, the selected design approaches have the potential to offer significant advantage for high seismic design as well. The investigation in the previous chapter included one configuration of each of the two proposed design approaches. It is conjectured that strength, stiffness and energy dissipation might be tunable by adjusting the perforation spacing and size. To test the tunability and further check the viability of the two proposed design approaches a parametric study is conducted.

The parametric study uses FE models in ABAQUS 6.10. The SPSW models consist of the web panels made of shell elements and boundary elements which are frame elements (beam elements). The frame elements are tied to the web panel using tie constraints. This reduces the number of shell elements drastically in comparison with a full scale model and also reduces the run time for the analysis. Furthermore, the use of beam elements allows easier definition of a truly pinned connection between the beams and columns.

The models consist of a single SPSW panel with cyclic horizontal displacement history applied at the top. The boundary elements are fully elastic. Realistic beam and column sections are assigned to the frame elements to simulate potential actual SPSW configurations. The SPSWs are 12ft x 12ft models. The displacement history consists of a sine wave distribution of displacement values ranging from 0.25 inches to 5.5 inches which is a maximum drift of 3.8% drift.

6.1 Application of Initial Imperfections and Mesh Size Selection

The initial imperfections due to manufacturing processes are simulated in ABAQUS 6.10 by applying a constant out of plane pressure load. The out-of-straightness tolerance for new construction as given in the AISC code of standard practice (AISC 2010) is L/1000. The goal is to apply this amount of out of straightness in the model to simulate the expected worst case for new construction. The values of the pressure loads required to obtain an imperfection of L/1000

are calculated for a solid plate by a trial and error method in ABAQUS 6.10. The same value of pressure load is used for all of the perforated plates without recalibrating the out of plane pressure. It is seen from Table 6-1 that there is a slight variation in the out of plane deformation from the value of L/1000. The values of pressure load for different plate thicknesses used in the parametric study are summarized in Table 6-1 below.

Table 6-1 Values of Pressure load applied to the plate to simulate the Out of plane deformations

Thickness of plate inches	Applied pressure ksi	Applied pressure psf	δ_{ini} Abaqus inches	Out of plane Straightness inches	Recommended Out of Plane Straightness (L/1000 in)
0.1875	9.03E-06	1.3	0.141	L/1021	0.144
0.25	1.39E-05	2	0.141	L/1021	0.144
0.375	2.78E-05	4	0.143	L/1007	0.144
0.5	4.51E-05	6.5	0.14	L/1028	0.144
0.75	9.03E-05	13	0.144	L/1000	0.144

Beyond the selection of an out-of-plane pressure to produce the target out-of-straightness, it was desired to investigate the sensitivity of the load-deformation behavior (including yield strength) to the value of the pressure load. This was studied by applying a range of out-of-plane pressure loads on a 3/16 inch thick plate between 1 psf to 10 psf. It was found that the out of plane pressure did not result in a significant difference in the value of the yield strength of the plate. For pressures ranging from 1psf to 10 psf, the yield strength of the plate remained constant at 500 kips. This is seen from the Table 6-2 below. This is also seen from the Figure 6-1.

Table 6-2 Values of yield strength of the plate for varying values of pressure load applied

Applied pressure ksi	Applied pressure psf	δ_{ini} abaqus inches	δ_{final} abaqus inches	Out of Straightness inches
6.94E-06	1	0.11	8.38	L/1309
1.04E-05	1.5	0.1616	8.38	L/891
1.39E-05	2	0.2102	8.4	L/685
2.08E-05	3	0.296	8.33	L/486
6.94E-05	10	0.688	8.24	L/209

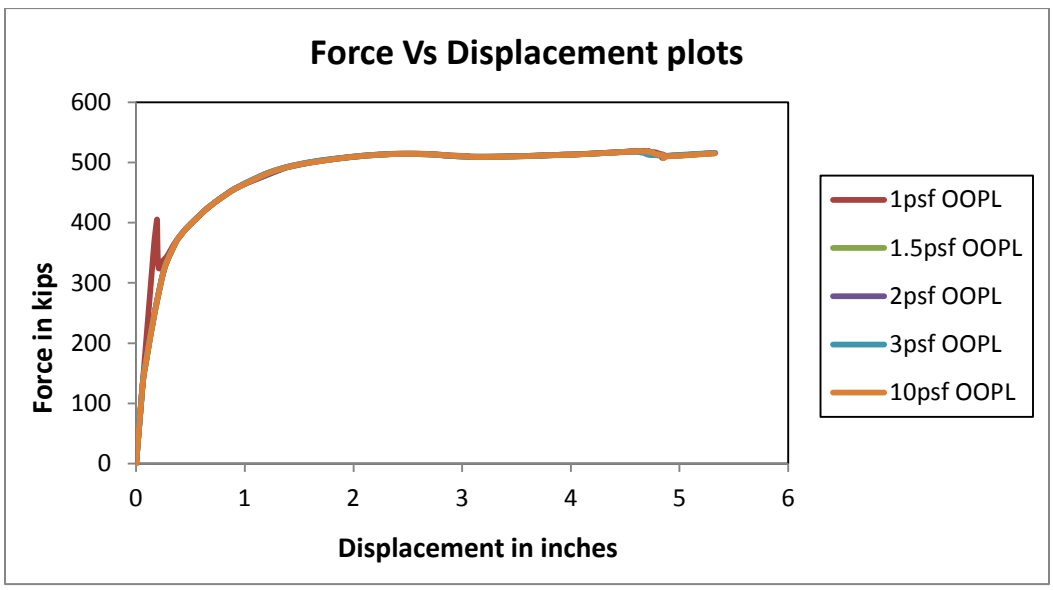

Figure 6-1 Force Vs Displacement plot for different values of out of plane pressure loads on the plate

In order to verify the sensitivity of the results to the mesh size, different mesh sizes were tested. A coarser mesh with 2.5-8 seeding and a finer mesh with 1.75-6 seeding were used and the variation of the output parameters was examined. It was found that there was little variation in the values obtained for the coarse and fine mesh sizes. Figure 6-3 shows that there is not much variation in the force – displacement hysteresis plot for a coarser and a finer mesh size. It is seen

from Table 6-4 that there is less than 0.5% difference in the values of initial imperfection and 1.5% difference in the values of the maximum out of plane deformation at the end of the displacement history. Since the maximum equivalent plastic strain (PEEQ) values are found to be highly mesh size dependent, these values are recorded but not compared between models. Because there was little difference between the results, mesh seeding of 2.5-8 corresponding to the coarser mesh is used for the entire parametric study. Coarser and finer mesh sizes used in the mesh sensitivity study are shown in Figure 6-2.

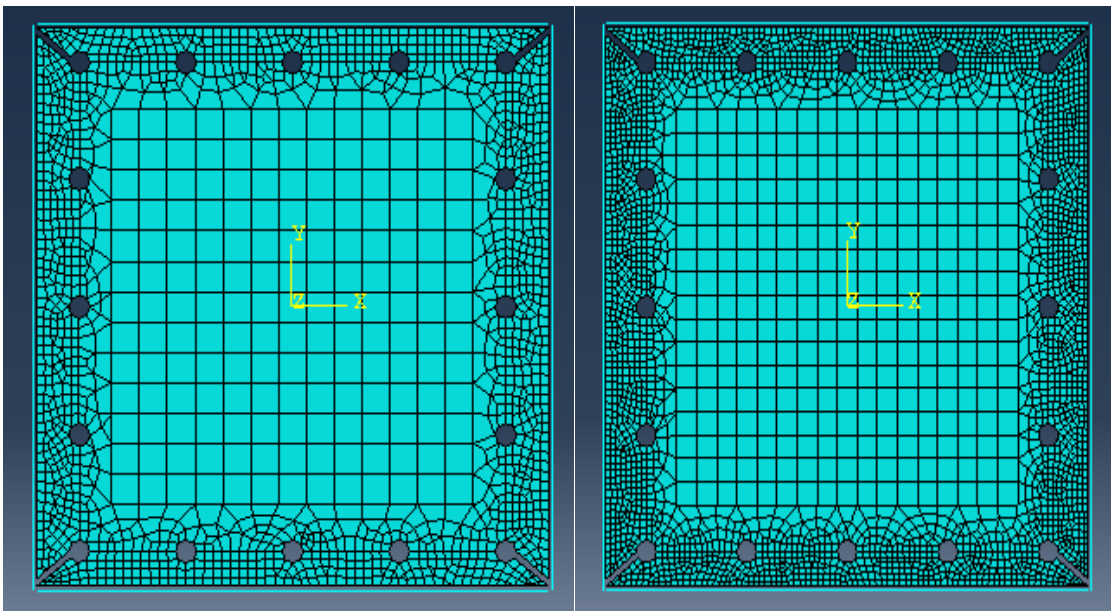

(a) (b)

Figure 6-2 (a) FE model of SPSW with coarser mesh (2.5-8), (b) FE model of SPSW with finer mesh (1.75-6)

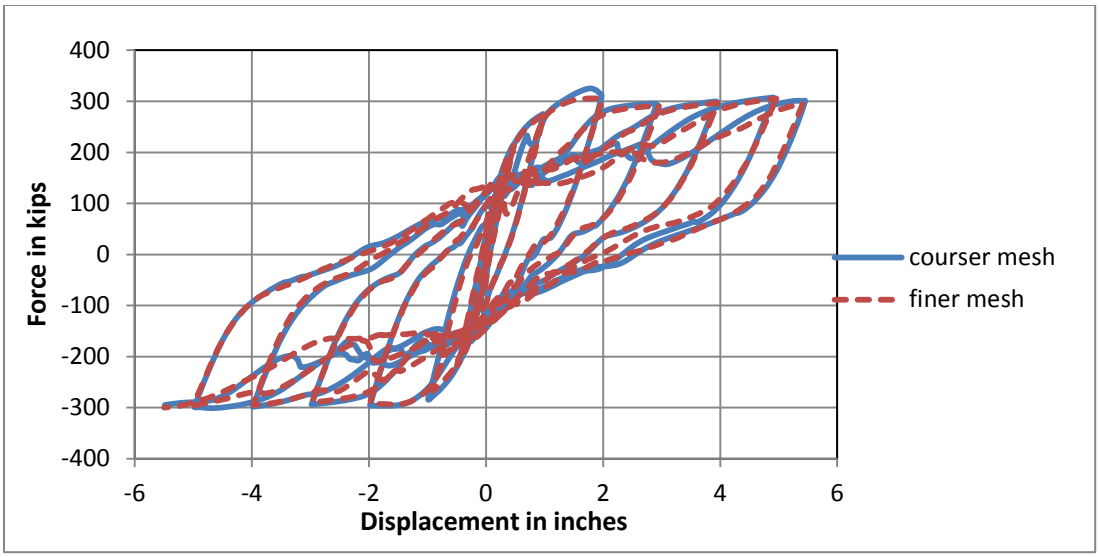

Figure 6-3 Force Vs Displacement plot for a coarser and a finer mesh

Table 6-3 Values of input parameters for comparison of a coarse and a finer mesh size in Abaqus models

Plate name	Mesh Seeding size	Plate thickness (inches)	Spacing of the holes (inches)	Perforation diameter D (inches)
Coarser	2.5-8	0.1875	24	6
Finer	1.75-6	0.1875	24	6

Table 6-4 Values of the output parameters for comparison of a course and finer mesh in Abaqus models

Plate name	Strength of wall Abaqus V_{abq} kips	Stiffness of wall Abaqus kips/in.	Energy dissipation of panel kips-in.	Max PEEQ	Max OOPD at end of cyclic disp. history inches	Initial OOPD inches
Coarser	200	645	1982	0.25	9.2	0.22
Finer	200	600	1791	0.46	9.3	0.22

6.1 Parametric Study Plan

As a part of the parametric study, two configurations of cutouts namely the perimeter circular holes and perimeter butterfly shaped cutouts are studied. A FE analysis was performed on a total of 40 FE models. The study performed on both these cutout configurations are explained in the following sections.

6.1.1 Perimeter Circular Hole Configuration

A total of 30 models were created to study the perimeter circular hole configuration. The study was broken into two parts. The thickness of the web panels was kept constant in the first twenty models to allow a more thorough investigation of hole size and spacing. A thickness of 3/8 inch was selected to represent a possible typical thickness. The D/S (diameter/spacing) ratio was varied from 0.2 to 0.8 with an interval of 0.2. This gave different values of spacing between the holes for diameters of holes varying from 6 inches to 18 inches with a 3 inch interval.

The second part of the study consisted of ten models, with web panel thickness varying from 3/16 inch to ¾ inch. The D/S ratio was kept constant at 0.6 for two values of hole diameters of 9 and 15 inches. The input and the output parameters recorded in the parametric study tables for circular holes around the perimeter of the panel are summarized below.

Input parameters:

- Thickness of the web panel
- Perforation ratio, D/S (where D is the hole diameter and S is the hole center to center spacing)
- D/H ratio (where D is the hole diameter and H is the length of one side of the square web panel)

Output parameters:

- Expected strength of the panel using the equation for solid and perforated panels from the AISC 360-10 specifications for SPSWs.
- Strength of the panel obtained from FEM results

- Stiffness of the panel
- Maximum equivalent plastic strain of the panel (PEEQ)
- Length of cut to be made on the panel (L_{cut})
- Cost of cutting
- Openness of the panel
- Energy dissipation ratio (EDR) of the panel
- Maximum out of plane deformation at end of the applied displacement history (OOPD)
- Initial imperfection in the web panel

The Table 6-5 gives a summary of the model details with the geometry in the form of input parameters used for the first 20 models in the parametric study.

Table 6-5 Geometry and input parameters for the first set of 20 models for perimeter circular holes with varying size and diameter

Plate Name	Thickness of Plate t inches	Clear Spacing between Holes (inches)	Perforation Diameter D inches	Perforation Ratio D/S	Input Parameter D/H
C1	0.375	24	6	0.2	0.04
C2	0.375	9	6	0.4	0.04
C3	0.375	4	6	0.6	0.04
C4	0.375	1.50	6	0.8	0.04
C5	0.375	36	9	0.2	0.06
C6	0.375	13.5	9	0.4	0.06
C7	0.375	6	9	0.6	0.06
C8	0.375	2.25	9	0.8	0.06
C9	0.375	48	12	0.2	0.08
C10	0.375	18	12	0.4	0.08
C11	0.375	8	12	0.6	0.08
C12	0.375	3	12	0.8	0.08
C13	0.375	60	15	0.2	0.10
C14	0.375	22.5	15	0.4	0.10
C15	0.375	10	15	0.6	0.10
C16	0.375	3.75	15	0.8	0.10
C17	0.375	72	18	0.2	0.13
C18	0.375	27	18	0.4	0.13
C19	0.375	12	18	0.6	0.13
C20	0.375	4.5	18	0.8	0.13

Table 6-6 gives the geometry and input parameters used in the parametric study for the next set of 10 models with perimeter circular holes configuration with varying thickness.

Table 6-6 Geometry and input parameters for the set of 10 models for perimeter circular holes with varying thickness

Plate Name	Thickness of Plate t inches	Clear Spacing between Holes inches	Perforation Diameter D inches	Perforation Ratio D/S	Parameter #1 D/H	Parameter #2 H/t
A1	0.1875	6	9	0.6	0.06	768
B1	0.25	6	9	0.6	0.06	576
C7 = C1	0.375	6	9	0.6	0.06	384
D1	0.5	6	9	0.6	0.06	288
E1	0.75	6	9	0.6	0.06	192
A2	0.1875	10	15	0.6	0.10	768
B2	0.25	10	15	0.6	0.10	576
C15 = C2	0.375	10	15	0.6	0.10	384
D2	0.5	10	15	0.6	0.10	288
E2	0.75	10	15	0.6	0.10	192

6.1.2 Butterfly Shaped Cutouts along the Perimeter of the Web Panel

A total of ten models were used for this configuration of cutouts. The thicknesses of the web plate used were 0.1875, 0.25, 0.375, 0.5 and 0.75 inches. Two cutout geometries were considered to produce a weak and a strong SPSW. The width and the spacing of the butterfly cutout were varied slightly to obtain these configurations. The input and the output parameters used in this study are the same as that for the circular holes configuration. A typical layout of the strong and weak configurations of the butterfly shaped cutout is shown in the Figure 6-4.

Table 6-7 gives the geometry and the input parameters of the 10 models with butterfly shaped cutouts with varying thickness used for the parametric study.

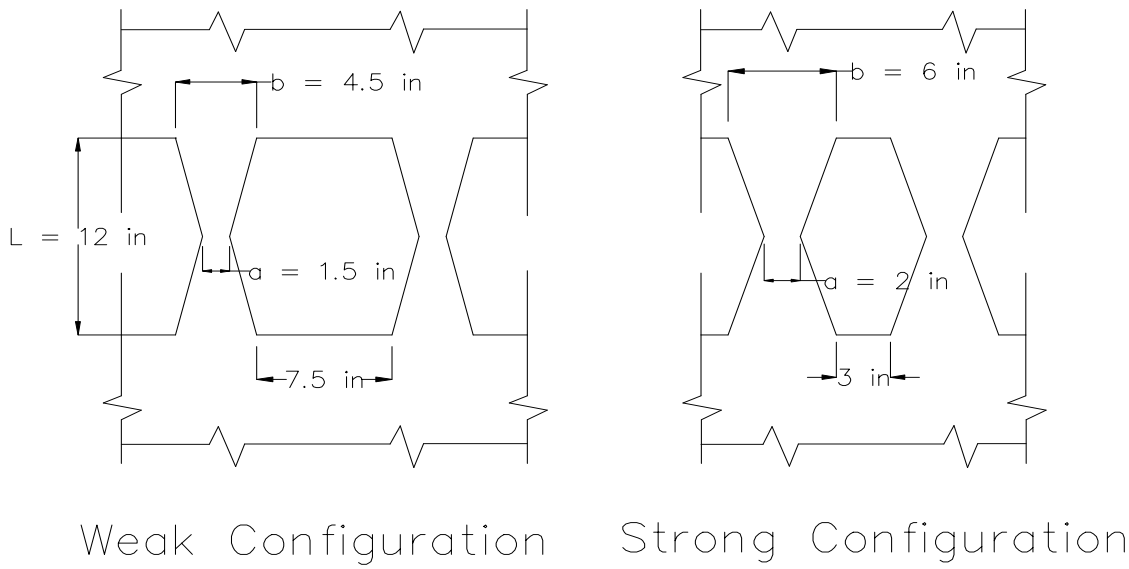

Figure 6-4 Typical layout of the weak and strong configurations of the butterfly shaped cutout

Table 6-7 Geometry and input parameters of set of 10 models with butterfly shaped links for varying plate thickness

Plate Name	Thickness of Plate t inches	Spacing of the Cutouts S inches	Cutout Width D inches	B with L = 12 in inches	Perforation Ratio D/S	Input Parameter #1 H/t	Input Parameter #2 D/t
A3	0.1875	2	7	6	3.5	768	37.33
B3	0.25	2	7	6	3.5	576	28.00
C3bf	0.375	2	7	6	3.5	384	18.67
D3	0.5	2	7	6	3.5	288	14.00
E3	0.75	2	7	6	3.5	192	9.33
A4	0.1875	1.5	10.5	4.5	7	768	37.33
B4	0.25	1.5	10.5	4.5	7	576	28.00
C4bf	0.375	1.5	10.5	4.5	7	384	18.67
D4	0.5	1.5	10.5	4.5	7	288	14.00
E4	0.75	1.5	10.5	4.5	7	192	9.33

6.1.3 Input Parameters

A brief explanation of each of the input parameters and the method used to record them is given below.

6.1.3.1 Thickness of the Web Plate

The thickness of the web plate for the parametric study is varied from 3/16 inch to 3/4 inch. This range is used to study the buckling and yielding behavior as the plate goes from thin to thick. Five values of thickness have been used: 0.1875, 0.25, 0.375, 0.5 and 0.75 inches.

6.1.3.2 Diameter of the Holes / Width of the Butterfly Cutout

This input parameter affects the strength, stiffness, length of cut and openness of the panel. The diameter of the hole in the circular hole configuration is varied from 6 to 18 inches in 3 inch increments. The width of the butterfly shaped cutouts used for the strong panel configuration is 7 inches and for the weak panel configuration is 10.5 inches. The strong panel configuration is the shear wall which has a shear strength of the panel ranging from 100 to 500 kips and the weak configuration shear wall has a shear strength of the panel ranging from 40 to 150 kips.

6.1.3.3 Spacing between the Perforations

This parameter is the key to determine the openness of the panel and affects strength and stiffness of the panel. This is because the diagonal tension field action or the shear yielding in the plate is developed between the perforations and the width of the strip for the governing action is determined by the spacing of these cutouts. The spacing between the perforations is determined for the circular holes configuration by the D/S ratio depending upon the diameter of the hole chosen for the wall. As the diameter is varied from 6 to 18 inches with 3 inch increments, the spacing also varies depending on the D/S ratio which is predefined to vary from 0.2 to 0.8 with an increment of 0.2. For the butterfly shaped cutouts the spacing for the strong configuration used is 2 inches (B = 6 inches) and for the weak configuration it is 1.5 inches (B = 4.5 inches).

6.1.3.4 Perforation Ratio

This is the parameter defined as the ratio of the diameter of the perforation to the spacing between the perforations. The perforation ratio (D/S) for circular holes along the perimeter of the shear wall is varied from 0.2 to 0.8 with an increment of 0.2. This range was used to study the behavior of walls with a small to a large perforation ratio. A D/S ratio for the butterfly shaped cutout has also been defined as the ratio of the width of the cutout at mid height of the cutout to the spacing at the mid height of the cutout.

6.1.4 Output Parameters

A brief explanation of each of the output parameters and the method used to record them is given below.

6.1.4.1 Expected Strength of the Web Plate of the SPSW

For the two configurations of cutouts – circular and butterfly shaped cutouts, the values of shear strengths of the web panel are recorded using the equations available in the current design aids. For the panels with circular holes along the perimeter, the equations for shear strength of a solid and perforated panel from the AISC specification (AISC 2010) are given by Equations 34 and 35 respectively. The terms in the equations have been explained in Chapter 2. Modifications to these equations have been done to incorporate the circular holes along the perimeter of the plate to calculate the shear strength. The $L_{cf}{}^{*}$ in Equation 34 is calculated by subtracting the number of holes times the diameter of each hole from the width of the plate and the angle α has been taken as 45 degree. The λ in Equation 35 is taken as 0.7 as specified in the code with the strength of the solid panel calculated using the Equation 34.

$$V_{exp} = 0.9 * 0.42\, F_y\, t_w\, L_{cf}{}^{*}\ \sin 2\alpha \ldots\ldots\ldots\ldots\ldots\ldots\ldots\ldots\ldots\ldots\ldots\ldots\ldots\ldots\ldots\ldots Eqn.(34)$$

$$V_{exp} = \left[1 - \lambda \left(\frac{D}{S_{diag}}\right)\right] V_{solid\ panel} \ldots\ldots\ldots\ldots\ldots\ldots\ldots\ldots\ldots\ldots\ldots\ldots\ldots\ldots\ldots\ldots Eqn.(35)$$

The following equation is used to determine the shear strength of the web panel with butterfly cutouts. The terms in the equation have been explained in Chapter 2.

$$V_{exp} = \frac{4\, b^2\, t}{9\, L}\, n\, F_y \ldots\ldots\ldots\ldots\ldots\ldots\ldots\ldots\ldots\ldots\ldots\ldots\ldots\ldots\ldots\ldots\ldots\ldots\ldots\ldots\ldots\ldots\ldots\ldots\ldots Eqn. (36)$$

6.1.4.2 Shear Strength of the Web Panel from Abaqus 6.10

The shear strengths of the web panel obtained from the above equations are compared with the values obtained from the force – deformation plots generated using the results from Abaqus 6.10 analysis for monotonic loading on the panels. The strength is calculated as the value at the intersection of two lines. The first line represents the initial stiffness and the second represents the final stiffness which is the plateau region of a very small slope. Conclusions about whether or not the existing equations in the current design codes could be used for the particular configuration of perforations are made from the results obtained in this comparison.

6.1.4.3 Stiffness of the Web Panel

The initial stiffness of the web panel is obtained from the initial slope of the force deformation plot obtained from the Abaqus analysis of the models subjected to a monotonic loading on the SPSW.

6.1.4.4 Maximum Equivalent Plastic Strain in the Panel

The value of the maximum equivalent plastic strain (PEEQ) in the panel at the end of the cyclic displacement history is recorded.

6.1.4.5 Length of Cutting in the Panel

This is calculated as the perimeter of the cutout times the number of cutouts in the panel. This value would be related to the cost of the panel. The length of cutting does not include the perimeter of the plate.

6.1.4.6 Cost of Cutting

This is calculated as the cost of cutting per length of cutting per thickness of the plate multiplied by the length of cutting in the plate times the thickness of the plate. The cost of cutting was obtained for a 3 ft x 3 ft panel with a different pattern of cutouts. The cost obtained was specified for the highest quality of cutting (Quality = 5) and water jet cutting from the vendor. This is an approximate estimation and has been rounded off to the nearest integer value. The cost of cutting obtained for the sample panel from the vendor was $2.40 per inch of cutting per inch of thickness.

6.1.4.7 Openness of the Panel

This parameter is calculated as the ratio of the cutout area in the panel to the area of the solid panel. The cutout area is calculated as the area of each cutout times the number of cutouts in the panel. The openness gives a sense of the amount of material used compared to a solid plate of similar thickness.

6.1.4.8 Energy Dissipation Ratio

The energy dissipation capacity ratio of the web plate is calculated as the ratio of the area under the last cycle of the hysteresis curve for the panel subjected to a cyclic displacement history to the energy dissipation of an equivalent elastic plastic system. This parameter is a measure of the ductility of the panel.

6.1.4.9 Maximum Out of Plane Deformation in the Web Panel

The maximum out of plane deformation in the web panel is obtained from the Abaqus 6.10 model at the end of the analysis by subjecting the SPSW to a cyclic displacement history. The displacement history has been applied in a separate step in the step module in Abaqus 6.10 during analysis.

6.1.4.10 Initial Imperfection in the Web Panel

The initial imperfection in the web panel is simulated by applying a pressure load described at the beginning of this chapter. The pressure load is applied in a separate step prior to the step in which the displacement history is applied to the SPSW in Abaqus 6.10. The value of initial imperfection is taken at the end of this initial step from the analysis results.

6.2 Load Deformation Results for some Typical Models

A typical layout of the circular perforations in two steel plate shear walls and their hysteretic response to cyclic displacement history is shown below in Figure 6-5 and Figure 6-6.

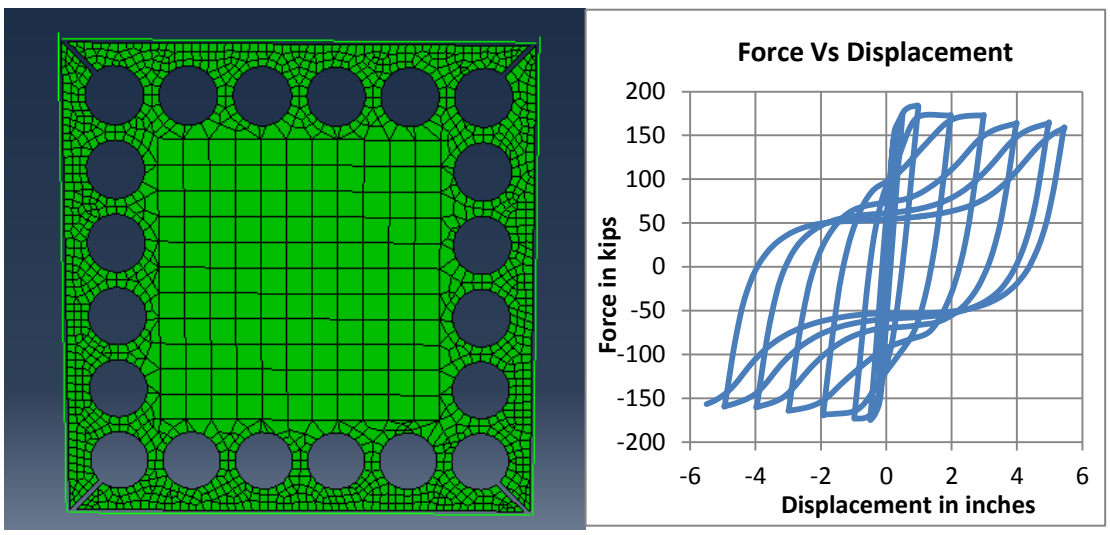

(a) (b)

Figure 6-5 (a) Layout of circular perforations with the coarse mesh, (b) Hysteresis curve for the cyclic displacement history applied

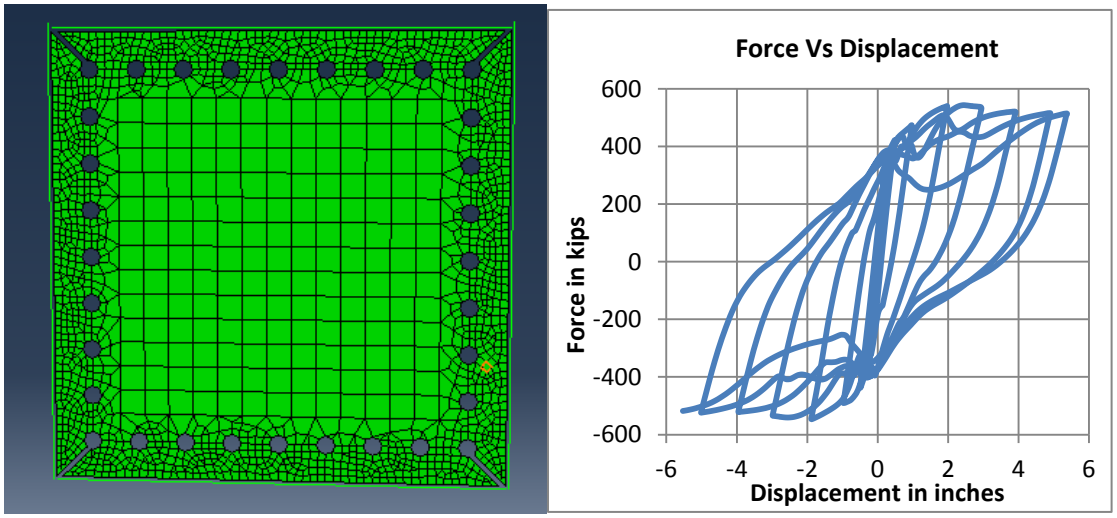

(a) (b)

Figure 6-6 (a) Layout of circular perforations with the coarse mesh, (b) Hysteresis curve for the cyclic displacement history applied

Figure 6-7 and Figure 6-8 show the hysteresis and layout for strong and weak configurations.

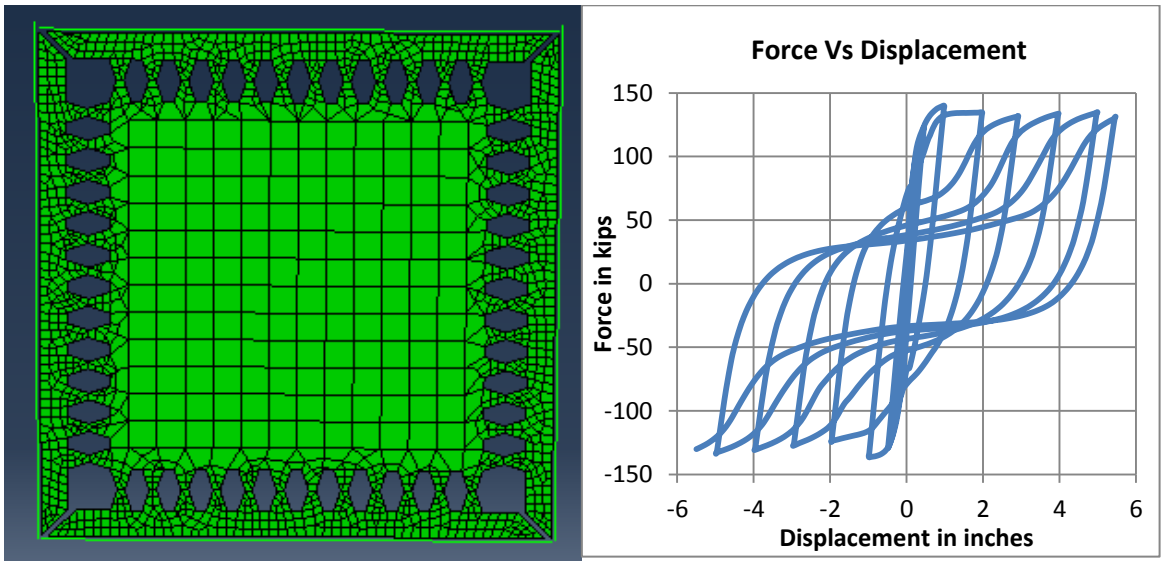

(a) (b)

Figure 6-7 (a) Layout of butterfly shaped cutouts B3 with the coarse mesh for strong configuration, (b) Hysteresis curve for the cyclic displacement history applied

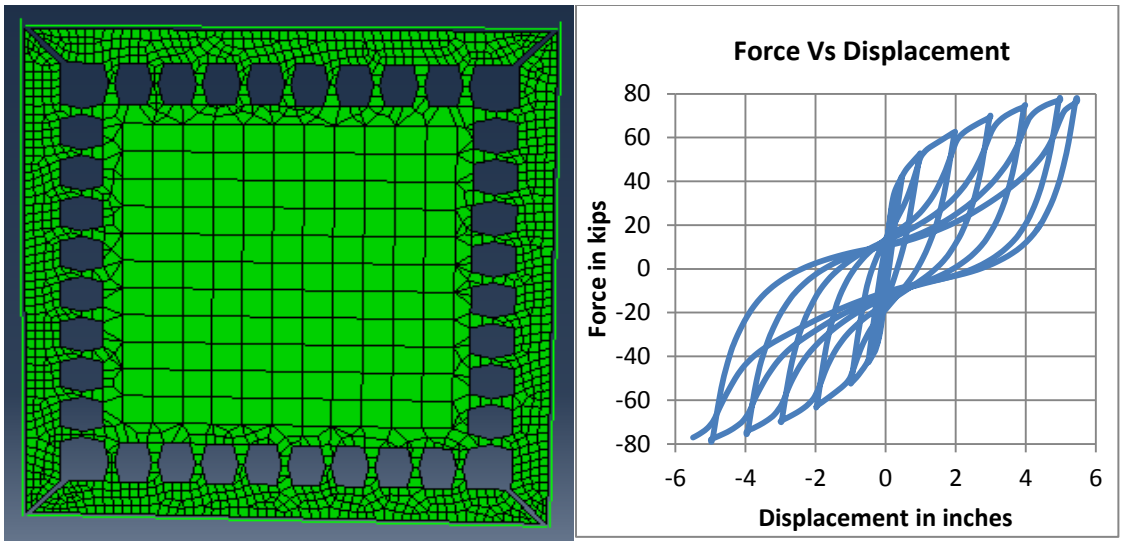

(a) (b)

Figure 6-8 (a) Layout of butterfly shaped cutouts B3 with the coarse mesh for weak configuration, (b) Hysteresis curve for the cyclic displacement history applied

Figure 6-9 and Figure 6-10 show the deformed shapes at 3.8% drift and hysteresis for web plates of 0.1875 inches and 0.75 inches with perimeter circular holes.

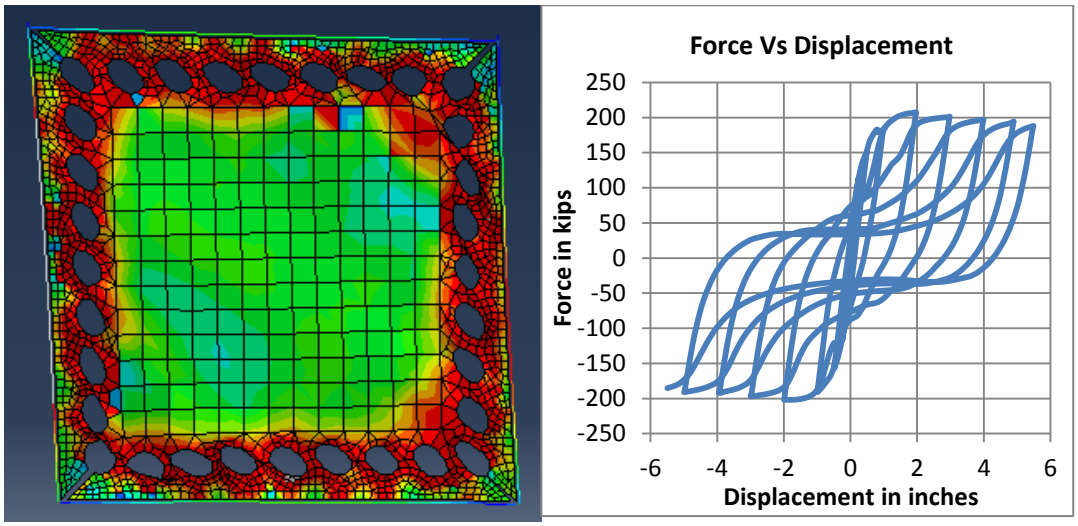

(a) (b)

Figure 6-9 (a) Layout of circular perforations for a plate thickness of 0.1875 inches, (b) Hysteresis curve for the cyclic displacement history applied

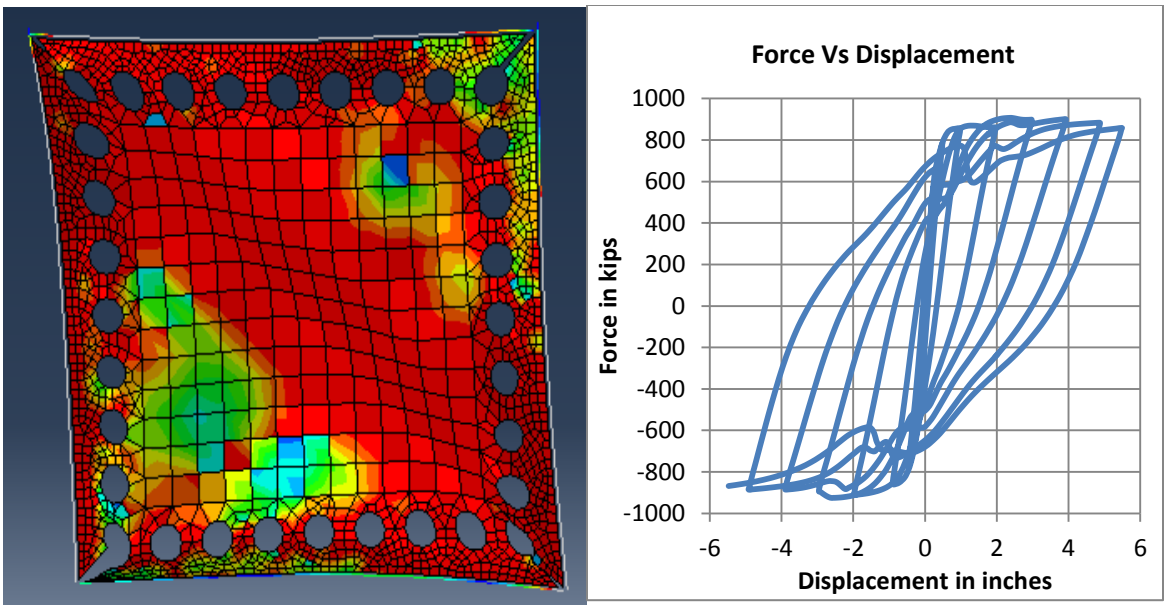

(a) (b)

Figure 6-10 (a) Layout of circular perforations for a plate thickness of 0.75 inches, (b) Hysteresis curve for the cyclic displacement history applied

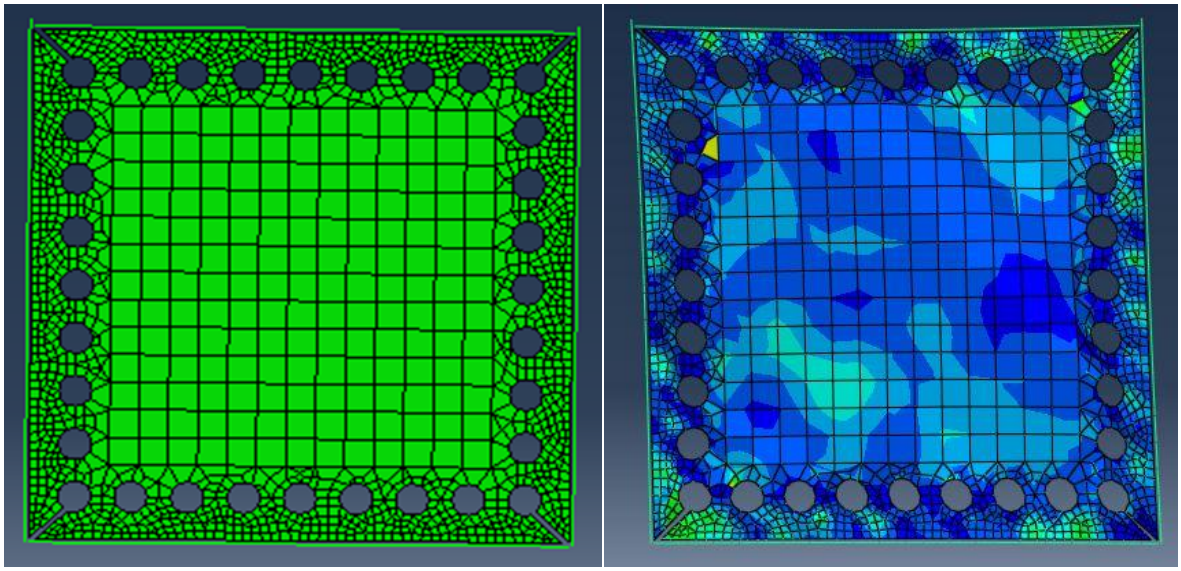

(a) (b)

Figure 6-11 (a) Undeformed shape of a 0.375 inch thick plate with D/S = 0.6 and 9 inch diameter holes, (b) Stress contour – S12 from Abaqus 6.10

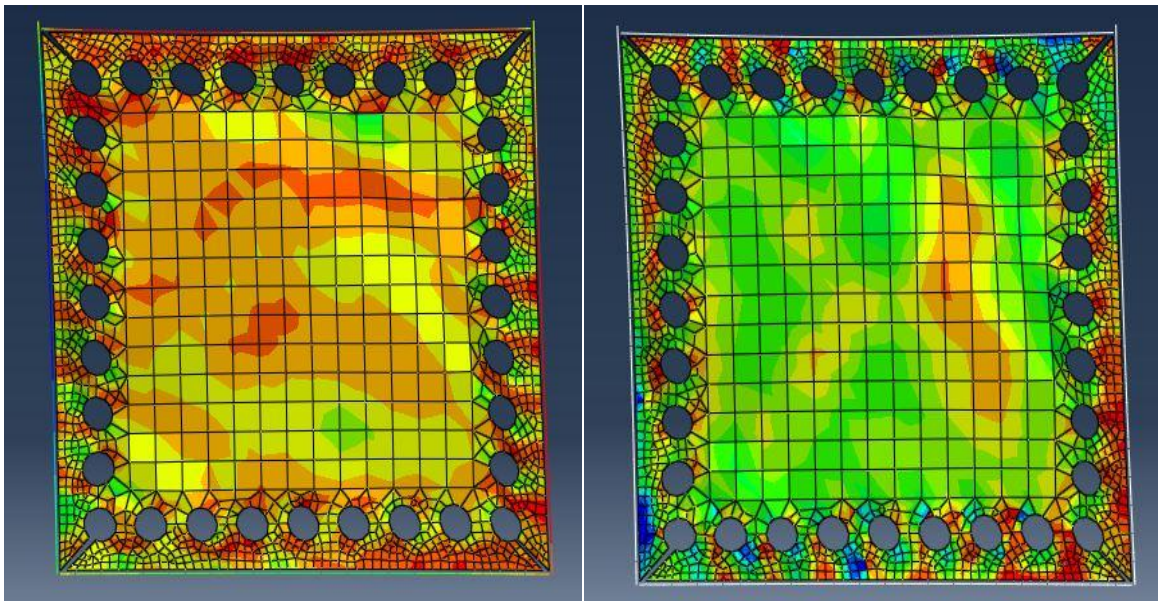

(a) (b)

Figure 6-12 (a) Stress Contour – S11 from Abaqus 6.10, (b) Stress Contour – S22 from Abaqus 6.10

Figure 6-11(a) shows the undeformed shape of the plate with a D/S ratio of 0.6 and Figure 6-11(b) shows the S12 (shear stress) contour from Abaqus 6.10. It was found that the magnitude of shear stresses in the links between the perforations were negligible. Figure 6-12 (a) shows the axial stresses in the plate in the X direction (S11) and Figure 6-12(b) shows the axial stresses in the plate in the Y direction. The magnitude of S11 in the links was of the order of 25 ksi and the magnitude of S22 in the links was of the order of 20 ksi. It can be inferred that the links are deforming more in bending than in shear.

6.3 Output Parameter Plots

The plots from the parametric study for circular and butterfly shaped cutouts are summarized in this section.

6.3.1 Results for Perimeter Circular Hole Configuration – Varying Size and Spacing

It is seen from the Figure 6-13 that the shear strength of the web panel decreases with increase in the hole diameter and with increase in the perforation ratio (D/S). With the increase in D/S ratio the spacing between the holes reduces leaving lesser plate material available to undergo shear yielding between the holes. The relationship between shear strength and the perforation ratio appears to be relatively linear for small diameter holes implying a linear relationship between panel shear strength and the length of solid material. However, as the hole diameter increases, there is a nonlinear relationship between shear strength and the perforation ratio implying that buckling is making the links less effective at resisting shear when the links become more slender.

It is also shown in Figure 6-13 that the hole diameter can be used to adjust shear capacity. For a set value of plate thickness, t=0.375", and perforation ratio equal to, D/S=0.6, the shear capacity can be adjusted from 320 kips to 480 kips.

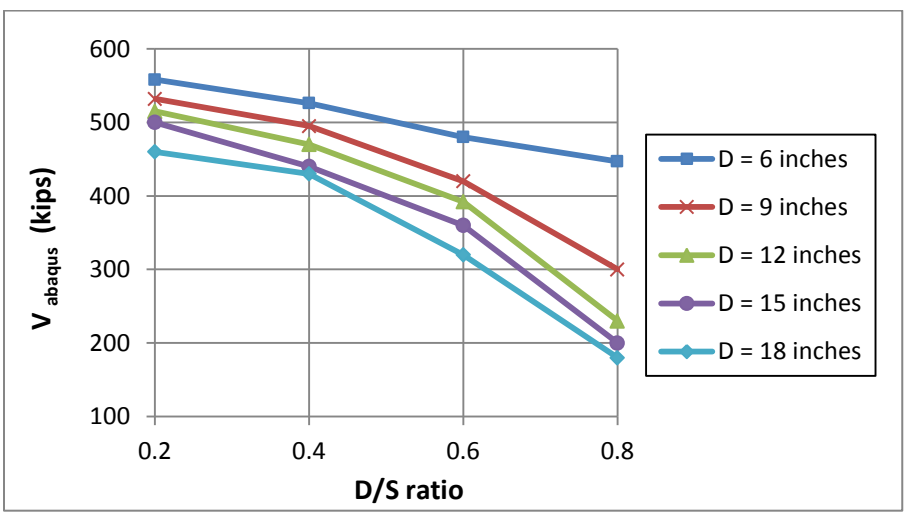

Figure 6-13 Plot showing the variation of shear strength of the panel with D/S ratio for varying hole diameter

It is seen from the Figure 6-14 that the stiffness of the web panel decreases with increase in the hole diameter and with increase in the D/S ratio. For perforation ratios between 0.2 to 0.6 there is relatively small effect on panel stiffness (between 5% and 25% reduction). This is an important result in that the stiffness is somewhat independent of the hole spacing in the range of perforation

ratio between 0.2 to 0.6. The perforation ratio can therefore be used effectively to adjust the strength of the wall while the stiffness is not affected as much.

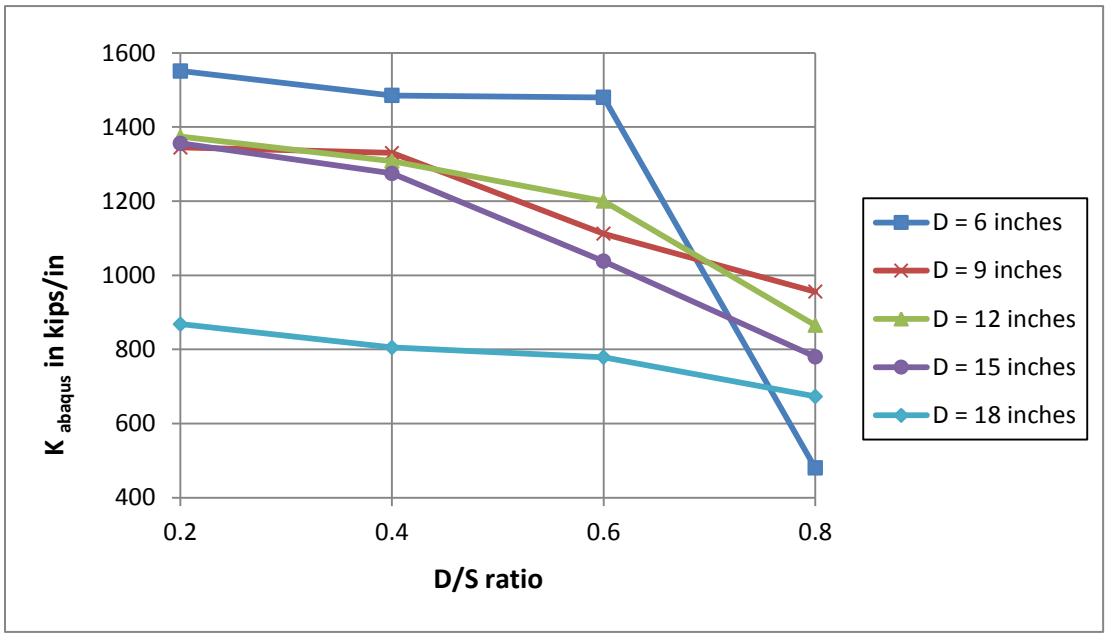

Figure 6-14 Plot showing the variation of stiffness of the panel with D/S ratio for varying hole diameters

It is seen from the Figure 6-15 that the energy dissipation ratio of the web panel decreases with increase in the D/S ratio from 0.2 to 0.8 and also it decreases with increase in the hole diameter from 6 to 18 inches. As the D/S ratio reaches a value of 0.8, the SPSW loses stiffness and becomes a soft system since the open area in the panel is large and there is little plate material remaining between the holes to undergo shear yielding in the plate. Hence there is a steep downward slope at a D/S ratio of 0.8.

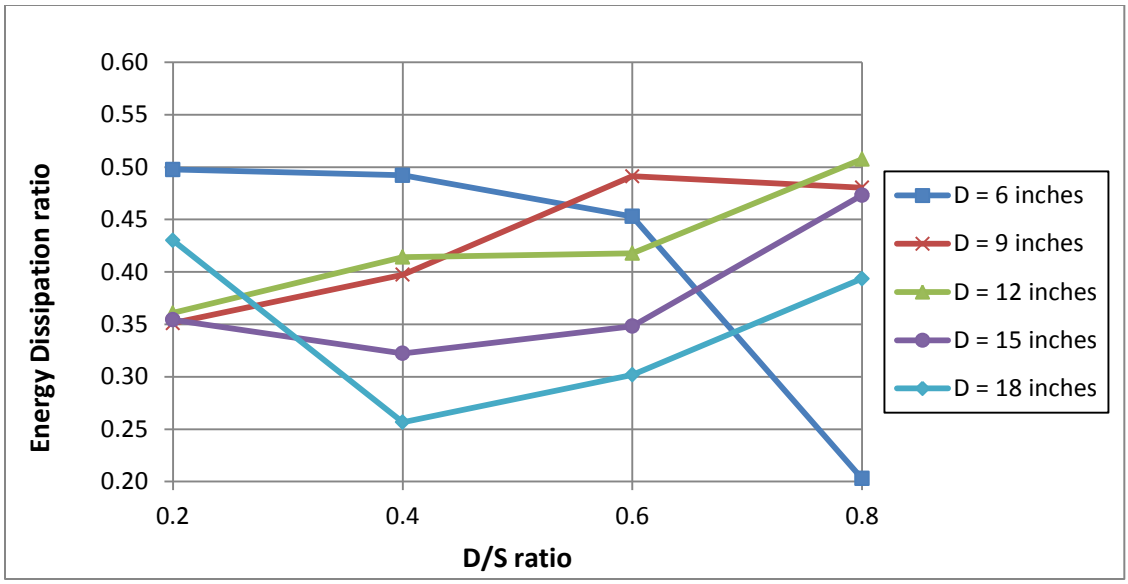

Figure 6-15 Plot showing the variation of energy dissipation ratio of the web panel with D/S ratio for varying hole diameters

Table 6-8 shows the values for output parameters – shear strength, stiffness and energy dissipation of the web plate with perimeter circular holes with varying size and spacing.

Table 6-8 Strength, stiffness and energy dissipation ratio of the set of 20 models for the perimeter circular holes with varying size and spacing

Plate Name	Expected Strength of Wall V_{exp} kips		Strength of Wall Abaqus kips	Stiffness of Wall Abaqus kips/in	Energy Dissipation (ED) of Panel kips-in	ED of Equiv EPPS kip-in	ED Ratio
	Eqn 1	Eqn 2					
C1	573	632	558	1687	4935	9917	0.50
C2	453	529	534	1591	4634	9415	0.49
C3	332	426	500	1578	3896	8601	0.45
C4	211	323	470	480	1512	7449	0.20
C5	588	632	540	1345	3349	9539	0.35
C6	452	529	500	1330	3518	8851	0.40
C7	317	426	433	1112	3672	7475	0.49
C8	226	323	308	956	2366	4925	0.48
C9	543	632	520	1374	3412	9452	0.36
C10	422	529	475	1308	3367	8127	0.41
C11	302	426	400	1200	2843	6805	0.42
C12	181	323	235	865	1930	3802	0.51
C13	573	632	500	1356	3047	8595	0.35
C14	422	529	450	1275	2625	8144	0.32
C15	347	426	360	1038	2034	5840	0.35
C16	196	323	200	780	1538	3250	0.47
C17	543	632	470	868	3505	8150	0.43
C18	452	529	430	805	1887	7351	0.26
C19	362	426	320	779	1622	5371	0.30
C20	181	323	180	673	1195	3035	0.39

It is seen from the Figure 6-16 that there is a relatively linear increase in the length of cutting in the web panel as the D/S ratio increase from 0.2 to 0.8. However, there is not much variation in cutting length with hole diameter. The number and size of holes is varying but the total length of

cutting in the plate almost remains uniform with increasing hole diameter. This implies that the perforation ratio is a better measure for the cost of cutting the plate than the hole diameter by itself.

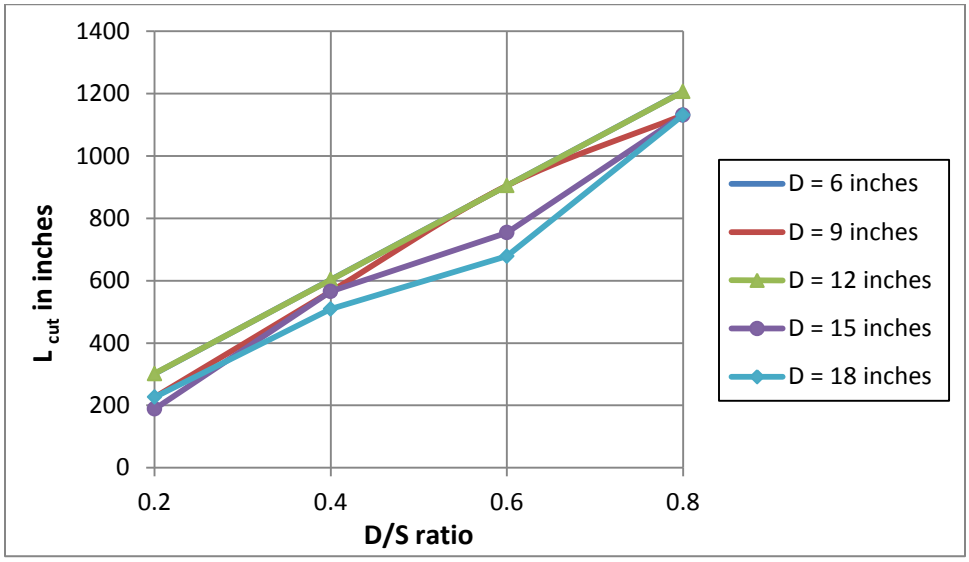

Figure 6-16 Plot showing the variation of length of cutting in the wall with D/S ratio for varying hole diameters

Figure 6-17 shows that the openness of the panel increases with increase in D/S ratio and with increase in diameter of the holes along the perimeter of the panel. The range of openness for the configurations examined in this parametric study varied from 2% to 25%.It was found that openness of the panel is more sensitive to D/S ratio at larger hole diameters. There is an 81% increase in the openness of the panel as the diameter of the holes increases from 6 to 18 inches at a D/S ratio of 0.8 and there is a 25% increase at a D/S ratio of 0.2.

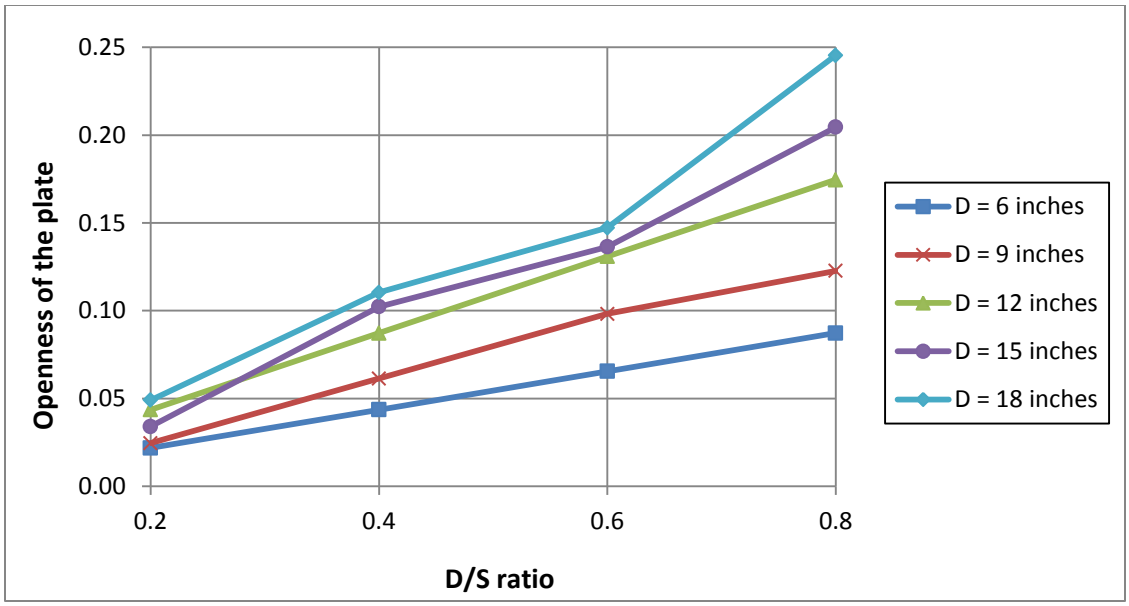

Figure 6-17 Variation of the openness of the web panel with D/S ratio for varying hole diameters

Table 6-9 shows the values of output parameters – length of cutting and openness of the panel for perimeter circular holes configuration with varying size and spacing.

Table 6-9 Length of cutting and openness of the panel for the set of 20 models for the perimeter circular holes with varying size and spacing

Plate Name	Length of Cutting inches	Openness of Panel	Max PEEQ	Max OOPD at End of Displ. History inches	Initial Imperfection inches	Cost of Cutting in the plate dollar
C1	302	0.02	0.69	8.6	0.21	300
C2	603	0.04	1.11	8.2	0.21	550
C3	905	0.07	1.36	7.8	0.21	800
C4	1206	0.09	0.67	5.9	0.22	1100
C5	226	0.02	0.43	8.4	0.24	200
C6	566	0.06	0.45	5.3	0.22	500
C7	905	0.10	0.88	4.8	0.22	800
C8	1131	0.12	2.91	5.8	0.22	1000
C9	302	0.04	0.58	8.5	0.22	300
C10	603	0.09	0.34	5.9	0.22	550
C11	905	0.13	0.69	4.7	0.22	800
C12	1206	0.17	1.56	5.3	0.22	1100
C13	189	0.03	0.44	6.5	0.27	200
C14	566	0.10	0.41	75	0.23	500
C15	754	0.14	0.35	5.2	0.24	700
C16	1131	0.20	1.05	5.9	0.23	1000
C17	226	0.05	0.40	9.9	0.25	200
C18	509	0.11	0.28	8.6	0.25	500
C19	679	0.15	0.35	6.0	0.25	600
C20	1131	0.25	0.49	4.5	0.23	1000

6.3.2 Results for Perimeter Circular Hole Configuration – Varying Thickness

Plots showing the variation of various output parameters for circular holes along the perimeter of the plate for the set of 10 models with varying thickness and a constant D/S ratio are shown below. Figure 6-18 shows the variation of shear strength with increasing thickness of the web panel from 0.1875 inches to 0.75 inches for two hole diameters. It can be seen that the shear strength decreases as the hole diameter increases from 9 inches to 15 inches. The shear strength also increases as the thickness of the plate increases. The increase in shear strength with panel thickness appears to be approximately linear implying that buckling did not significantly change the shear strength between these models. Since shear strength has a nonlinear relationship with the perforation ratio and hole diameter, it is suspected that the buckling of the links may be more related to the link slenderness in plane (length divided by width) than the out of plane slenderness (length divided by thickness).

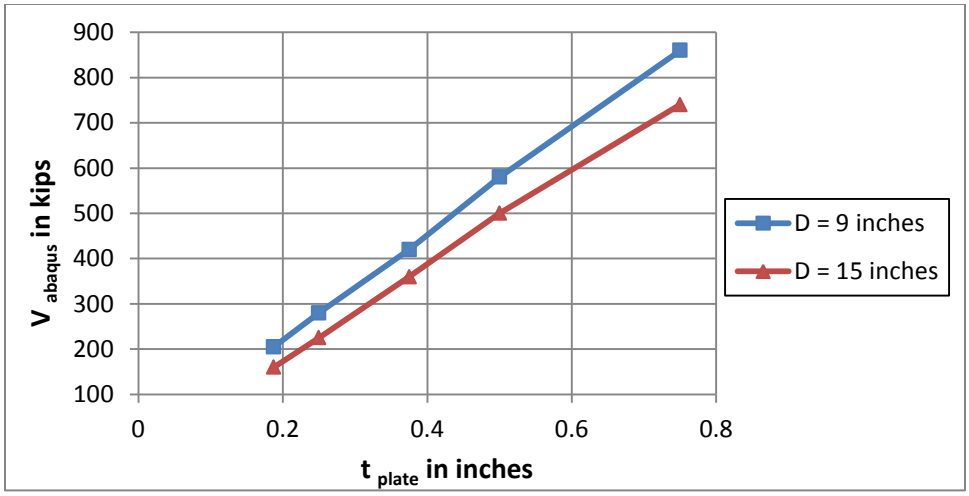

Figure 6-18 Variation of shear strength of the web panel with thickness of the plate for varying hole diameters

The same trend is observed for the stiffness and energy dissipation of the web panel as seen from Figure 6-19 and Figure 6-20. The stiffness increases with increase in thickness of the panel and the panel with bigger holes is less stiff.

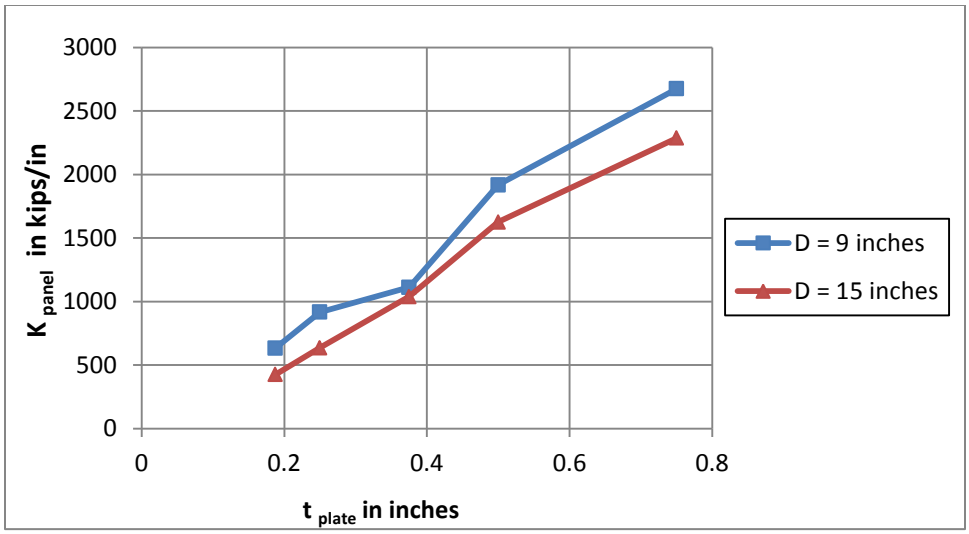

Figure 6-19 Variation of stiffness of the web panel with thickness of the plate for varying hole diameters

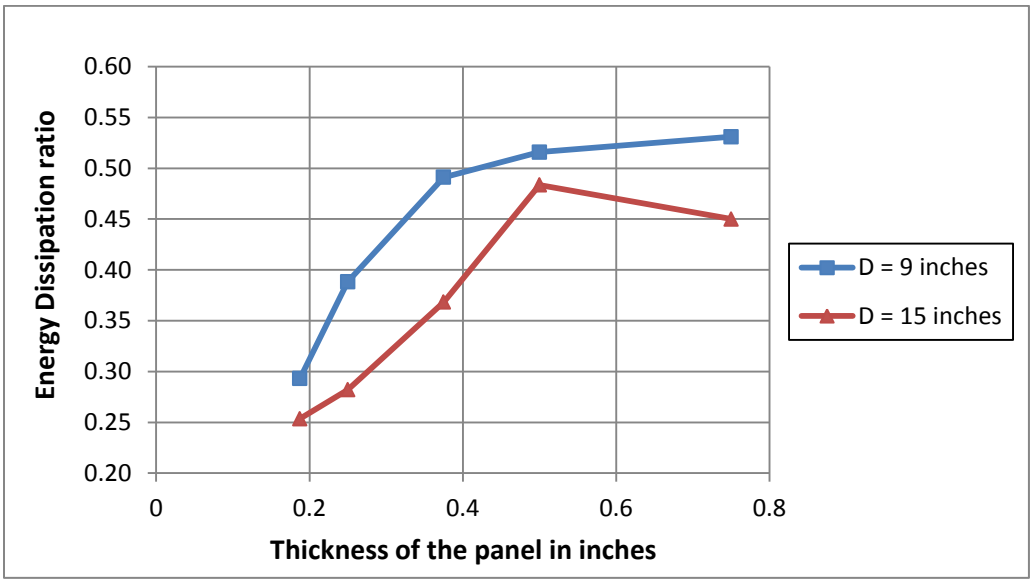

Figure 6-20 Variation of the energy dissipation capacity of the web panel with thickness of the panel for varying hole diameters

Table 6-10 shows the values for the output parameters – strength, stiffness and energy dissipation ratio for the set of 10 models with perimeter circular holes with varying thickness.

Table 6-10 Strength, stiffness and energy dissipation ratio for the set of 10 models with perimeter circular holes configuration with varying thickness

Plate Name	Expected Strength of Wall V_{exp} kips		Strength of Wall Abaqus kips	Stiffness of Wall Abaqus kips/in	Energy Dissipation of the Panel kips-in	ED of Equiv EPPS kips-in	ED Ratio
	Eqn 1	Eqn 2					
A1	158	213	205	633	1031	3516	0.29
B1	211	284	280	916	1848	4758	0.39
C7 = C1	317	426	420	1112	3871	7475	0.49
D1	422	568	580	1917	5285	10242	0.52
E1	633	852	860	2675	8320	15668	0.53
A2	173	213	160	425	717	2828	0.25
B2	231	284	225	635	1096	3886	0.28
C15 = C2	347	426	360	1038	2151	5840	0.37
D2	462	568	500	1625	3895	8054	0.48
E2	694	852	740	2287	5936	13189	0.45

Figure 6-21 shows the variation of maximum out of plane deformation in the plate with the thickness of the plate for varying hole diameter. The maximum out of plane deformation is recorded at the end of the displacement history. The maximum out of plane deformation increases with increase in thickness and also with increase in the hole diameter. The increase in out of plane displacement with thicker plates shown in Figure 6-21 can be explained by the fact that as the plate thickness increases the buckling half wave is longer leading to higher amplitude of the maximum out of plane deformation.

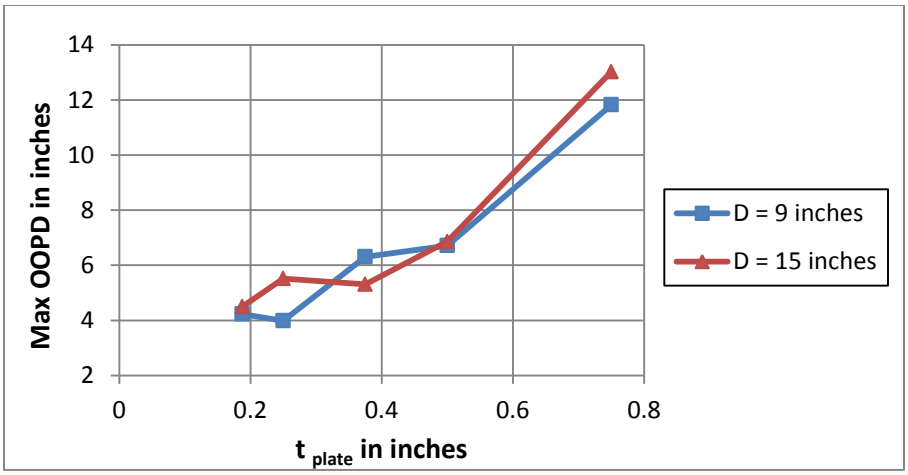

Figure 6-21 Variation of maximum out of plane deformation in the plate with the thickness of the plate for varying hole diameter

Table 6-11 shows the values of output parameters – length of cutting and openness of the panel for perimeter circular holes configuration with varying thickness.

Table 6-11 Length of cutting and openness of the panel for the set of 10 models for the perimeter circular holes with varying thickness

Plate Name	Length of Cutting inches	Openness of Cutting	Max PEEQ	Max OOPD at End of Disp. History inches	Initial Imperfection inches	Cost of Cutting in the Plate dollar
A1	905	0.09	0.64	4.2	0.22	400
B1	905	0.09	0.88	4.0	0.22	550
C7 = C1	905	0.09	0.94	6.3	0.23	800
D1	905	0.09	0.88	6.7	0.22	1100
E1	905	0.09	0.84	11.8	0.22	1600
A2	754	0.14	0.32	4.6	0.22	350
B2	754	0.14	0.34	5.5	0.22	450
C15 = C2	754	0.14	0.43	5.3	0.24	700
D2	754	0.14	0.44	6.9	0.24	900
E2	754	0.14	0.65	13.0	0.24	1400

6.3.3 Butterfly Shaped Cutouts along the Perimeter of the Panel

The plots showing the variation of the output parameters for the butterfly shaped cutouts have been summarized in this section. A brief explanation for the observed trend and the reason for the behavior are also given for each of the plots.

It is seen from Figure 6-22 that the shear strength of the web panel increases with increase in thickness of the plate. The shear strength is higher for the strong configuration where the links are wider and there is more plate material to resist the story shear. Both geometries appear to produce a linear variation in shear strength with plate thickness. The equation predicting the strength of the panel produced reasonable results varying from 18% below to 35% above the observed shear capacity of the panels. See Table 6-12 for values of shear strength as calculated from the equation and calculated from the FE model results.

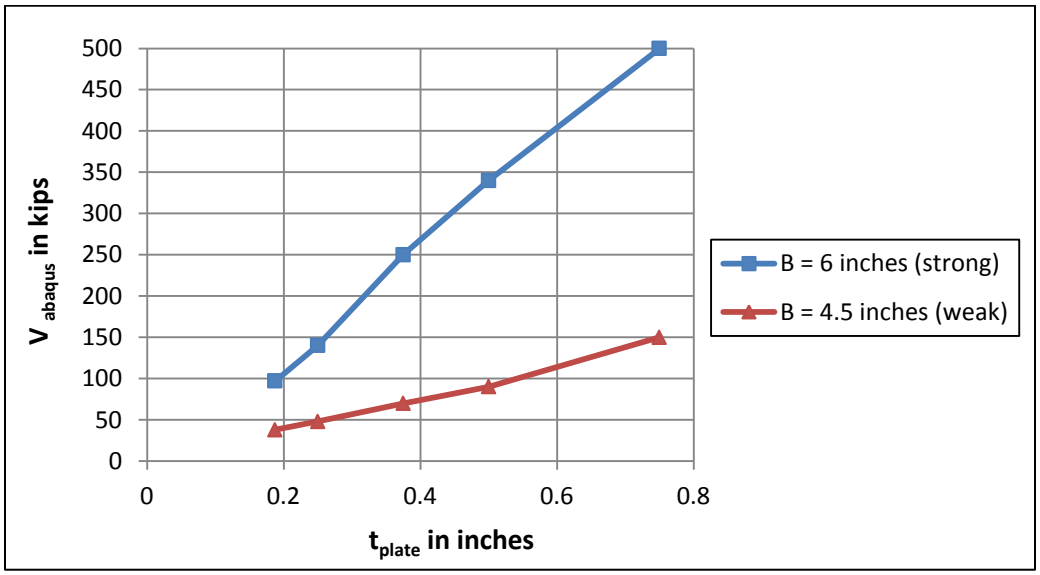

Figure 6-22 Plot showing the variation of shear strength of the web panel with thickness of the panel for strong and weak configurations

Figure 6-23 shows the variation of stiffness of the panel with the thickness of the plate. As the thickness increases, the stiffness of the plate increases. The slightly nonlinear relationship

implies a reducing increase in stiffness with increasing plate thickness. The different plate geometries (strong vs. weak) were shown to produce significantly different stiffness. It is concluded that adjusting the butterfly link geometry may be a more effective way to change the stiffness than changing the plate thickness. The same trend is seen for the energy dissipation capacity of the plate from Figure 6-24.

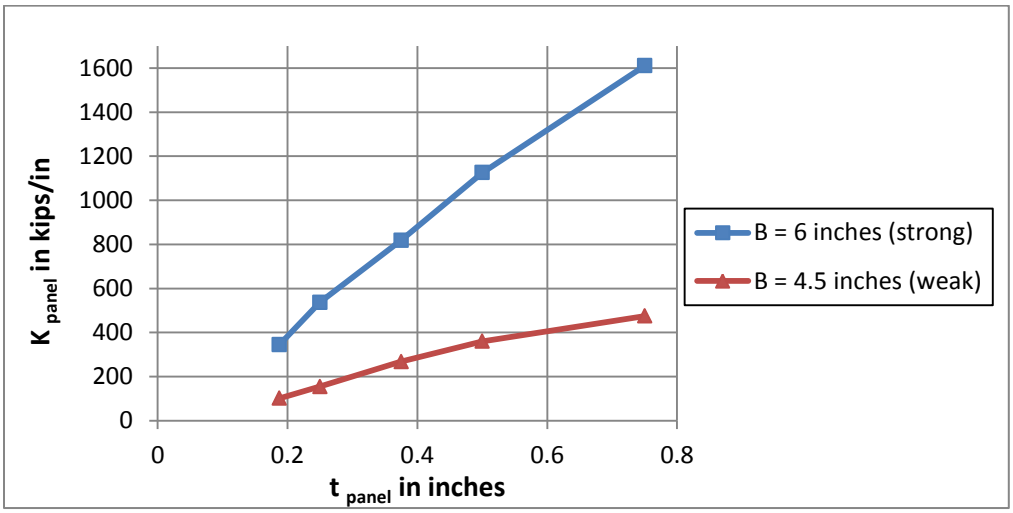

Figure 6-23 Plot showing the variation of the stiffness of the panel with thickness of the panel for strong and weak configurations

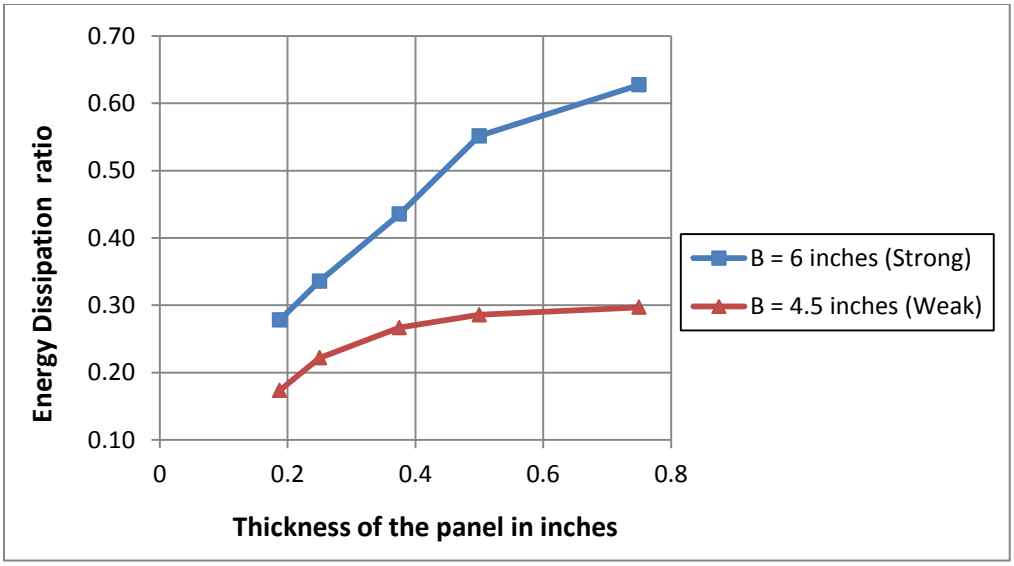

Figure 6-24 Plot showing the variation of energy dissipation capacity of the panel with the thickness of the panel for strong and weak configurations

Table 6-12 shows the values of the output parameters – strength, stiffness and energy dissipation for the set of 10 models with strong and weak butterfly shaped cutouts.

Table 6-12 Strength, stiffness and energy dissipation ratio for the set of 10 models with strong and weak perimeter butterfly shaped cutout configurations

Plate Name	Expected Strength of Wall V_{exp} kips	Strength of Wall Abaqus kips	Stiffness of Wall Abaqus kips/in	Energy Dissipation of the Panel kips-in	Energy Dispn. of Equiv EPPS kip-in	Energy Dissipation Ratio
A3	108	97	345	482	1732	0.28
B3	144	140	537	830	2472	0.34
C3bf	216	250	818	1774	4075	0.44
D3	288	340	1125	3241	5876	0.55
E3	432	500	1610	6857	10928	0.63
A4	46	38	102	163	940	0.17
B4	61	48	155	300	1355	0.22
C4bf	91	70	268	651	2440	0.27
D4	122	90	360	1014	3546	0.29
E4	182	150	475	1796	6048	0.30

From the Figure 6-25 it is observed that the maximum out of plane deformation increases with the thickness of the plate. This is due to the fact that as the thickness increases, the buckling half wave length increases leading to larger amplitude buckling waves. The plate with smaller links (weak configuration) has larger out of plane deformation. It is expected that the increased frequency and strength of the links in the strong configuration better restrains the out of plane motion of the plate.

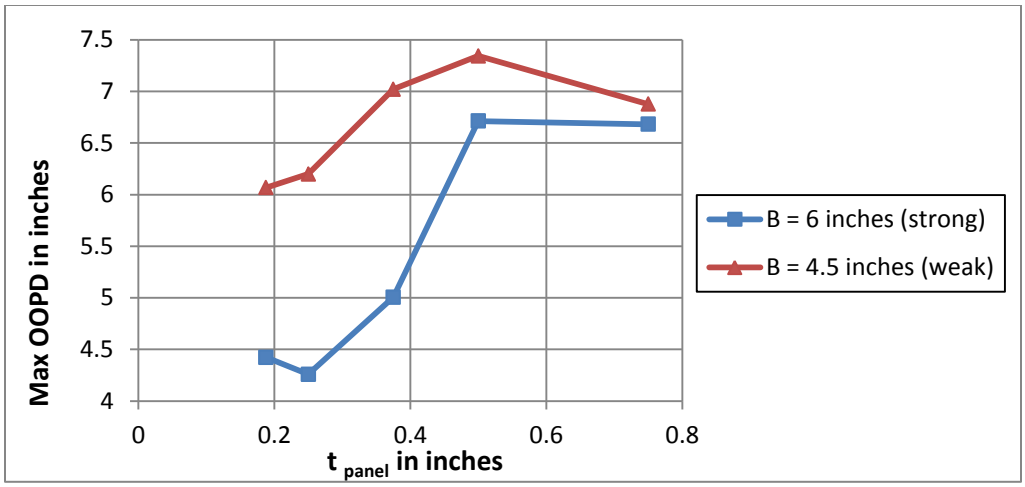

Figure 6-25 Variation of the maximum out of plane deformation with the thickness of the plate for strong and weak configurations of cutouts

Table 6-13 shows the values of output parameters – length of cutting and maximum out of plane deformation for the set of 10 models with perimeter strong and weak butterfly shaped cutouts.

Table 6-13 Length of cutting, openness of panel and maximum out of plane deformation for the set of 10 models with perimeter strong and weak butterfly shaped cutouts

Plate name	Length of cutting Lcut inches	Openness of cutting	Max PEEQ	Max OOPD at end of disp history inches	initial imperfection inches	No. of holes	Cost of Cutting in Plate dollar
A3	1574	0.16	0.64	4.4	0.22	48	700
B3	1574	0.16	0.87	4.3	0.23	48	950
C3bf	1574	0.16	1.19	5.1	0.24	48	1400
D3	1574	0.16	1.43	6.7	0.23	48	1900
E3	1574	0.16	1.84	6.7	0.23	48	2900
A3	1467	0.20	0.53	6.1	0.22	36	700
B3	1467	0.20	0.64	6.2	0.23	36	900
C3bf	1467	0.20	1.10	7.0	0.24	36	1300
D3	1467	0.20	1.15	7.3	0.24	36	1800
E3	1467	0.20	1.20	6.9	0.23	36	2700

6.4 Behavioral Trends Observed from Hysteresis Curves and Force – Displacement Plots of the Parametric Study

The parametric study for SPSW with circular and butterfly shaped cutouts resulted in a number of hysteresis curves and force – displacement plots. The numerous observations made regarding the behavior of the SPSW when subjected to cyclic and monotonic loading are summarized in this section.

6.4.1 Perimeter Circular Holes with Varying Size and Spacing

Some of the salient features observed from the hysteresis plots for perimeter circular holes with varying size and thickness are summarized in this section. The fullest hysteresis curves occur for D/S=0.6. It could be suggested that using a D/S = 0.6 is a good value to use in design of these systems. A transition in behavior is observed as D/S goes from a small value of 0.2 (holes are far apart and plate acts in tension field) to medium (D/S=0.6 for instance where there is the most shear yielding and energy dissipation) to large where D/S = 0.8 (where links between the holes may be subjected to buckling which reduces energy dissipation). It can be concluded that larger diameter holes create more pinching in the hysteretic behavior. Because of this, smaller diameter holes are suggested.

6.4.2 Perimeter Circular Holes with Varying Thickness

The energy dissipation capacity clearly increases with increase in plate thickness from 0.1875 inches to 0.75 inches. The hysteretic behavior is highly pinched for plates of lower thickness and is more complete as the thickness increases. Therefore providing for thicker plates is suggested for this configuration. This set of models supports the result discovered in the first part of the study that smaller holes result in more energy absorption. It is therefore suggested that SPSW with smaller holes and higher thickness will have better performance as seismic force resisting systems.

6.4.3 Perimeter Butterfly Links

It is observed that thicker plates result in more energy dissipation. The panels with thickness of 0.5 inches and higher had especially good energy dissipation. A thickness of 0.5 inches or greater is suggested for the panel dimensions similar to that discussed in the parametric study. The weak and strong configurations demonstrate the ability to tune the strength to a good range of values from large to small values while continuing to produce good energy dissipation ability.

Chapter 7. CONCLUSIONS

7.1 Finite Element Modeling of SPSW

In order to validate modeling of SPSWs with and without perforations in a finite element environment, two experiments conducted at the MCEER facility in the University of Buffalo, NY were chosen. Finite element models of SPSWs with shell elements were made and were used to simulate tests found in the literature. It was found that the agreement between the finite element models and the experiments was quite good for solid and perforated panels. Finite element modeling with different elements was done in the thesis. The modeling techniques validated were used to simulate the behavior of new forms of SPSW.

7.2 Adaptation of High Seismic Design for Moderate Seismic Zones

The approach that was followed was to start with a high seismic design for a prototype building found in the literature and demonstrate the design procedure and then examine approaches to reduce the cost and sizes of the boundary elements (mostly the VBE), amount of steel required and construction complexity. The three methods attempted to achieve these goals were the capacity design of VBE without moment connections, the over strength factor design of VBE without moment connections and plastic mechanism design for VBE without moment connections. Beyond the elimination of moment connections, the proposed design approaches were intended to reduce the design strength demands on the boundary elements. It was observed that drifts controlled the design, the strength was greater than what it need to be and hence the proposed design approaches did not result in reduced steel weight. It was concluded that to achieve improved efficiency in a SPSW system it was necessary to decouple strength and stiffness. This provided the motivation to develop tunable SPSW for which strength, stiffness and ductility might be separately tuned.

7.3 Alternate SPSW Detailing to Create More Efficient Solutions for SPSW

Several new methods for reducing web plate strength while sustaining or increasing system stiffness were investigated. Seven approaches were attempted. The approaches were separated

into two parts: approaches using solid plates, and approaches with web cut-outs. After preliminary analyses of the seven approaches, two approaches that gave promising results were chosen – circular holes along the perimeter of the web plate and butterfly shaped cutouts along the perimeter of the web plate. Moment connections were eliminated between the beam and columns and instead simple shear connections were used in all these approaches. Since the stiffness of the SPSW is related to the web plate thickness, it was observed that the plate thickness increased for the new approaches in which moment connections were eliminated. The new approaches allowed the strength and stiffness to be tuned separately and the observed strength was better controlled. The boundary elements selected using the preliminary design procedures were dramatically smaller for the new approaches. Furthermore the hysteretic behavior of the two new approaches was found to be significantly better than the typical SPSW. Because of the tunability, reduced steel weight, elimination of moment connections and improved energy dissipation, the two proposed approaches were considered promising and a parametric study was conducted.

7.4 Parametric Study for the Two Proposed Configurations of Cutouts

Steel plate shear walls with two types of cutouts namely perimeter circular hole panels and perimeter butterfly link panels have been investigated. A computational study using the finite element software Abaqus 6.10 was performed. The parametric study was conducted by varying the sizes, spacing and thickness for the perimeter circular holes configuration. Strong and weak configurations of the perimeter butterfly shaped cutouts were defined and variation in the output parameters was investigated for varying plate thicknesses.

For plates with perimeter circular holes, it was found that the fullest hysteresis curves occured for D/S=0.6. A D/S = 0.6 is a suggested value to use in design of these systems. A transition in behavior was observed as D/S goes from a small value of 0.2 (holes far apart and plate acts in tension field) to medium (D/S=0.6 for instance, where there is the most shear yielding and energy dissipation) to large where D/S = 0.8 (where links between the holes may be subjected to buckling which reduces energy dissipation). It was concluded that larger diameter holes create more pinching in the hysteretic behavior. Because of this, smaller diameter holes are suggested. The energy dissipation capacity clearly increased with increase in plate thickness from 0.1875

inches to 0.75 inches. The hysteretic behavior was highly pinched for plates of lower thickness and was more complete as the thickness increased. Therefore use of thicker plates is suggested.

The equations from the existing codal specifications with modifications to predict the shear strength of the panel with circular perforations along the perimeter of the panel were attempted and the values obtained by using these modified equations are tabulated in the tables under the heading – expected strength of wall. It was found that the equation for a solid panel was able to predict the same capacity as obtained from Abaqus 6.10 with an error of less than 10 percent for small values of D/S ratio upto 0.4. For higher values of D/S ratios (0.6-0.8) the equation for perforated panels was able to predict the same capacity obtained from Abaqus 6.10 with an error of 5% for a diameter of 12 inches. There is varying trend where a particular equation predicts the capacity with the least percentage error. With more analysis, an equation to closely predict the shear strength of the web plate with this configuration of perforations could be arrived at. This is recommended as part of the future work.

For perimeter butterfly shaped cutouts, it was observed that thicker plates resulted in more energy dissipation. The panels with thickness of 0.5 inches and higher had especially good energy dissipation. A thickness of 0.5 inches or greater is suggested for the panel dimensions similar to that discussed in the parametric study. The weak and strong configurations demonstrate the ability to tune the strength to a good range of values from large to small values while continuing to provide good energy dissipation. The equation for prediction of the shear strength proposed by Borchers et al (2010) for butterfly shaped cutouts predicts the capacity obtained from Abaqus with a maximum error of 30%. Thus it is suggested that with more analysis, an equation to closely predict the shear strength of the web plate with this configuration of cutouts could be arrived at. This is recommended as part of the future work.

7.5 Recommendations for Future Work

Experimental testing is needed to verify the expected behavior and to check the accuracy of the models for the configuration with circular holes along the perimeter and butterfly links along the perimeter of the plate. The modeling done so far is not capable of predicting tearing, ductility and final failure of the SPSW. These quantities should be investigated either computationally or

experimentally for both the proposed configuration of cutouts. Equations to predict the strength and stiffness of the two configurations with cutouts along the perimeter of the plate need to be developed. More analysis needs to be done to develop reliable design procedures for SPSW with circular and butterfly shaped cutouts along the perimeter of the web plate. Different patterns of cutouts could be experimented with and better approaches to reduce the sizes of boundary elements could be implemented. A more thorough parametric study with variation in thickness and a detailed study of the variation in output parameters are required for a better understanding of the behavior of the SPSWs with perforations.

References:

1. Astaneh-Asl, A. "Seismic Behavior and Design of Steel Shear Walls – SEANC Seminar", Distributed at 2001 SEOANC Seminar, Structural Engineers Association of Northern California, November 7, 2001, San Francisco.

2. Astaneh-Asl, Abolhassan, and Zhao, Qiuhong (2002) "Cyclic Behavior of Steel Shear Wall Systems", Proceedings, Annual Stability Conference, Structural Stability Research Council, April, Seattle.

3. Astaneh-Asl, Abolhassan "Seismic Behavior and Design of Steel Shear Walls" Steel Tips published by the Structural Steel Educational Council, July 2001.

4. Baldelli, Joseph A. Jr. (1983) "Steel Shear Walls for Existing Buildings" Engineering Journal, AISC, Vol. 20, No. 2, pp 70-77.

5. Behbahanifard, Mohammad R., Grondin, Gilbert Y. and Elwi, Alaa E. "Experimental and Numerical Investigation of Steel Plate Shear Wall" Structural Engineering Report No. 254, Department of Civil & Environmental Engineering – University of Alberta at Edmonton, September 2003.

6. Berman, Jeffrey, and Bruneau, Michel (2003) "Plastic Analysis and Design of Steel Plate Shear Walls" Journal of Structural Engineering, ASCE, Vol. 129, No. 11. Nov. 2003.

7. Berman, Jeffrey W. and Bruneau, Michel "Steel Plate Shear Walls are Not Plate Girders" Engineering Journal, Third Quarter 2004

8. Berman, Jeffrey W., and Bruneau, Michel "Experimental Investigation of Light-Gauge Steel Plate Shear Walls" ASCE Journal of Structural Engineering, Vol. 131, No. 2, Feb 2005

9. Berman, Jeffrey W., Celik, Oguz C., and Bruneau, Michel "Comparing Hysteretic Behavior of Light-Gauge Steel Plate Shear Walls and Braced Frames" Engineering Structures 27 (2005) pp 475-485

10. Berman, Jeffrey W., and Bruneau, Michel "Seismic Behavior of Code designed Steel Plate Shear Walls" Engineering Structures 33 (2011) pp 230-244

11. Caccese, Vincent; Elgaaly, Mohamed and Chen, Ruobo (1993) "Experimental Study of Thin Steel-Plate Shear Walls Under Cyclic Load" Journal of Structural Engineering, ASCE, Vol. 119, No. 2, February, 1993.

12. CAN/CSA S16-01 "Limit States Design of Steel Structures" published by Canadian Standards Association

13. CSI (2010) - SAP 2000 User manual

14. Driver, Robert G., Kulak Geoffrey L., Kennedy, D.J. Laurie and Elwi, Alaa E. (1998) "Cyclic Test of Four-Story Steel Plate Shear Wall" Journal of Structural Engineering, ASCE, Vol. 124, No. 2, February, 1998.

15. Driver, Robert G., Kulak Geoffrey L., Elwi, Alaa E. and Kennedy, D.J. Laurie (1998) "FE and Simplified Models of Steel Plate Shear Wall" Journal of Structural Engineering, ASCE, Vol. 124, No. 2, February, 1998

16. Driver, Robert George, "Seismic Behaviour of Steel Plate Shear Walls" PhD Thesis, University of Alberta, Spring 1997

17. Driver, Robert G., Grondin, Gilbert Y., Behbahanifard, Mohammad R., Hussain, Munawar A. "Recent Developments and Future Directions in Steel Plate Shear Wall Research" North American Steel Construction Conference, Ft. Lauderdale, FL May 9-12, 2001

18. Elgaaly, Mohamed and Liu, Yinbo (1997) “Analysis of Thin-Steel-Plate Shear Walls” Journal of Structural Engineering, ASCE, Vol. 123, No. 11, November, 1997.

19. Hitaka, Toko and Matsui, Chiaki (2003) “Experimental Study on Steel Shear Wall With Slits” Journal of Structural Engineering, ASCE, Vol. 129, No. 5, May, 2003.

20. Hitaka and Matsui (2006) “Seismic Performance of Steel Shear Wall with slits integrated with Multi-story Composite Moment Frame” STESSA, pp 241-246

21. Lubell, Adam S., Prion, Helmut G. L., Ventura, Carlos E. and Rezai, Mahmoud (2000) “Unstiffened Steel Plate Shear Wall Performance Under Cyclic Loading” Journal of Structural Engineering, ASCE, Vol. 126, No. 4, April, 2000.

22. Ma, X., Borchers, E., Peña, A., Krawinkler, H., and Deierlein, G. (2010) *Design and Behavior of Steel Shear Plates With Openings as Energy-Dissipating Fuses*, Internal Report, Blume Earthquake Engineering Center, Stanford University.

23. Purba, Ronny and Bruneau, Micheal (2007) “Design Recommendation for Perforated Steel Plate Shear Walls” MCEER Report – 07-0011

24. Roberts, T. M. and Ghomi, S. Sabouri (1992) “Hysteretic Characteristics of Unstiffened Plate Shear Panels” Thin-Walled Structures, Elsevier Science Publishers, Great Britain, 1992.

25. Roberts, T.M. “Seismic Resistance of Steel Plate Shear Walls” Engineering Structures, Vol. 17, No. 5, pp 344-351, 1995

26. Similia (2010) - ABAQUS 6.10 user manual

27. Thorburn, L. Jane, Kulak, G.L. and Montgomery, C.J. “Analysis of Steel Plate Shear Walls” Structural Engineering Report No. 107, Department of Civil Engineering – University of Alberta at Edmonton, May, 1983.

28. Timler, P.A. and Kulak, G.L. (1983) “Experimental Study of Steel Plate Shear Walls”. Structural Engineering Report No. 114, Department of Civil Engineering, The University of Alberta, November 1983.

29. Vian, Darren and Bruneau, Micheal (2005) “Steel Plate Shear Walls for Seismic Design and Retrofit of Building Structures” MCEER Report -05-0010

30. Xue, M. and Lu, L-W. (1994b). “Monotonic and Cyclic Behavior of Infilled Steel Shear Panels”, The Seventeenth Czech and Slovak International Conference on Steel Structures and Bridges, Bratislava, Slovakia September 1994.

APPENDIX A

Compilation of the plots for the first 20 models for perimeter circular holes configuration with varying size and spacing

From the models C1 to C20 the following trends can be observed.

1. For each value of the diameter of the hole there are four models with the D/S ratio varying from 0.2 to 0.8 with an increment of 0.2. Therefore C1 to C4, C5 to C8, C9 to C12, C13 to C16 and C17 to C20 are the five sets of models with each set having a constant diameter of holes around the perimeter of the plate.
2. There is an improvement in the hysteretic behavior as the D/S ratio increases from 0.2 to 0.6 for the first set of models C1 – C4. The energy dissipation capacity of the web panel improves from C1 to C3. But for model C4 it is observed to drastically reduce. The system is very flexible and has very low stiffness.
3. The story shear is resisted in the first set of models C1-C4 mainly due to the shear yielding of the links between the circular holes. The plate buckles at a very small value of force and then gains strength immediately. The shear resistance by the shear links stays constant through the entire set over a D/S ratio of 0.2 to 0.8.
4. As the D/S ratio increases from 0.2 to 0.8 the spacing between the perforations reduces. There are more holes and lesser plate area in the links for shear resistance as the D/S ratio increases. This is reflected in the reduction of the shear capacity of the panel as seen from the force – displacement plots for the panels subjected to monotonic loading. The shear strength of the web panel reduces from about 550 kips to 450 kips as the D/S ratio increases from 0.2 to 0.8.
5. The monotonic force – displacement curves have four distinct regions with gradually reducing stiffness. The first region has a high initial stiffness and the second region with a lower secondary stiffness and the third region with a tertiary reduced slope and the fourth region with almost zero slope with very little or no strength gain or degradation. For C4 the fourth region of constant strength is not reached within the applied displacement range and hence the onset of the fourth region is seen and not the stabilized strength region as seen for models C1, C2 and C3.

6. The load at which the plate buckles is observed to reduce as the D/S ratio increases from 0.2 to 0.8 from about 415 kips for C1 to 75 kips for C4.
7. As the diameter of the holes increases from 6 to 9 inches or higher, the monotonic force – displacement curves are smoother with a smoother transition from the regions of primary, secondary and tertiary stiffness.
8. There is a transition in the behavior that is predominant in resisting the story shear from shear yielding of the links between the perforations to the diagonal tension filed action in the web panel. This could be seen from the hysteresis curves which get smoother with the increase in D/S ratio from 0.2 to 0.8. For the first set of models C1 – C4 this transitional behavior is seen at a D/S ratio of 0.8 and for the second set C5 – C8 at a D/S ratio of 0.6 – 0.8, for the third set C9 – C12 at a D/S ratio of 0.6, for the fourth set C12 – C15 at a D/S ratio of 0.4 – 0.6 and for the fifth set C16 – C20 at a D/S ratio of 0.4.
9. We see that for hole diameters of 9 and more inches as the D/S ratio reaches a value of 0.8 there is a slight strength gain as opposed to a constant strength plateau for lower D/S values.

1. C1 – Diameter = 6 inches, D/S = 0.2

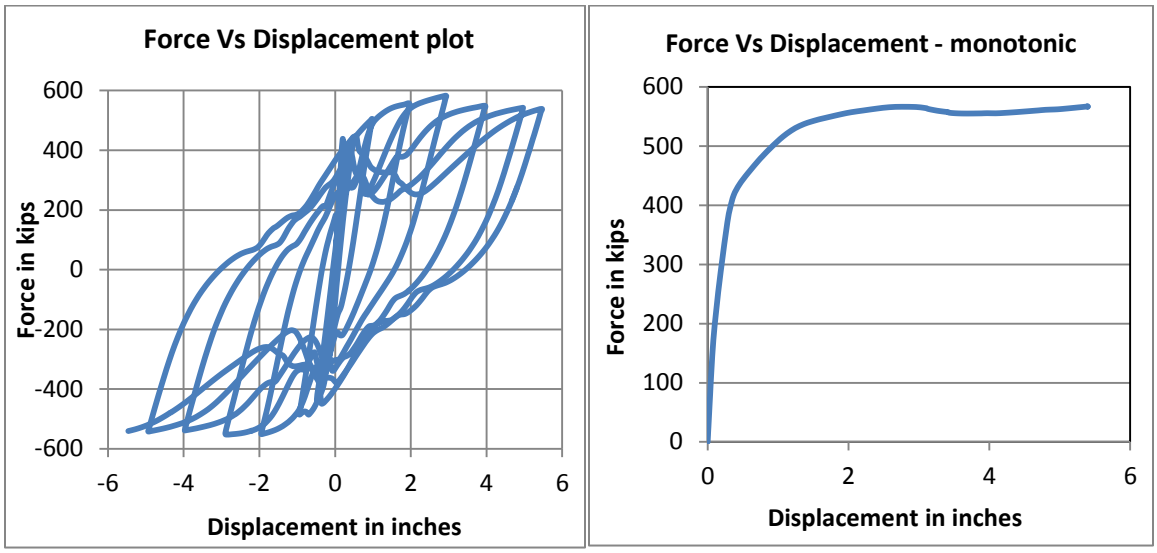

(a) (b)

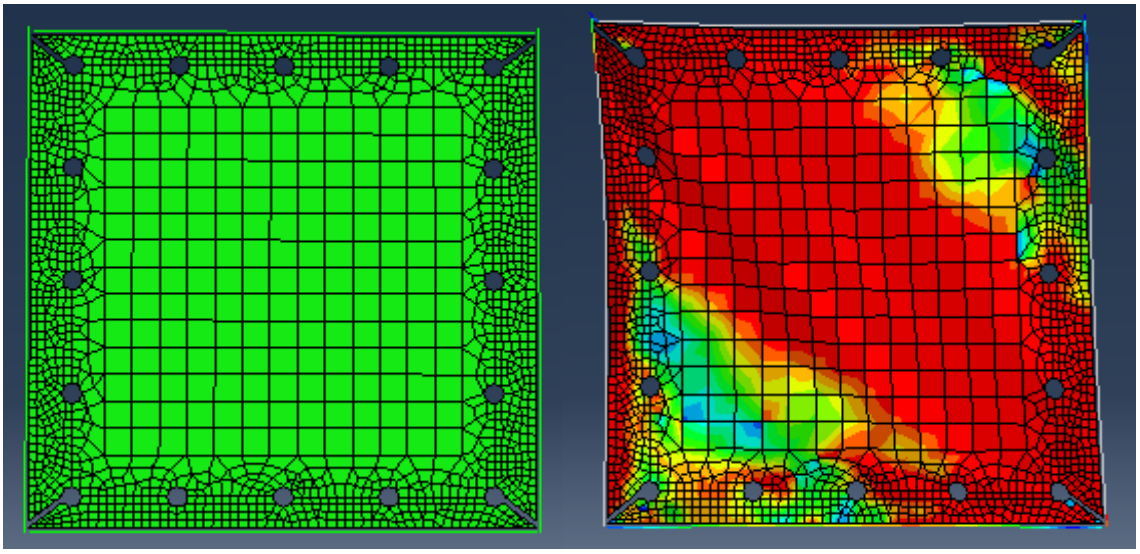

(c) (d)

Figure A-1 (a) Hysteresis curve, (b) Monotonic Force Vs Displacement curve, (c) Undeformed shape, (d) Deformed shape at 3.8% drift for Plate C1 with 6 inches hole diameter and D/S = 0.2

2. C2 – Diameter = 6 inches, D/S = 0.4

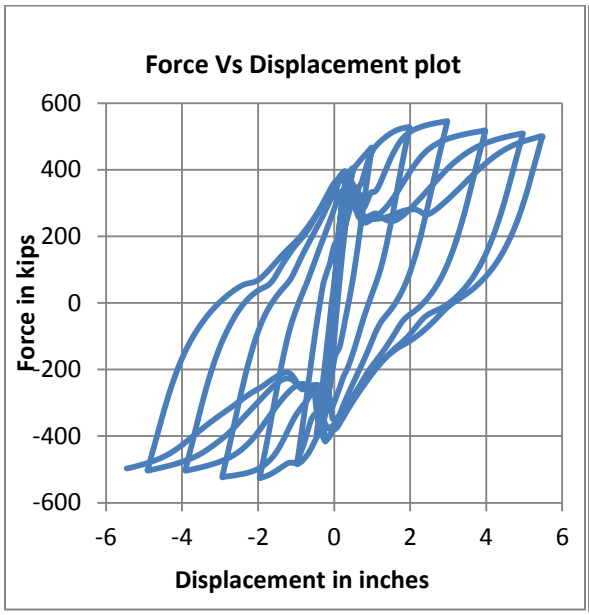

(a)

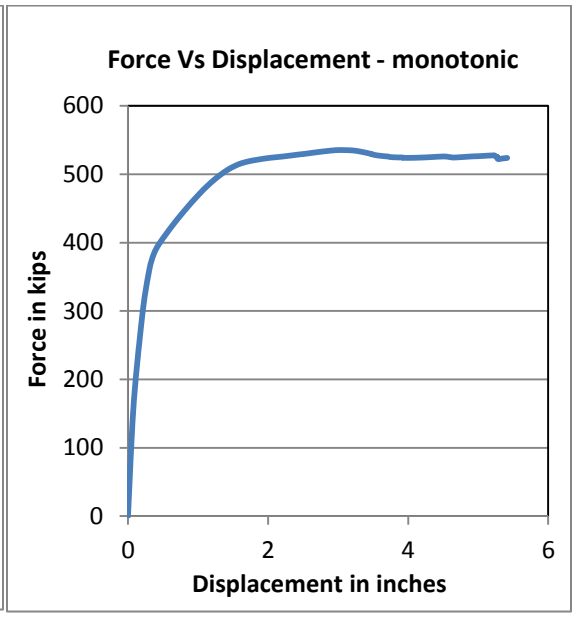

(b)

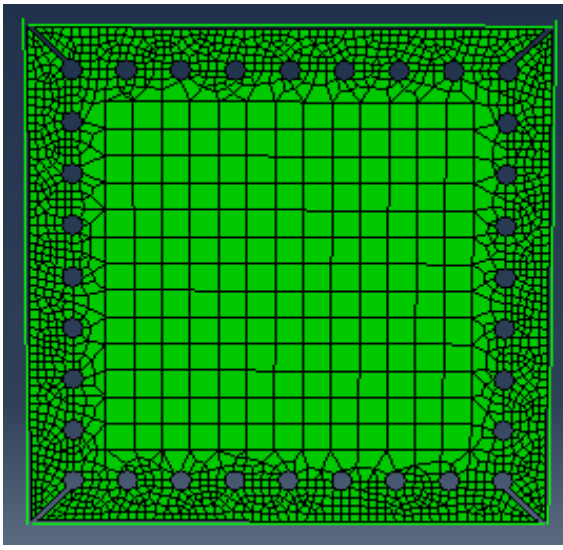

(c)

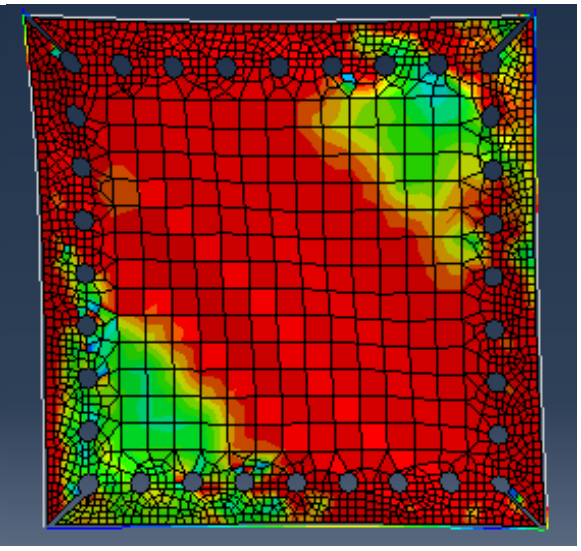

(d)

Figure A- 2 (a) Hysteresis curve, (b) Monotonic Force Vs Displacement curve, (c) Undeformed shape, (d) Deformed shape at 3.8% drift for Plate C2 with 6 inches hole diameter and D/S = 0.4

3. C3 – Diameter = 6 inches, D/S = 0.6

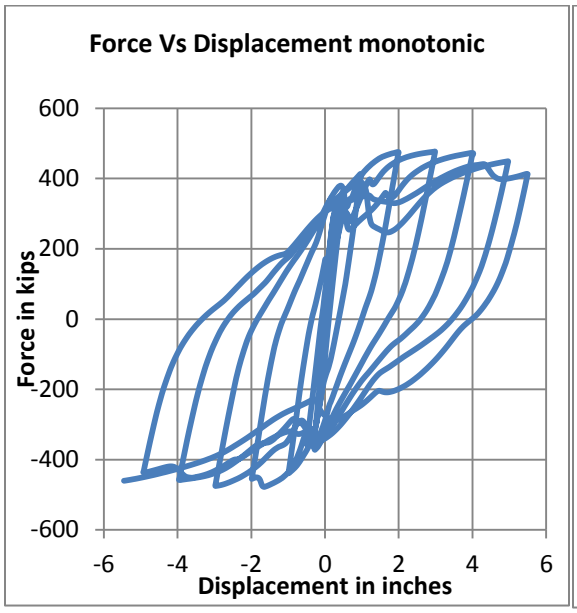

(a)

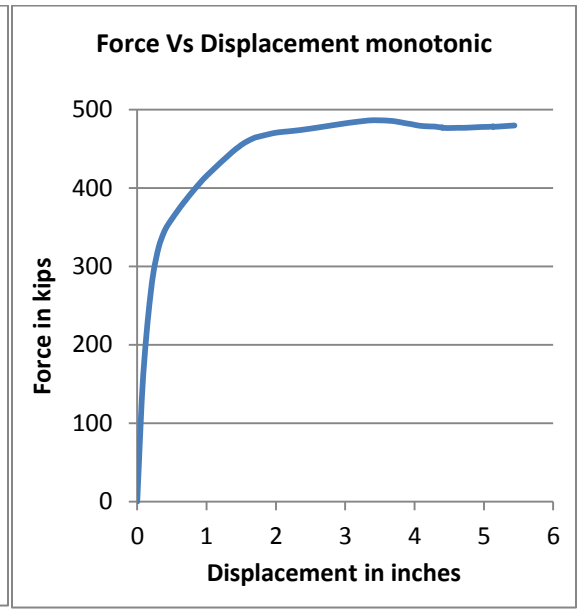

(b)

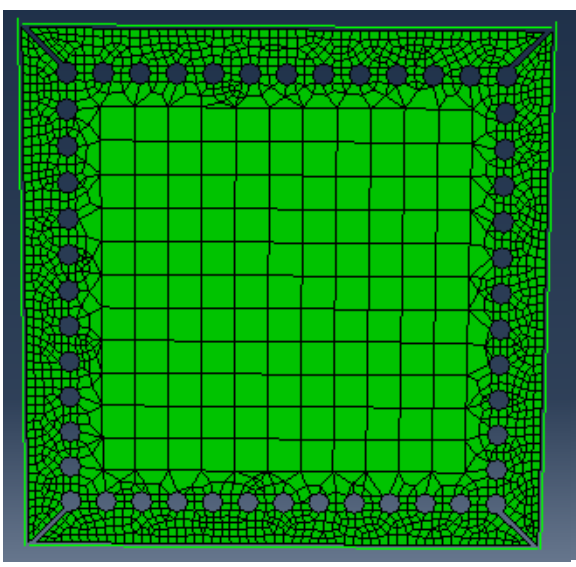

(c)

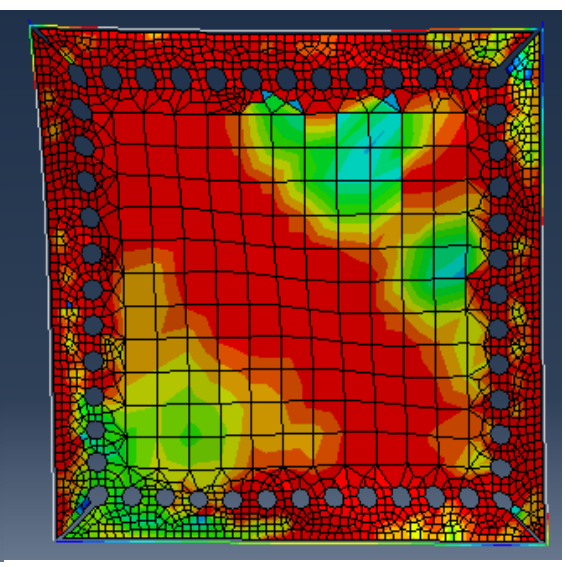

(d)

Figure A- 3 (a) Hysteresis curve, (b) Monotonic Force Vs Displacement curve, (c) Undeformed shape, (d) Deformed shape at 3.8% drift for Plate C3 with 6 inches hole diameter and D/S = 0.6

4. C4 – Diameter = 6 inches, D/S = 0.8

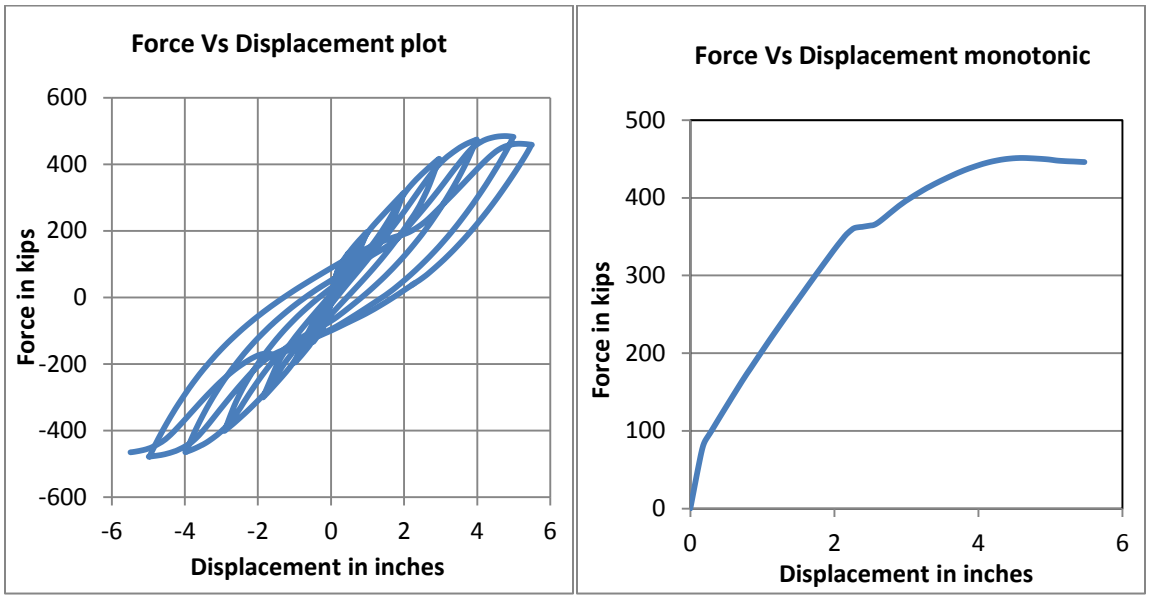

(a) (b)

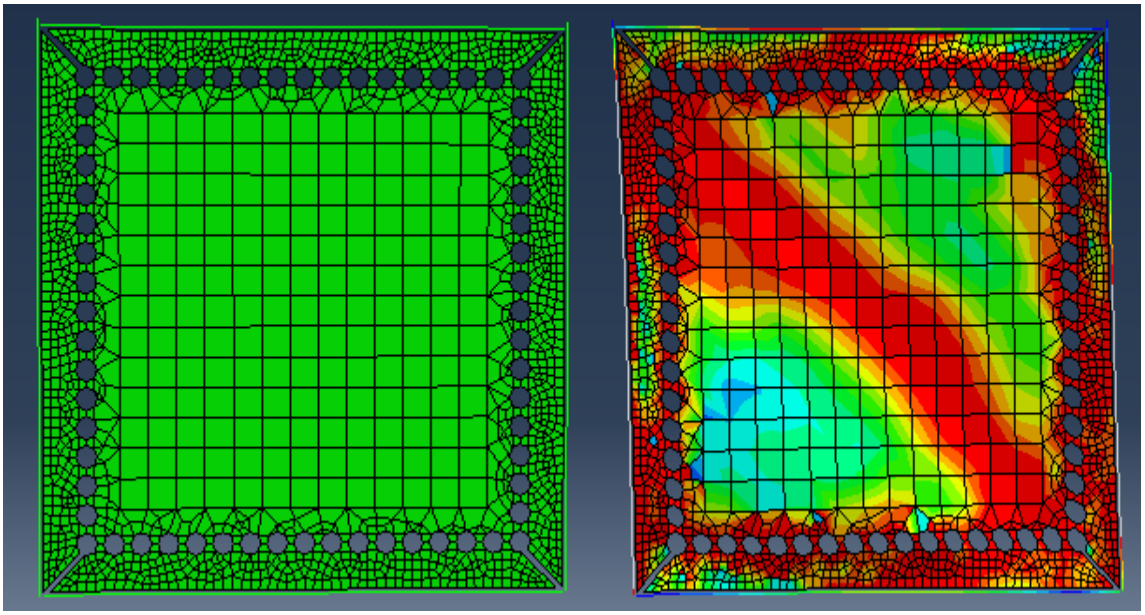

(c) (d)

Figure A- 4 (a) Hysteresis curve, (b) Monotonic Force Vs Displacement curve, (c) Undeformed shape, (d) Deformed shape at 3.8% drift for Plate C4 with 6 inches hole diameter and D/S = 0.8

5. C5 – Diameter = 9 inches, D/S = 0.2

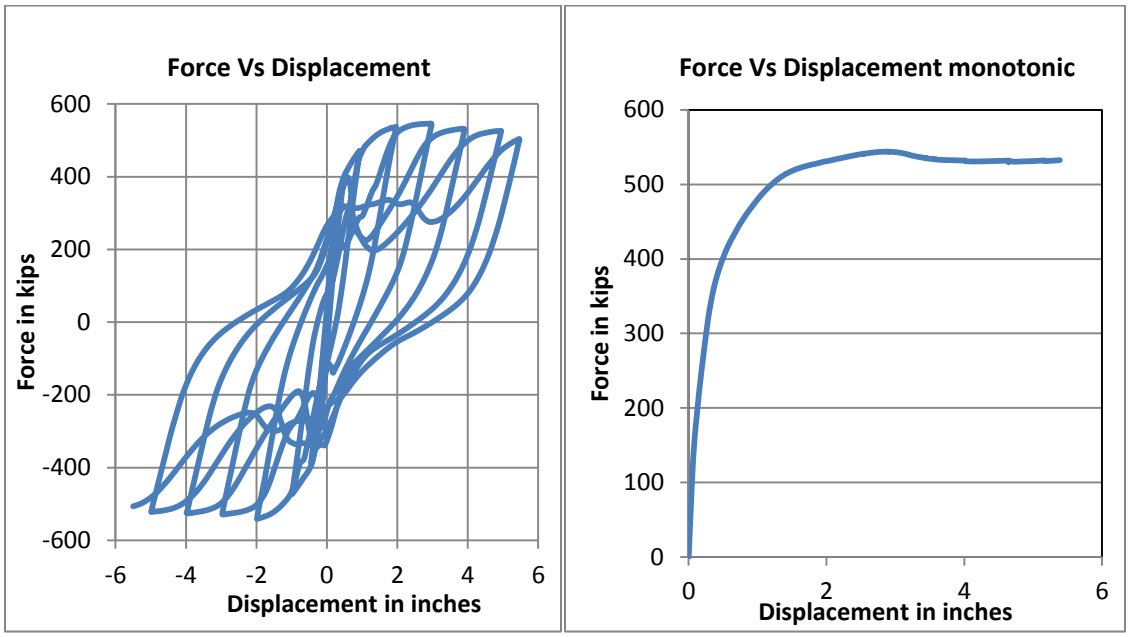

(a) (b)

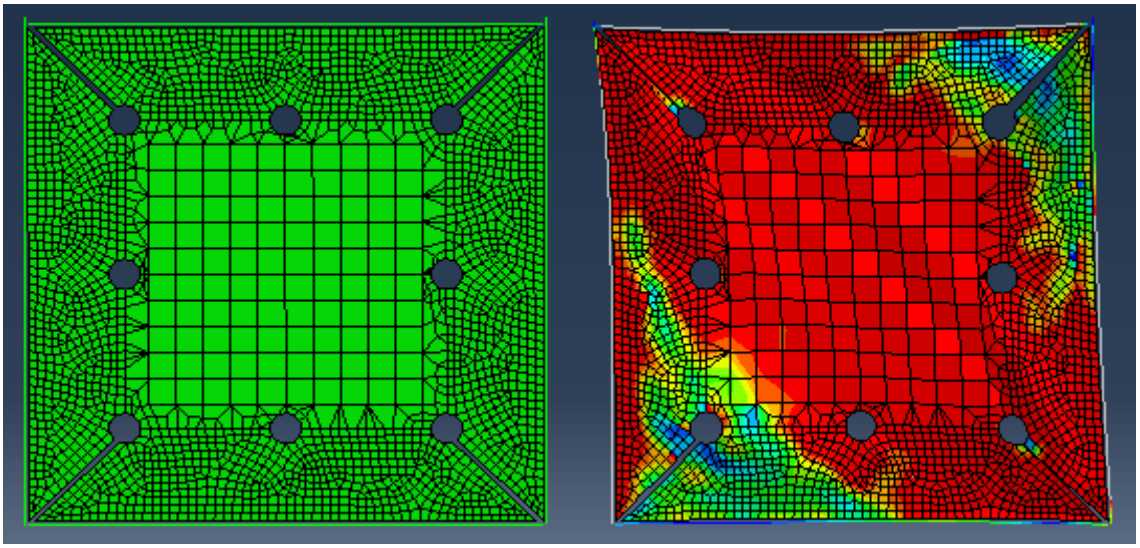

(c) (d)

Figure A- 5 (a) Hysteresis curve, (b) Monotonic Force Vs Displacement curve, (c) Undeformed shape, (d) Deformed shape at 3.8% drift for Plate C5 with 9 inches hole diameter and D/S = 0.2

6. C6 – Diameter = 9 inches, D/S = 0.4

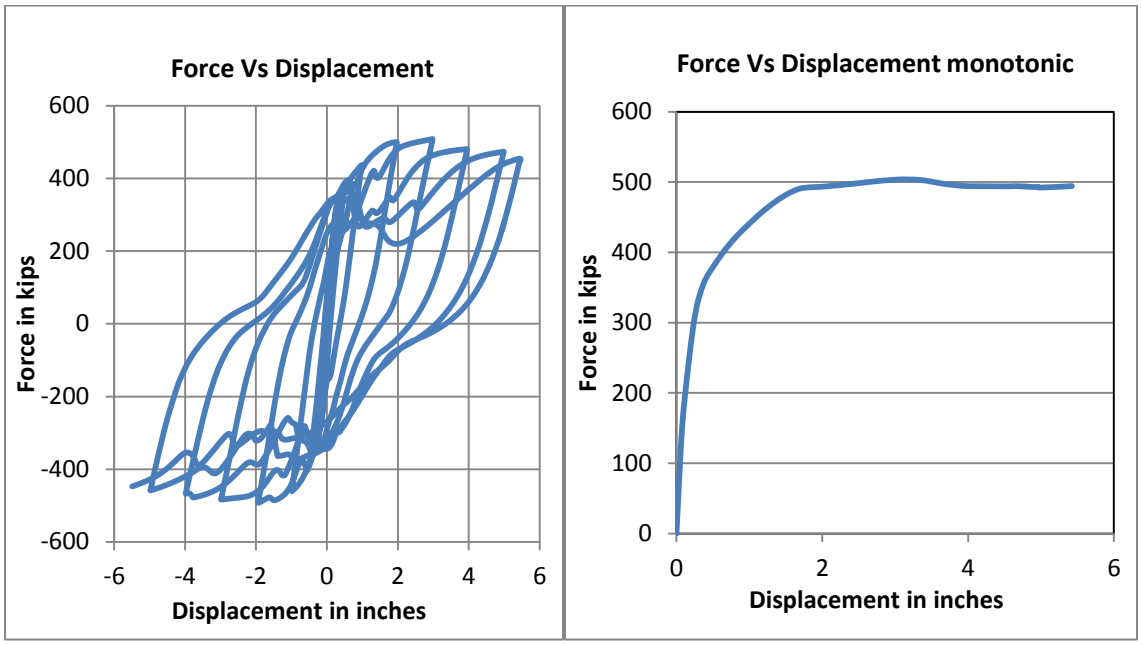

(a) (b)

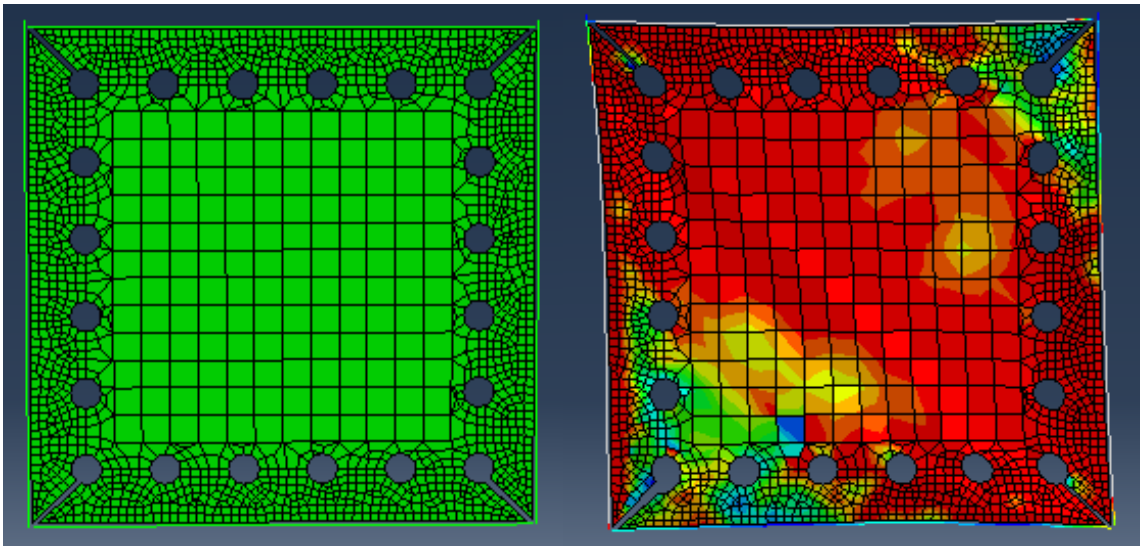

(c) (d)

Figure A- 6 (a) Hysteresis curve, (b) Monotonic Force Vs Displacement curve, (c) Undeformed shape, (d) Deformed shape at 3.8% drift for Plate C6 with 9 inches hole diameter and D/S = 0.4

7. C7 – Diameter = 9 inches, D/S = 0.6

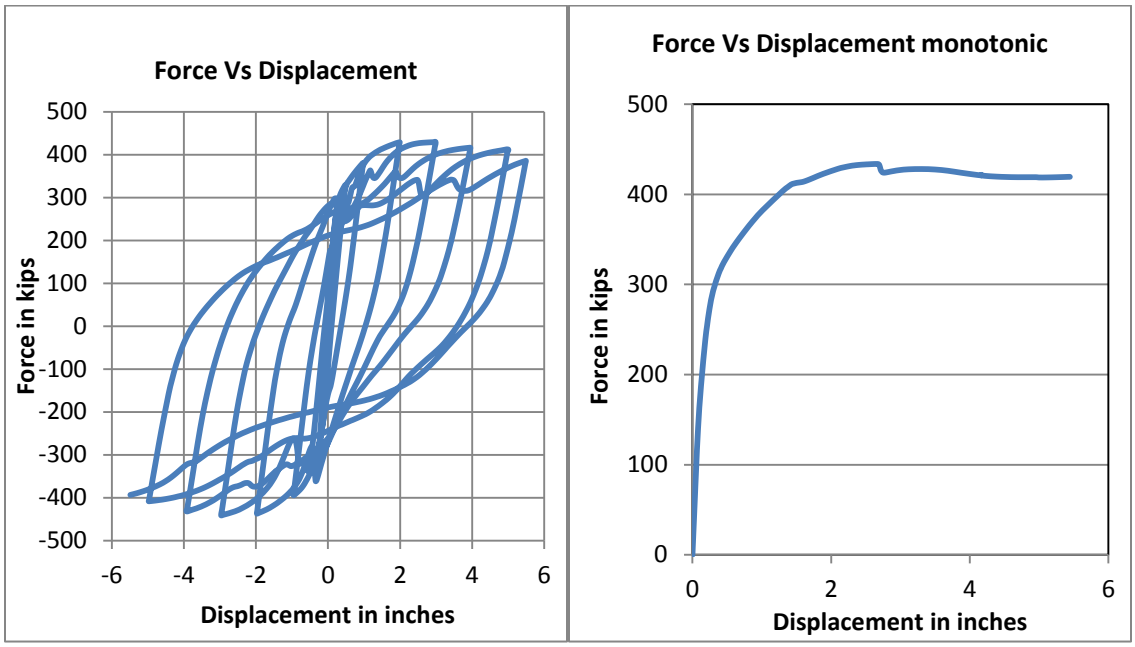

(a) (b)

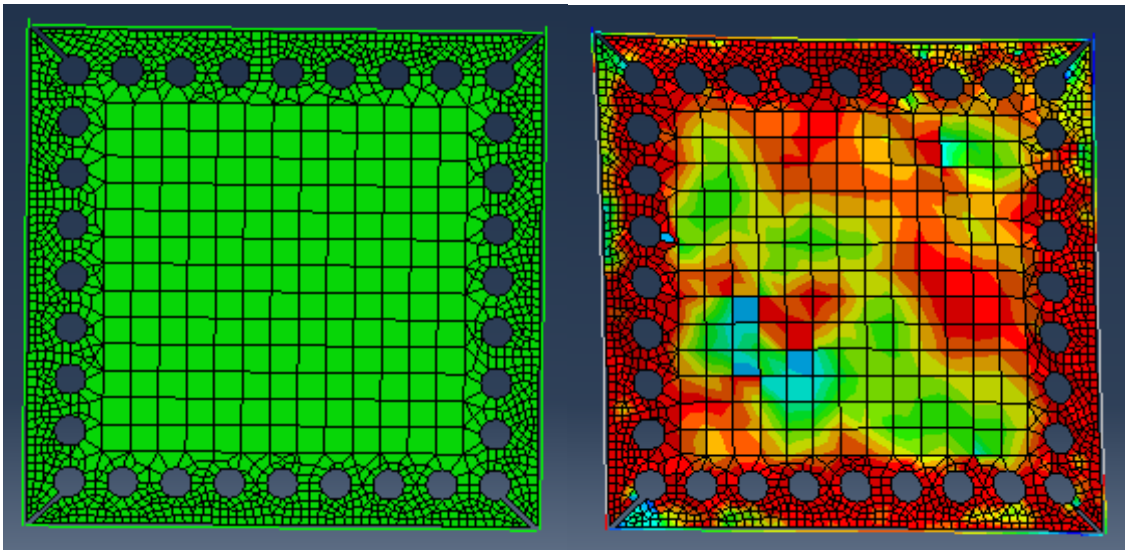

(c) (d)

Figure A- 7 (a) Hysteresis curve, (b) Monotonic Force Vs Displacement curve, (c) Undeformed shape, (d) Deformed shape at 3.8% drift for Plate C7 with 9 inches hole diameter and D/S = 0.6

8. C8 – Diameter = 9 inches, D/S = 0.8

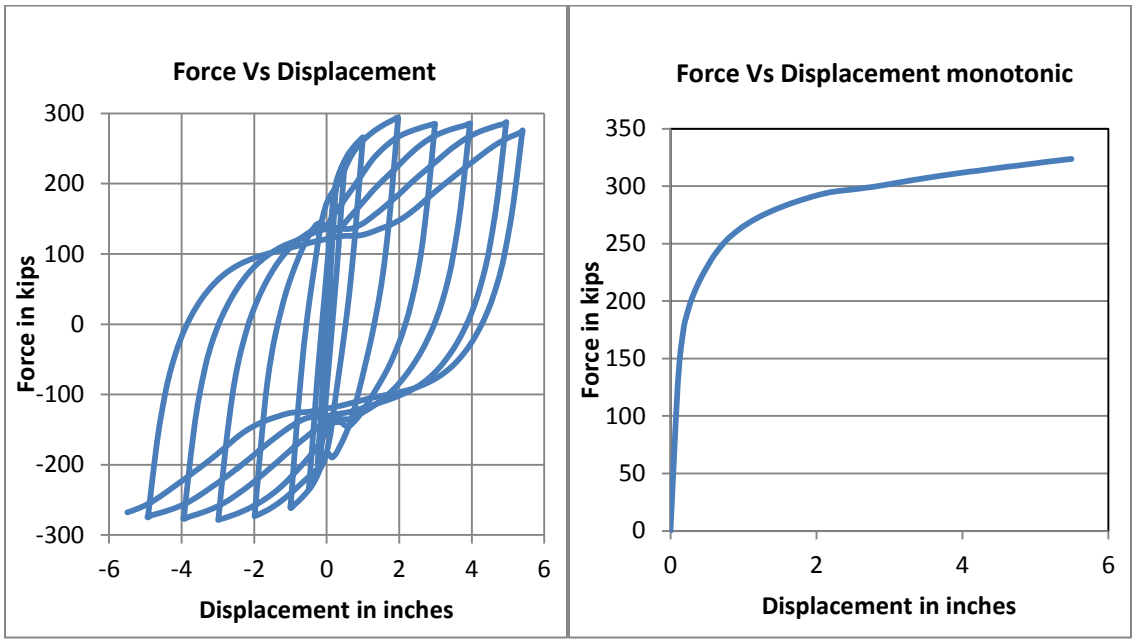

(a) (b)

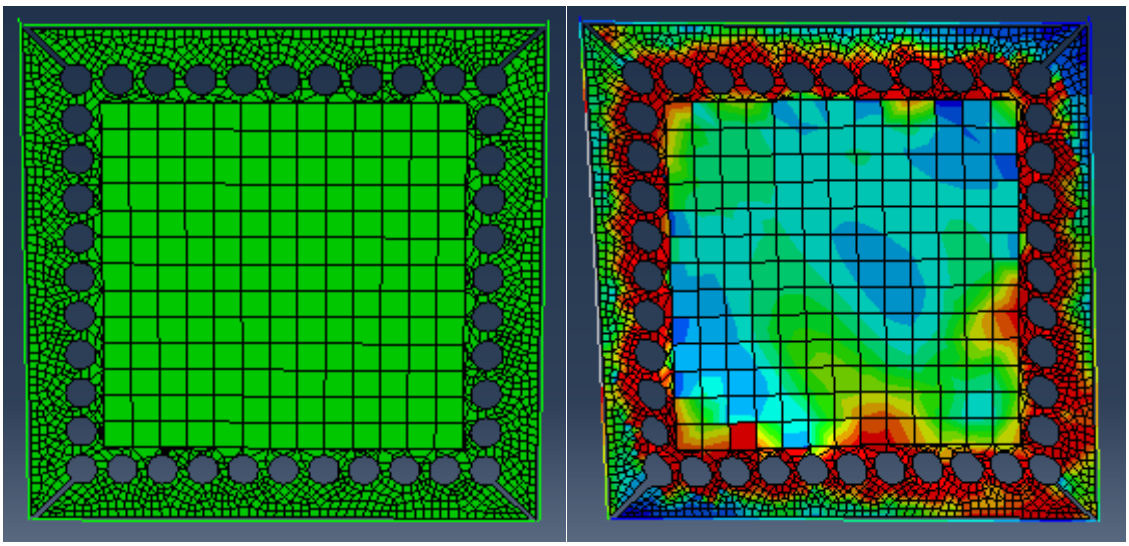

(c) (d)

Figure A- 8 (a) Hysteresis curve, (b) Monotonic Force Vs Displacement curve, (c) Undeformed shape, (d) Deformed shape at 3.8% drift for Plate C8 with 9 inches hole diameter and D/S = 0.8

9. C9 – Diameter = 12 inches , D/S = 0.2

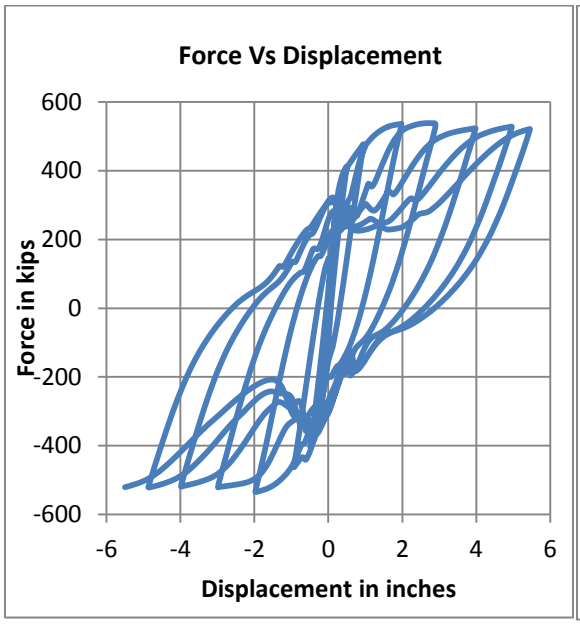

(a)

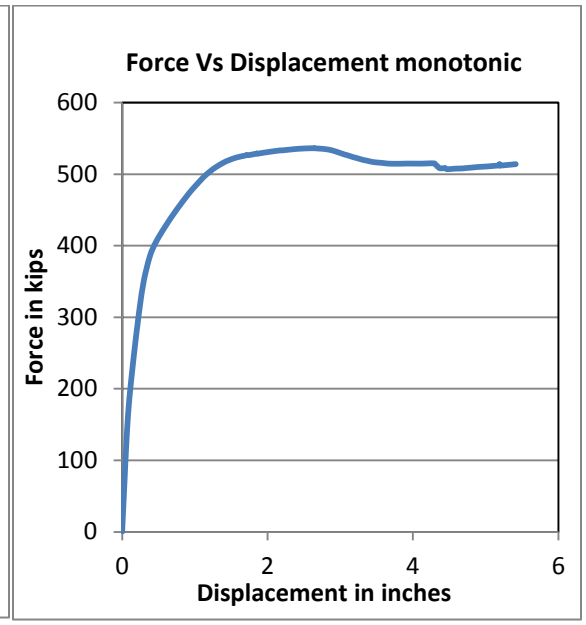

(b)

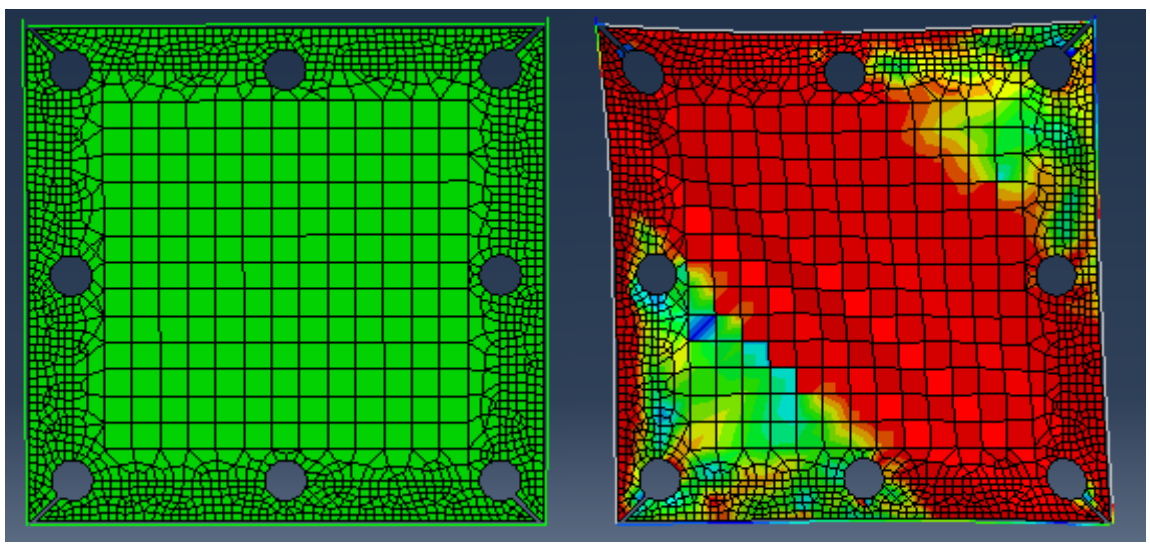

(c) (d)

Figure A- 9 (a) Hysteresis curve, (b) Monotonic Force Vs Displacement curve, (c) Undeformed shape, (d) Deformed shape at 3.8% drift for Plate C9 with 12 inches hole diameter and D/S = 0.2

10. C10 – Diameter = 12 inches, D/S = 0.4

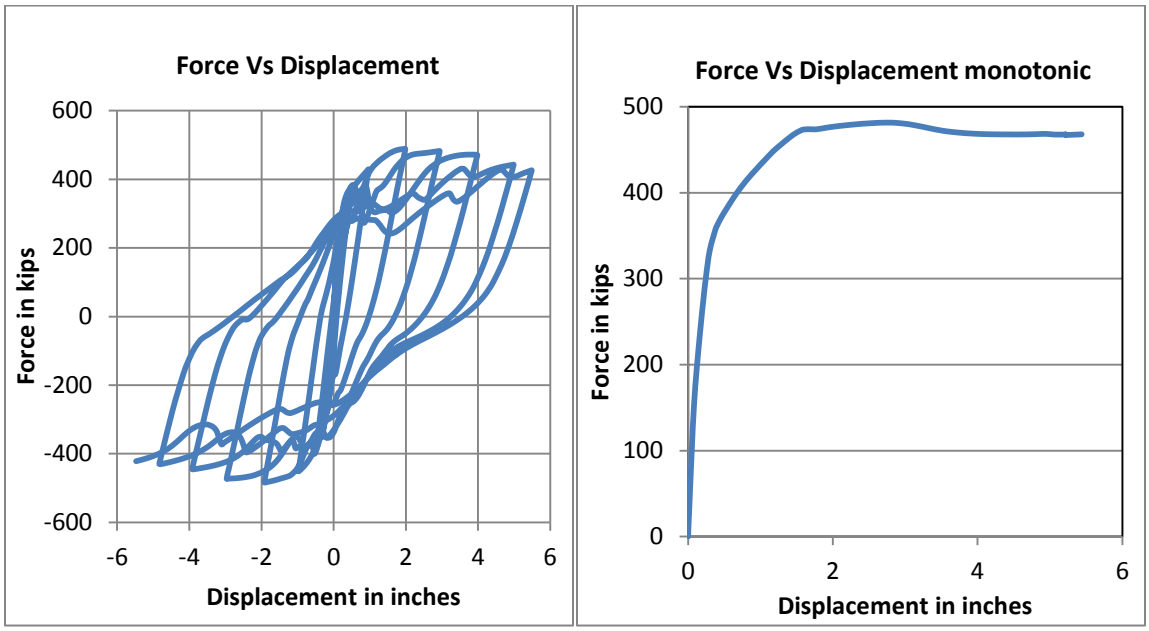

(a) (b)

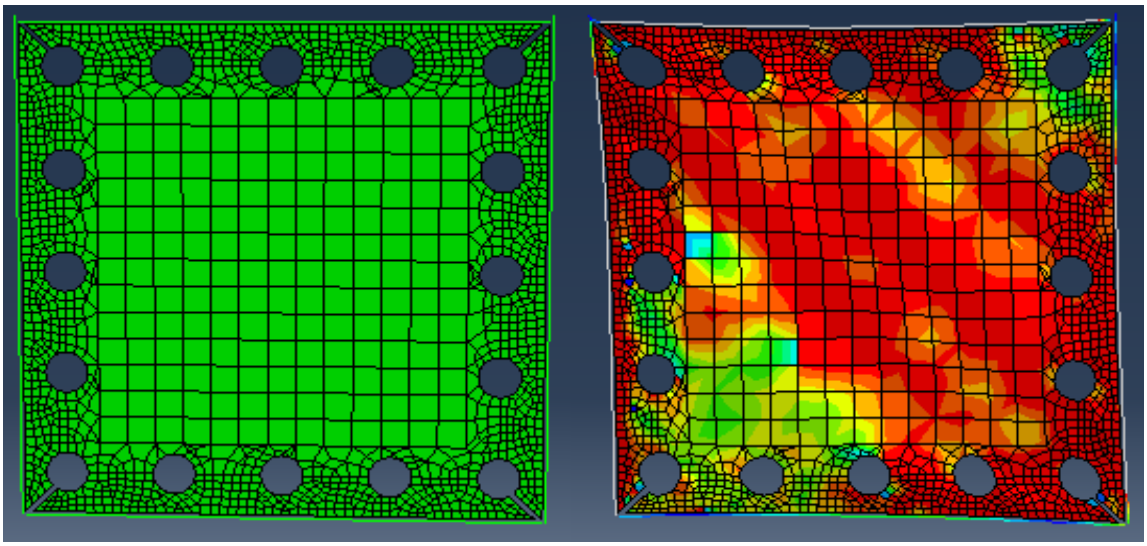

(c) (d)

Figure A- 10 (a) Hysteresis curve, (b) Monotonic Force Vs Displacement curve, (c) Undeformed shape, (d) Deformed shape at 3.8% drift for Plate C10 with 12 inches hole diameter and D/S = 0.4

11. C11 – Diameter = 12 inches, D/S = 0.6

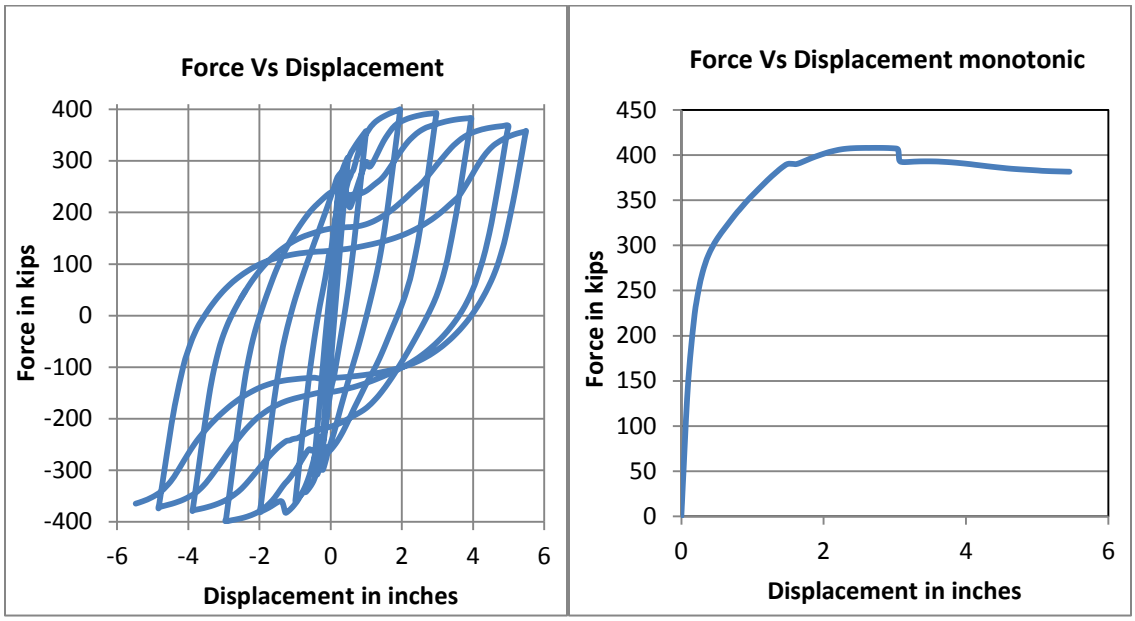

(a) (b)

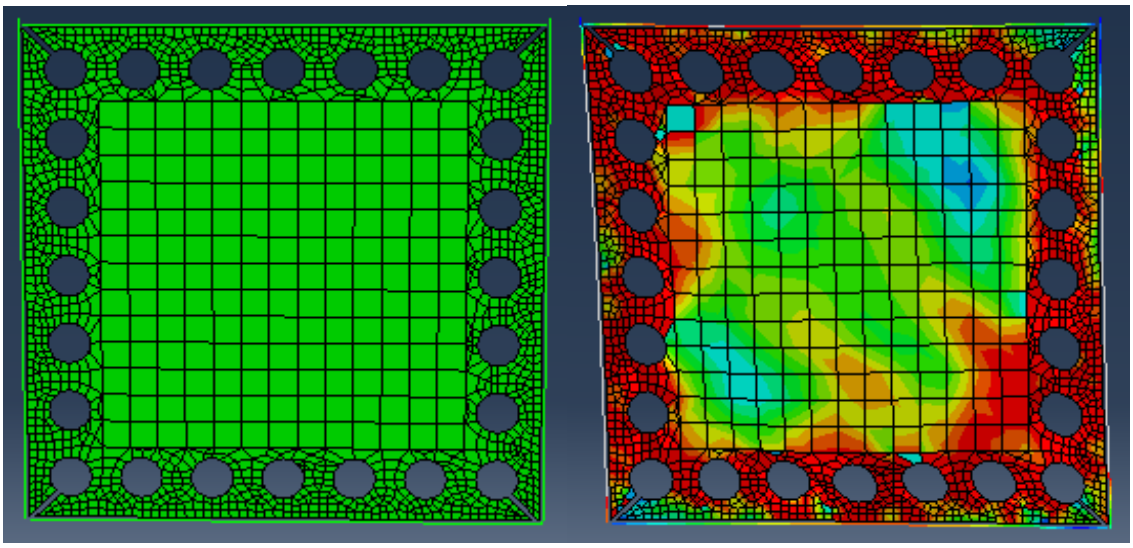

(c) (d)

Figure A- 11 (a) Hysteresis curve, (b) Monotonic Force Vs Displacement curve, (c) Undeformed shape, (d) Deformed shape at 3.8% drift for Plate C11 with 12 inches hole diameter and D/S = 0.6

12. C12 – Diameter = 12 inches, D/S = 0.8

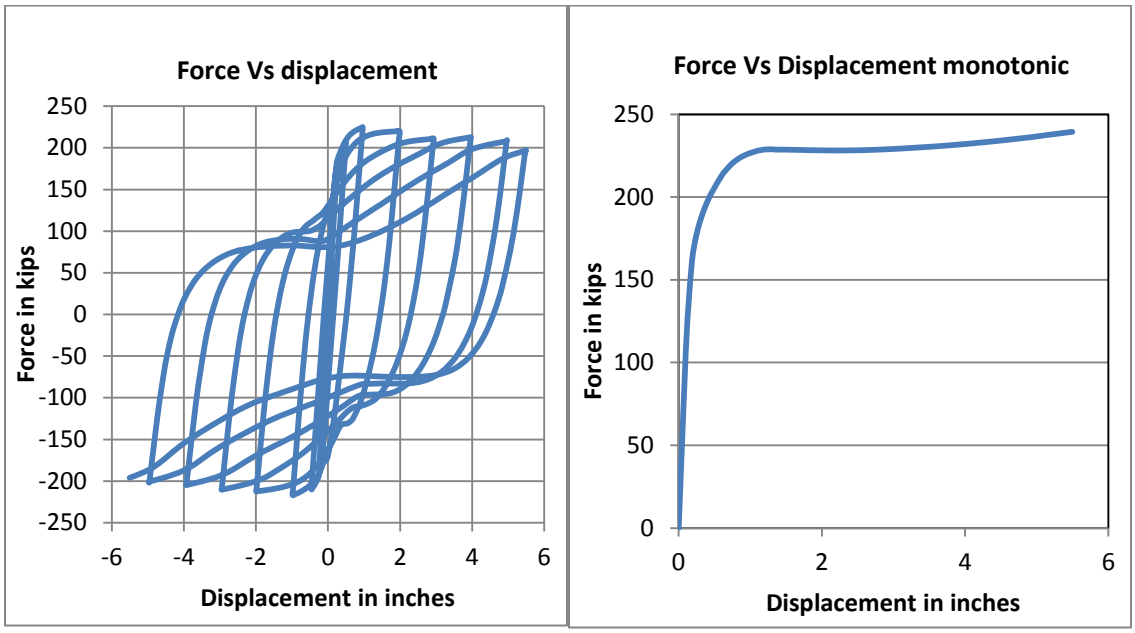

(a) (b)

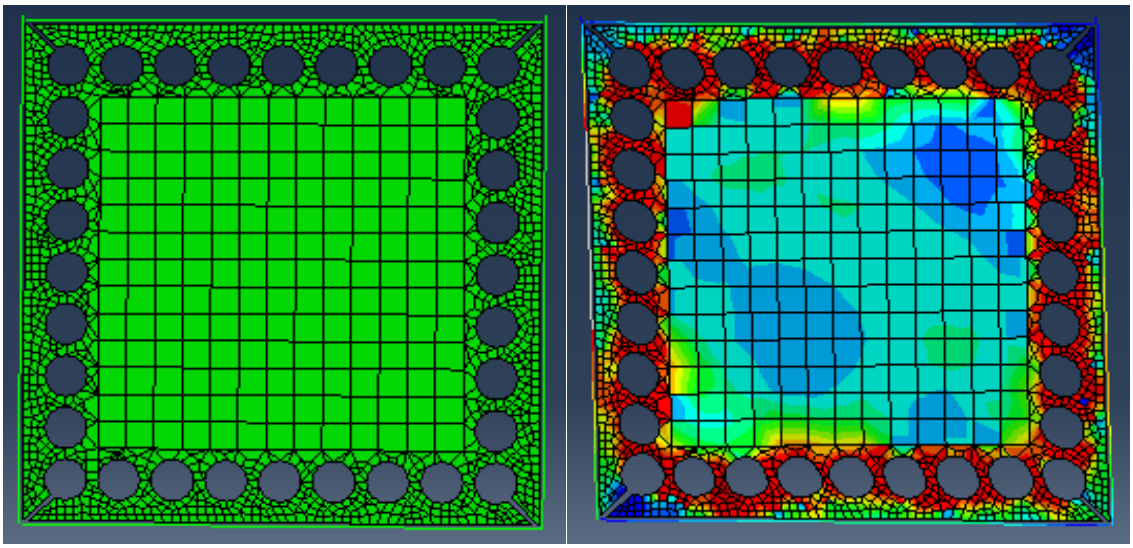

(c) (d)

Figure A- 12 (a) Hysteresis curve, (b) Monotonic Force Vs Displacement curve, (c) Undeformed shape, (d) Deformed shape at 3.8% drift for Plate C12 with 12 inches hole diameter and D/S = 0.8

13. C13 – Diameter = 15 inches, D/S = 0.2

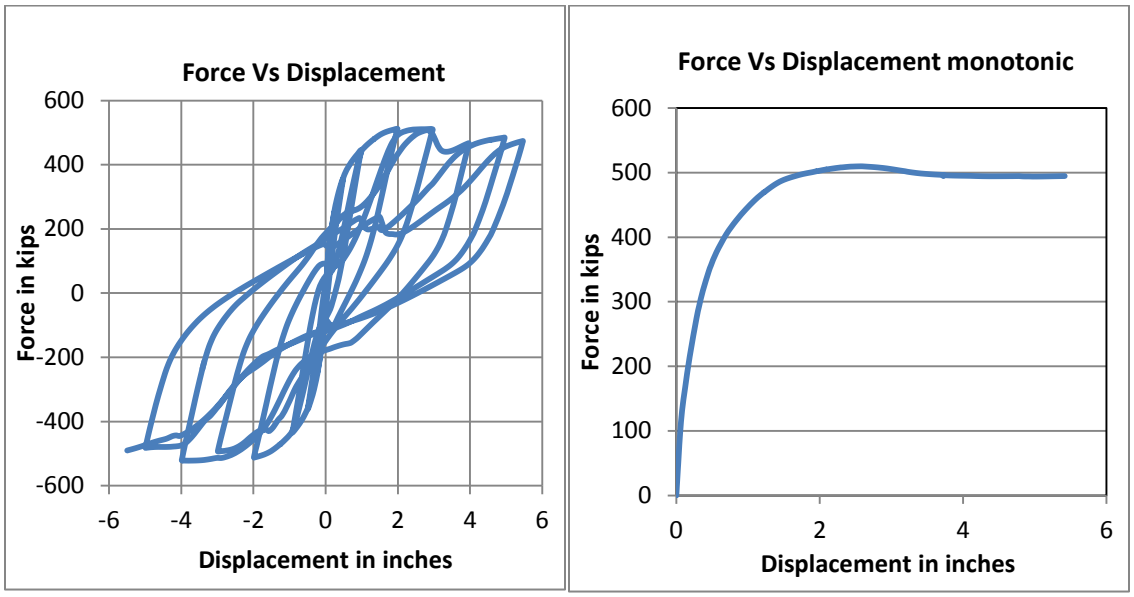

(a) (b)

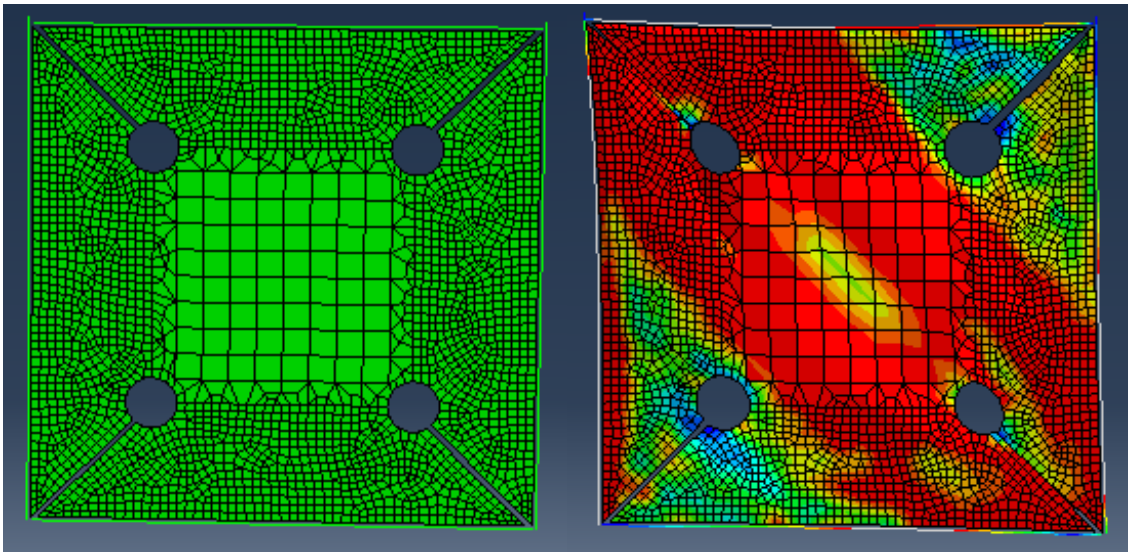

(c) (d)

Figure A- 13 (a) Hysteresis curve, (b) Monotonic Force Vs Displacement curve, (c) Undeformed shape, (d) Deformed shape at 3.8% drift for Plate C13 with 15 inches hole diameter and D/S = 0.2

14. C14 – Diameter = 15 inches, D/S = 0.4

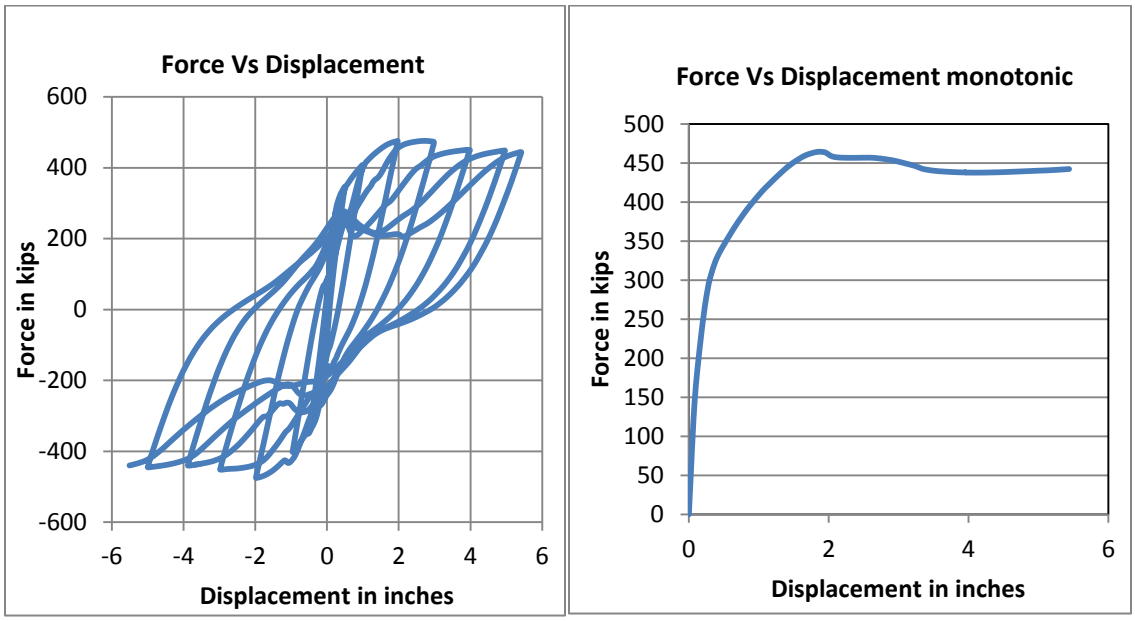

(a) (b)

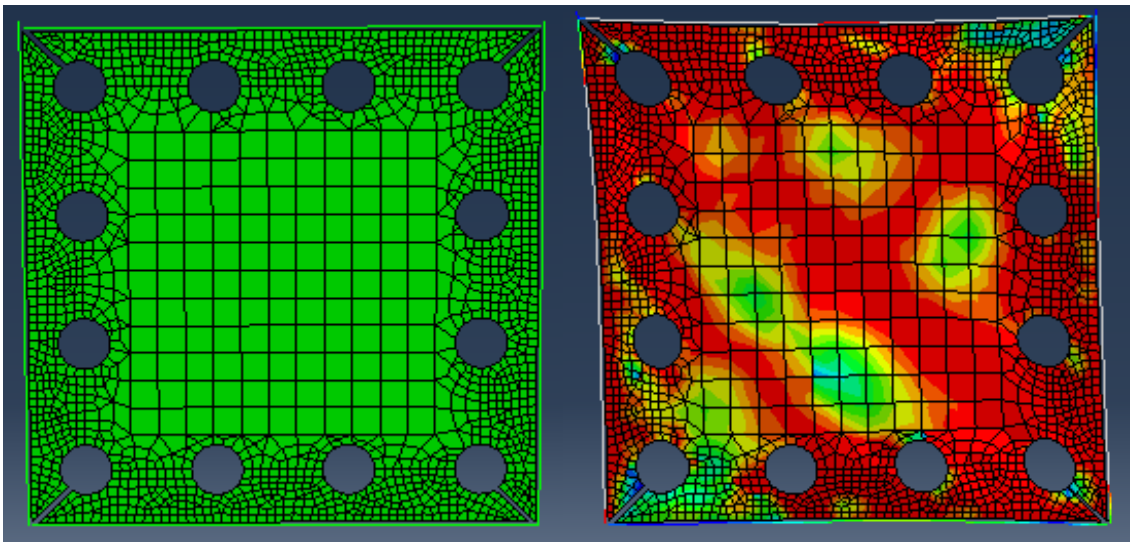

(c) (d)

Figure A- 14 (a) Hysteresis curve, (b) Monotonic Force Vs Displacement curve, (c) Undeformed shape, (d) Deformed shape at 3.8% drift for Plate C14 with 15 inches hole diameter and D/S = 0.4

15. C15 – Diameter = 15 inches, D/S = 0.6

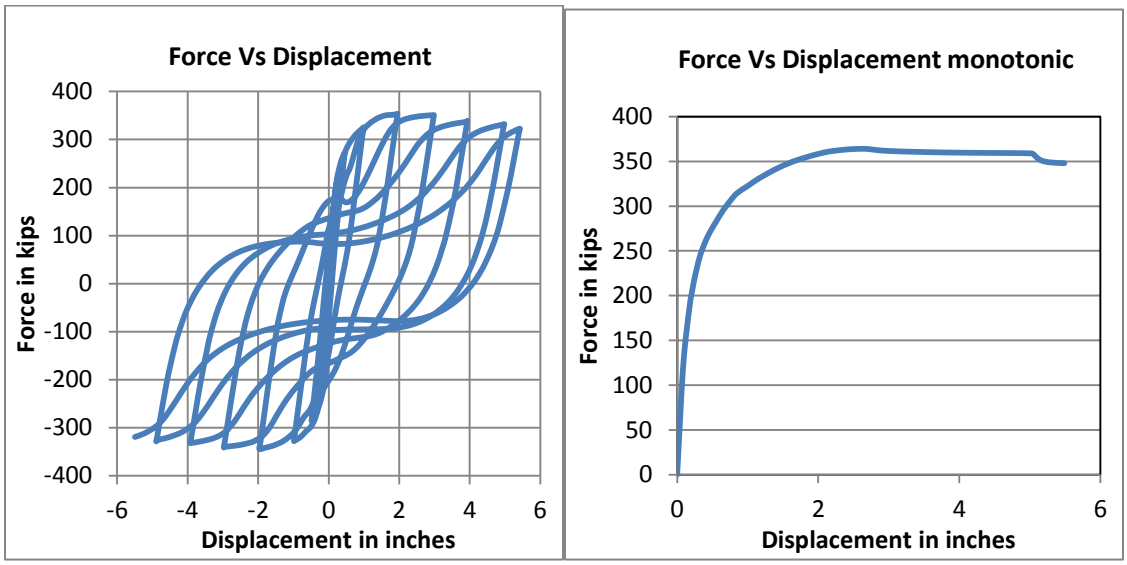

(a) (b)

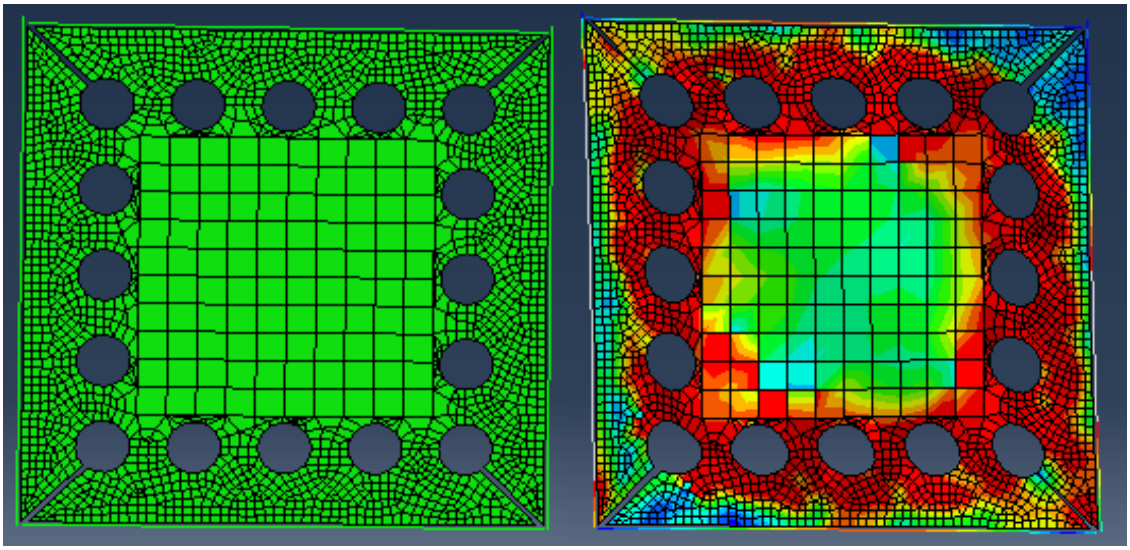

(c) (d)

Figure A- 15 (a) Hysteresis curve, (b) Monotonic Force Vs Displacement curve, (c) Undeformed shape, (d) Deformed shape at 3.8% drift for Plate C15 with 15 inches hole diameter and D/S = 0.6

16. C16 – Diameter = 15 inches, D/S = 0.8

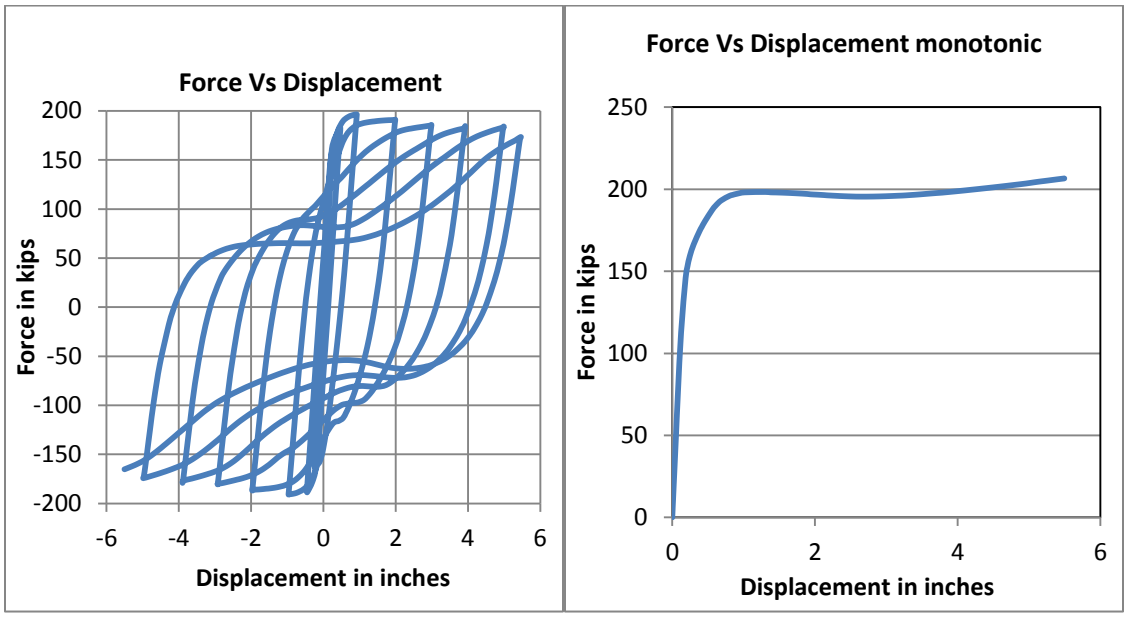

(a) (b)

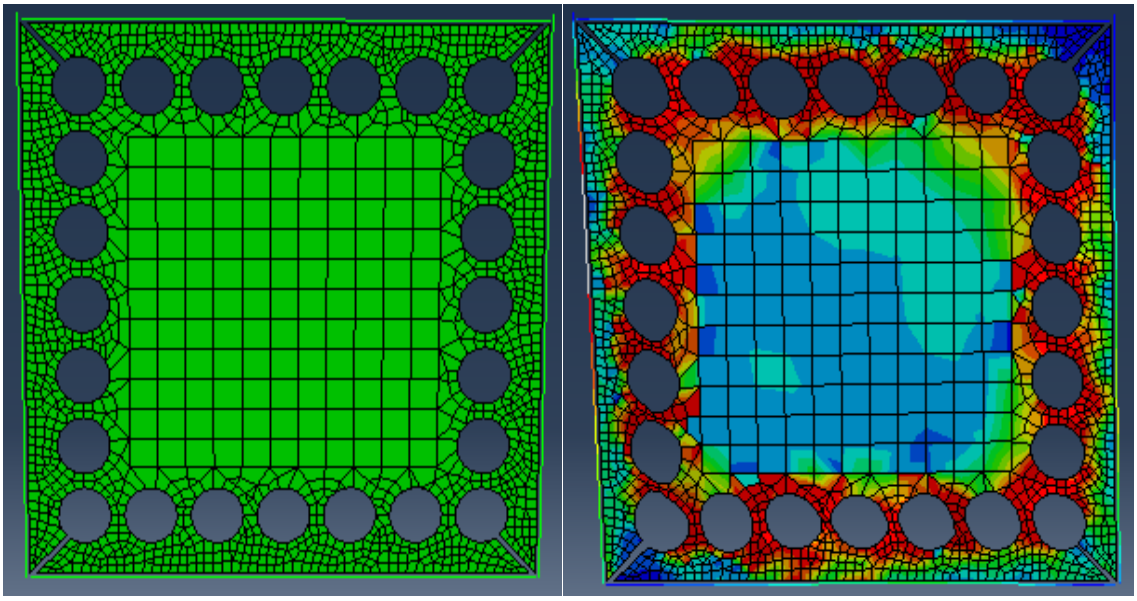

(c) (d)

Figure A- 16 (a) Hysteresis curve, (b) Monotonic Force Vs Displacement curve, (c) Undeformed shape, (d) Deformed shape at 3.8% drift for Plate C16 with 15 inches hole diameter and D/S = 0.8

17. C17 – Diameter = 18 inches, D/S = 0.2

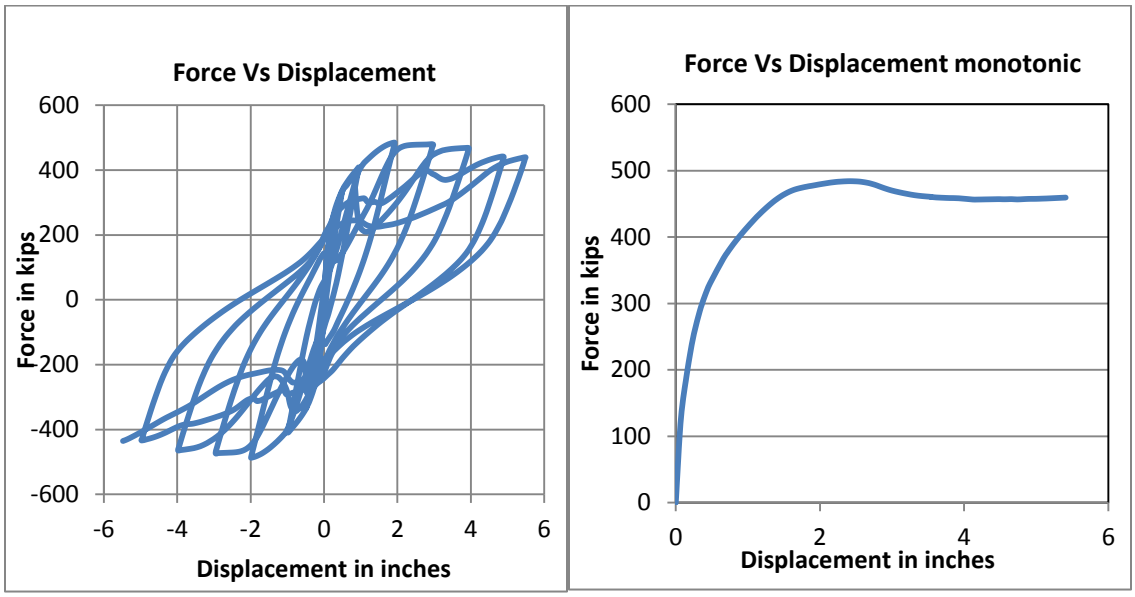

(a) (b)

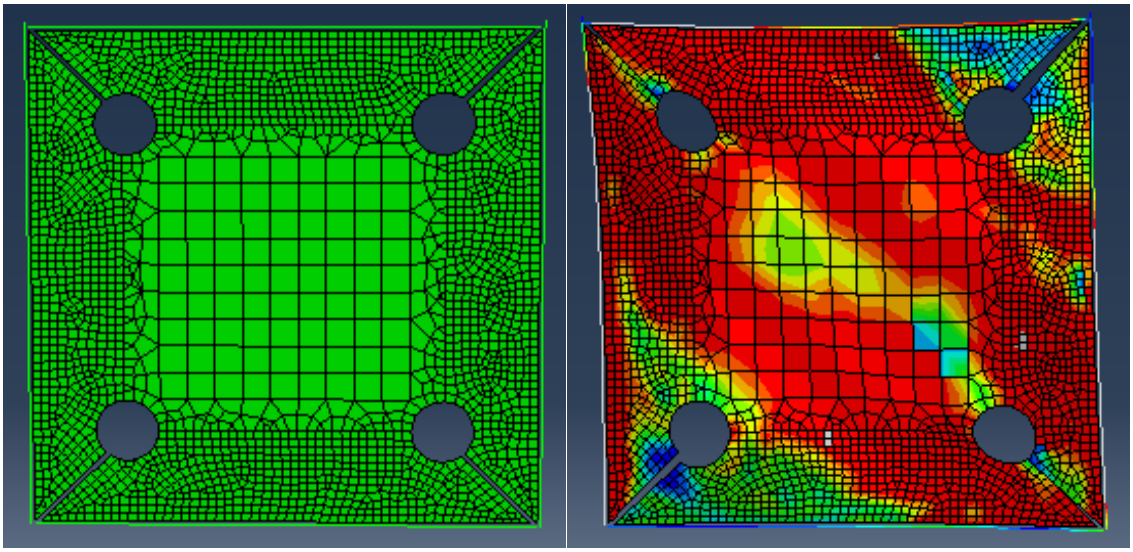

(c) (d)

Figure A- 17 (a) Hysteresis curve, (b) Monotonic Force Vs Displacement curve, (c) Undeformed shape, (d) Deformed shape at 3.8% drift for Plate C17 with 18 inches hole diameter and D/S = 0.2

18. C18 – Diameter = 18 inches, D/S = 0.4

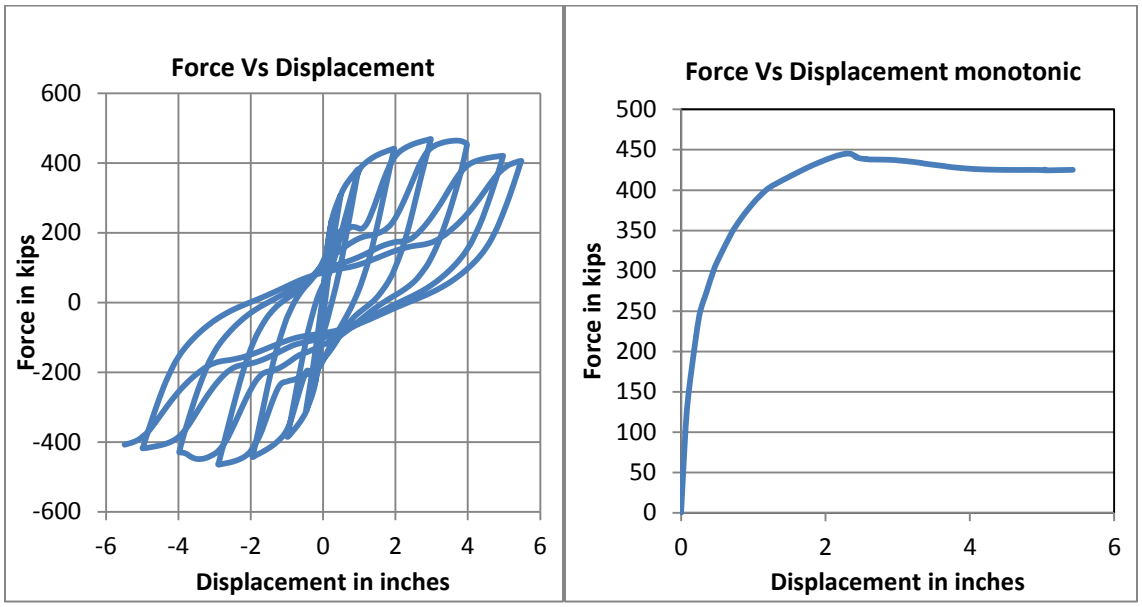

(a) (b)

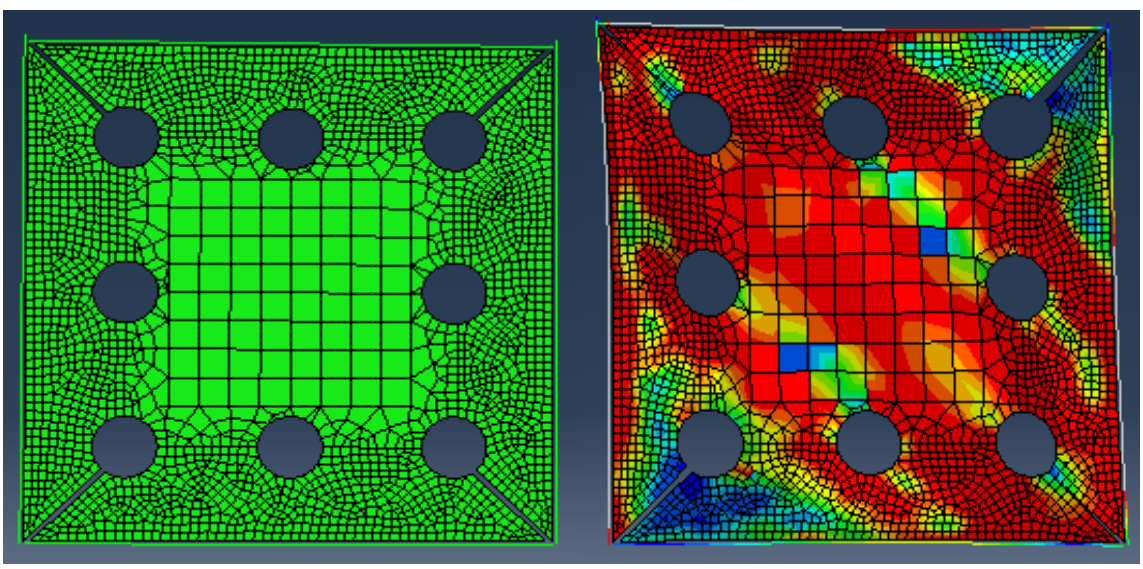

(c) (d)

Figure A- 18 (a) Hysteresis curve, (b) Monotonic Force Vs Displacement curve, (c) Undeformed shape, (d) Deformed shape at 3.8% drift for Plate C18 with 18 inches hole diameter and D/S = 0.4

19. C19 – Diameter = 18 inches, D/S = 0.6

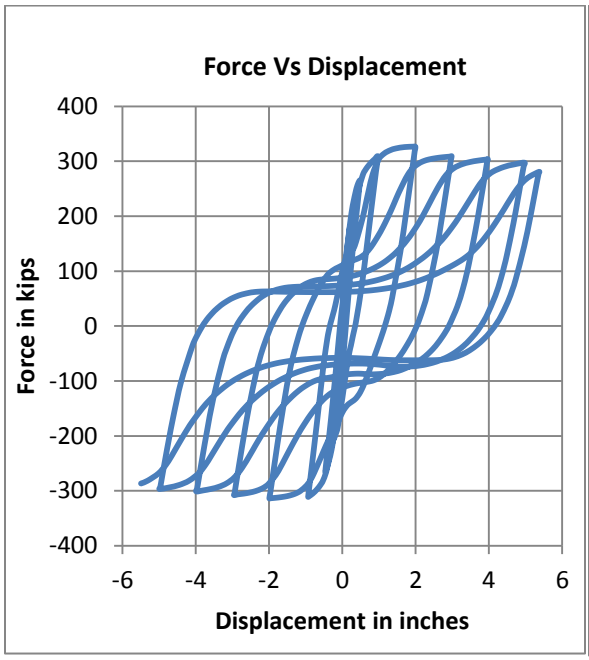

(a)

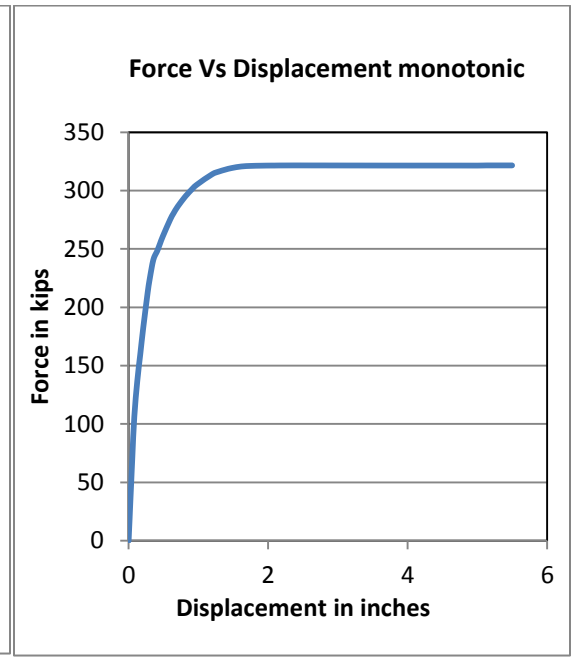

(b)

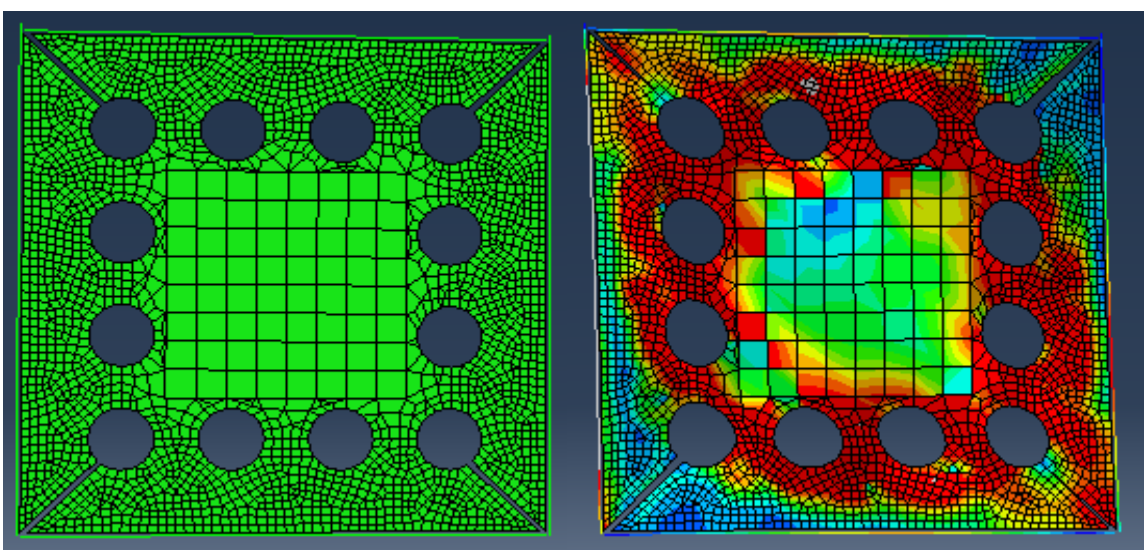

(c) (d)

Figure A- 19 (a) Hysteresis curve, (b) Monotonic Force Vs Displacement curve, (c) Undeformed shape, (d) Deformed shape at 3.8% drift for Plate C19 with 18 inches hole diameter and D/S = 0.6

20. C20 – Diameter = 18 inches, D/S = 0.8

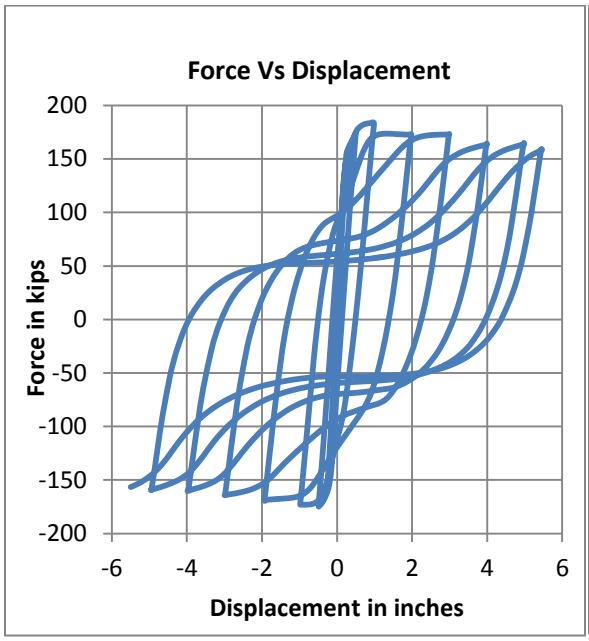

(a)

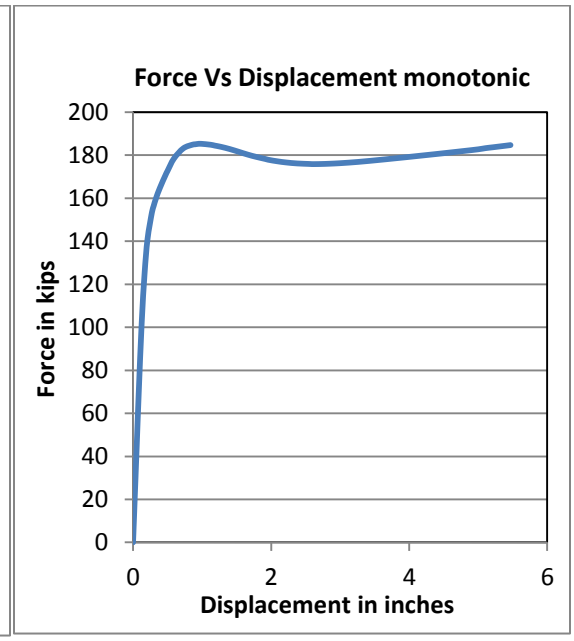

(b)

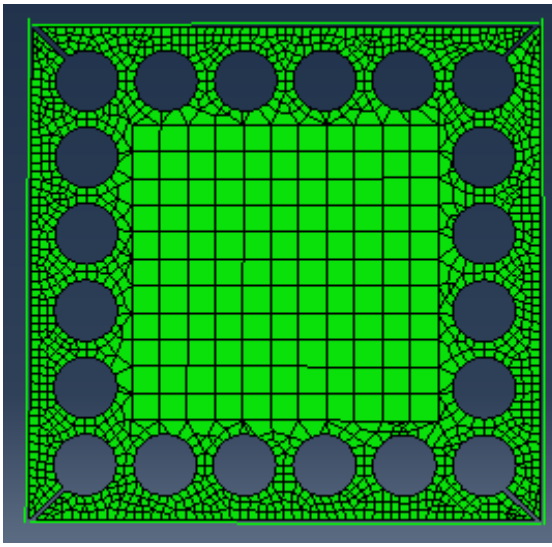

(c)

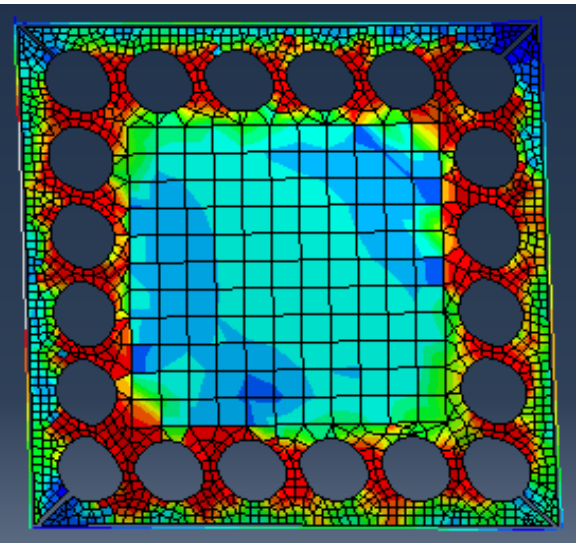

(d)

Figure A- 20 (a) Hysteresis curve, (b) Monotonic Force Vs Displacement curve, (c) Undeformed shape, (d) Deformed shape at 3.8% drift for Plate C20 with 18 inches hole diameter and D/S = 0.8

Trends from hysteresis plots and force-deformation plots for the set of 10 models with perimeter circular holes with varying thickness are presented below:

1. The energy dissipation capacity clearly increases with increase in plate thickness from 0.1875 inches to 0.75 inches. The hysteretic behavior is highly pinched for plates of lower thickness and is more complete as the thickness increases.
2. The D/S ratio and the diameter of holes is kept constant throughout the first set from C21 – C25. As observed in the previous set of models C1 – C20, for a D/S ratio of 0.6 and 9 inch diameter of holes, the diagonal tension field action is the predominant mechanism for shear resistance; the same trend is seen in the models C21 and C22 for a plate thickness of 0.1875 and 0.25 inches. But as the thickness increases, the controlling behavior shifts to shear yielding of the links between the perforations for models C23, C24 and C25.
3. The monotonic force displacement curve shows a gain in strength for the model with a plate thickness of 0.75 inches as opposed to a final strength plateau as seen in the other models with lower plate thickness.
4. The peak shear strength of the plate increases with increase in plate thickness from 0.1875 to 0.75 inches from 205 kips for C21 to 850 kips for C25 and from 160 kips for C26 to 750 kips for C30.
5. The force displacement curves have a smoother transition of stiffness for plates with higher thickness as compared to that for the ones with lower plate thickness.

   For the next set of models C25 – C30 the D/S ratio is still 0.6 but the diameter of the holes is increased to 15 inches. For these models the hysteresis curves are smoother and the predominant shear resistance mechanism is diagonal tension field action irrespective of the plate thickness and shear yielding of the links has very slight influence as opposed to a transition in the behavior observed in the set of models with 9 inch diameter holes.

21. A1 – Diameter 9 inches, D/S = 0.6, t = 0.1875 inches

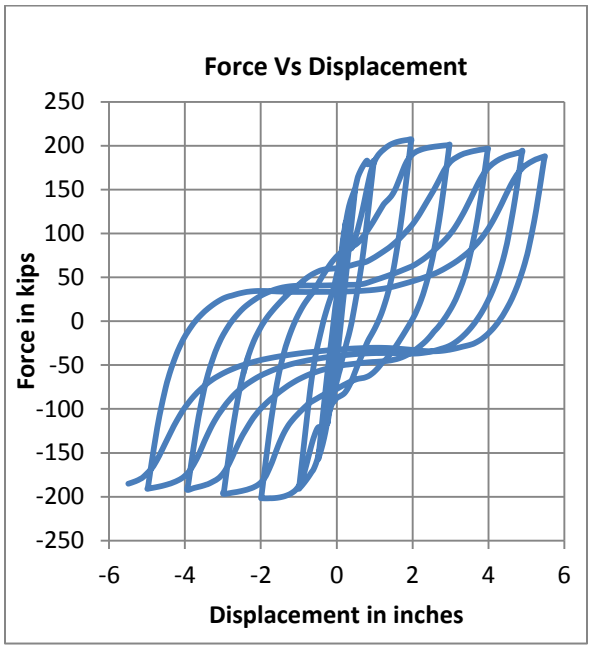

(a)

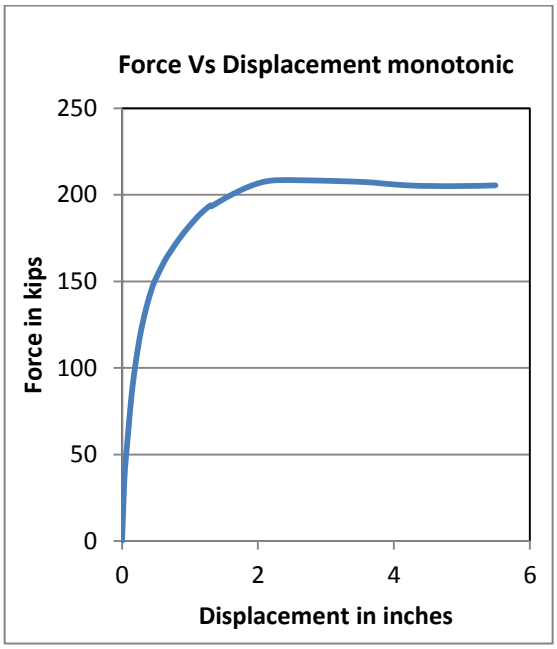

(b)

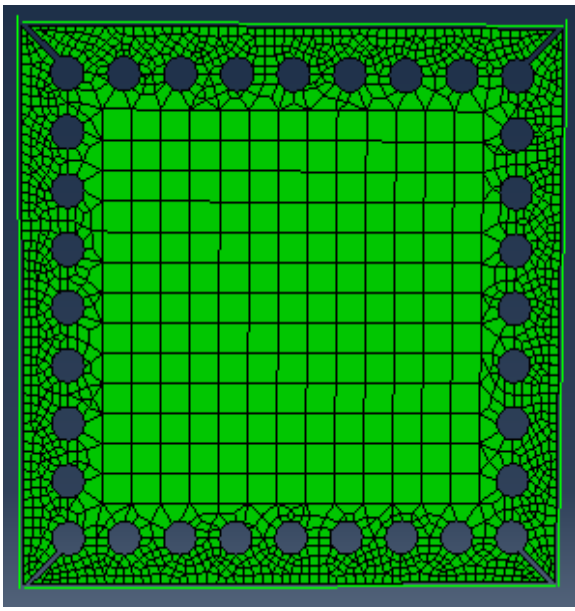

(c)

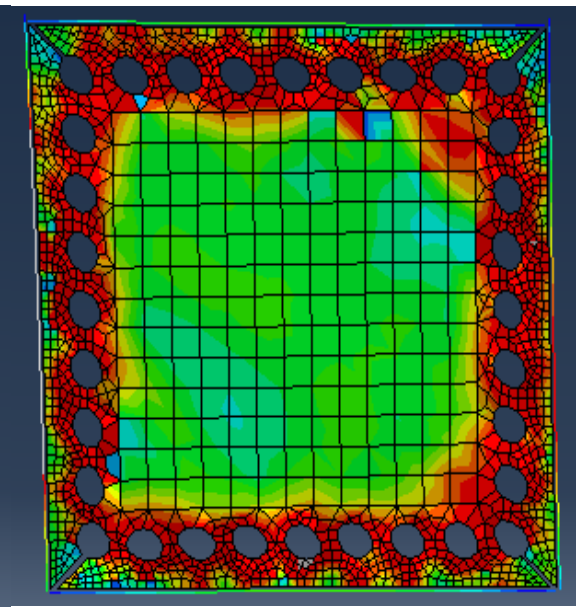

(d)

Figure A- 21 (a) Hysteresis curve, (b) Monotonic Force Vs Displacement curve, (c) Undeformed shape, (d) Deformed shape at 3.8% drift for Plate A1 with 9 inches hole diameter, D/S = 0.6 and t = 0.1875 inches

22. B1 – Diameter = 9 inches, D/S = 0.6, t = 0.25 inches

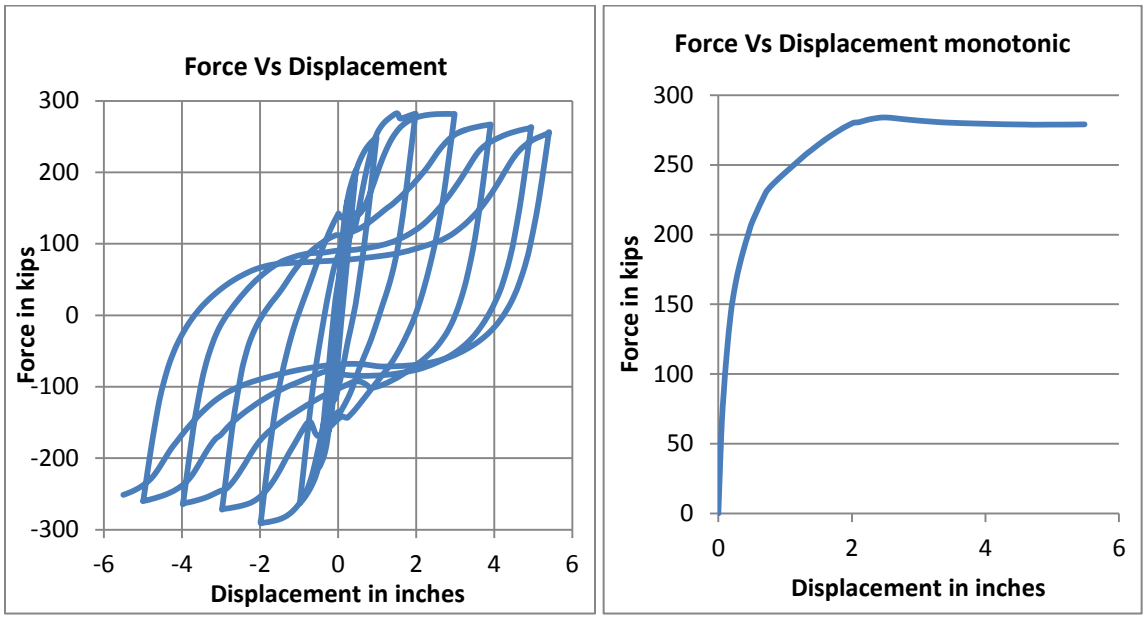

(a) (b)

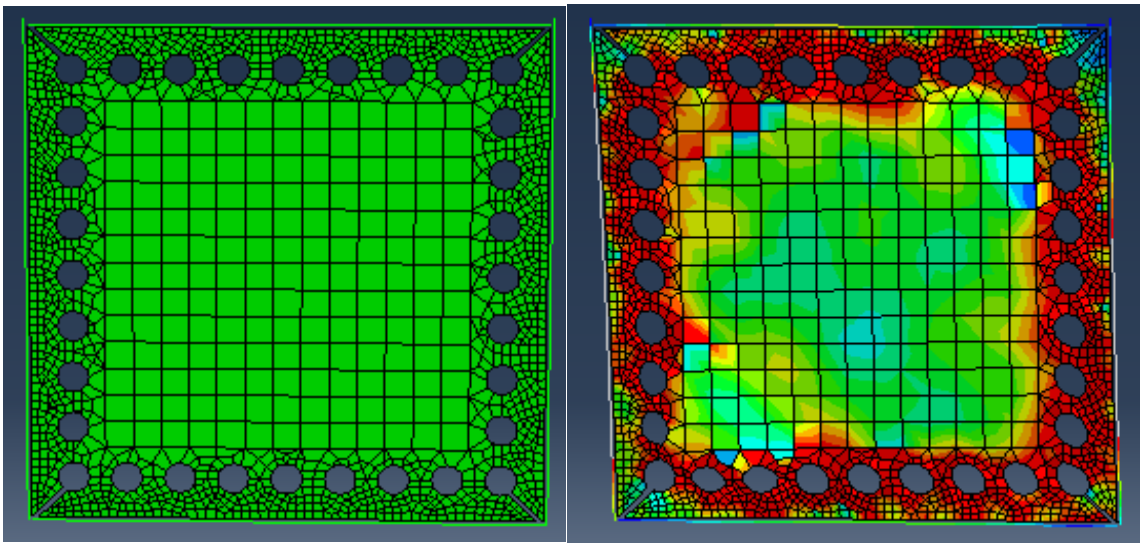

(c) (d)

Figure A- 22 (a) Hysteresis curve, (b) Monotonic Force Vs Displacement curve, (c) Undeformed shape, (d) Deformed shape at 3.8% drift for Plate B1 with 9 inches hole diameter, D/S = 0.6 and t = 0.25 inches

23. C1 – Diameter – 9 inches, D/S = 0.6, t = 0.375 inches

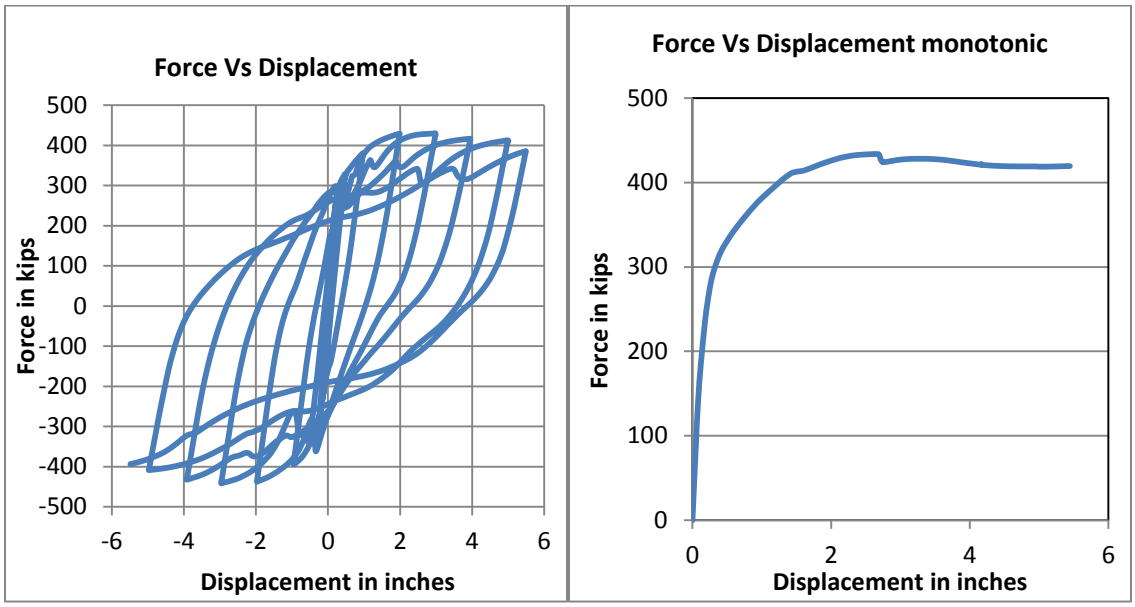

(a) (b)

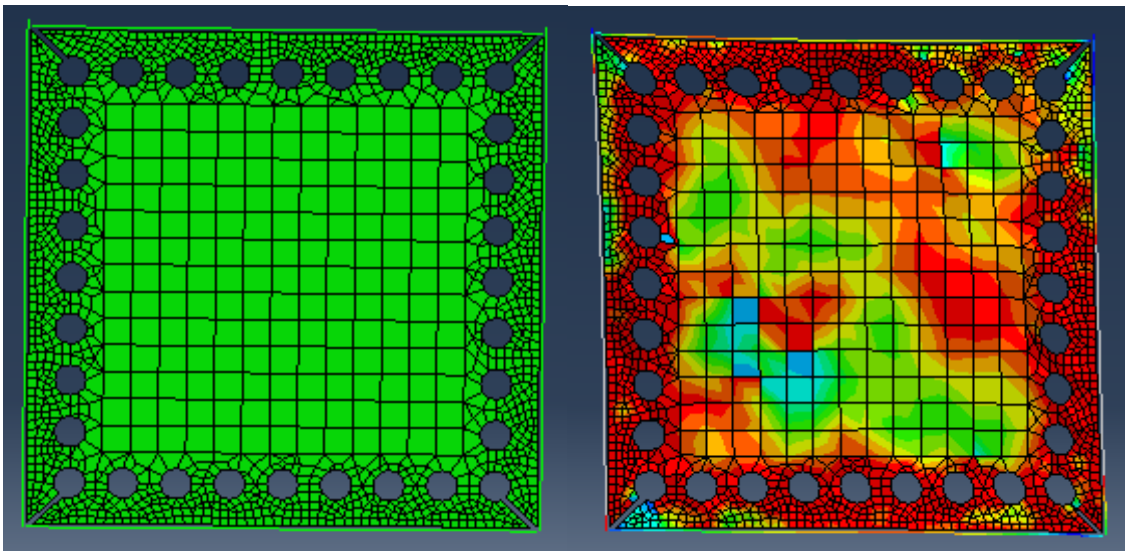

(c) (d)

Figure A- 23 (a) Hysteresis curve, (b) Monotonic Force Vs Displacement curve, (c) Undeformed shape, (d) Deformed shape at 3.8% drift for Plate C1 with 9 inches hole diameter, D/S = 0.6 and t = 0.375 inches

24. D1 – Diameter – 9 inches, D/S = 0.6, t = 0.5 inches

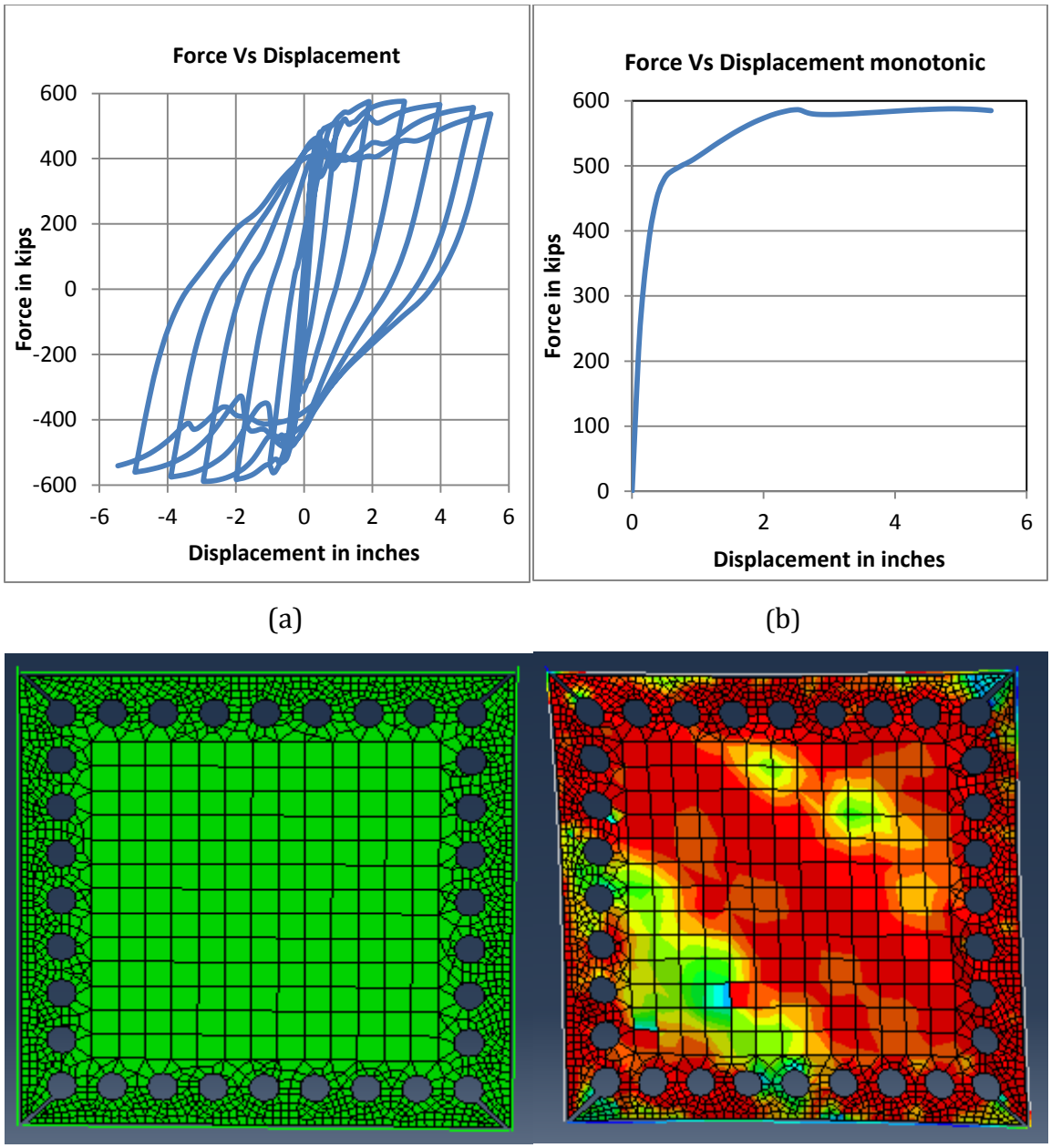

(a) (b)

(c) (d)

Figure A- 24 (a) Hysteresis curve, (b) Monotonic Force Vs Displacement curve, (c) Undeformed shape, (d) Deformed shape at 3.8% drift for Plate D1 with 9 inches hole diameter, D/S = 0.6 and t = 0.5 inches

25. E1 – Diameter – 9 inches, D/S = 0.6, t = 0.75 inches

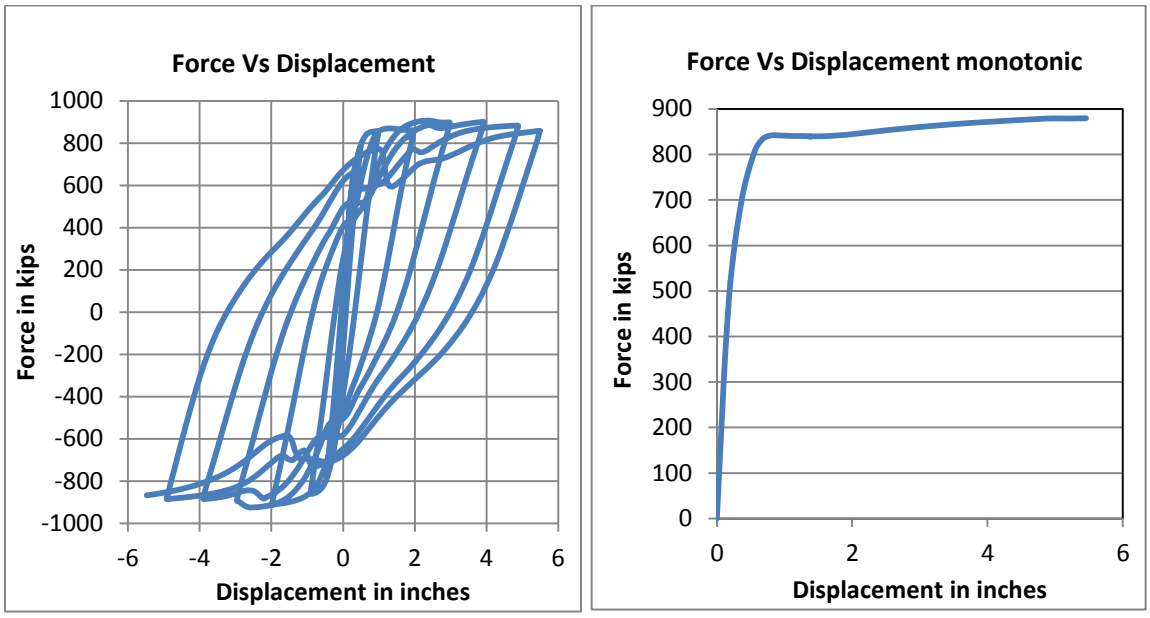

(a) (b)

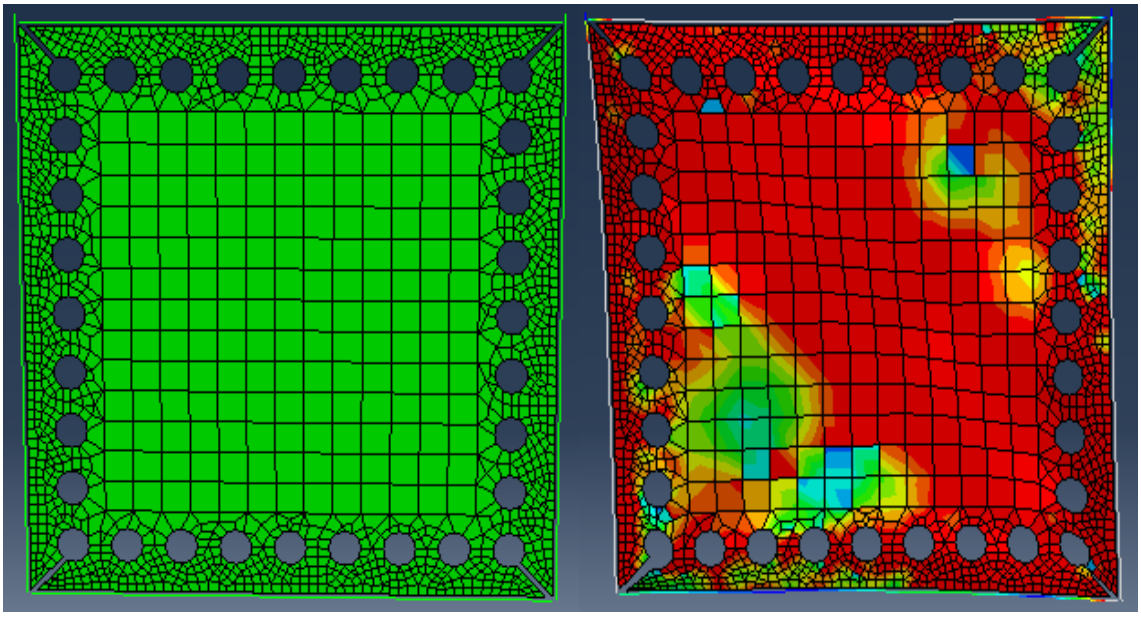

(c) (d)

Figure A- 25 (a) Hysteresis curve, (b) Monotonic Force Vs Displacement curve, (c) Undeformed shape, (d) Deformed shape at 3.8% drift for Plate E1 with 9 inches hole diameter, D/S = 0.6 and t = 0.75 inches

26. A2 – Diameter = 15 inches, D/S = 0.6, t = 0.1875 inches

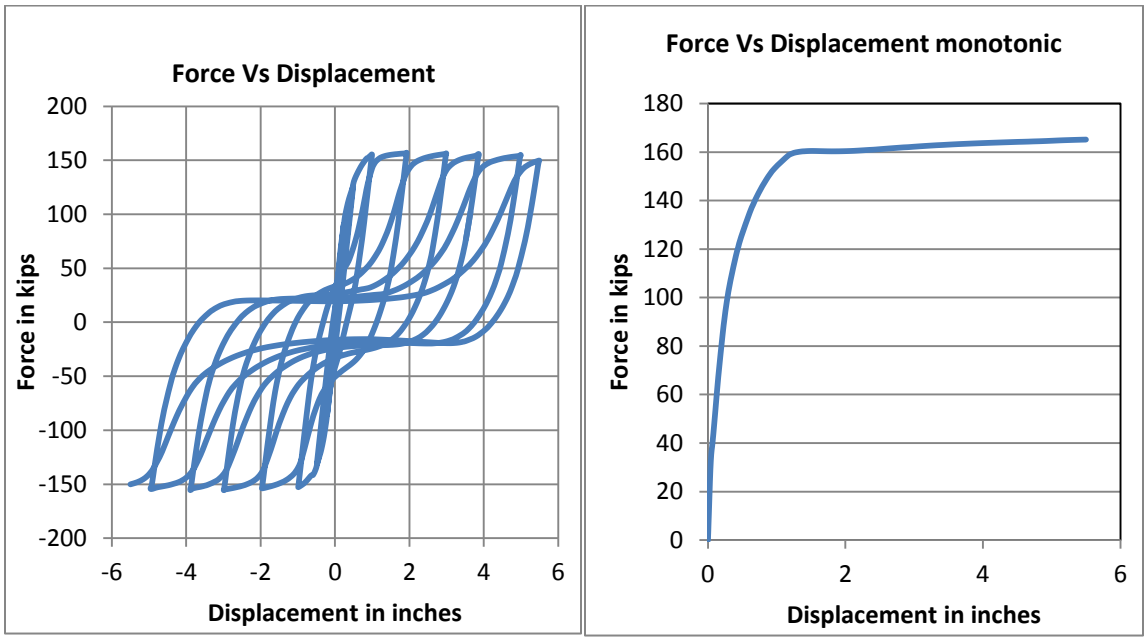

(a) (b)

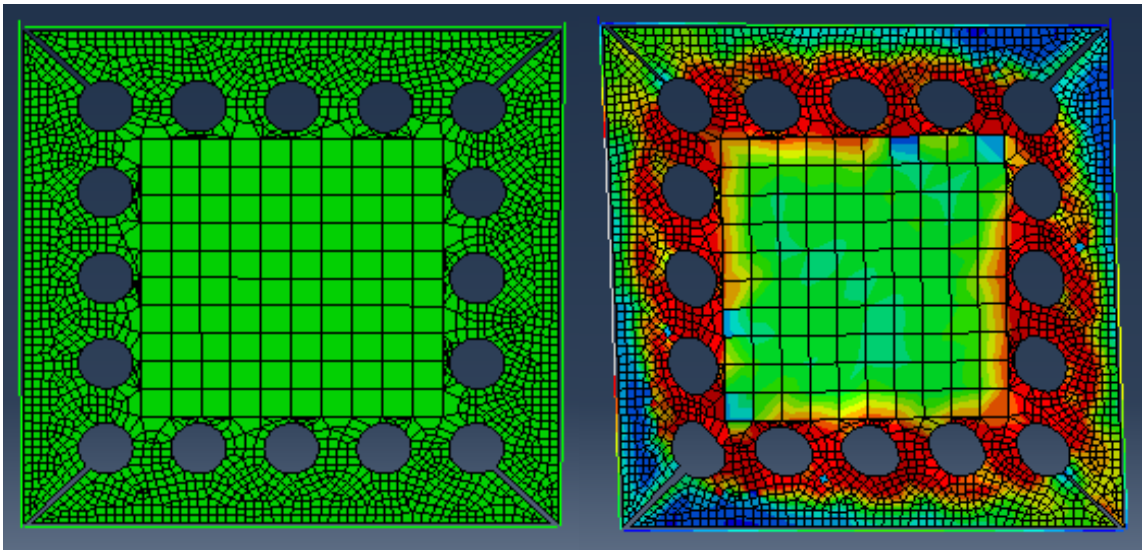

(c) (d)

Figure A- 26 (a) Hysteresis curve, (b) Monotonic Force Vs Displacement curve, (c) Undeformed shape, (d) Deformed shape at 3.8% drift for Plate A2 with 15 inches hole diameter, D/S = 0.6 and t = 0.1875 inches

27. B2 – Diameter = 15 inches, D/S = 0.6, t = 0.25 inches

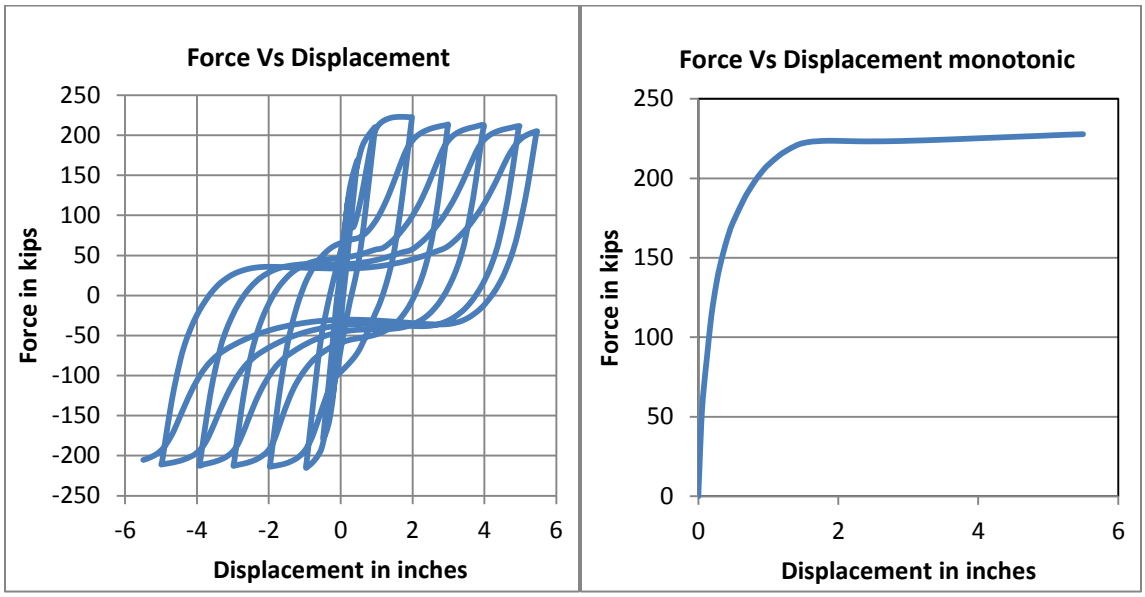

(a) (b)

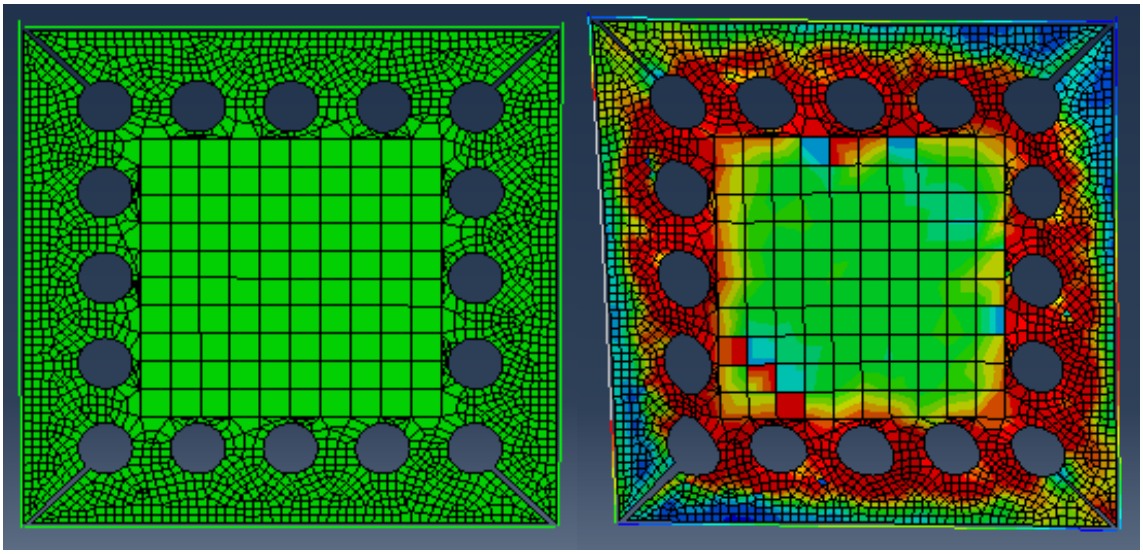

(c) (d)

Figure A- 27 (a) Hysteresis curve, (b) Monotonic Force Vs Displacement curve, (c) Undeformed shape, (d) Deformed shape at 3.8% drift for Plate B2 with 15 inches hole diameter, D/S = 0.6 and t = 0.25 inches

28. C2 – Diameter = 15 inches, D/S = 0.6, t = 0.375 inches

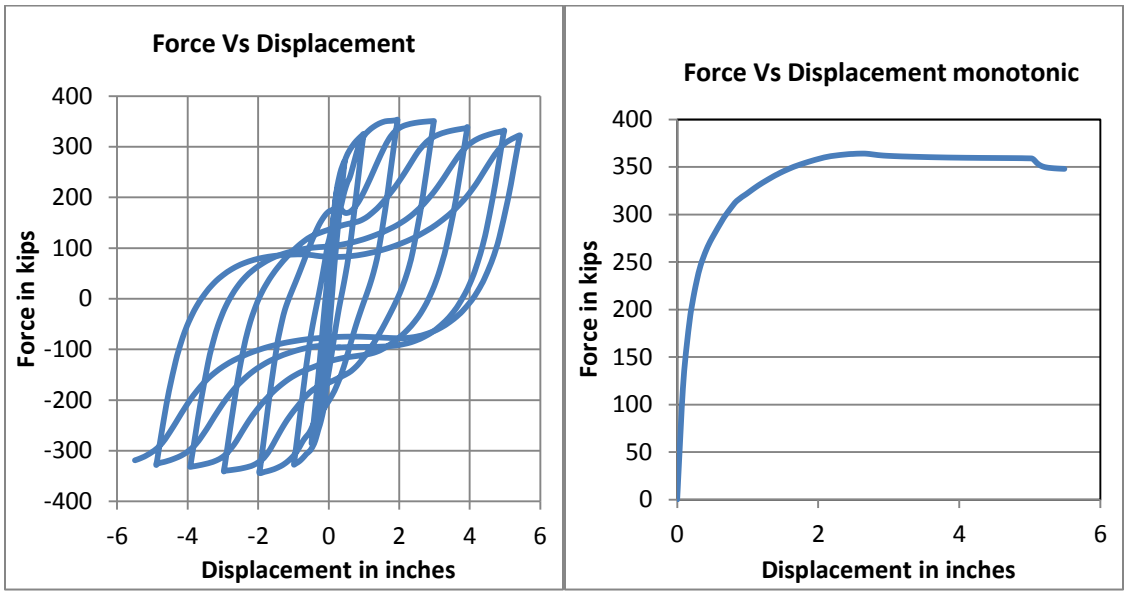

(a) (b)

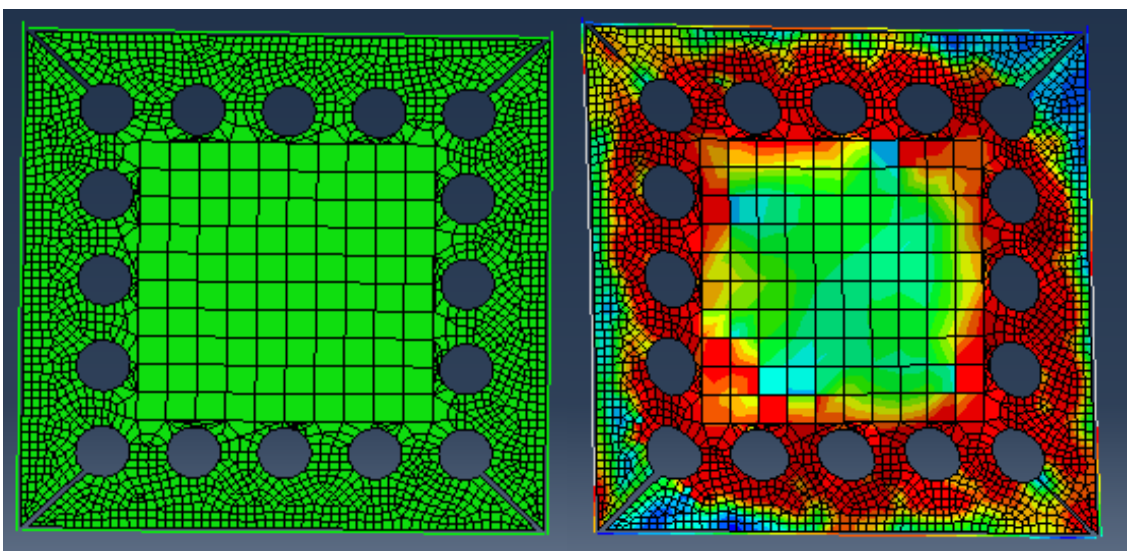

(c) (d)

Figure A- 28 (a) Hysteresis curve, (b) Monotonic Force Vs Displacement curve, (c) Undeformed shape, (d) Deformed shape at 3.8% drift for Plate C2 with 15 inches hole diameter, D/S = 0.6 and t = 0.375 inches

29. D2 – Diameter = 15 inches, D/S = 0.6, t = 0.5 inches

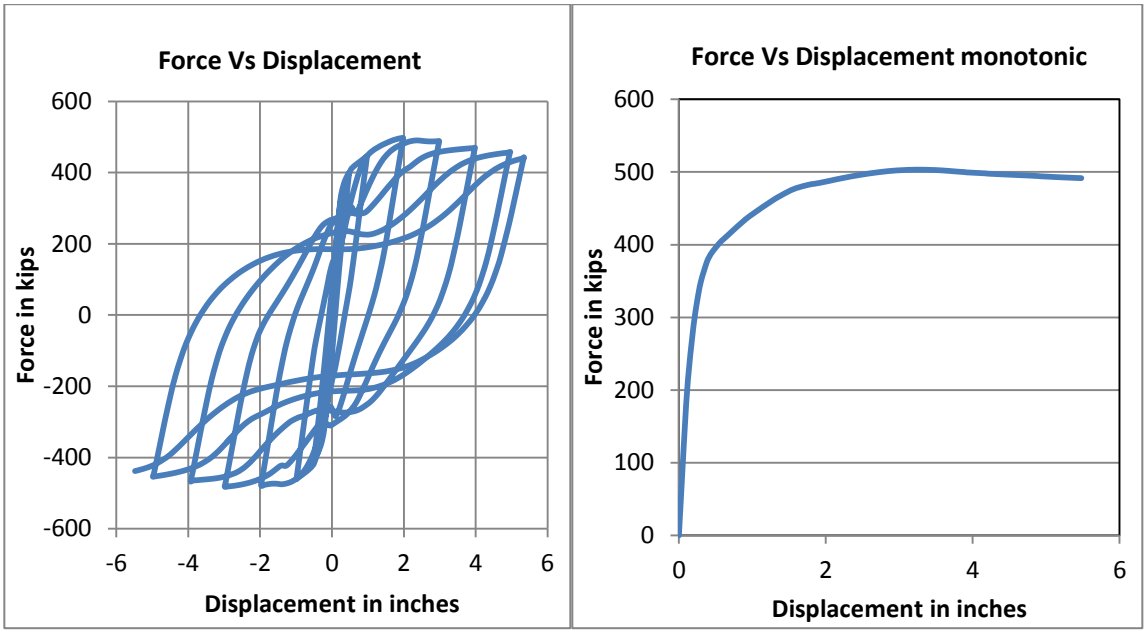

(a) (b)

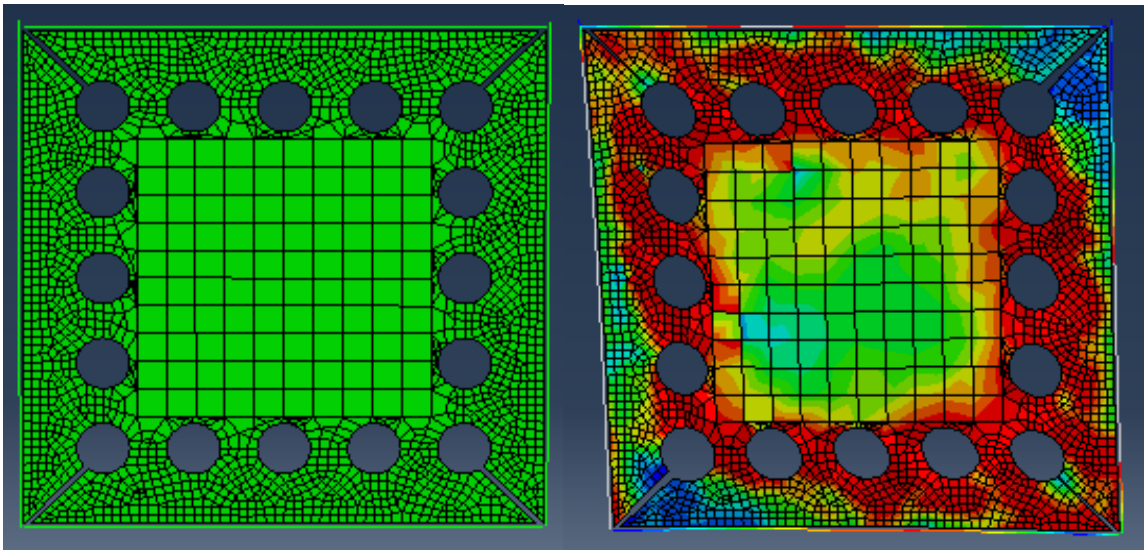

(c) (d)

Figure A- 29 (a) Hysteresis curve, (b) Monotonic Force Vs Displacement curve, (c) Undeformed shape, (d) Deformed shape at 3.8% drift for Plate D2 with 15 inches hole diameter, D/S = 0.6 and t = 0.5 inches

30. E2 – Diameter = 15 inches, D/S = 0.6, t = 0.75 inches

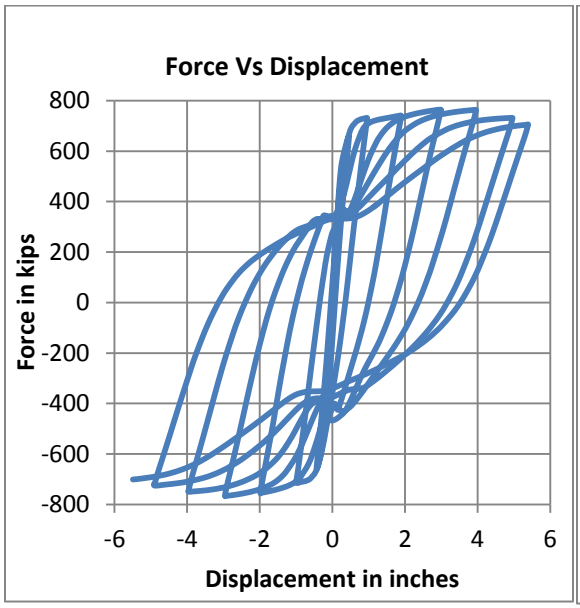

(a)

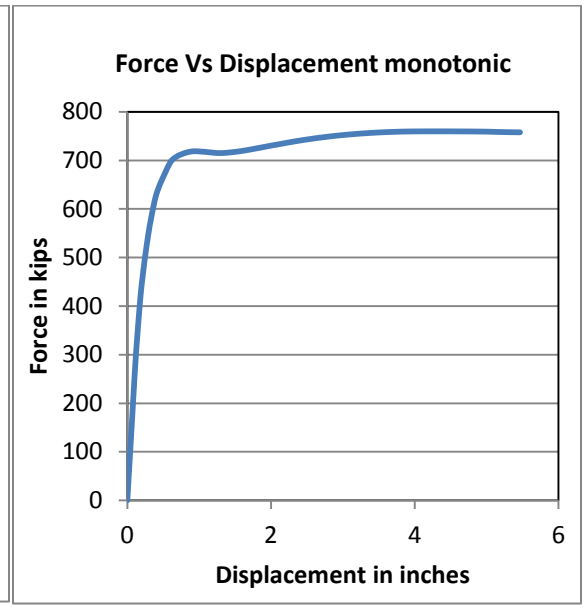

(b)

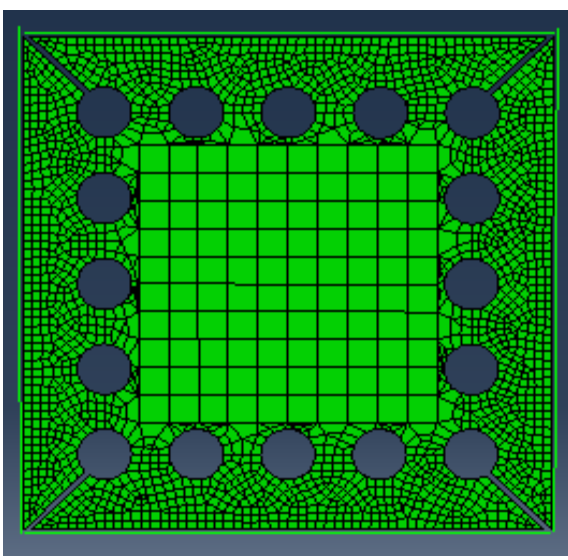

(c)

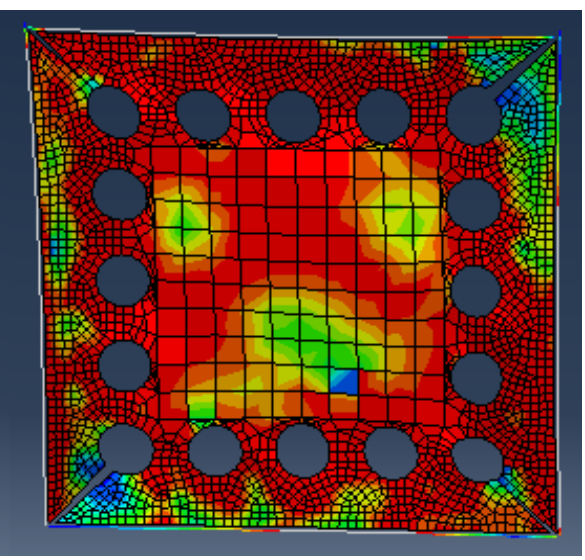

(d)

Figure A- 30 (a) Hysteresis curve, (b) Monotonic Force Vs Displacement curve, (c) Undeformed shape, (d) Deformed shape at 3.8% drift for Plate E2 with 15 inches hole diameter, D/S = 0.6 and t = 0.75 inches

The trends observed from the hysteresis plots and the force deformation plots for the set of 10 models with perimeter strong and weak butterfly shaped links are as shown below:

1. The hysteresis loops for the strong configuration are very less pinched and a stable hysteresis is observed. Hence the energy dissipation capacity is much higher for this configuration in comparison to its weaker counterpart. The strong links are resisting the shear predominantly.
2. The monotonic force – displacement curves are smooth and the distinct regions of stiffness is not observed.
3. There is gain in strength for all the models in this set.
4. The hysteresis of the weak configuration of links is highly pinched and suggests that the primary mode of shear resistance is diagonal tension field action in the plate.
5. There is an increase in the buckling load from 35 kips for model C36 to 150 kips for the model C40.
6. An increase in the peak load is also seen as the plate thickness increases from 0.1875 inches to 0.75 inches for both the strong and the weak configuration of cutouts.

31. Strong model A3 – t = 0.1875 inches

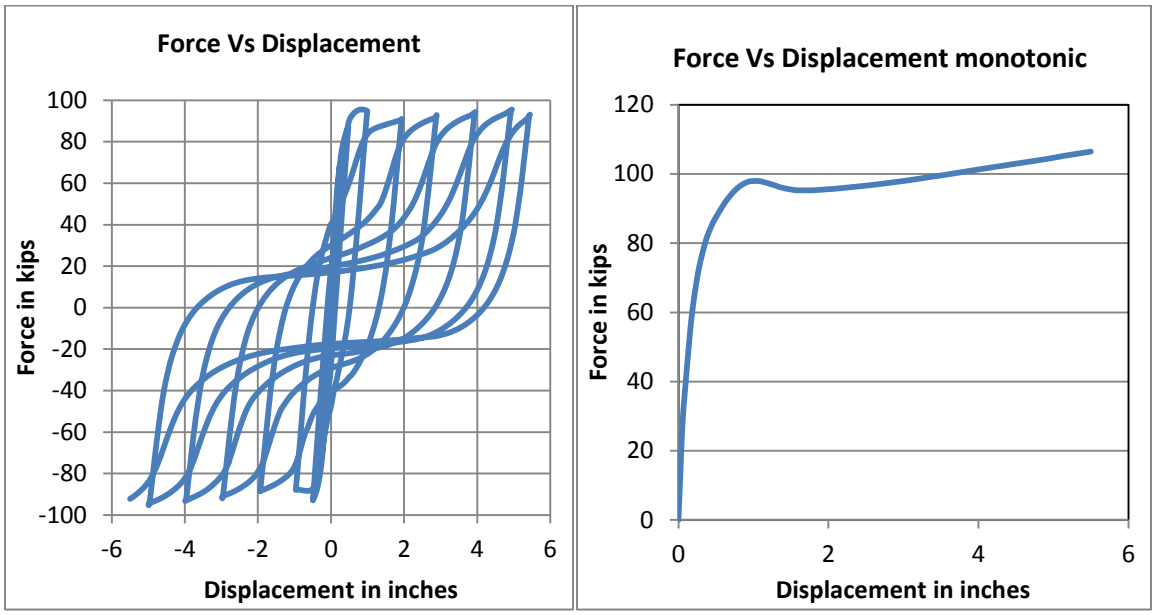

(a) (b)

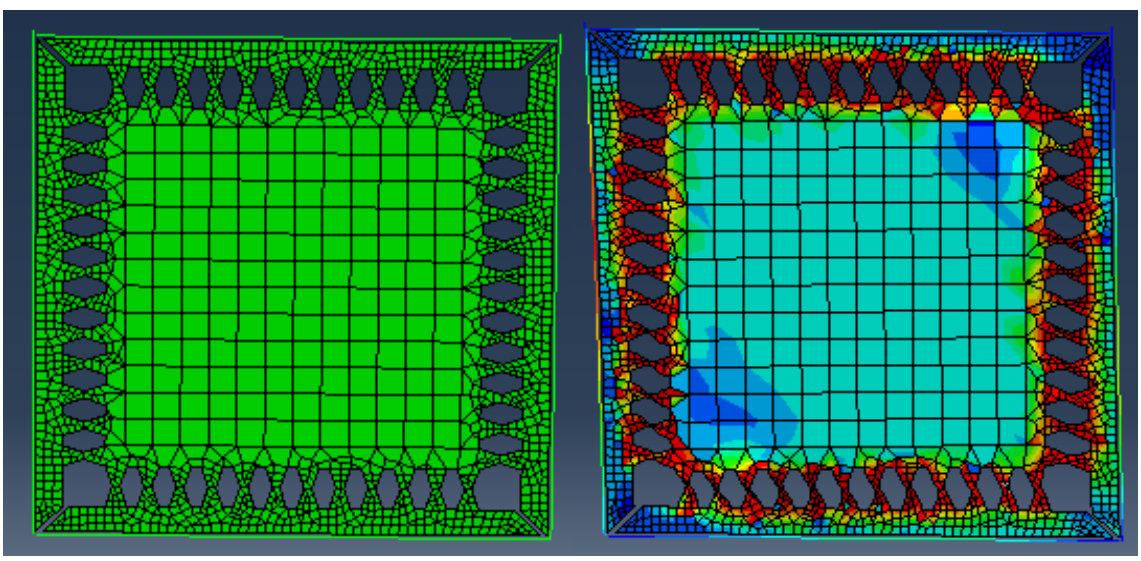

(c) (d)

Figure A- 31 (a) Hysteresis curve, (b) Monotonic Force Vs Displacement curve, (c) Undeformed shape, (d) Deformed shape at 3.8% drift for Plate A3 (Strong Configuration) and t = 0.1875 inches

32. Strong model B3 – t = 0.25 inches

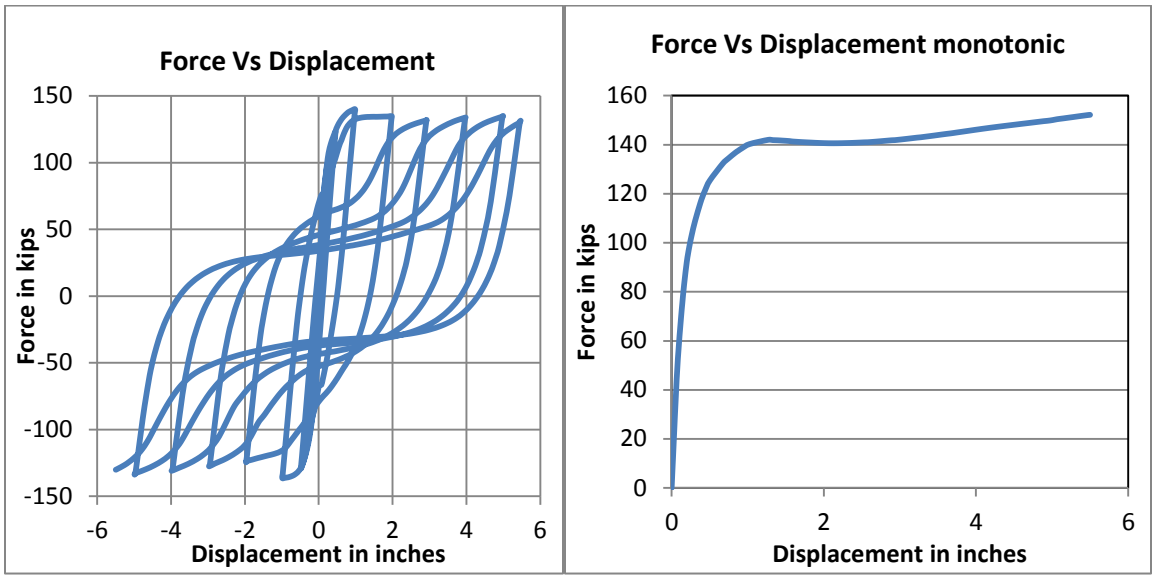

(a) (b)

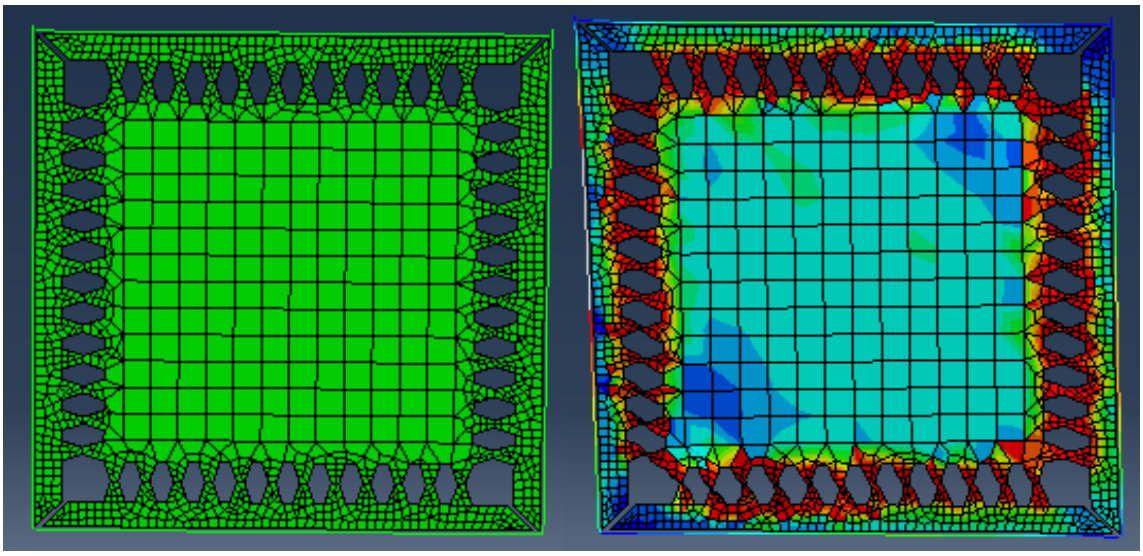

(c) (d)

Figure A- 32 (a) Hysteresis curve, (b) Monotonic Force Vs Displacement curve, (c) Undeformed shape, (d) Deformed shape at 3.8% drift for Plate B3 (Strong Configuration) and t = 0.25 inches

33. Strong model C3 – t = 0.375 inches

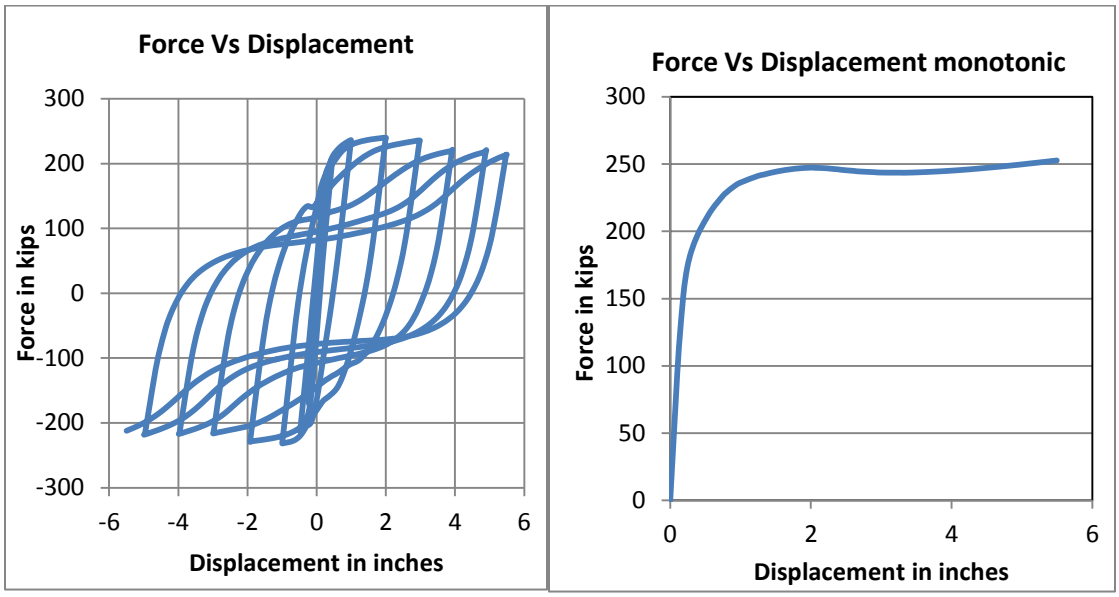

(a) (b)

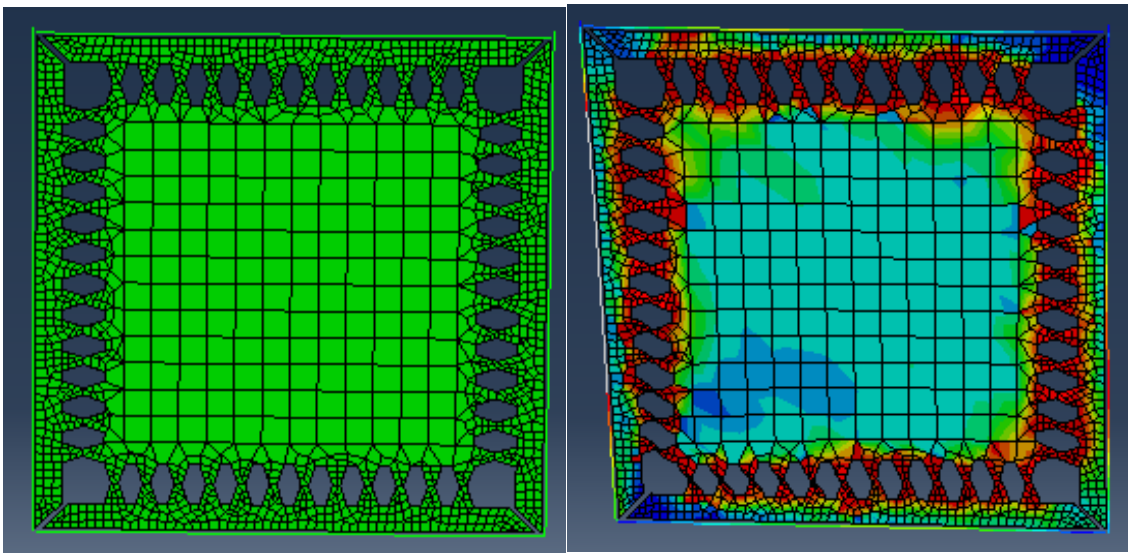

(c) (d)

Figure A- 33 (a) Hysteresis curve, (b) Monotonic Force Vs Displacement curve, (c) Undeformed shape, (d) Deformed shape at 3.8% drift for Plate C3 (Strong Configuration) and t = 0.375 inches

34. Strong model D3 – t = 0.5 inches

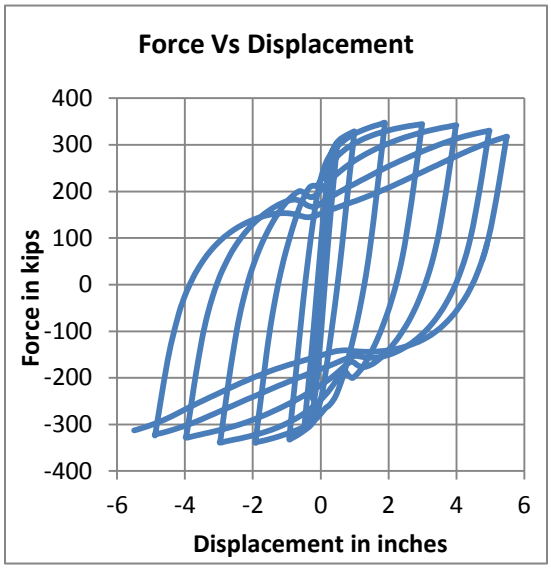

(a)

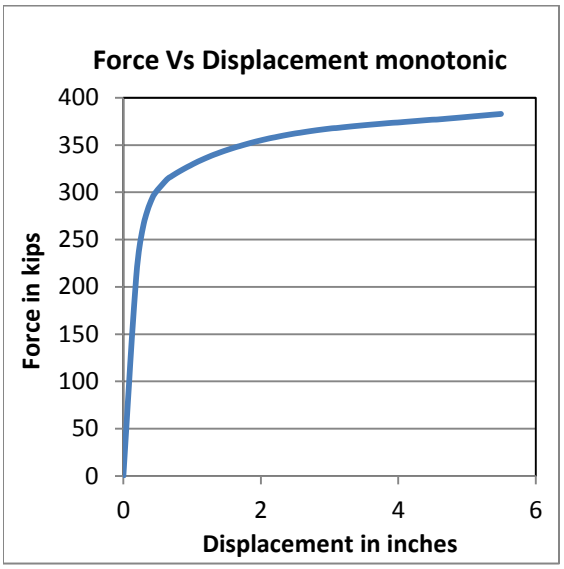

(b)

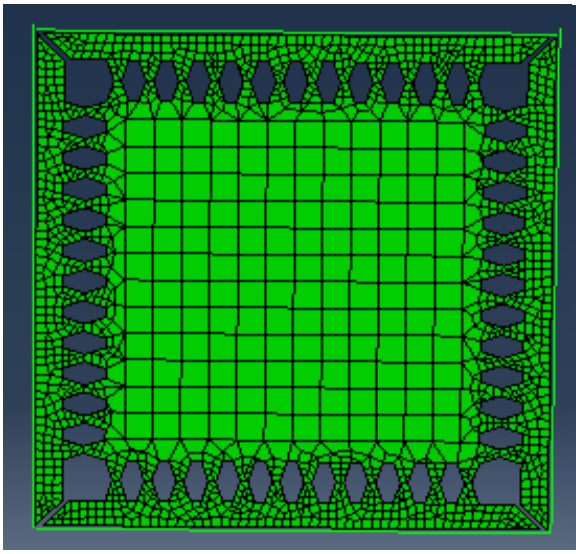

(c)

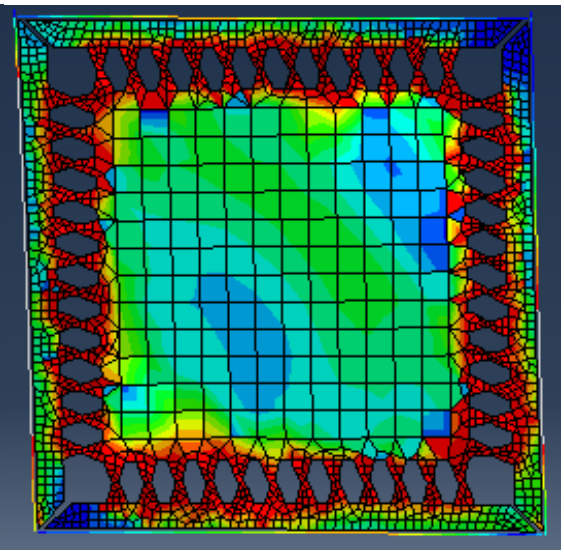

(d)

Figure A- 34 (a) Hysteresis curve, (b) Monotonic Force Vs Displacement curve, (c) Undeformed shape, (d) Deformed shape at 3.8% drift for Plate D3 (Strong Configuration) and t = 0.5 inches

35. Strong model E3 – t = 0.75 inches

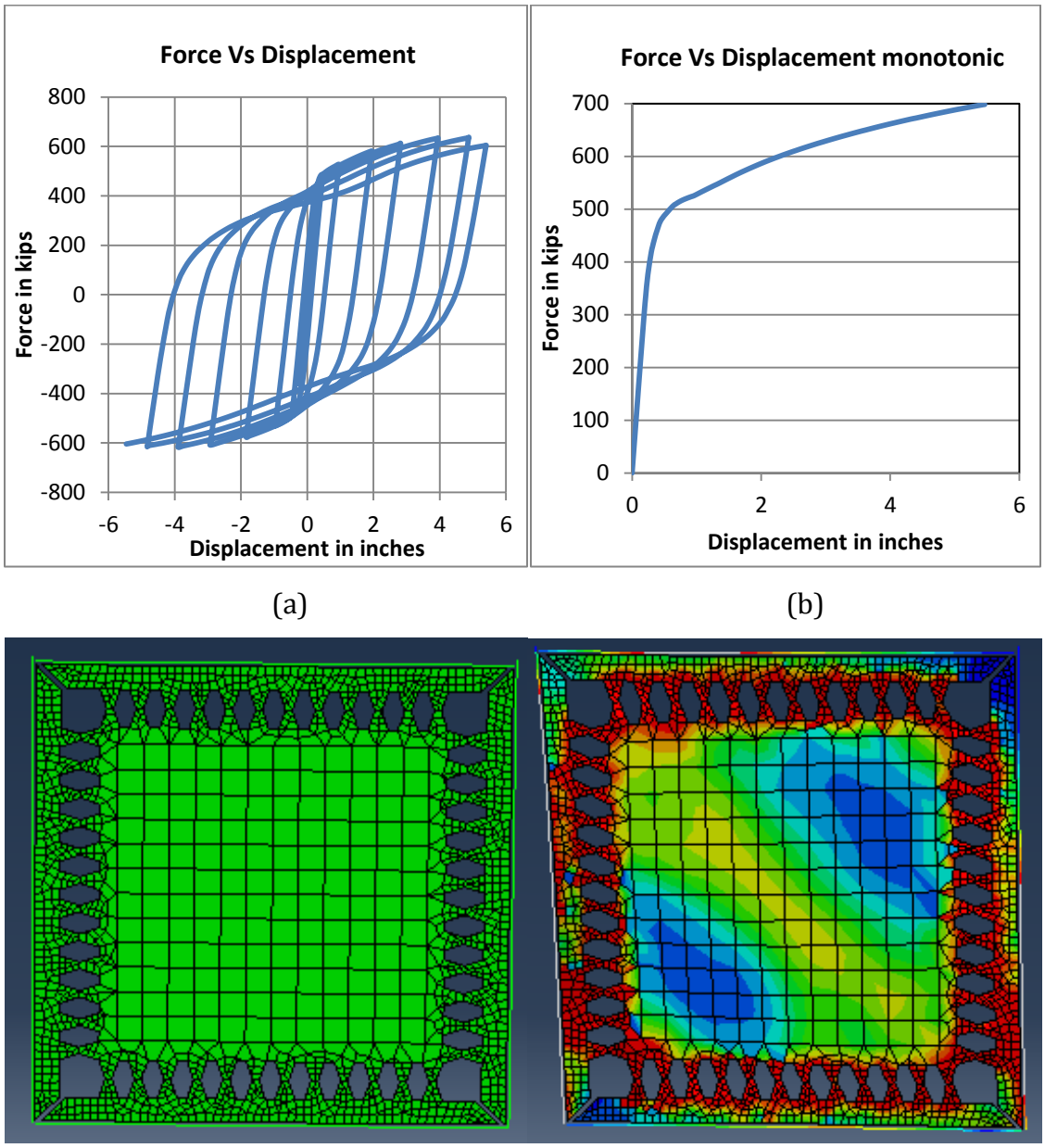

(a) (b)

(c) (d)

Figure A- 35 (a) Hysteresis curve, (b) Monotonic Force Vs Displacement curve, (c) Undeformed shape, (d) Deformed shape at 3.8% drift for Plate E3 (Strong Configuration) and t = 0.75 inches

36. Weak model – A4 – t = 0.1875 inches

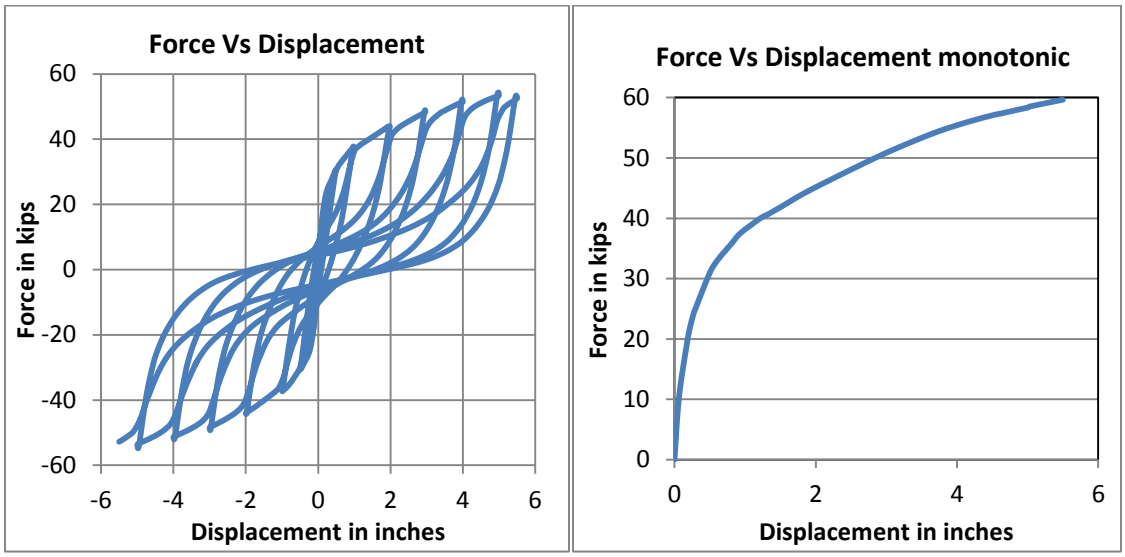

(a) (b)

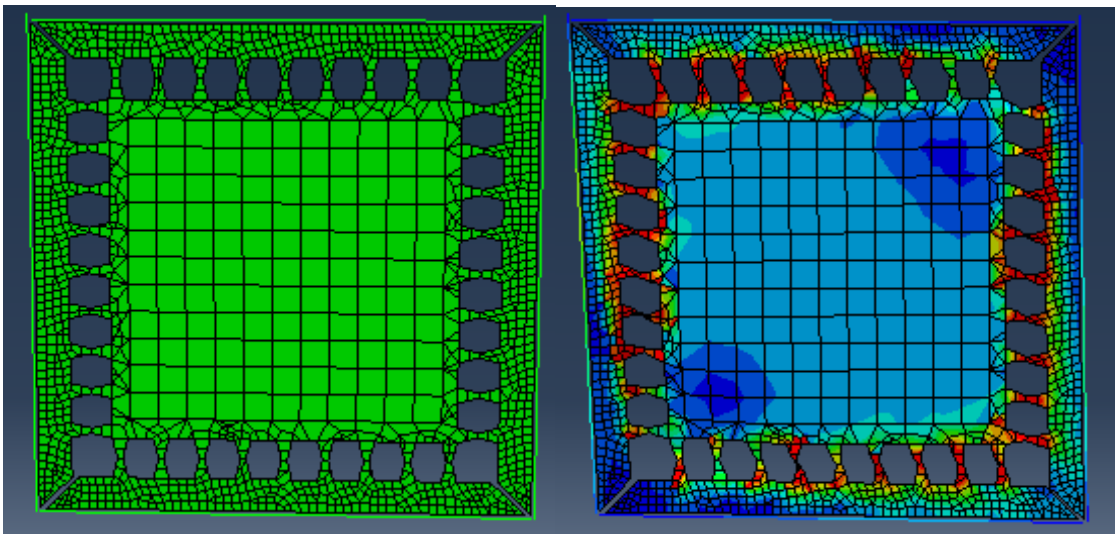

(c) (d)

Figure A- 36 (a) Hysteresis curve, (b) Monotonic Force Vs Displacement curve, (c) Undeformed shape, (d) Deformed shape at 3.8% drift for Plate A4 (Weak Configuration) and t = 0.1875 inches

37. Weak model – B4 – t = 0.25 inches

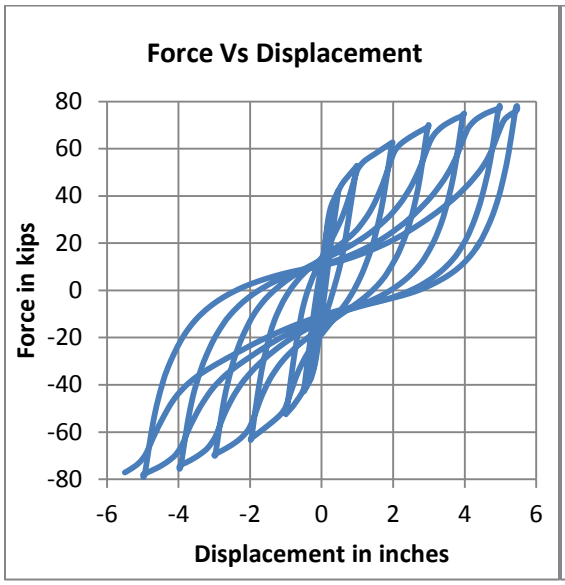

(a)

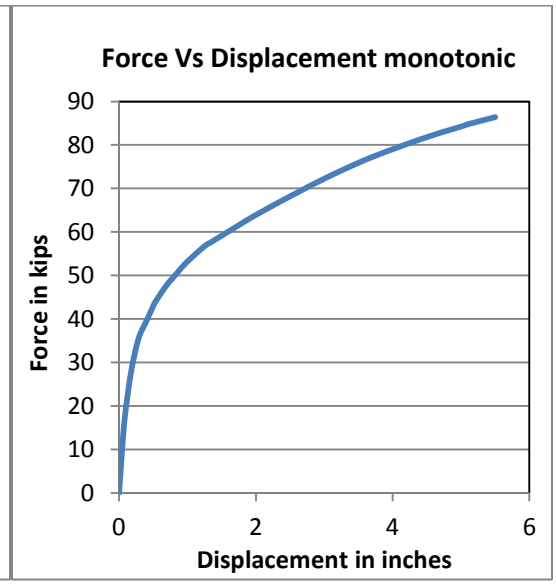

(b)

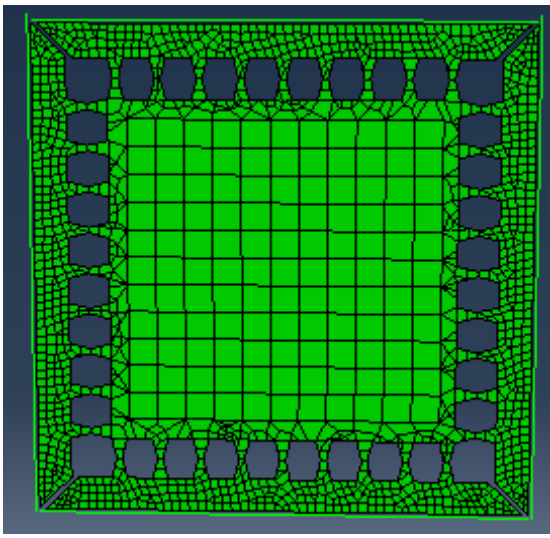

(c)

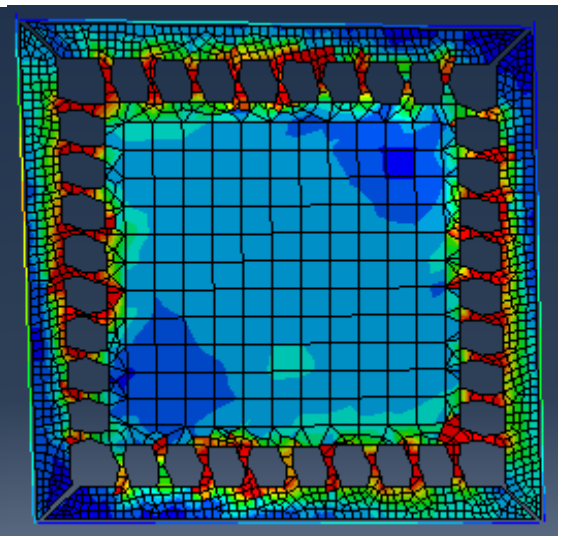

(d)

Figure A- 37 (a) Hysteresis curve, (b) Monotonic Force Vs Displacement curve, (c) Undeformed shape, (d) Deformed shape at 3.8% drift for Plate B4 (Weak Configuration) and t = 0.25 inches

38. Weak model – C4bf – t = 0.375 inches

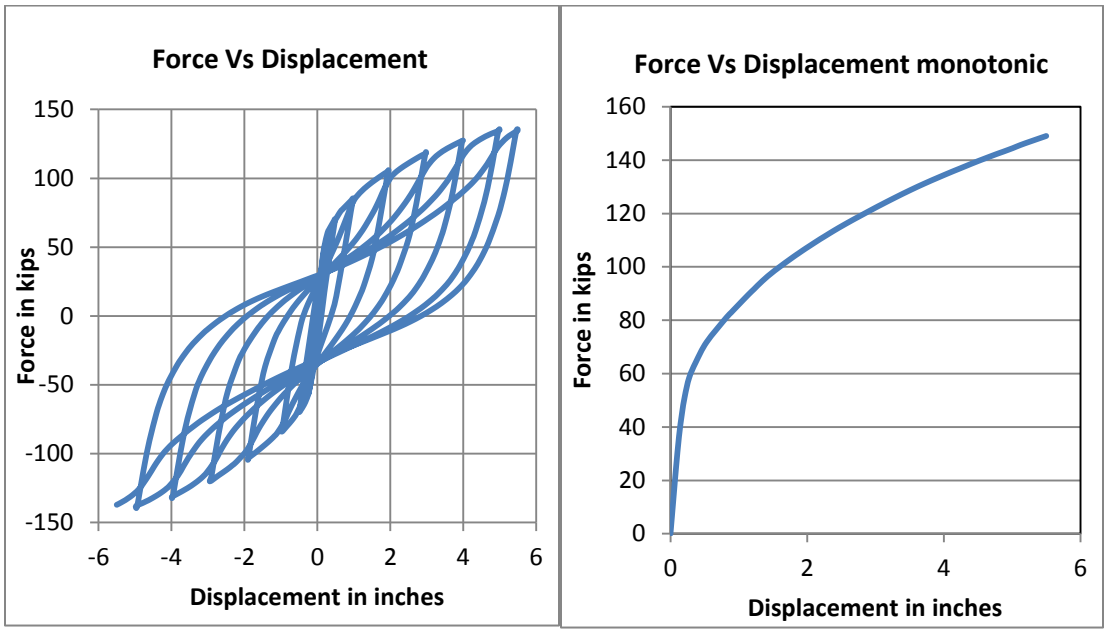

(a) (b)

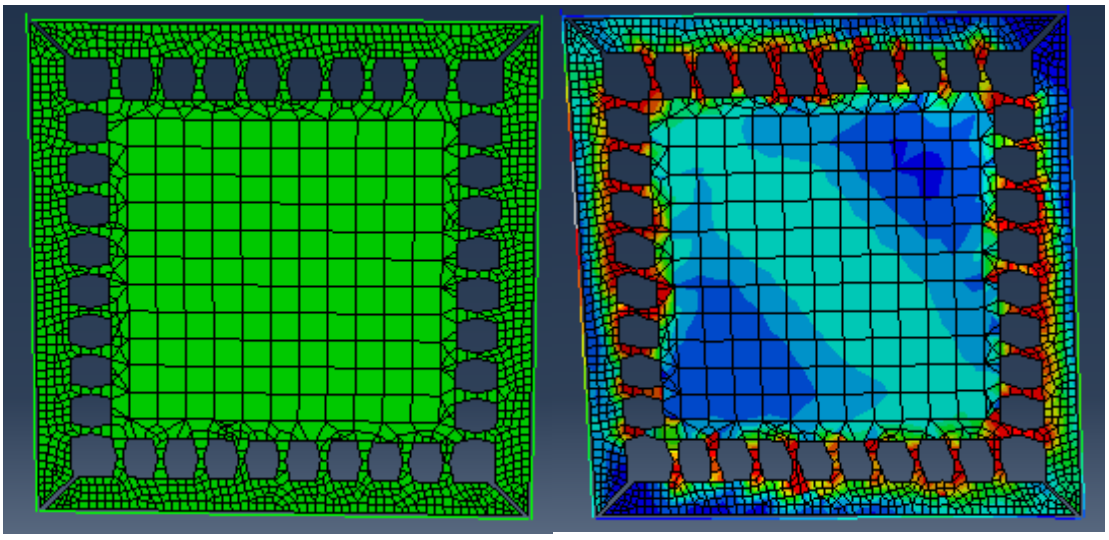

(c) (d)

Figure A- 38 (a) Hysteresis curve, (b) Monotonic Force Vs Displacement curve, (c) Undeformed shape, (d) Deformed shape at 3.8% drift for Plate C4bf (Weak Configuration) and t = 0.375 inches

39. Weak model – D4 – t = 0.5 inches

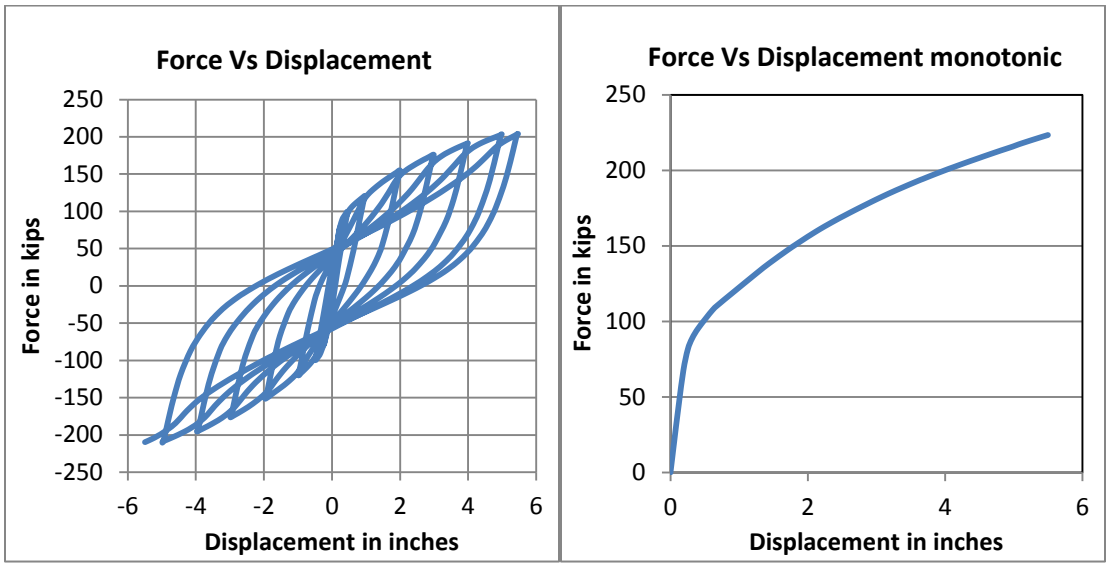

(a) (b)

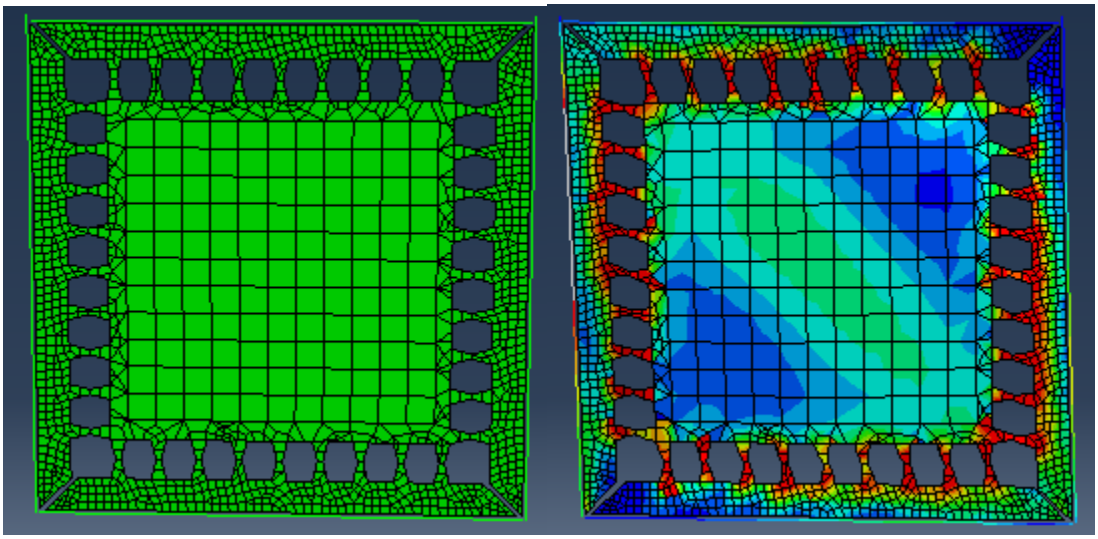

(c) (d)

Figure A- 39 (a) Hysteresis curve, (b) Monotonic Force Vs Displacement curve, (c) Undeformed shape, (d) Deformed shape at 3.8% drift for Plate D4 (Weak Configuration) and t = 0.5 inches

40. Weak model – E4 – t = 0.75 inches

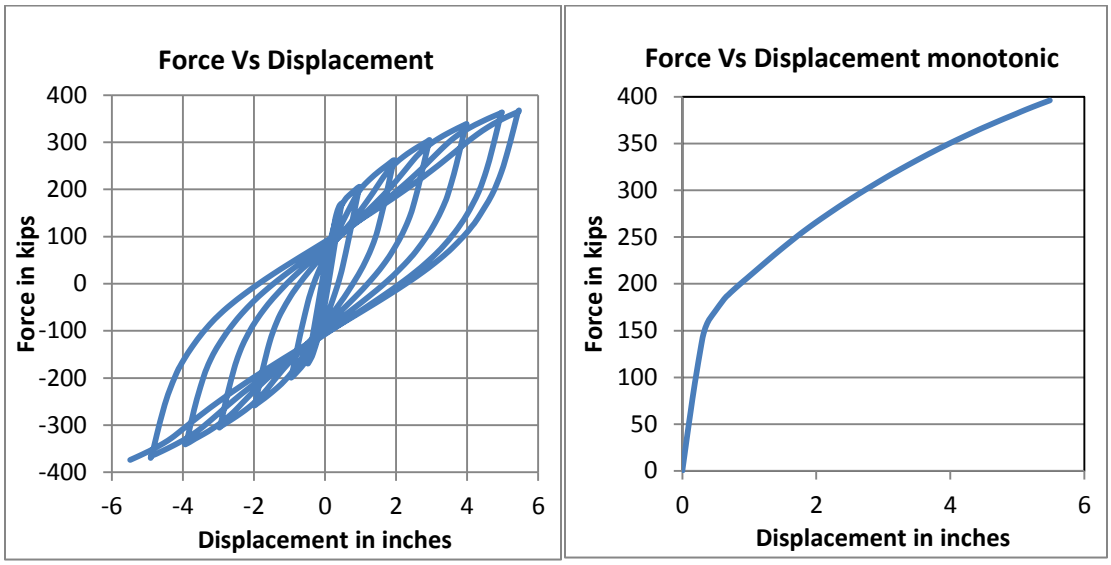

(a) (b)

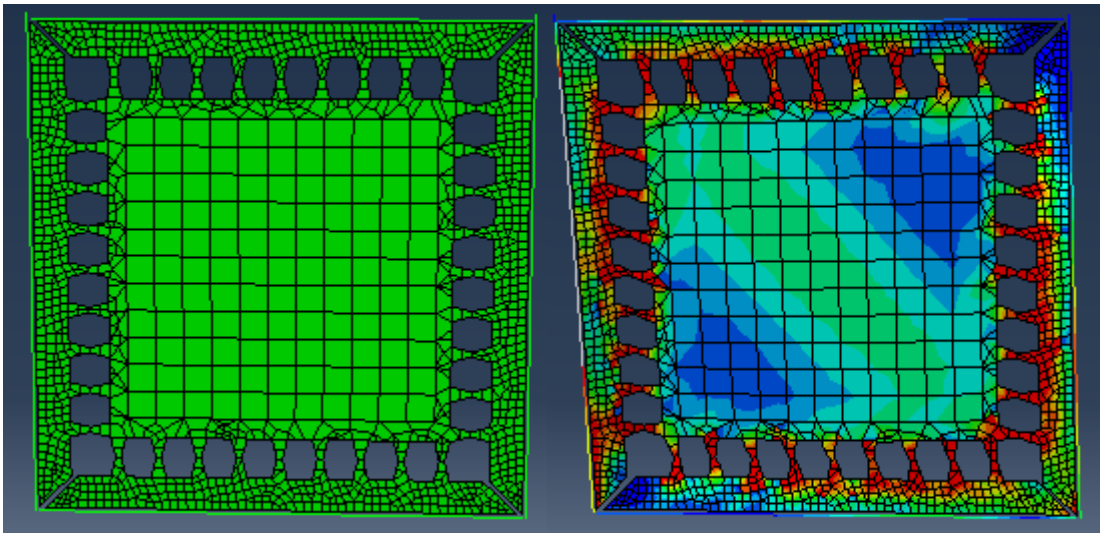

(c) (d)

Figure A- 40 (a) Hysteresis curve, (b) Monotonic Force Vs Displacement curve, (c) Undeformed shape, (d) Deformed shape at 3.8% drift for Plate E4 (Weak Configuration) and t = 0.75 inches